Investigation of zebrafish gills as a model to study respiratory immunology

Madina Racky Wane

Imperial College London

Department of Life Sciences

Thesis submitted for the degree of

Doctor of Philosophy (PhD)

2021

Acknowledgments

This thesis, like all scientific endeavours, could not have been completed without the support of many people. Firstly, I want to thank Maggie and Laurence for giving me the opportunity to work on this project, providing valuable guidance and feedback, and challenging me to grow as a scientist. Thanks also to Fränze for being a wonderful supervisor during my Master's and starting the work on which this thesis builds on. Working in the Dallman lab has been a huge joy and I must also thank fellow members of the lab: Dory, Marie-Christine, Ralf, Anna, Håkon, Hannah, Natalie and Jon for creating such a supportive and fun environment. I have learnt a lot from all of them and am grateful for their company, scientific input and for making those 3 fish room moves bearable!

During this PhD I have been able to supervise some brilliant undergraduate and Masters' students whose enthusiasm and diligent work helped this project progress. I particularly thank Katie, Alisha, Morgan and Sabrina whose work are all included in this thesis.

I am also very grateful for my project advisors and collaborators who took the time to work with me and provided advice and resources: Cecilia Johansson, Freja Kirsebom, Trevor Hansel, Akhilesh Jha, Wendy Barclay, Jay, Jie Zhou, Jennifer Shelley, Bhakti Mistry, Federica Bottiglione, Adam Hurlstone, Marc Dionne, Jon Pavelin and Ross Houston. The staff of the Facility for Imaging by Light Microscopy, and Flow Cytometry Facility also provided excellent training and continuous support during this project. Particular thanks to David Gaboriau, Stephen Rothery, Andreas Bruckbauer, Jane Srivastava, Jess Rowley and Radhika Patel.

I could not have gone through this PhD without the incredible support of my friends, particularly Nirmz, Amy, Jenny, Tamzin, Bernadett, Maria, Mo, Supreet, Helen, Zara and many others who've stuck with me through many years. I can't thank Dory enough for the many hours spent helping each other and sharing our struggles and excitement throughout our projects. This PhD would not have been nearly as fun without her! Thanks also to friends and colleagues in SAF and my fellow Wellcome cohort who have been great company over the last 4 years – you know who you are!

Finally, I am always thankful for the support from family, especially Mum and Dad who have always believed in me and supported my pursuit of education.

Statement of originality

The work presented in this thesis is original work produced by myself. Contributions from others have been clearly specified and referenced in relevant sections.

Copyright declaration

The copyright of this thesis rests with the author. Unless otherwise indicated, its contents are licensed under a Creative Commons Attribution-Non Commercial 4.0 International Licence (CC BY-NC). Under this licence, you may copy and redistribute the material in any medium or format. You may also create and distribute modified versions of the work. This is on the condition that: you credit the author and do not use it, or any derivative works, for a commercial purpose. When reusing or sharing this work, ensure you make the licence terms clear to others by naming the licence and linking to the licence text. Where a work has been adapted, you should indicate that the work has been changed and describe those changes. Please seek permission from the copyright holder for uses of this work that are not included in this licence or permitted under UK Copyright Law.

Funding

Abbreviations

AEC	Airway epithelial cells
AIM-2	Absent in melanoma-2
ALI	Air-liquid interface
ALR	Absent in melanoma-2-like receptor
AM	Alveolar macrophage
AMP	Antimicrobial peptide
APC	Antigen presenting cell
ATI	Alveolar type 1 epithelial
ATII	Alveolar type 2 epithelial
BALT	Bronchus-associated lymphoid tissue
BrdU	5-bromo-2′-deoxyuridine
cDNA	complementary DNA
CHIKV	Chikungunya virus
CHSE214 cells	Chinook salmon embryo cells
CLR	C-type lectin receptor
COPD	Chronic obstructive pulmonary disease
CoV	Coronavirus
cRNA	Complementary RNA
CSV	Chum salmon reovirus
CT	Cycle threshold
CyHV-3	Cyprinid herpesvirus 3
DAB	Diaminobezindine tetrahydrochloride
DAMP	Danger-associated molecular pattern
DAPI	4′,6-diamidino-2-phenylindole
DC	Dendritic cell
dCT	Difference in cycle threshold
DMEM	Dulbecco's modified Eagle's medium
DMSO	Dimethyl sulfoxide
DoC	Duct of Cuvier
dpc	Days post challenge
dpf	Days post fertilisation

dpi	Days post infection
dsRNA	Double-stranded RNA
EHV-1	Equine herpesvirus-1
ESV	European sheatfish virus
FACS	Fluorescence activated cell sorting
FCS	Fetal calf serum
FDC	Follicular dendritic cell
FISH	Fluorescence *in situ* hybridisation
FSC	Forward scatter
FSC-A	Forward scatter area
FSC-H	Forward scatter height
GC	Germinal centre
GCRV	Grass carp reovirus
GIALT	Gill-associated lymphoid tissue
HA	Haemagglutinin
HAE	Human airway epithelium
HCV	Hepatitis C virus
HE-p2	Human epithelial type 2
HEV	High endothelial venule
hpc	Hours post challenge
hpi	Hours post infection
hPSC	Human pluripotent stem cell
hpt	Hours post treatment
HSPC	Haematopoietic stem and progenitor cell
HSV-1	Herpes simplex virus-1
HuNoV	Human norovirus
i.p.	Intraperitoneal
i.v.	Intravenous
IAV	Influenza A virus
iBALT	Induced bronchus-associated lymphoid tissue
IBS	Interbranchial septum
IEL	Intraepithelial lymphocyte
IFN	Interferon

Ig	Immunoglobulin
IHNV	Infectious Hematopoietic Necrosis Virus
ILC	Innate lymphoid cell
ILC1	Group 1 innate lymphoid cell
ILC2	Group 2 innate lymphoid cell
ILC3	Group 3 innate lymphoid cell
ILT	Interbranchial lymphoid tissue
iNKT	Invariant natural killer T
IPNV	Infectious pancreatic necrosis virus
IRF	Interferon regulatory factor
ISAV	Infectious salmon anaemia virus
ISG	Interferon-stimulated gene
ISKNV	Infectious spleen and kidney necrosis virus
Lck	Lymphocyte-specific protein tyrosine kinase
LGP2	Laboratory of genetics and physiology 2
LN	Lymph node
LPS	Lipopolysaccharide
LRR	Leucine-rich repeat
LTi	Lymphoid tissue inducer
Lyz	Lysozyme
M	Mean
M cell	Microfold cell
MALT	Mucosal-associated lymphoid tissue
MB	Methylene blue
MDA5	Melanoma differentiation-associated factor 5
MDCK	Madin-Darby Canine Kidney
MERS-CoV	Middle East respiratory syndrome-coronavirus
MFI	Median intensity fluorescence
MHC	Major histocompatibility complex
MNP	Mononuclear phagocyte
Mpeg	Macrophage expressed
mpf	Months post fertilisation
Mpx	Myeloperoxidase

MyD88	Myeloid differentiation primary response 88
NA	Neuraminidase
NALT	Nasopharyngeal-associated lymphoid tissue
NCC	Non-specific cytotoxic cell
NF-κB	Nuclear factor kappa B
NHP	Non-human primate
NK	Natural killer
NKL	Natural killer-like
NLR	Nucleotide-binding oligomerization domain-like receptors
NNV	Nervous necrosis virus
NOD	Nucleotide-binding oligomerization domain
NS	Nonstructural
ODN	Oligonucleotide
OPT	Optical projection tomography
OTC	Oxytetracycline
OVA	Ovalbumin
PAMP	Pathogen-associated molecular pattern
PBS	Phosphate-buffered saline
PCLS	Precision cut lung slice
PCNA	Proliferating cell nuclear antigen
PCV	Posterior cardinal vein
PFA	Paraformaldehyde
PFU	Plaque forming units
pL	Primary lamellae
Poly(I:C)	Polyinosinic:polycytidylic acid
PRR	Pattern recognition receptor
PVM	Pneumonia virus of mice
qRT-PCR	Real time reverse transcriptase polymerase chain reaction
R848	Resiquimod
R848-F	Resiquimod-ATTO488
RdRP	RNA-dependent RNA polymerase
RIG-I	Retinoic acid-inducible gene-I
RLR	Retinoic acid-inducible gene-I-like receptor

RSV	Respiratory syncytial virus
RVI	Respiratory viral infection
SARS-CoV	Severe acute respiratory syndrome-coronavirus
scRNA-Seq	Single cell RNA sequencing
SD	Standard deviation
SEM	Standard error mean
SHRV	Snakehead rhabdovirus
SINV	Sindbis virus
sL	Secondary lamellae
SMG	Submucosal gland
SSC	Side scatter
SSC-A	Side scatter area
ssRNA	Single-stranded DNA
SVCV	Spring viremia of carp virus
TCR	T cell receptor
TEP	Transepithelial protrusion
Tfh	T follicular helper
Th1	Type 1 helper
Th17	Type 17 helper
Th2	Type 2 helper
Th22	Type 22 helper
TiLV	Tilapia lake virus
TIR	Toll/interleukin-1
TLR	Toll-like receptor
Treg	Regulatory T cell
TRIF	TIR-domain-containing adapter-inducing IFN-β
VHSV	Viral haemorrhagic septicemia virus
vRNA	Viral RNA
VSV	Vesicular Somatitis Virus
WGD	Whole genome duplication
WKM	Whole kidney marrow
wpf	Weeks post fertilisation
WT	Wildtype

ZfPV   Zebrafish picornavirus

Abstract

Respiratory viral infections are routinely studied with animal models or *in vitro* culture which mimic but do not fully recapitulate elements of human immune responses or pathology. Studying events at the respiratory mucosa where infection is established is crucial to further our understanding of immune responses to these infections. In this thesis I evaluated the zebrafish gills as a novel *in vivo* model to study respiratory immunity. Using transgenic zebrafish, flow cytometry and several microscopy techniques I characterized immune cell composition and function in this tissue. In addition, I assessed the stimulatory effects of pathogen mimetics and derivatives on immune response pathways using RNA analysis. The stimulatory and pathological effects of live viral challenges were also assessed.

These experiments highlighted the abundance and diversity of innate and adaptive immune cells in the gills from early to adult developmental stages. Some of these immune cells were capable of antigen-uptake and formed dynamic cell-cell interactions. Aggregates of T and B cells were identified as interbranchial lymphoid tissue which had some similarities but also some architectural differences to mammalian mucosal-associated lymphoid tissue. Different responses were stimulated by resiquimod and lipopolysaccharide highlighting these pathogen-related compounds as tools to interrogate immune pathways in the gills. On the other hand, zebrafish had limited responses to human respiratory or fish-endemic viruses and were resistant to pathological infection. These results highlight zebrafish gills as a useful model to investigate several aspects of immune cell function and inflammation in a respiratory mucosal *in vivo* setting. Further investigation with pathogens is needed to expand the use of this model for infection studies.

Table of Contents

List of figures

List of tables

List of appendices

1. Chapter 1 – Literature review

1.1 Respiratory mucosal tissues and their role in host defense against infection

Mucosal tissues are found in both vertebrates and invertebrates, forming the interface between the host and the external environment. These tissues are therefore critical in the defense against infection and this is reflected in their features. In mammals, mucosal tissues include but are not limited to the gastrointestinal tract, the respiratory tract, and the urogenital tract (McGhee et al., 2012).

The major feature of mucosal tissues is a mucus-covered epithelium that acts as a physical and chemical barrier to particles, pathogens, and commensal organisms. The constant exposure to foreign materials means that these tissues must adopt strategies to respond quickly to pathogens, whilst limiting excessive and pathological inflammation at homeostasis. This is important as loss of integrity of the epithelial barrier, due to infection or injury, increases the susceptibility to further damage and infection (Vareille et al., 2011). In the respiratory tract, the epithelium performs the important function of gas exchange and therefore epithelial damage can also impair lung function (Short et al., 2014). To protect against infection, mucosal tissues contain abundant immune cells and account for some of the largest immune cell populations in the body (Mowat and Viney, 1997). In addition to immune cells, each mucosal tissue is associated with a specific and abundant commensal microbiome that is increasingly appreciated for its role in establishing immune tolerance and whose dysregulation can lead to inflammatory diseases (Neish, 2014).

Section 1 of the literature review will address the features of the mammalian respiratory mucosa and the current understanding and remaining questions about its role in infection, particularly with regards to viral infections. This will highlight the features that are important to consider when developing a model to study the respiratory system and provide a basis for comparison with fish respiratory tissue.

1.1.1 Respiratory mucosal structure

1.1.1.1 Respiratory system structure

The respiratory tract (Figure 1.1A) can be functionally divided into two main regions, the conducting airways where air is inhaled, and the respiratory zone where gas exchange takes place (Ganesan et al., 2013). Both of these regions are covered by a mucosal epithelium but show differences in cell composition.

The conducting airway begins with the nasal passages where air is inhaled. However, only part of the nasal epithelium consists of respiratory epithelium, the other part consists of olfactory epithelium which has a significantly different cellular composition to allow for olfactory function (Harkema et al., 2006). The conducting airway continues along the trachea then branches to form the bronchi, one entering each lung. These bronchi branch many more times to form bronchioles. The respiratory zone consists of the smallest airways: respiratory bronchioles connected with alveolar ducts and finally alveolar sacs where gas exchange takes place.

In the conducting zone, the mucosal structure consists of a mucus layer covering the apical surface of ciliated epithelium (Figure 1.1A). Underneath the epithelium is the lamina propria where resident immune cells, lymphatic vessels and nerve fibers reside (Bustamante-Marin and Ostrowski, 2017; Veres, 2018). Below this layer is the submucosa which contains submucosal glands. Of note, these glands are restricted to the upper airways in mice and are absent in rabbits (Widdicombe et al., 2001). This may reflect differences in particle clearance between humans and these smaller mammals. It has been suggested that smaller mammals filter particles in the upper airways and therefore have less of a need for mucus strands from submucosal glands to trap large particles in lower airways (Widdicombe and Wine 2015; Fischer et al. 2019). As the conducting airways transition to the respiratory zone, the mucosal structure changes to a thinner epithelium required for efficient gas exchange and lacking submucosal glands (Bustamante-Marin and Ostrowski, 2017). The mucus layer is also reduced as the airways get smaller, eventually being replaced in the alveoli by a thin mixture of phospholipids and proteins, known as surfactant (Taherali et al., 2018).
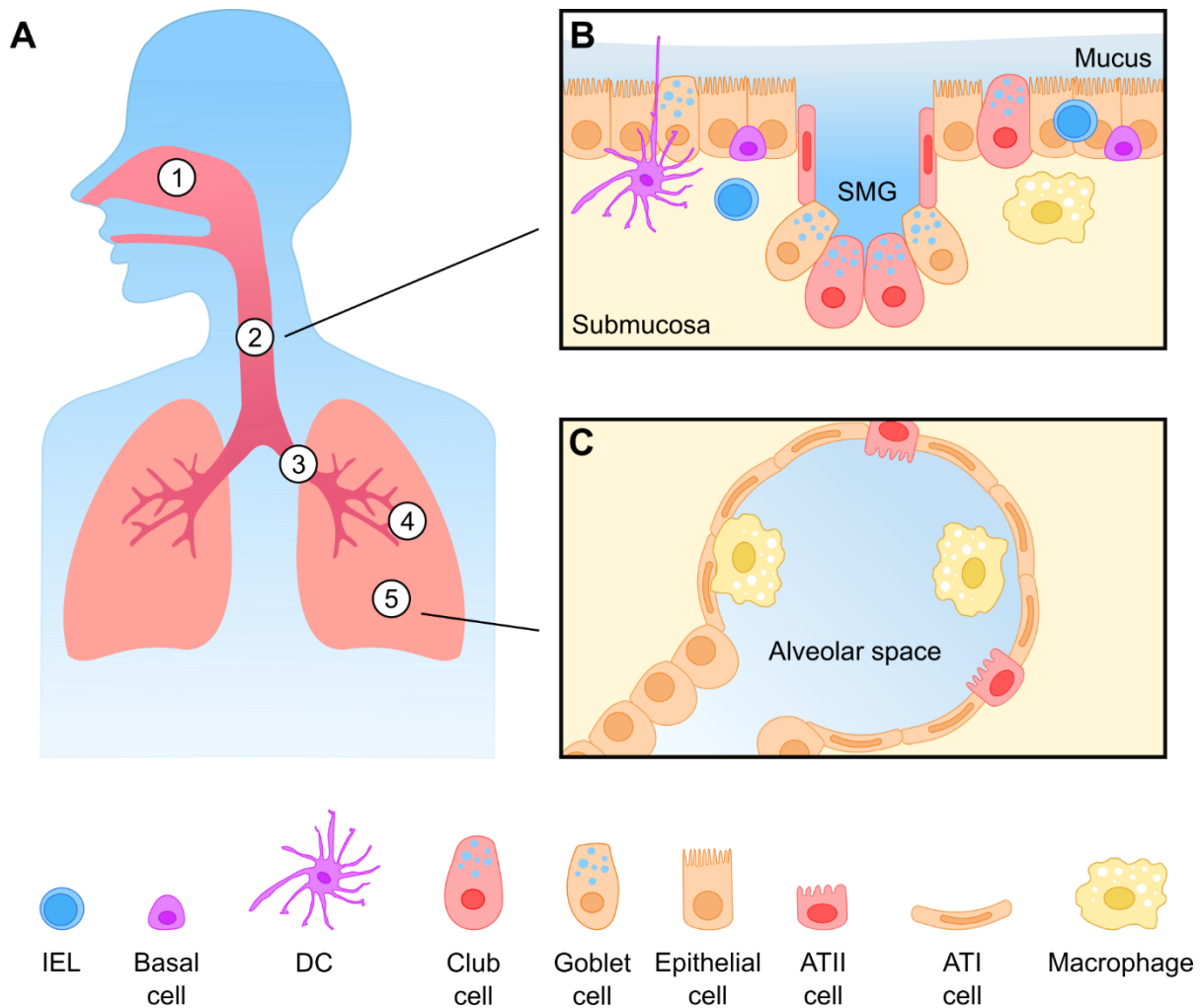
Figure 1.1 Gross anatomy of the human respiratory tract and cellular composition of its epithelium.

A) The human respiratory tract beginning in the nasal passages (1) and continuing distally along the trachea (2) and the bronchi (3) making up the conducting airways. The lung parenchyma contains the bronchioles (4) and alveoli (5) which make up the respiratory zone. B) Simplified diagram of the mucosal epithelium in the conducting airways. SMG: submucosal gland, DC: dendritic cell, IEL: intraepithelial lymphocyte. C) Simplified diagram of the alveolar epithelium in the respiratory zone. ATII: alveolar epithelial type II cell, ATI: alveolar epithelial type I cell.

1.1.1.2 Epithelial barrier

In the conducting zone (Figure 1.1B), it is estimated that 50% of the cells in the epithelium are ciliated (Ganesan et al., 2013). These terminally differentiated cells arise from basal cells which are also present in the epithelium. Basal cells have the ability to self-renew and differentiate into all cell types in the respiratory epithelium of the conducting zone and are therefore considered to be stem cells (Montoro et al., 2018). Basal cells generate ciliated cells and mucus-producing goblet cells through a club cell intermediary, which

itself is a secretory cell involved in generating respiratory fluid (Montoro et al., 2018; Whitsett et al., 2019). Other cells in the epithelium include brush cells which sense inhaled and bacterial compounds and regulate neural reflexes, neuroendocrine cells, and ionocytes (Krasteva et al., 2011, 2012; Plasschaert et al., 2018). Intraepithelial dendritic cells (DCs) and T lymphocytes are also present in the airways and survey the airways for antigen and quickly respond to immune challenge. Specialised alveolar type 1 epithelial (ATI) cells make up the vast majority of the alveolar epithelium (Figure 1.1C) whilst alveolar type 2 epithelial (ATII) cells produce surfactant to maintain the alveolar fluid layer (Dobbs et al., 2010).

These cell types are not equally distributed throughout the respiratory tract. As the respiratory tract branches into smaller airways the numbers of basal, ciliated, and goblet cells decrease. In contrast the number of club cells increases. In addition, submucosal glands are not present in smaller airways (Ganesan et al., 2013). Differences in the distribution of immune cells have also been reported in human lungs, with these cells comprising a larger percentage in distal airways (Deprez et al., 2020). However, the latter analysis included cells not directly within the epithelium.

Cells in the epithelium are connected by junctions which establish an impermeable barrier and regulate paracellular transport of small molecules including ions, metabolites, and secondary messengers (Georas and Rezaee, 2014; Vareille et al., 2011). These junctions also establish cell polarity with tight junctions and adherens junctions distinguishing the apical and basolateral domains of cells respectively (Georas and Rezaee, 2014). Cell polarity is important in the respiratory tract since only the apical surface of the epithelium is exposed to environmental air in the lumen. This is obvious in the formation and role of cilia, which are found on the apical surface, but also has important implications for viral infection. The distribution of host receptors for viral entry usually determines whether a virus will preferentially infect the apical or basolateral surface. For example, several human coronaviruses, including the recently emerged severe acute respiratory syndrome-coronavirus 2 (SARS-CoV 2), infect cells and release virions through the apical surface (Dijkman et al., 2013; Tseng et al., 2005; Vanderheiden et al., 2020; Wang et al., 2000). These infection dynamics correlate with greater apical expression of viral receptors in host cells. In contrast, some viruses, like equine herpesvirus-1 (EHV-1), preferentially infect the basolateral surface (Van

Cleemput et al., 2017). EHV-1 was found to require loss of epithelial integrity to access this surface. This indicates that polarisation could have important implications on the initiation of immune responses and on therapeutic strategies.

There are also differences in gene expression between different regions of the respiratory tract which can have consequences on viral infection. For example, *ACE2* transcript levels, one of the receptors for SARS-CoV 2, are higher in nasal epithelium than in the lower airways (Sungnak et al., 2020). This difference was found to mimic viral load in primary airway cells (Hou et al., 2020). Similarly, α2-6 sialic acid linkages, which bind human influenza A virus, are predominately found in the upper respiratory tract which correlates with viral distribution (Zanin et al., 2016).

The epithelial barrier can be damaged by chemical, physical or infectious insult leading to loss of integrity and impaired pathogen clearance. This is thought to increase susceptibility to infection, and if not repaired appropriately promote chronic inflammation and microbial dybiosis (Invernizzi et al., 2020; Ishak and Everard, 2017; Vareille et al., 2011). Renewal of dying and damaged cells by stem and progenitor cells is therefore crucial to maintaining a healthy respiratory system. This process is dependent on migration and proliferating epithelial cells but also involves resident immune cells (Allard et al., 2018).

1.1.1.3   Role of the airway epithelium in immune responses to infection

At homeostasis epithelial cells can interact with leukocytes to regulate their function. This involves production and activation of regulatory cytokines, or expression of inhibitory ligands that interact with leukocyte receptors (Weitnauer et al., 2016). This limits inappropriate inflammation at homeostasis but can also impair the response to infection (Branchett and Lloyd, 2019). Epithelial cells also contribute directly to innate defense against pathogens. In addition to forming a barrier, epithelial cells produce a range of antimicrobial products. These include lactoferrin, beta-defensins, and nitric oxide which can act directly against microorganisms (Ricciardolo, 2003; Rogan et al., 2006). Epithelial cells also produce polymeric immunoglobulin (Ig) receptor which transports polymeric IgA into the respiratory lumen. IgA helps to restrict commensal microorganisms to the lumen and contributes to defense against exogenous antigens and pathogens (Gohy et al., 2016).

Epithelial cells are also important in the initial response against infection. They are targets of many respiratory viruses and can detect viral material through different pattern recognition receptors (PRRs). Viral infection and detection induces an innate response which includes production of interferons (IFNs), cytokines, and additional antimicrobial products (Vareille et al., 2011). These can have direct effects on pathogens or trigger activation of neighbouring immune cells. Furthermore, secreted chemokines promote recruitment of immune cells from circulation to the site of infection (Iwasaki et al., 2016). The actions of epithelial cells highlight the importance of cross-talk between immune and non-immune compartments in mucosal tissue, both at homeostasis and during infection.

1.1.1.4 Mucus barrier

Mucus is a visoelastic gel composed of large, highly glycosylated proteins known as mucins. Mucins polymerize and bind water, creating the gelatinous properties of mucus (Johansson and Hansson, 2016; Thornton et al., 2008). In humans there are 21 mucin genes which produce either transmembrane or secreted proteins (Ma et al., 2018). Expression of mucins varies between tissues, for example, human airway mucus consists mostly of secreted MUC5AC and MUC5B, whilst gastrointestinal mucus is predominately composed of secreted MUC2 (Johansson and Hansson, 2016; Rose and Voynow, 2006). Mucus is produced by goblet cells which continuously secrete mucins, including both MUC5B and MUC5AC (Fahy and Dickey, 2010). Mucus is also produced by club cells which secrete MUC5B in addition to glandular fluid that hydrates the mucus (Fahy and Dickey, 2010; Ganesan et al., 2013).

Mucus is selectively permeable for compounds including gases and water but acts as a barrier for pathogens (Witten et al., 2018). Following inhalation, the majority of pathogens and particulates are trapped by the mucus and are transported up the respiratory tract by the beating of cilia. The mucus is eventually cleared through the esophagus or by coughing action. This process is known as mucocilliary clearance and is an important feature of host defense. In order to overcome this barrier some pathogens have evolved strategies including cleavage of mucin glycans, flagellar motility, and direct binding to mucin proteins (Zanin et al., 2016). In addition to its role as a physical barrier, mucus also contains many antimicrobial compounds including those secreted by epithelial cells which can directly inhibit infection (Rogan et al., 2006).

The composition and properties of mucus can be altered by environmental change or in disease states. Viral infection, cigarette smoke, and allergens have been found to increase mucus production through upregulation of mucin expression or increased proliferation of goblet cells (Rose and Voynow, 2006; Shaykhiev, 2019; Stier and Peebles, 2018). This can be exacerbated by genetic conditions like cystic fibrosis, or chronic inflammatory conditions like chronic obstructive pulmonary disorder (Kreda et al., 2012; Shaykhiev, 2019). Although a moderate increase in mucus can assist with particle clearance, too much mucus, or altered mucus properties can lead to impaired clearance. This can lead to an accumulation of pathogens and increase the risk of infection. Understanding the properties of the mucus barrier is also important for designing drugs, vaccines, and other therapeutics that target mucosal surfaces.

1.1.1.5 Microbiota

The lungs were originally thought to be a sterile environment however, next generation sequencing has revealed that the respiratory tract contains a commensal microbiome. Microbial colonization in human lungs occurs during birth and commensal communities develop in the first weeks of life, stabilising by about 2 months (Pattaroni et al., 2018). The microbial composition has been found to vary in different regions of the respiratory tract, although the upper airways seem to influence the lower airways (Man et al., 2017). There is increasing evidence that early colonization influences immune tolerance and responses both during infancy and in later life. The incidence of asthma and allergy have been epidemiologically linked to microbial exposure suggesting that the microbiome is important in establishing immune tolerance (Ege et al., 2006; Risnes et al., 2011; Stein et al., 2016). Experimental studies have also found that commensal bacteria in other mucosal tissues, in this case the gut, can influence immune cell presence in the lungs and thus promote protective responses to infection (Gray et al., 2017). The microbiota in adult lungs also seems to have an impact as shown in lung transplant patients where bacterial dysbiosis was linked to different expression and activation profiles of immune cell populations (Bernasconi et al., 2016). There is also evidence that the lung microbiota influences the immune response to respiratory viruses. Commensal bacteria were found to be necessary for the maintenance of CD8+ memory T cells and establishment of protective inflammatory responses in cytomegalovirus and influenza-infected mice respectively (Ichinohe et al., 2011; Tanaka et al., 2007). In addition, viral infection is associated with changes in microbial composition, although whether this is a

consequence or driver of infection is unclear (Chonmaitree et al., 2017; De Steenhuijsen Piters et al., 2016). Current evidence points to the microbiota as an important factor in immune homeostasis and respiratory infection.

1.1.2 Immune cell compartments

Like all mucosal tissues, the respiratory tract contains resident immune cells at homeostasis and additional recruited immune cells in inflammatory conditions. These immune cells, along with epithelial cells, can detect pathogens and initiate immune responses. In addition, they also have effector functions to clear pathogens and regulate the mucosal epithelium and commensal microbiota. Another hallmark of mucosal tissues is the presence of secondary lymphoid tissues including mucosal-associated lymphoid tissues (MALT) and in mammals and some birds, lymph nodes (Boehm et al., 2012). These lymphoid tissues form specialised environments for activation, expansion and differentiation of adaptive immune cells which can then migrate to peripheral sites of infection or inflammation. The mammalian respiratory tract is associated with draining lymph nodes, nasopharyngeal-associated lymphoid tissue (NALT) and bronchus-associated lymphoid tissue (BALT), although these structures vary between species.

1.1.2.1 Innate immune cells

Alveolar macrophages (AMs) are one of the few immune cells in the airspaces (Figure 1.1C) and are involved in clearance of cellular debris and apoptotic cells at homeostasis and during infection, supporting effective function of respiratory tissue. Non-alveolar tissue-resident macrophages are present beneath the respiratory epithelium (Figure 1.1B) and are involved in antigen processing and antigen transport to lymph nodes (Braciale et al., 2012).

Several subsets of dendritic cells have been described in the respiratory tract of mammalian species at homeostasis. These include intraepithelial DCs that are closely associated with the epithelium and can extend dendrites into the airway lumen to sample antigens (Braciale et al., 2012). Other subsets of DCs beneath the epithelium and in the alveolar airspaces contribute to T cell activation, chemokine production and type I IFN production promoting type I immunity (Braciale et al., 2012; Kim and Lee, 2014; Lambrecht and Hammad, 2009; Vareille et al., 2011). DCs are therefore important regulators of the innate and adaptive immune responses.

Monocytes are recruited from the blood and are thought to differentiate into DCs and macrophages (Braciale et al., 2012). Neutrophils are often the earliest immune cells to be recruited to the respiratory tract during inflammatory conditions and directly contribute to pathogen clearance. Both of these cell types have inflammatory phenotypes (Iwasaki et al., 2016).

Mast cells, eosinophils, and basophils are key players during helminth infections and allergic inflammation through their release of effector molecules and pro-inflammatory cytokines. However, mast cells and eosinophils have also been linked to innate defenses during respiratory viral infections and in the case of mast cells, some pathology (Campillo-Navarro et al., 2005; Flores-Torres et al., 2019).

Resident innate lymphocytes in the respiratory tract can respond rapidly to pathogens, modulating the immune environment or performing effector functions. Group 1, 2 and 3 innate lymphoid cells (ILCs) are all found in the respiratory tract and natural killer (NK) cells make up the largest population of these cell types in the lungs of mice and humans (Kim et al., 2016; Simoni et al., 2017). NK cells are a type of group 1 ILCs and are cytotoxic once activated, killing infected target cells. They also produce large amounts of type II IFNγ, which promotes antiviral responses, macrophage activation and type 1 immunity (Stehle et al., 2018). The other ILCs, ILC1, ILC2 and ILC3 contribute to type I, type 2 and type 3 immunity respectively through cytokine production. They are involved in responses to different pathogens in the respiratory tract including fungal pathogens and helminths (Denney and Ho, 2018; Iwasaki et al., 2016; Stehle et al., 2018). Each ILC population has also been linked to respiratory viral infections although further investigation is required to assess their direct involvement in some cases (Ardain et al., 2019; Paget et al., 2012; Stehle et al., 2018). Invariant natural killer T (iNKT) cells and γδ T cells are innate T lymphocytes that express unconventional T cell receptors (TCR). During infection these cells can produce a range of immunomodulatory cytokines (Chen and Kolls, 2013; Paget et al., 2012). Overall, innate lymphocytes seem to play an important role in modulating the respiratory cytokine environment and in the case of NK cells, directly clearing infected cells.

1.1.2.2 Adaptive lymphocytes

Conventional αβ CD4+ or CD8+ T cells are present in the draining lymph nodes or in the MALT of the respiratory tract. Naïve T cells are activated upon recognition of cognate

antigen on antigen-presenting cells (APCs) such as DCs or macrophages. This induces proliferation and differentiation of T cells into different effector phenotypes. CD4+ T cells have been observed to differentiate into several subsets characterised by distinct cytokine and gene expression profiles. One of these subsets is T follicular helper cells (Tfh) which are specialised to activate naïve B cells within germinal centres of lymphoid tissues (Miyauchi, 2017). Other subsets include the T helper (Th) cells (Th1, Th2, Th17, Th22) and regulatory T cells (Treg) which can migrate to the site of infection and modulate the immune environment through cytokine secretion. These cytokines can activate other immune cells and promote different types of immune responses (type 1, 2, or 3), characterized by different effector cells and immune mediators. Th1 cells promote type 1 immunity which is particularly associated with antiviral responses. These cells typically produce IFNγ, IL-12, IL-2, and TNFα and promote activation of CD8+ cytotoxic T cells (Chen and Kolls, 2013). In contrast to the other T helper cells, Treg cells produce anti-inflammatory cytokines like IL-10 which inhibit immune responses and inflammation (Allie and Randall, 2017).

Naïve CD8+ T cells are activated by APCs and differentiate into cytotoxic effector cells. Following migration to the site of infection, these cells can induce the killing of infected cells (Hamada et al., 2013). They can also amplify type 1 responses by producing Th1-associated cytokines (Schmidt and Varga, 2018). Activated CD4+ and CD8+ T cells can also differentiate into long-lived memory T cells which patrol respiratory tissue following infection. These cells form the basis of immunological memory, allowing rapid adaptive immune responses following re-exposure to the same antigen.

B cells in respiratory lymphoid tissues undergo clonal expansion (proliferation) and antibody class switching following stimulation by T cells. IgE, IgA, IgG or IgD can be produced following class switching but this is dependent on the cytokine environment, highlighting the importance of T helper cells in directing the humoral response (Miyauchi, 2017). IgA is often the dominant class in mucosal environments but the mechanisms of IgA class-switching have been more thoroughly studied in the gut than in the respiratory tract (Miyauchi, 2017; van Riet et al., 2012). There is some evidence that AMs, DCs, Toll-like receptor (TLR) signalling and TGFβ signalling play a role, although not all studies have investigated the precise mechanisms behind this (Bessa et al., 2009; Borsutzky et al., 2004; Wang et al., 2010a). Activated B cells can differentiate into short-lived antibody

producing plasmablasts, long-lived antibody producing plasma cells, or long-lived memory cells which do not produce antibodies, the latter two cells being important for long-term immunity (Chiu and Openshaw, 2015).

1.1.2.3 *Lymphoid tissue of the respiratory tract*

Draining lymph nodes

Lymph nodes are encapsulated structures which contain segregated accumulations of B and T cells (Figure 1.2A) that are recruited via specialised blood vessels known as high endothelial venules (HEVs). The lymph nodes (LNs) associated with the respiratory tract are found in the head and neck region and along the trachea and bronchi (Patel and Metcalf, 2018). Lymph and mature APCs drain into the LNs from the lungs through afferent lymphatic vessels, bringing soluble antigens and migratory antigen-bearing APCs in contact with resident APCs and naïve or memory lymphocytes (Haig et al., 1999). Both LN-resident DCs and migratory DCs can activate T cells, but in some cases have different abilities to stimulate CD4+ and CD8+ cells (GeurtsvanKessel et al., 2008). In addition, imaging studies of lymph nodes have shown that B cells can acquire cognate antigen from LN-resident macrophages (Junt et al., 2007; Phan et al., 2007). Some activated CD4+ effector T cells remain in the LNs to activate antigen-bearing B cells in germinal centres. In these structures, resident follicular dendritic cells (FDCs) present antigen from internalised immune complexes, to activated B cells. This promotes the clonal expansion and survival of B cells with higher affinity for antigen. FDCs obtain antigen from a separate population of B cells which transport non-cognate immune complexes from resident macrophages (Phan et al., 2009).

At homeostasis, lymphocytes migrate through LNs, and exit back to circulation if they do not encounter antigen, at a steady rate. However, studies in sheep have shown that during antigen challenge, lymphocyte entry to LNs is increased whilst lymphocyte exit is transiently reduced for a few hours. This is later followed by a significant increase in lymphocyte exit (Cahill et al., 1976; Mackay et al., 1992). Activated T and B cells can exit the LNs via efferent lymphatic vessels, re-entering circulation and homing back to peripheral tissues where they can perform their effector functions (Agace, 2006). The receptors which mediate homing of activated lymphocytes to the respiratory tract are still being investigated but include CCR4, CCR3 and CXCR4 (Allie and Randall, 2017;

Sackstein et al., 2017). These receptors associate with endothelium-expressed ligands to facilitate lymphocyte entry into respiratory tissue from circulation.

Lymphocytes in the lymph nodes are supported by specialised stationary stromal cells which direct lymphocytes into T or B cell regions. One of these stromal cells, fibroblastic reticular cells, also form conduit networks which guide the transport of antigen to cells in the LN (Stein and F. Gonzalez, 2017). In addition, LN-resident macrophages can phagocytose some pathogens, including influenza virus, and limit their spread (Gonzalez et al., 2010).
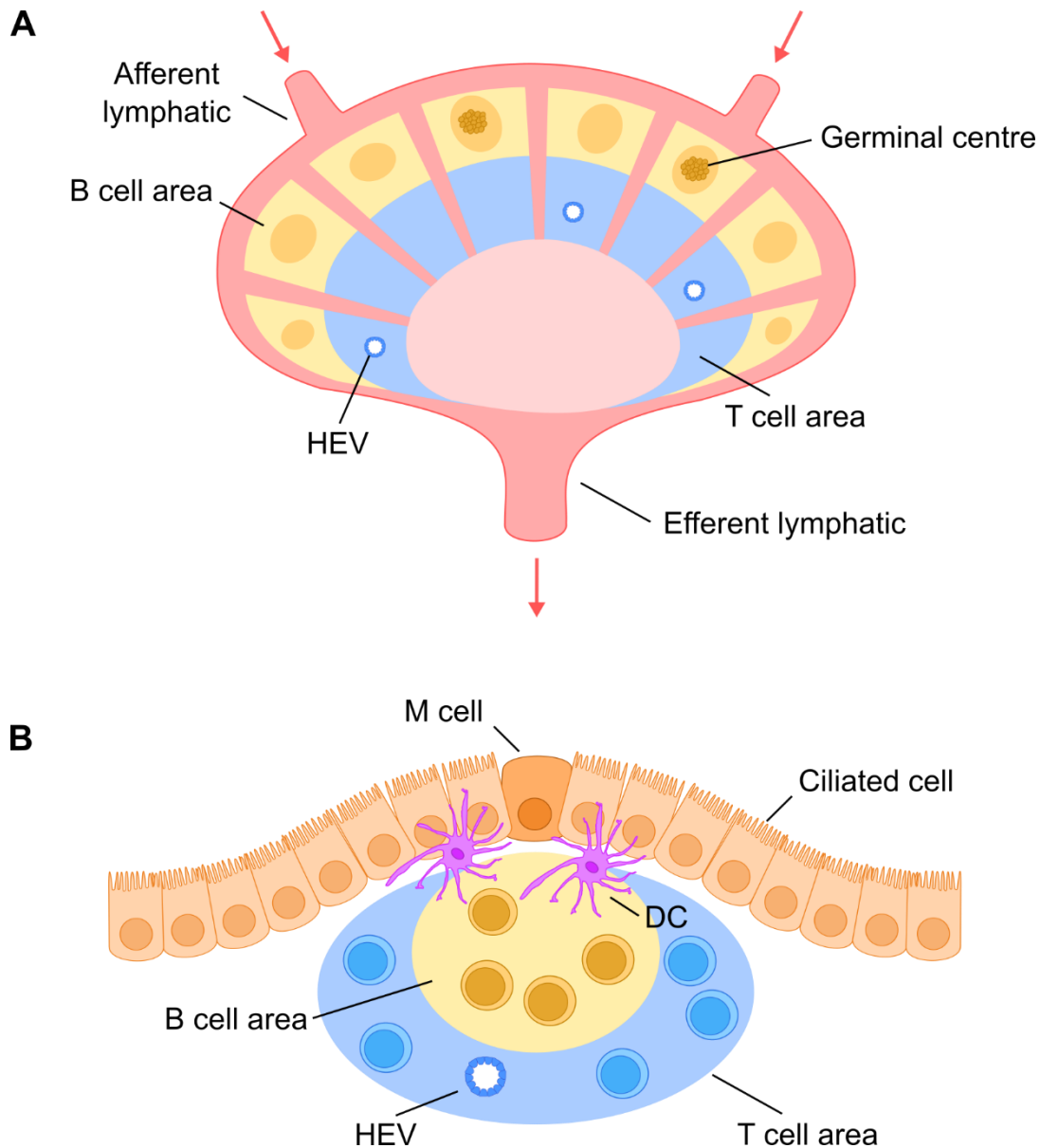
Figure 1.2 Generalised anatomy of lymph nodes and mucosal-associated lymphoid tissue.

A) Simplified diagram of a lymph node showing the key vessels and B cell and T cell areas. Lymph and APCs enter the lymph node via afferent lymphatics. Circulating lymphocytes enter the lymph node via HEVs. Lymph and circulating cells exit the lymph node via efferent lymphatics. During antigenic stimulation, B cells form additional clusters known as germinal centres. B) Simplified diagram of the ciliated epithelium and key lymphocyte regions of MALT. Microfold (M) cells are specialised for antigen uptake and closely associated with DCs and other immune cells. Circulating lymphocytes can traffic to MALT through HEVs which are often found in the T cell area. The exact composition of MALT varies between structures and tissues.

Mucosal-associated lymphoid tissue

MALT also contains accumulations of lymphocytes, however, unlike LNs these structures are found in association with the mucosal epithelium (Figure 1.2B). These structures are therefore suited to initiating rapid local responses whilst LNs allow surveillance of circulating antigen of an entire tissue. It is tempting to speculate that this would lead to a faster response in MALT than in the LNs however, current evidence suggests the kinetics of the response are more complicated. In one study in mice infected with influenza virus, the LNs and respiratory MALT generated T cell effector responses with similar kinetics (Richert et al., 2013). Studies using reovirus or *Francisella tularensis* bacterial challenges have reported less efficient and delayed responses in the LNs compared to the respiratory MALT (Chiavolini et al., 2010; Zuercher et al., 2002). In addition, the nature of the response between these structures can also differ with respiratory MALT showing a stronger IgA response, and LNs showing a stronger IgG2a response in reovirus infected mice (Zuercher et al., 2002). Indeed, IgA is a characteristic feature of MALT (McGhee et al., 2012).

MALT was historically categorised as "organised" structures and "diffuse" regions of lymphocytes, but the field has moved away from these categories. Instead, MALT structures are now more commonly referred to by their function. Lymphocyte activation, proliferation & differentiation occurs at inductive sites which, for some MALT structures, involves germinal centres (Sato and Kiyono, 2012). Differentiated lymphocytes can then migrate to other mucosal sites via the blood, and perform their functions (cytokine secretion, antibody production, cytotoxic activity) at effector sites. It is not recommended to refer to these effectors site as MALT due to their functional differences to inductive lymphoid tissue (Brandtzaeg et al., 2008). However, it is important to note there is not always a clear anatomical distinction between effector and inductive sites (Kuper, 2006).

Unlike LNs, MALT lacks afferent lymphatic vessels therefore, antigen uptake is facilitated by direct exposure to the luminal space. Antigen uptake is performed by intraepithelial DCs and specialised epithelial cells, known as microfold (M) cells (Figure 1.2B). These M cells are phenotypically and morphologically distinct from conventional ciliated epithelial cells. They are closely associated with immune cells on the basal side and transfer antigen to underlying DCs (Sato and Kiyono, 2012).

Nasopharyngeal-associated lymphoid tissue

NALT has been identified in mammals, birds and fish with significant species differences. In humans, NALT consists of the tonsils and adenoids, 8 structures found in the pharynx at the back of the nasal and oral cavities. Collectively these are known as Waldeyer's ring. In contrast, mouse and rat NALT consists of a single pair of structures and no tonsils (Sepahi and Salinas, 2016). There is little information on the consequences of these anatomical differences on respiratory immunity. However, the differences in distribution and abundance of NALT could affect the kinetics of immune responses and the progression of infections. The differences in anatomy may reflect differences in antigen exposure and retention. This emphasises the need to study NALT in several animal models rather than making generalisations from one species.

NALT has received attention for its potential in vaccination against respiratory pathogens. It is thought that administering vaccines at the site of infection is more likely to result in protective immunity than systemic administration. In fact, nasal vaccine challenges have been reported to induce both mucosal and systemic immune responses in animal models and humans (Ascough et al., 2019; Mizuno et al., 2016; Zhao et al., 2016). In addition, the nasal mucosa is easily accessible and can be challenged with non-invasive methods. Licensed human intranasal vaccines currently only exist for influenza A virus although vaccines for other pathogens are being investigated (Zheng et al., 2018).

Bronchus-associated lymphoid tissue

BALT is formed during normal lung development in some species, such as rabbits and rats. BALT is also found in the healthy lungs of human children but not in adults or in mice (Carragher et al., 2008; Tschernig and Pabst, 2000). BALT can also be induced (iBALT) by inflammation, autoimmunity and infection including in humans and mice. These transient tertiary lymphoid structures contain many of the same components as secondary lymphoid tissue but do not develop in predictable locations (Carragher et al., 2008; Yadava et al., 2016). The main features of iBALT are B cell follicles surrounded by T cells and supported by follicular dendritic cells and other stromal cells. BALT can also contain HEVs and lymphatic vessels and localise underneath a domed epithelium containing M cells (Hwang et al., 2016; Randall, 2015). In this respect iBALT is often anatomically similar to other secondary lymphoid tissues.

The mechanisms behind the formation, resolution and function of iBALT are only partially understood. Unlike secondary lymphoid tissue, iBALT does not depend on lymphoid tissue inducer (LTi) cells which may reflect the comparatively later development of iBALT when mature lymphocytes are present (Hwang et al., 2016). In experimental models iBALT can be induced with overexpression of cytokines, microbial compounds, and pathogens (Foo et al., 2015; Lee et al., 1997; Slight et al., 2013). Innate cells including neutrophils and eosinophils can also promote iBALT formation (Silva-Sanchez and Randall, 2020). In addition, in mice iBALT forms more readily in neonates than in older animals, mimicking the presence of BALT in human infants but not in adults (Foo et al., 2015). In humans iBALT formation must depend on multiple factors since not every patient with a particular inflammatory condition develops these structures (Jones and Jones, 2016). The diverse factors that can induce iBALT may reflect the diverse functions of this lymphoid tissue.

iBALT can be protective against infection in some contexts. In mice, induction of iBALT by nonreplicative virus-like particles was associated with enhanced immune responses and protection against subsequent influenza virus challenge (Richert et al., 2013). This study demonstrated that iBALT can respond to different antigen challenges beyond their initial formation. In addition, iBALT structures can last for several months and appear to contribute to longer-term immune responses (Foo et al., 2015; Rangel-Moreno et al., 2011). More research is needed to understand the mechanisms of these protective responses and how different stimulants may affect iBALT function. In some chronic infections and inflammatory diseases iBALT is positively correlated with disease severity (Marin et al., 2019). It is still unclear whether iBALT structures are increased due to the inflammatory environment or whether they drive disease pathology, though both could be possible. Improving our understanding of iBALT is important for developing vaccination and therapeutic strategies that enhance protective effects whilst limiting pathological effects. Furthermore, studying iBALT may provide additional insights into ectopic tertiary lymphoid tissue in other tissues such as the gut and thyroid (Neyt et al., 2012).

1.2 Respiratory viral infections

Respiratory infection in humans is a leading cause of death and disability; lower tract respiratory infections and tuberculosis are the fourth and twelfth most common causes of deaths globally (Forum of International Respiratory Societies, 2017). These infections are caused by a variety of pathogens including bacteria like *Mycobacterium tuberculosis,* and viruses, which this project focuses on. This section of the literature review will address the different types of respiratory viruses, the molecular determinants of infection, the immune response, the existing tools to investigate these infections, and the gaps that remain in the field.

1.2.1 Types of respiratory viruses and associated disease

Multiple virus families cause respiratory infection, including those with DNA and RNA genomes. The major disease-causing viruses in humans include influenza viruses (A or B), parainfluenza virus, coronaviruses (CoVs), rhinoviruses, adenoviruses, enteroviruses, respiratory syncytial virus (RSV) and measles virus. Animals are also susceptible to human or animal respiratory viral infections (RVIs) and this can have negative impact on livestock and contribute to zoonotic transmission (Bailey et al., 2018).

1.2.1.1 Epidemiology

Many human respiratory viruses circulate in the global population causing seasonal outbreaks or infections throughout the year. Some of these viruses, such as rhinoviruses and RSV, commonly cause mild disease but do not confer lasting protective immunity leading to potential reinfections in individuals throughout life (Openshaw et al., 2017). In contrast, influenza virus infection does confer protective immunity but due to high viral mutation rates, individuals can be reinfected with new strains (Rajão and Pérez, 2018; Sridhar et al., 2015).

Influenza A virus (IAV) is also highly capable of major genetic changes (antigenic shift) due to gene reassortment between different viral strains. This can result in new pandemic strains of human IAV emerging from animal IAV strains. These strains are more virulent due to their limited adaptation to the human host, but also more easily transmitted due to the lack of pre-existing immunity in the global population (Thangavel and Bouvier, 2014). Historically, IAV has been a major cause of disease outbreaks, most notably

causing the 1918-20 pandemic which claimed an estimated 50 million lives (Johnson and Mueller, 2002). In this case, young healthy adults were more susceptible than expected as the virus induced a highly inflammatory and pathological response, known as a 'cytokine storm'. In contrast, infection with circulating IAV virus in young adults causes mostly mild disease (Ahmed et al., 2007). This shows that disease susceptibility and progression can vary significantly between respiratory viruses and between virus strains.

Development of new viruses through animal vectors has also been observed with the emergence of SARS-CoV which caused an epidemic in 2003 and had a high case fatality rate of 11%. At the end of 2019, a new coronavirus, SARS-CoV 2 emerged which though less fatal, spread more widely leading to an ongoing global pandemic (Yang et al., 2020). Research on RVIs is therefore essential to tackle existing pathogens but also to increase preparedness for future emerging pathogens.

1.2.1.2 *Disease traits*

RVIs most commonly cause respiratory symptoms since this is the initial site of infection. Milder symptoms can include fever, rhinorrhea, and coughing, which are all host defense mechanisms to clear the virus. However, these symptoms also contribute to viral transmission. Mild infection tends to be restricted to the upper respiratory tract (nasopharyngeal region) whilst severe disease is associated with lower respiratory tract pathology. Both viral infection of epithelial cells and activation of immune cells can damage the alveolar epithelium. This impairs gas exchange and leads to fluid accumulation in the airways (Short et al., 2014). In addition, viral infection can induce changes in mucus secretion and properties, further impairing respiratory function (Stier and Peebles, 2018). Damaged epithelium may also increase the risk of secondary bacterial infections (Tavares et al., 2017). Progression to severe disease can also involve dissemination of virus and symptoms in other organs such as renal dysfunction and diarrhea (Lee and Kim, 2020). Severe respiratory symptoms can be fatal but even in recovered patients, these symptoms can have long-term effects (Ngai et al., 2010). For emerging and widely-transmitted pathogens like SARS-CoV 2, the potential long-term consequences are unknown and therefore a major area of concern that is under investigation (Fraser, 2020). RVIs are also associated with exacerbations of non-infectious respiratory conditions such as chronic obstructive pulmonary disease (COPD)

and asthma (Hansel et al., 2013). In certain demographics RVIs can have more severe effects; RSV is a leading cause of infant hospitalisation and can cause more severe disease in elderly and immunocompromised individuals (Iwane et al., 2004; Jansen et al., 2007).

1.2.1.3 Therapeutic strategies

Vaccination is the most effective strategy to control and eliminate infectious diseases when available and widely used. The measles vaccine is one of the few vaccines against RVIs that provides long-term protection and as a result has drastically reduced cases since its introduction in the 1960s. Influenza vaccines are also currently in use however, due to virus mutations, these must be altered every year and do not always have high efficacy (Rajão and Pérez, 2018). In addition, vaccines against circulating IAV do not necessarily protect against reassorted, epidemic causing viruses.

Despite decades of research, there are no available vaccines for many RVIs including RSV, rhinoviruses and SARS-CoV although clinical trials for some vaccine candidates have been ongoing (Alturki et al., 2020; Anderson et al., 2017; Xu et al., 2019). Some of the challenges in vaccine development include high antigenic variability of some viruses, poor understanding of correlates of protection, ensuring vaccine safety, and having high enough levels of viral transmission to test for efficacy in populations.

Effective prophylaxis and antiviral therapeutics are similarly limited for many RVIs. Therapeutics exist for RSV but issues remain over their high costs and debated efficacy (Hynicka and Ensor, 2012; Jorquera and Tripp, 2017). Although some antivirals exist to treat influenza these must be administered in the early stages of infection and are ineffective against drug-resistant strains (Thorlund et al., 2011). Some viruses, including rhinoviruses and coronaviruses, lack specific therapeutics and are instead treated by broadly acting antivirals such as IFN and ribavirin or drugs for symptom relief. With these issues in mind, new monoclonal antibodies, antivirals and host modulatory drugs are being developed for many RVIs (Basnet et al., 2019; Behzadi and Leyva-Grado, 2019). Both vaccine and therapeutic candidates must be tested extensively prior to clinical trials highlighting the importance of having a range of models for different research questions.

1.2.2 Molecular determinants of viral infection

In order to establish a productive infection in the respiratory tract, viruses must overcome several barriers. They have evolved different mechanisms to do this including co-opting host machinery. Therefore, both host and viral factors are important in determining the cell, tissue, and species tropism of a virus strain. These factors can be targeted in drug and vaccine design to block infection or enhance protective immune responses.

1.2.2.1 Viral access to target tissues and cells

Viruses must first escape mucocilliary clearance and penetrate the mucus barrier in order to reach the cells of the respiratory tract. This can involve enzymatic activity to disrupt the mucus architecture. Several studies have suggested that IAV penetrates the mucus barrier by using its neuraminidase (NA) protein to cleave sialic acid residues on glycosylated mucus proteins (Cohen et al., 2013; Yang et al., 2014; Zanin et al., 2015). One study found that swine IAV penetrated porcine mucus *in vitro* and this was inhibited by a NA inhibitor but enhanced by exogenous NA (Yang et al., 2014). Alveolar surfactant proteins can also restrict viral infection by binding viruses thus blocking entry into target cells (Denney and Ho, 2018; Garcia-Verdugo et al., 2010). However, the mucosal surface does not just act as a physical barrier. Antimicrobial molecules secreted into the airway lumen can also act against viruses. For example, defensin proteins, which are produced by epithelial cells, can disrupt the viral lipid envelope, inhibiting viral and host cell membrane fusion and blocking virus uncoating within cells (Wilson et al., 2013).

If a virus manages to evade the mucous and fluid barrier, it then needs to bind to cell-surface receptors to enter its target cells. These co-opted host molecules include proteins and glycans and vary considerably between viruses. They are therefore an important restriction factor in viral tropism. As previously mentioned, some receptors have polarized distribution which restricts infection to one side of the epithelium.

Once bound to the target cell, the virus needs to be internalized for the infection process to continue. For enveloped viruses like RSV, CoVs, and influenza viruses, this involves the fusion of the viral and cell membranes. This occurs with the plasma membrane, or if the virus has been endocytosed, with the endosomal membrane (Griffiths et al., 2017; Samji, 2009; Simmons et al., 2013). For SARS-CoV, this requires proteolytic cleavage of the viral spike protein by host proteins (Simmons et al., 2013). For influenza virus, the acidic

environment of the endosome induces a conformation change in the haemagglutinin (HA) protein which facilitates membrane fusion (Samji, 2009). Non-enveloped viruses, such as rhinoviruses, lack a lipid membrane but can be internalized by endocytosis and micropinocytosis (Jacobs et al., 2013). The endosomal membrane is then disrupted, allowing release of viral particles into the cytosol (Smith et al., 2010).

1.2.2.2 Viral replication

The viral genome must be released from the viral nucleocapsid to allow production of new virions. This process, known as 'uncoating', can be mediated by host receptor binding or by acidic endosomal environments (Fuchs and Blaas, 2012; Samji, 2009). The next stages in the viral lifecycle vary depending on the virus. Released genomes are either exported to the nucleus or remain in the cytosol for transcription and replication.

Viral RNA genomes encode RNA-dependent RNA polymerase (RdRP) which can both replicate and transcribe the genetic material. Some DNA viruses, such as adenoviruses, encode DNA polymerase (Hoeben and Uil, 2013). Host proteins are also important in genome replication and transcription. For example, the host protein ANP32A has been shown to support IAV polymerase function. Avian IAV polymerase is adapted to using avian ANP32A but not human ANP32A showing that this protein is an important species restriction factor (Long et al., 2016).

For viruses that are transcribed in the nucleus, mRNA must be exported into the cytosol for translation. Following viral protein synthesis and genome replication, new virions are assembled in the cytosol or in the nucleus (Charman et al., 2019; Ruch and Machamer, 2012). For enveloped viruses, assembly takes place at a lipid membrane, either on the plasma membrane or in the ER-Golgi. Assembled virions are released through membrane scission at the plasma membrane or by exocytosis (Ruch and Machamer, 2012; Shaikh and Crowe, 2013). For IAV, virion release is mediated by NA which cleaves cell surface sialic acid residues attached to viral HA (Dou et al., 2018).

1.2.3 Immune responses to RVIs

The immune response to RVIs can vary considerably depending on the virus and the age, genetics and health status of the host. This can affect the magnitude and kinetics of the response, the immune mediators involved, and the disease outcomes. However, some key

features of the immune response are broadly consistent across different RVIs. Understanding the similarities and differences in the immune response is important for designing vaccines or therapeutics that are safe and protective against infection.

1.2.3.1 Molecular mechanisms of virus recognition

Viruses are detected by the host through both innate and adaptive mechanisms. Innate recognition of viruses and other pathogens is achieved by germline-encoded pattern recognition receptors (PRRs) which recognise broadly conserved pathogen-associated molecular patterns (PAMPs). Each PRR can recognize a particular type of PAMP, for example, TLR3 recognises dsRNA whilst TLR7 recognises ssRNA (Kawasaki and Kawai, 2014). On the other hand, somatically rearranged immunoglobulins or TCRs recognise highly specific antigen epitopes. Immunoglobulins and TCRs are expressed exclusively by B cell and T cells respectively whilst PRRs are expressed by a variety of immune and non-immune cells. This includes epithelial cells, the main targets for respiratory viruses (Vareille et al., 2011).

PRRs include Toll-like receptors (TLRs), retinoic acid-inducible gene-I (RIG-I)-like receptors (RLRs), nucleotide-binding oligomerization domain (NOD)-like receptors (NLRs) and C-type lectin receptors (CLRs). Activation of these receptors induces downstream signalling of different pathways leading to IFN production, inflammasome activation, cytokine production, and positive or negative feedback loops. PRR expression varies between cell types which could mediate differences in responses and functions during RVIs (Kim and Lee, 2014). Indeed, human lung dendritic cell subsets were found to respond differently to TLR agonists and this was associated with differences in TLR expression (Demedts et al., 2006).

The host can detect different viral components, including genetic material and proteins, depending on which part of the virus is accessible and which PRR the virus is exposed to. This is determined by the structure of virions, the life cycle stage of the virus, and the subcellular localisation of PRRs. At different stages of the life cycle, the virus can be found in different cellular compartments, such as the cell surface, the cytoplasm, and endosomes. Initially, viral genetic material, and certain proteins, are shielded from the host by the viral coat and in some cases, envelope. However, as the virus is internalised, its genome and additional proteins become exposed in the different cellular compartments. The products of viral genome replication and transcription can also be

recognized by the host. This includes intermediate products like dsRNA which forms during the genome replication of ssRNA viruses (Ascough et al., 2018).

Effective antiviral immune responses rely on host detection and viruses have evolved mechanisms to evade this. This includes virus encoded or co-opted host proteins which inhibit PRR-ligand binding or interfere in downstream signalling (Ascough et al., 2018; Wong et al., 2016). In addition, some viruses, like influenza, have a high mutation rate leading to frequent changes in viral epitopes. This means that antibodies and cytotoxic T cells generated in a primary infection may not be as effective during a secondary infection with the same type of virus (Kreijtz et al., 2011). This explains why influenza viruses can reinfect individuals, and why influenza vaccines only provide short-term protection.

Antibody recognition of viruses can lead to several outcomes including phagocytosis by immune cells, antibody-dependent cell-mediated cytotoxicity, or complement-dependent cytotoxicity (Van Erp et al. 2019). Although these mechanisms promote viral clearance antibodies can also enhance disease. This has been observed for a particular inactivated RSV vaccine candidate where lack of antibody affinity maturation led to poor control of RSV infection (Delgado et al., 2009). This has also been observed in influenza vaccines when the antigen in the vaccine differs from the antigen of the subsequent viral challenge (Khurana et al., 2013; Rajão et al., 2016). In some cases, antibodies can promote viral cell entry by enhancing membrane fusion (Winarski et al., 2019). Antibody-dependent enhancement of disease has critical implications for vaccine safety.

1.2.3.2 *Cellular immune responses*

Epithelial cells are usually the first cells to be infected by respiratory viruses, and their response contributes directly to clearing the virus and recruiting and activating immune cells. Epithelial-derived molecules including nitric oxide and beta-defensins, are upregulated by respiratory viruses and can have antiviral effects (Kao et al., 2001; Proud et al., 2004; Vareille et al., 2011). Other cells can also be infected by respiratory viruses, such as DCs which have been infected with RSV *in vitro* (Ugonna et al., 2014), although this has not been assessed *in vivo*. Human influenza virus has been found to infect endothelial cells *in vitro* and *in vivo* leading to increased apoptosis and vascular permeability (Armstrong et al., 2012).

PRR recognition in infected epithelial cells can induce type I and type III IFN production although evidence indicates that type III IFN is predominately expressed (Denney and Ho, 2018; Glaser et al., 2019; Ioannidis et al., 2012; Okabayashi et al., 2011; Wang et al., 2009). IFNs stimulate expression of interferon-stimulated genes (ISGs) in an autocrine and paracrine manner (Ivashkiv and Donlin, 2014). There are hundreds of ISGs encoded in mammalian genomes and they can directly inhibit viral infection or enhance innate immune responses through regulation of PRR signaling pathways (Crosse et al., 2018; Schoggins, 2019; Turan et al., 2004). Some viruses, like RSV, have been found to suppress IFN induction and interfere with IFN-signalling pathways, impairing the antiviral response (Ramaswamy et al., 2004; Spann et al., 2004).

Epithelial cells also produce chemokines upon viral recognition which are important for the early recruitment of innate immune cells. For example, in mice, higher levels of neutrophils have been found in the respiratory tract following IAV infection (Tate et al., 2008). In IAV-infected ferrets, neutrophil levels were also higher in the lungs, with neutrophils accumulating around infected epithelial cells (Camp et al., 2015). Polymorphonuclear phagocyte infiltration (which includes neutrophils) is also a feature of human influenza infection (Sweet and Smith, 1980). The chemotactic properties of epithelial-derived chemokines have been demonstrated for several models of RVIs (Becker and Soukup, 1999; Kulkarni et al., 2019; Rzepka et al., 2012).

Resident and recruited innate immune cells contribute to a pro-inflammatory environment and have effector functions against respiratory viruses. For example, alveolar macrophages produce type I IFNs in RSV-infected mice which promote monocyte chemoattractant production and monocyte recruitment (Goritzka et al., 2015). Neutrophils have been found to produce molecules with direct activity against several respiratory viruses and can also phagocytose some viruses (Geerdink et al., 2015). However, neutrophil infiltration is also associated with disease severity suggesting a pathological role in some contexts (Camp and Jonsson, 2017). The exact role of neutrophils in different RVIs is poorly understood. The role NK cells in RVIs is similarly complex. NK cells can kill cells expressing IAV antigens but can also contribute to pathology in IAV-infected mice (Zhou, Juang, and Kane 2013; Vanderven et al. 2016).

Epithelial cell responses are also important in promoting the maturation of airway-resident dendritic cells into APCs. For example, RSV-infected rat airway epithelial cells

(AECs) were found to upregulate thymic stromal lymphopoietin which increased expression of major histocompatibility complex II (MHCII) and co-stimulatory molecule CD86 in DCs (Qiao et al., 2011). Infection of DCs themselves, such as with RSV, can also induce DC maturation as well as inhibitory molecules showing a complex modulation of DC function by viruses (Tognarelli et al., 2019). Maturation is necessary for DCs to present antigen to and activate T cells, representing a key link between the innate and adaptive immune response. However, different DC subsets have distinct phenotypes and functional roles. Migratory DCs from the lungs were found to stimulate both CD8+ and CD4+ T cells in the lymph nodes of influenza-infected mice, but resident DCs only stimulated CD8+ T cells (GeurtsvanKessel et al., 2008). In RSV-infected mice, migratory DCs displayed a more mature phenotype than lymph node-resident DCs and induced greater IFNγ production in T cells than other DCs (Lukens et al., 2009a). Recruited monocyte-derived DCs in the lungs do not express co-stimulatory molecules or MHCII but produce the chemokines MCP-1 and IP-10. They are therefore thought to be involved in enhancing monocyte recruitment but lack the necessary components to act as APCs (Neyt and Lambrecht, 2013). Plasmacytoid DCs have been found to lack antigen-presentation abilities but are known to produce type I IFNs (GeurtsvanKessel et al., 2008; Kim and Lee, 2014).

Innate immune cell recruitment and DC migration occurs in the first few days of infection, with T cell proliferation and differentiation following a few days later. In influenza infection, virus-specific T cells are significantly elevated in the lungs from 7 days post infection, peaking a few days later (Hornick et al., 2019). T cell responses are therefore thought to be involved in clearing the virus from the host rather than limiting the initial infection. Cytotoxic CD8+ T cells are protective in various RVIs including influenza, RSV and CoV infections, correlating with lower viral load and disease severity (Channappanavar et al., 2014; Russell et al., 2017; Sridhar et al., 2013). CD4+ Th1 cells are important in supporting cytotoxic T cells through IFNγ secretion and their activity follows similar kinetics to CD8+ recruitment in the lungs (Hornick et al., 2019). NK cells also seem to be important as NK depletion was found to reduce CD8+ T cell recruitment into the airways in IAV-infected mice (Verbist et al., 2012). RVIs can also induce Th2 and Th17 cell differentiation which have been implicated in pathological responses (Miyauchi, 2017). In influenza-infected mice, lung-resident memory T cells have been found to exhibit significant differences to circulating memory T cells, such as increased

IFNγ production and a larger proportion of virus-specific T cells (Turner et al., 2014). This highlights the importance of studying immune responses at the respiratory mucosa instead of relying on data from peripheral sites.

B cell responses also occur later than innate responses; in influenza-infected mice and ferrets, antibody producing cells increase in the lungs and lymph nodes within a week and peak 1-3 weeks from primary infection (McLaren and Butchko, 1978). In addition, B cell dynamics differ between tissues, with germinal centre B cells reported to peak in the lungs later than in the lymph nodes during influenza infection (Boyden et al., 2012). Different tissues also have different antibody isotype profiles; whilst BALT can produce a range of antibody isotypes NALT appears to be a more significant producer of IgA (Boyden et al., 2012; Liang et al., 2001; Shimoda et al., 2001; Zuercher and Cebra, 2002). Different isotypes are also associated with different disease outcomes; systemic IgG and mucosal IgA are often associated with protection in RVIs whereas IgE is associated with pathology in RSV infections (Ascough et al., 2018; Van Erp et al., 2019).

Long-lasting antibody and memory B cell levels are associated with protection against recurrent infections, but for some viruses, such as SARS-CoV, these levels decline within a few years (Liu et al., 2006; Wu et al., 2007). Other viruses, such as RSV, are poor at inducing IgA+ B cell memory cells (Habibi et al., 2015). Reasons for these impairments are not understood and have not been extensively researched. Antibody responses are often T cell-dependent although short-lived antibody responses can be driven by T cell-independent mechanisms (Allie and Randall, 2017). Development of memory T cells has also been observed in responses to RVIs and can provide long-term protection (Channappanavar et al., 2014). Some of the molecular regulators and signalling processes involved in generating memory T cells have been described but there remain questions about why memory T cells decline after some infections (Pizzolla and Wakim, 2019). Understanding how to induce protective and long-term and B and T cell responses is therefore a key area of focus for vaccine development.

Inflammatory responses are important in clearing viral load but they have also been linked with disease pathology. In severe influenza infections, pathology has been linked to uncontrolled, systemic levels of inflammatory mediators; a phenomenon known as a "cytokine storm" (Tavares et al., 2017). In severe RSV infections in infants, disease has been linked to both high viral load and significant levels of immune cells and

inflammatory mediators in the airways (Openshaw et al., 2017). Some of the mechanisms underlying immunopathology are poorly understood but it is clear that the magnitude and type of response is important for controlling viral replication without additional pathogenesis.

Mechanisms that regulate inflammation are also under investigation and are known to involve immune cells. CD4+ Treg cells generated during RVI can inhibit effector T cell proliferation, differentiation and activity through anti-inflammatory cytokine production and cell-cell contacts (Miyauchi, 2017). In addition, effector T cells themselves can produce anti-inflammatory cytokines like IL-10 (Braciale et al., 2012). Removing Tregs or blocking anti-inflammatory cytokines can lead to worse disease outcomes and increased inflammation (Lee et al., 2010; Loebbermann et al., 2012). Innate immune cells and epithelial cells also contribute to immune regulation depending on their phenotype and gene expression (Braciale et al., 2012). Ensuring immune responses are appropriately controlled is therefore another important aspect in therapeutic and vaccine design.

1.2.4 Models in respiratory viral infection research

1.2.4.1 *In vitro and ex vivo model systems*

In vitro or *ex vivo* culture systems have been widely used in RVI research as they are easier to manipulate and sample than animals or humans. In addition, their relative simplicity makes it easier to determine the functions of individual host or viral components. However, these systems do not reflect the true complexities of the respiratory and immune systems. This limits their use in studying the immune response which we know relies on interactions and migration of many cell types. In addition, most culture systems are static and lack a commensal microbiome, thus lacking key features of the respiratory tract which have important consequences on cell physiology (Douville et al., 2011; Hauptmann and Schaible, 2016). Furthermore, although it is easy to administer substances or pathogens in culture systems, this does not recapitulate physiological exposure in living organisms.

Types and sources of cells and tissues

Immortalised cell lines have been extensively used in biological research for decades and are well characterized and widely available. These cells can grow indefinitely due to their cancerous properties or transgenic telomerase activity. However, this can create differences in their biology which are not reflected *in vivo.* In addition, due to extensive passaging and possible contamination, individual cell lines can show considerable variability, potentially affecting the validity and reproducibility of experiments (Kaur and Dufour, 2012). There are several commercially available human epithelial cell lines that derive from different parts of the respiratory tract and in some cases can differentiate into multiple cell types (Bhowmick and Gappa-Fahlenkamp, 2016). Other cell lines, including those for immune cells, are also available.

Primary cells are obtained directly from living humans, cadavers or animals. Respiratory cells are obtained from lung biopsies and nasal or bronchial brushings, whilst circulating immune cells can be obtained from peripheral blood. These cells are not extensively passaged so more closely resemble the phenotype of respiratory cells *in vivo.* However, human primary cells have limited availability especially from certain groups, such as infants. In addition, since primary human cells are often obtained during medical treatment produces, tissue from healthy donors can be more difficult to source than tissue from donors with respiratory conditions. Furthermore, there can be considerable variability between donors making it difficult to draw conclusions about specific features or factors. However, using primary cells allows researchers to study the effects of viral infection in the context of conditions like COPD and asthma, which are exacerbated by RVIs and associated with increased susceptibility to infection.

Human pluripotent stem cells (hPSCs) can be used to generate multiple respiratory cell types in 2D and 3D culture systems. However, despite their broad differentiation potential, these cells require complex culture conditions, are not easily available, and reflect fetal tissue more than mature respiratory tissue (Miller and Spence, 2017).

Cell cultures have been particularly useful for studying host cell immune responses and host-virus interactions of individual cell types (Jonsdottir and Dijkman, 2016; Proud et al., 2004; Wang et al., 2000). In addition, multiple cell types can be co-cultured to study cell interactions and infection dynamics (Deng et al., 2018; Zhang et al., 2015b).

As well as individual cells, tissue explants from human donors or experimental animals can also be cultured *ex vivo*. This maintains some of the tissue structure with multiple relevant cell types. *Ex vivo* tissue cultures therefore bridge a gap between easily manipulated culture systems and physiologically relevant *in vivo* systems. Cultured tissue can be analysed for changes in gene expression, protein levels and viral load like cell cultures but they can also be analysed by histology to better understand changes within the tissue structure (Chan et al., 2010, 2013). However, this does mean that the selection of the tissue region could introduce variability and must be carefully considered in experimental design. One type of tissue explant system used in respiratory research is precision cut lung slices (PCLS). This involves infusing dissected lung tissue with agarose to maintain an inflated structure, slicing into sections, and culturing for up to two weeks (Liu et al., 2019a). This can be achieved with tissue from human donors or experimental animals. PCLS have been used to study the effect of pollutants, immune responses to RVIs, and viral cell tropism and differences have been observed between PCLS and primary cell cultures (Goris et al., 2009; Maikawa et al., 2016; Wu et al., 2011).

Culture systems

The simplest method to culture cells is by maintaining them in 2D monolayer cultures. This can be achieved by submerging cells in media or by culturing cells at an air-liquid interface (ALI). Media submerged cultures are simpler to set up but do not reflect the air-liquid environment of the respiratory epithelium. ALI cultures are established using specialised supports where culture medium is removed from apical side of cells, exposing them to air. Medium remains on the basolateral side and the resulting ALI allows cells to form a polarized epithelium. This approach can be used for cells from different respiratory regions and promotes differentiation of multiple cell types including ciliated cells, goblet cells and basal cells (Jonsdottir and Dijkman, 2016). This allows a mucus layer to form on apical side. ALI cultures of human primary cells have more similar gene expression to epithelium *in vivo* than media submerged cultures or ALI cultures of immortalized cells (Pezzulo et al., 2011). However, these human airway epithelium (HAE) cultures can still lack some of the cells and epithelial junctions found *in vivo*, such as neuroendocrine cells, club cells and paracellular junctions (Davis et al., 2015). HAE cultures have been used to study the polarity of infection and viral receptor expression, epithelium integrity, changes in mucus, the effects of drugs, and the innate immune

response in the context of RVIs. The presence of multiple cell types also allows investigation into the cell tropisms of different viruses.

Cells can also be grown in 3D cultures which mimic *in vivo* respiratory structures more closely than 2D cultures. This can be achieved by allowing cells to self-assemble in droplets or gels or seeding cells onto scaffolds (Miller and Spence, 2017). These systems can be used with hSPCs to form organoids – miniature tissue-like structures that contain a variety of cell lineages. These have been used to monitor infection dynamics and structural changes during infection, reflecting some of the changes observed *in vivo* (Chen et al., 2017; Porotto et al., 2019). Another recent development is the lung-on-a-chip platform which recapitulates some physiological dynamics of respiratory epithelium. This consists of specialised supports where epithelial cells are seeded at an ALI to generate the polarized epithelium. Endothelial cells are seeded beneath the epithelium and a microfluidics system circulates media, mimicking blood flow. In one study, this system was found to consist of a mucous ciliated epithelium with underlying extracellular matrix (Benam et al., 2016). Furthermore, the cultures responded to polyinosinic:polycytidylic acid [poly(I:C)] – a TLR3 agonist and dsRNA mimic – by secreting cytokines. Organoids and lung-on-a-chip systems have not yet been used in many studies of RVIs, likely because of the complexity of these systems.

1.2.4.2 *In vivo animal models*

Although many insights can be gained from culture systems, *in vivo* models are more suitable for studying the response of an intact immune system and the effects of infection or medical interventions on disease pathology. Natural infections or experimental challenges can be studied in humans but there are necessary ethical limitations to these studies. For example, highly pathogenic viruses like SARS-CoV cannot be used in experimental challenges. Less pathogenic virus like RSV have been used in human challenges but these studies can be costly and may require quarantine centres. One alternative is to study human responses to non-infectious viral mimics and immunostimulants (Progatzky et al., 2019). Human studies are further complicated by genetic variability, co-morbidities and lifestyle factors which can be difficult to control. Therefore, animal models, which can be used in highly controlled conditions, are often a more appropriate choice. No single model recapitulates all aspects of human disease and therefore, biological and practical factors must be considered in order to choose the most

appropriate model for the research question. Mammalian species are most widely used in RVI research, but fish and avian species also offer some advantages.

Many studies have focused on systemic responses to RVIs since peripheral blood is easily accessible and less invasive than sampling of respiratory tissue. However, systemic responses do not always correlate with mucosal respiratory responses and can be poor indicators of protective immunity following vaccination (Waffarn and Baumgarth, 2011).

Biological differences between model organisms

Some species are permissive to infection by human respiratory viruses although this varies with the virus and host strain. Some viruses, like IAV, can infect several species including non-human primates (NHPs), ferrets, guinea pigs, hamsters and cotton rats (Bouvier and Lowen 2010). However, differences have been observed in cell tropism: in macaques, avian influenza viruses preferentially bind to ATII cells whilst in humans these viruses preferentially bind ATI cells (van Riel et al., 2007). Furthermore, mice are not permissive for circulating IAV strains but are permissive for some highly pathogenic strains. Other viruses have a more restricted species tropism, for example, Middle East respiratory syndrome-CoV (MERS-CoV) cannot infect ferrets, mice or hamsters (Lee and Kim, 2020).

To overcome lack of infection or pathology, some studies use animal viruses that are similar to human respiratory viruses. For RSV, these include bovine RSV and ovine RSV which infect cattle and sheep respectively, and pneumonia virus of mice (PVM). However, not all human viruses have a related animal counterpart. Furthermore, despite some similarities, animal viruses are clearly antigenically and genetically different to human viruses. Some animal viruses are more frequently used for veterinary studies bu this can still improve our broader understanding of RVIs.

Species-restrictions can also be tackled by using lab-adapted viruses, grown in specific conditions or genetically modified to infect animals. Several lab-adapted mouse strains exist for IAV and these can show differences in pathogenicity (Bouvier and Lowen 2010). Furthermore, wild mice and certain inbred mice strains are resistant to the mouse-adapted PR8 strain of IAV due to presence of Mx1, an ISG that has been shown to be protective against infection. Mx1 is non-functional in commonly used inbred strains, e.g.

C57BL/6J, highlighting the importance of immunological differences within species (Shin et al., 2015).

Viral susceptibility is determined in part by the presence of viral receptors and these can vary genetically between species. In mice, the ACE2 protein can interact with human SARS-CoV leading to infection, albeit with only mild symptoms (Lee and Kim, 2020). In contrast, mice epithelial cells lack the α-2,6 sialic acid linkages used by human IAV which may explain differences in infection susceptibility (Ibricevic et al., 2006). Transgenic animals expressing human receptors have been developed to overcome this barrier for certain viruses. This includes transgenic mice expressing human ACE2, ICAM-1 or dPP4 which can be infected with SARS-CoV and SARS-CoV 2, human rhinoviruses, and MERS-CoV respectively (Agrawal et al., 2015; Bao et al., 2020; Bartlett et al., 2008; Yang et al., 2007). However, this strategy requires prior knowledge of the relevant receptors. In addition, some viruses use multiple receptors therefore infection dynamics might not be reflective of infection in humans.

For established infections, disease pathology is another important consideration. Some species can be infected with human viruses but show few or no clinical symptoms. Whilst ferrets closely recapitulate human symptoms during IAV infection, they show only mild symptoms with SARS-CoV 2. Furthermore, although some animals do not display clinical symptoms, they may show pathology at a cellular level, as observed in guinea pigs infected with IAV (Van Hoeven et al., 2009). For species that develop clinical symptoms, there may still be differences to human symptoms. In contrast, to most IAV infections in humans, infection in mice results in lower respiratory tract pathology rather than upper respiratory symptoms. Furthermore, mice lack a sneezing reflex which limits their use in transmission studies. Ferrets, who do sneeze during IAV infection, are more appropriate in this context (Bouvier and Lowen, 2010). Assessing the effects of therapeutics on disease pathology also requires models that recapitulate some symptoms of interest, and ideally most human symptoms. Species differences in pharmacokinetics and toxicities are also important for selecting models and dosages in pre-clinical studies (Bouvier and Lowen, 2010). All of these factors further emphasise the need to choose models based on the specific virus and research question.

Respiratory anatomy and physiology are also important to consider in the study of RVIs. Larger mammals like sheep, NHPs and pigs have a similar respiratory anatomy to humans

and can be used to perform and interpret pulmonary function tests more easily than smaller species. On the other hand, mice and small rodents have noticeable anatomical differences to the human respiratory system (Bem et al., 2011; Casadei and Salinas, 2019). This includes differences in the presence and structure of NALT as mentioned previously. Furthermore, mouse nasal tissue is poorly accessible, requiring euthanasia for sampling. Differences are also observed at a cellular level: the ratio of olfactory to respiratory epithelium in nasal tissue is smaller in humans and NHPs compared to other mammals (Smith and Bhatnagar 2004).

As with other biological components, the immune system and responses vary between species. NHPs are most genetically similar species to humans and are therefore often used for vaccine studies. Mice are one of the most extensively used model organisms but have many immunological differences to humans, such as a lack of the chemokine IL-8 and a TLR8 protein which does not respond to human TLR8 ligands (Hol, Wilhelmsen, and Haraldsen 2010; Liu et al. 2010). However, one of the hallmarks of the mucosal response to RVIs – IgA production – is observed in several species including birds, NHPs and mice (Casadei and Salinas, 2019; Nochi et al., 2018). In addition, differences in immune responses can also provide important information about factors that influence infection and pathology. For example, guinea pigs were found to rapidly upregulate genes involved in IFN signalling in response to avian H5N1 which may explain their resistance to infection (Zhang et al. 2017). In contrast, avian H5N1 is highly pathogenic in humans.

Closely related to the immune system is the microbiota which can show species-specific differences in composition and influencing factors. For example, the cotton rat nasal microbiota consists of some bacterial species not found in humans (Chaves-Moreno et al., 2015). In addition, mouse microbiota is significantly affected by the environment whereas the microbiota of human lungs is not as affected by changes in geography (McGinniss and Collman, 2018). With increasing evidence for the role of the microbiota in infection and respiratory health, this is an important factor to consider when translating findings from animal models to humans. We currently have limited understanding of how the microbiome is established and maintained in humans and other species and these gaps in knowledge can further complicate immunological studies.

Practical considerations

In addition to the numerous biological differences between model organisms, their practical use in laboratory research must also be considered. There are legislative regulations and ethical restrictions for animal research in many countries and studies using NHPs are particularly restricted.

Some model organisms, particularly mice have been extensively used in immunology and infectious disease research and therefore have many readily available reagents and immunological and genetic data. These are much more limited for other species such as sheep, cattle and cotton rats. In addition, genetic modification is well established for mice but more difficult to achieve in NHPs (Casadei and Salinas, 2019). The lack of availability of inbred strains for NHPs, guinea pigs and ferrets can introduce greater variability in experimental studies compared to inbred mice and other species (Bouvier and Lowen, 2010). On the other hand, the greater genetic diversity more closely reflects the diversity of human populations.

When studying the complex and dynamic immune system, it is particularly useful to visualise changes *in vivo* using intravital imaging. This has been achieved for imaging whole lungs of ferrets with positron emission tomography and computed tomography to assess the extent of inflammation during IAV infection (Camp et al., 2015). The respiratory system can be visualised at higher resolution in mice, but this requires invasive surgical exposure of the respiratory tissues, likely in itself to cause an inflammatory response, and complicated, custom microscope setups (Veres, 2018).

The housing and handling requirements for different species are also important as they determine the level of expertise required and the costs. Smaller animals like rodents are understandably cheaper to house than livestock and larger species. Very large species like horses are not generally used as model organisms for human disease partly because of these factors. Some species also require particularly careful handling including cotton rats and NHPs, meaning that researchers and animal technicians require more extensive training (Bem et al., 2011; Bouvier and Lowen, 2010).

Biosafety is another crucial consideration and depends on both the virus and the model organism. Housing facilities must have suitable pathogen containment, particularly when using animal viruses that could infect other animals in the facility e.g. PVM in mice. In addition, those working with the infected animals must be suitably protected. Some

pathogens are not infectious in humans, e.g. the lab-adapted IAV strain, PR8, but others, e.g. SARS-CoV, are highly pathogenic and lack vaccination or effective therapeutics (Beare et al., 1975).

1.2.4.3 Overview of gaps in tools and understanding

Overall, *in vitro* and *ex vivo* models for studying RVIs are well established but particularly limited for studying the dynamism of the immune response. *In vivo* animal models have been a powerful alternative and several strategies have been successfully used to overcome challenges in restrictive virus tropisms. However, existing animal models can be poorly accessible regarding access to the respiratory tract, research costs, and expertise required. Immunological studies in many species are also limited by the availability of tools. There is therefore a case for developing complementary *in vivo* models that allow easy access and manipulation of the respiratory mucosa.

1.3 Teleost gill structure and immunology

Gills are the respiratory organs for many vertebrate and invertebrate aquatic species including fish, amphibians, and mollusks (Griffith, 2017). They are important in the health of aquatic species and are studied to improve aquaculture and monitor aquatic environments. This section will review the main structural, functional and immunological features of the gills in order to highlight analogies to the mammalian respiratory tract. Differences to mammals will also be highlighted as this is an important consideration in model development. Since this project investigated the immunology of zebrafish gills, this section will focus on fish gills, and more specifically on teleost gills. Teleosts are a group of bony ray-finned fish which include zebrafish.

1.3.1 Structure and function of the gills

The gross anatomy of the gills is largely different to that of the mammalian respiratory system. However, at a basic level both structures consist of a thin mucosal epithelium with a large surface area essential for efficient gas exchange (Ohtani et al., 2014). Whilst the gills are the major site of gas exchange, they also perform several important functions not observed in the mammalian respiratory tract.

1.3.1.1 Gross anatomy of the gills

Teleost gills consist of two sets of arches on opposite sides of the head of the fish (Figure 1.3A). Each set of is made up of 4 arches and a pseudobranch (Evans et al., 2005). Individual branches are made up of two sets of filaments which protrude at a perpendicular angle from the cranial and caudal sides of a bony structure also known as the arch (Figure 1.3B). One set of filaments constitutes a hemibranch (Figure 1.3C), whilst the two sets of filaments are collectively named a holobranch. The hemibranches are connected by connective tissue known as the interbranchial septum. It is speculated that water flowing in this region is retained for longer leading to more mixing and potentially more exposure to particles and pathogens (Dalum et al., 2015; Rességuier et al., 2020).

Skeletal tooth-like structures known as rakers protrude from the arch, opposite to the filaments. Rakers are hypothesised to influence particle filtration in the branchial cavity (Smith and Sanderson 2013). Each filament consists of a primary lamella containing blood vessels, and multiple secondary lamellae protruding from two sides (Figure 1.3D). These disk-like structures are perpendicular to the primary lamellae and greatly increase the surface area of the gills. The secondary lamellae are covered by a single-cell layer epithelium made of squamous epithelial cells (Olson, 2002). These cells more closely resemble the squamous cells of mammalian alveoli rather than the epithelium of the conducting airways. The primary lamellae are also covered by an epithelium, but this is normally thicker than the lamellae, consisting of three or more layers of cells (Wilson and Laurent, 2002).
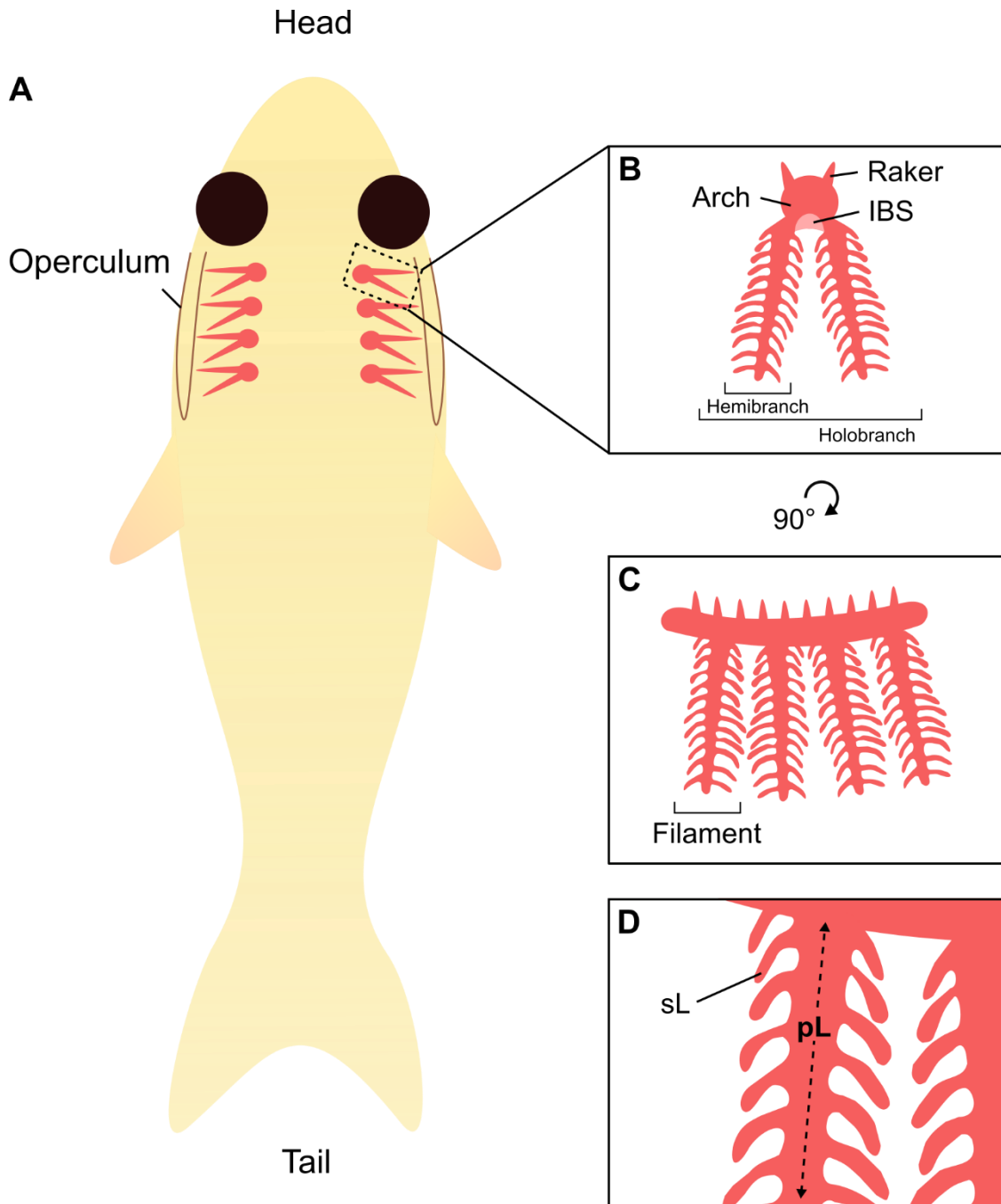
Figure 1.3 Gross anatomy of teleost gills.

A) Dorsal view of an adult fish. The gills exist as paired structures (holobranches) on each side of the fish, covered by a bony flap of skin (operculum). B) Transverse view of a gill holobranch showing the two hemibranches. Each hemibranch is joined by connective tissue known as the interbranchial septum (IBS). Bony tooth-like structures (rakers) project from the anterior region of the arch. C) 90° rotation showing a medio-lateral view of a gill hemibranch and its filaments. D) Magnified view of a gill filament showing the core primary lamellae (pL) and the branching secondary lamellae (sL).

1.3.1.2 Functions of the gills

Aside from gas exchange, the gills have important roles in ionoregulation, osmoregulation, pH regulation and waste secretion (Evans et al., 2005). In this respect they share similarities with mammalian kidneys.

The large surface area to volume ratio means that the gills are highly adapted for efficient gas exchange. All the deoxygenated blood from the heart travels directly to the gills where it enters individual branches through the branchial afferent artery. The blood flows into each filament via an afferent filament artery (Olson, 2002). Deoxgenated blood then reaches the secondary lamellae which do not contain blood vessels but instead contain specialised endothelial cells (pillar cells) which red blood cells pass by in a sheet flow system. This bears similarities to blood flow in the alveoli (Farrell et al., 1980). Gas exchange takes place in these secondary lamellae but not in primary lamellae (Rombough, 2007). This again bears similarities to the mammalian respiratory tract where gas exchange takes place in the alveoli, not the conducting zone. Water enters fish through the mouth and flows between secondary lamellae. In this system, blood flow is countercurrent to water flow enabling maximal gas exchange and affecting diffusion rates of ions (Evans et al., 2005). Oxygenated blood leaves the filaments via the efferent filament artery (Olson, 2002). The blood finally exits the gills to circulate around the rest of the body of the fish in a single circulatory system, before returning to the heart.

The bodily fluids of fish have significantly different ion levels to the surrounding aquatic environments therefore the gills actively transport ions to maintain homeostasis (Hwang and Lee 2007). The gills are also the primary site of excretion of nitrogenous waste – primarily ammonia and urea. This is essential for fish since storage of nitrogenous waste compounds has high energy costs and can have high toxicity (Evans et al., 2005). Therefore, it is clear that multiple selective pressures have influenced the evolution and properties of the gills. This is a clear difference to mammalian respiratory systems which are thought to have evolved partly due to higher oxygen demands (Hsia et al., 2013). The different selective pressures on the gills are likely to have influenced the immune properties and responses of this tissue. Specifically, the immune responses are likely to be adapted to avoid impairment of these crucial physiological functions.

1.3.1.3 Cells

In order to perform their numerous functions, teleost gills contain different specialised cells. As with the mammalian respiratory epithelium, the gill epithelium consists of epithelial cells, progenitor cells required for tissue repair, and mucus-producing cells. Since this project sought to investigate immune responses in the whole gill, this section will also review cells beyond the epithelium.

Pavement cells are epithelial cells that cover the gill arch and filaments. They are flat and have microvilli or microridges which are thought to increase the surface area for gas exchange and may support mucus adhesion (Evans et al., 2005; İşisağ and Karakişi, 1998; Leguen, 2018). These cells are the first to contact the external environment and their thin morphology make them well-suited for gas exchange. Unlike mammalian respiratory epithelium, pavement and other gill cells are not ciliated. Therefore, the gills must employ alternative mechanisms to clear pathogens and particles. These may include cough action to directly expel water and mucus and the regular flow of water over the gill surface (Derksen et al., 1998).

Mucus-producing cells are found in the epithelium of the gill arch, rakers and filaments but not in the secondary lamellae except in pathological conditions (Leguen, 2018; Macirella and Brunelli, 2017; Progatzky et al., 2015). Club cells also produce mucus but in some fish they are not exposed to the gill surface and are only found in the gill arch (Kumari et al., 2009b). Basal cells have also been described in the in the gill epithelium and exhibit features of undifferentiated cells (Wilson and Laurent 2002; Macirella and Brunelli 2017). However, the differentiation potential of these cells is unknown.

Like the lungs, the gills are highly vascularised. Endothelial cells make up these numerous blood vessels as well as lymphatic vessels (Okuda et al., 2012; Olson, 2002). Pillar cells are endothelial cells that structurally support the secondary lamellae and have morphological differences to vascular endothelial cells (Wilson and Laurent 2002).

Other cells in the gills include neuroepithelial cells which can detect changes in oxygen and carbon dioxide levels. Oxygen-sensing in the lungs also occurs via neuroepithelial cells (Jonz and Nurse, 2005; Qin et al., 2010). Nerves fibres innervate the gills and are observed throughout the filaments and lamellae. Ionocytes (also known as mitochondria-rich cells or chloride cells) are involved in ion exchange and ammonia secretion and

observed along gill filaments (Evans et al., 2005; Leguen, 2018). Ionocytes in murine lungs have a similar transcriptome to zebrafish skin ionocytes but it is not known whether the same is true for gill ionocytes (Montoro et al., 2018). The gills also contain secretory rodlet cells which have been associated with helminth infection (Reite and Evensen, 2006).

1.3.1.4 Mucosal components

Mucus

Like all mucosal compartments, the gill epithelium is covered by mucus composed of glycosylated proteins (Kumari et al., 2009b; Lumsden and Ferguson, 1994). The transcript levels of mucin genes has been described in the gills of several species. These genes include *Muc5B*, an orthologue of mammalian MUC5B expressed in the respiratory tract (Van Der Marel et al., 2012). In addition, multiple immune-related and antimicrobial proteins have been detected in gill mucus such as immunoglobulins (IgM and IgT), myeloperoxidase precursor and complement C3 factor (Igarashi et al., 2017; Valdenegro-Vega et al., 2014; Xu et al., 2016). Gill mucus can bind pathogens (Padra et al., 2019) but presence of antimicrobial components suggests that it is involved in immune defense beyond its role as a physical barrier. Transcripts for many other antimicrobial peptides (AMPs) have been detected in the gills but more work is needed to establish whether these are secreted in the gill mucus (Gomez et al., 2013; Van Der Marel et al., 2012).

Various parameters of gill mucus are affected during infection, including during viral infection. Changes have been observed in the numbers of mucous cells, mucus protein composition, and mucin gene transcript levels (Adamek et al., 2017; Roberts and Powell, 2005; Valdenegro-Vega et al., 2014). Whether these changes contribute to protection or pathology has not been determined.

Microbiota

Like mammalian respiratory tissue, teleost gills have a commensal microbiota which can change following exposure to chemical challenges or during disease (Aleshina et al., 2019; Legrand et al., 2018). Gill microbial composition in healthy gibel carp and bluntnose black bream were found to differ from surrounding water indicating that the gills provide a specialised environment that promotes colonization of certain bacterial species (Wang et al., 2010c). Gill microbial composition has also been found to differ from the skin mucosa

and may reflect the specialised gas exchange and nitrogenous waste secretion environment (de Bruijn et al., 2018; van Kessel et al., 2016). Furthermore, secretory IgT has been found to coat the microbiota in rainbow trout, suggesting that this fish-specific immunoglobulin has a mucosal function similar to IgA in mammals (Xu et al. 2016). IgT antibodies against the dominant gill commensal bacteria, *Flectobacillus major*, have also been detected in gill mucus (Sepahi et al., 2016a). Depletion of IgT+ B cells in rainbow trout led to greater bacterial penetration of gill tissues, dysbiosis of gill microbiota and higher inflammation and gill pathology (Xu et al., 2020). These studies indicate an important role for IgT in regulation of gill commensal homeostasis and clear similarities with mammalian mucosa. The interactions between the immune system and gill microbiota should continue to be investigated in a wider range of teleost species.

Gill-associated lymphoid tissue (GIALT)

Lymphoid tissue has been described in many fish mucosal tissues, including the gills. Teleosts lack lymph nodes, but lymphocytes in these mucosal tissues are thought to contribute to initiation and progression of immune responses. Many studies have investigated the responses of mucosal tissues to infection or immune challenge however further work is needed to determine the specific roles of immune cells in the different MALTs. (Salinas, 2015).

MALT in the gills, skin, gut, and nasal region consists of lymphocytes scattered in the tissue and in some teleosts, the gills also contain organised accumulations of T cells in the interbranchial region (Hetland et al., 2010; Rességuier et al., 2020). This structure is known as interbranchial lymphoid tissue (ILT) and extends along the filaments (Dalum et al., 2015). Lymphocytes in the ILT are encompassed by a network of epithelial cells and together with scattered lymphocytes in the rest of the gill make up the GIALT (Koppang et al., 2010; Salinas et al., 2011).

The ILT is responsive to bacterial and viral challenge indicating that is has an active role in gill immunity rather than being a passive store of lymphocytes (Aas et al., 2017; Hu et al., 2019). For antiviral responses, which typically engage the adaptive arm of the immune system, the ILT and GIALT may be particularly important. However, few studies on fish mucosa have investigated this structure, instead focusing primarily on the gut and skin. This is therefore a neglected area of research that could reveal many new insights in

mucosal and respiratory immunology. This will be discussed further in the introduction of Chapter 3.

1.3.2 Gill immunology

1.3.2.1 Immune cells

Innate and adaptive immune cells from the myeloid and lymphoid lineages have been identified in many teleosts including zebrafish. Some immune cells have been clearly established as equivalents to mammalian cells. However there are also reports of cells with immune-related properties that have not been clearly classified. In addition, it is not clear if some mammalian immune cells have teleost counterparts. This section will describe the immune cells currently identified in teleost gills.

Myeloid cells

Granulocytes, including neutrophils, mast cells, and eosinophils/basophils have all been identified in the gills (Balla et al., 2010; Powell et al., 1990; Progatzky et al., 2015). Cells with monocyte, macrophage or dendritic cell morphology and transcript profiles have also been identified in the gills. In rainbow trout, cells with these mononuclear phagocyte morphologies were reported to take up inactivated bacteria highlighting their phagocytic abilities (Kato et al., 2018). Macrophage expressed (*Mpeg*) 1.1 + cells, which include macrophages, have also been reported to take up nanoparticles in zebrafish gills (Rességuier et al., 2017). Furthermore, the numbers of Mpeg1+ cells were higher in the gills of grouper fish following parasitic infection with *Cryptocaryon irritans* (Ni et al., 2020). Analysis of zebrafish gills has also revealed a population of DCs with affinity for a commonly used DC marker, peanut agglutinin, and antigen-specific T cell activation abilities *in vitro* (Lugo-Villarino et al., 2010).

Natural killer cells and innate lymphoid cells

Non-specific cytotoxic cells (NCCs) have been described in teleosts. These cells have cytotoxic activities but express distinct markers and have different origins to another NK-cell-like population (Nakanishi et al., 2011). NCCs are also morphologically distinct from mammalian NK cells (Fischer et al., 2006, 2013; Nakanishi et al., 2011). Orthologues of mammalian NK-markers are not thoroughly characterised in teleosts but single cell RNA sequencing (scRNA-Seq) studies have recently identified cell populations with NK-like

cell transcriptomes in zebrafish (Pereiro et al. 2015; Moore et al. 2016; Tang et al. 2017). Despite these advances, reports of NK cells in the gills are lacking.

Characterisation for the other ILC populations (ILC1, 2 and 3) in teleosts is even more limited. One scRNA-Seq study in zebrafish revealed distinct clusters of kidney and gut cells that may correspond to ILC equivalents (Hernández et al., 2018). Furthermore, these cells responded to challenges with helminth extract or inactivated bacteria by upregulating cytokine transcripts associated with mammalian ILCs. However, more work is needed to compare the function and ontogeny of these cells to mammalian ILCs. Further work is also needed to assess presence of these cells in the gills.

B cells

In fish species, B cells can produce at least three antibody isotypes: IgM, IgD or IgT (also known as IgZ in zebrafish and carp) compared to the five classes (IgG, IgM, IgA, IgD, and IgE) produced in humans. A fourth isotype, IgZ-2, has also been identified in zebrafish and carp (Hu, Xiang, and Shao 2010; Ryo et al. 2010). IgZ+, IgM+IgD+, IgM+IgD-, and IgM-IgD+ cells have been identified in the gills of different species indicating that teleost gills contain heterogenous populations of B cells (Perdiguero et al., 2019; Rességuier et al., 2017). In addition, IgM and IgT antibodies have been found to bind to the parasite *Ichthyophthirius multifiliis* in rainbow trout gills showing direct interactions between antibodies and pathogens (von Gersdorff Jørgensen et al., 2011). This binding was only observed in fish previously immunized against the parasite indicating development of humoral immunity.

T cells

As previously mentioned, T cells are found in the gills both in the ILT and scattered in the rest of the tissue. Both CD4+ and CD8+ T cells have been identified in the gills but further characterisation of T cell subsets in the gills is limited (Hetland et al., 2010; Somamoto et al., 2015). *Cd4+* T cells with Th2 or Treg transcript profiles have been described in zebrafish gills but it is not clear how far the classification of T cells from mammalian species applies to teleosts (Dee et al., 2016; Hui et al., 2017). Notably, Tfh cells, which are important in supporting B cell activation in mammals, have not been described in teleosts. Since germinal centres have also not been described it is reasonable to speculate that this subset may also be lacking in teleosts.

CD8+ lymphocytes from the trout gut and nasal mucosa were found have some differences in transcript profiles but were both enriched for *IFNγ* (Sepahi et al., 2016b). This suggests that CD8+ gill cells may have tissue-specific gene expression but still have features of mucosal lymphocytes. Lymphocytes expressing the γδ TCR have also been detected in zebrafish gills with immunofluorescence (Wan et al., 2017). γ+δ+ cells from the kidney, spleen and blood expressed *cd8* and not *cd4*, but the transcript profile of γ+δ+ cells in gills was not investigated. More research is needed to assess potential cytotoxic activity, cell-cell interactions, and cytokine production of these different gill T cell subsets.

Overall, the immune cells required for pathogen recognition and innate and adaptive responses all seem to be present in the gills. Functional analyses of these cell types are limited so understanding how these cells contribute to viral infections, if at all, requires further investigation. Additional work is also needed to understand how these cells interact within the complex gill structure.

1.3.2.2 *The gill immune environment at homeostasis*

Some research suggests that gills have a Th2-skewed environment based on moderate levels *of GATA-3* and *IL-4/13A* transcripts and lower levels of *IFN-γ* and *T-bet* transcripts (Kumari, Bogwald, and Dalmo 2009; T. Wang et al. 2010; Takizawa et al. 2011). Furthermore, as previously mentioned, *cd4+* T cells in the gills have a Th2 phenotype at homeostasis (Dee et al., 2016). This contrasts with murine lungs which do not show enriched levels of IL-4, IL-13, or GATA3 (Takizawa et al., 2011). As a result, immune responses in the gills and in the mammalian lungs may differ, particularly with respect to viral infections which usually induce Th1 responses.

The gills also contain different anti-inflammatory and immunosuppressive components including *LAG-3*, *IL-11* and *IL-10* transcripts and presence of Treg cells at homeostasis (Wang et al. 2005; Zhang et al. 2005; Takizawa et al. 2011; Hui et al. 2017). *Il10* has been found to be essential in preventing excessive inflammation in zebrafish gills as *il10* mutants had pathological signs of inflammation and higher levels of *ifng1* at homeostasis (Bottiglione et al., 2020). *Il10* mutants also had prolonged inflammation following immune challenge with a synthetic TLR7/8 agonist, resiquimod. In a different study, *il10* transcript levels were higher in zebrafish gills following LPS challenge, indicating a role for this regulatory cytokine in other immune activation pathways (Zhang et al. 2005).

Il4/13a and *il4/13b* have also been found to regulate gill inflammation (Bottiglione et al., 2020). In this study, zebrafish double mutants for these genes had higher levels of *il6*, *tnfa* and *ifng1* transcripts in the gills at homeostasis. In addition, transcriptome analysis showed an enrichment of Th1 differentiation and IFNγ signaling suggesting that *il4/13a* and *il4/13b* are also important for maintaining a Th2 environment.

These data fit with the idea that mucosal tissues are tolerogenic environments. However, in Atlantic halibut the gills were found to express high levels of proinflammatory and Th1-associated genes, IL-1β, IL-12βc and IFNγ, and lower levels of IL-11 in contrast to the studies cited above (Øvergård et al., 2012). In addition to highlighting potential species differences, these conflicting findings indicate that assessment of gill responses to immune challenge may provide a better indication of how the gill environment influences immune responses.

1.3.2.3   Gill pathology and immune responses to infection

As an interface between host and environment, the gills are susceptible to infection by a range of pathogens including bacteria, parasites, and viruses (Mitchell and Rodger, 2011). They can also act as a route for pathogens to infect other tissues even if they are not infected themselves (Montero et al., 2011). Consequently, they are likely to be key for antigen surveillance and initiation of immune responses. This bears clear similarities to the mammalian respiratory system but also makes the gills an important tissue for understanding fish infections and designing effective aquaculture vaccines. This section will focus primarily on viral infections.

Fish infected with viruses can display a range of gill pathologies including anaemia, inflammation and infiltration of leukocytes, loss of clear lamellar structures and apoptotic cells (Bermúdez et al., 2018; Pikarsky et al., 2004; Thoen et al., 2020). In severe cases this can result in respiratory impairment and mortality (Office International des Épizooties, 2003).

Responses to viral infection in the gills vary by virus and by fish species but many studies have reported changes in transcript levels of immune-related genes. These include IFNs, ISGs, chemokines, and immunoregulatory mediators (Aas et al., 2017; Austbø et al., 2014; Ordás et al., 2012). In one study, chemokine transcript levels in the gills were altered despite a lack of viral presence (Montero et al., 2011). These studies show that the gills

contribute to local and possibly systemic defenses against viral infection. Indeed, viral load in ginbuna carp gills was lower in secondary challenge compared to primary challenge with crucian carp hematopoietic necrosis virus (Somamoto et al., 2015). However, the mechanisms of this apparent protection are still to be determined.

Some studies have reported changes in specific immune cells populations in the gills. Cd8+ and IgM+ cells in rainbow trout gills were both found in have altered gene transcript levels following viral haemorrhagic septicemia virus (VHSV) infection (Aquilino et al., 2014). The proportion of CCR7+ cells (mostly B cells) was also altered following viral infection (Castro et al., 2014). However, some studies also report a lack of change in certain immune cell populations (Aquilino et al., 2014; Scapigliati et al., 2010; Somamoto et al., 2015). Studies have also reported changes in transcript levels of immune cell markers, which can indicate changes in cellular activity but only provides an estimate of cell presence (Aquilino et al., 2014; Austbø et al., 2014). Furthermore, there is a lack of information on the proliferation and migration dynamics which may explain some of these cellular changes. Epithelial cells are also important in the response to RVIs and like the mammalian respiratory tract, gill epithelial cells can be infected by viruses (Thoen et al., 2020; Weli et al., 2013). However, information on their innate immune response is lacking. Overall, more information is needed to understand how changes, or lack of changes, in immune cell populations impact disease progression and antiviral immunity in the gills.

1.4 Zebrafish as a model for immunology research

Zebrafish (*Danio rerio)* are a vertebrate species belonging to the bony fish group, rather than the cartilaginous fish group which includes sharks and rays. More specifically, zebrafish are teleosts, a group of fish that make up the vast majority (98%) of extant ray-finned fish - *Actinopterygii* (Ravi and Venkatesh, 2018). Teleosts are a vastly diverse group of almost 30,000 identified species, including fish used in aquaculture, such as salmon and trout, and other model organisms, such as medaka. Studying zebrafish can therefore help answer questions on vertebrate biology, evolutionary biology, and food security.

1.4.1 Zebrafish as a model organism

Zebrafish have been used since the 1970s as a model organism in numerous fields including developmental biology, neuroscience and immunology. They are increasingly popular due to their genetic tractability, ease of *in vivo* imaging, small size and high fecundity. Zebrafish have orthologues with about 70% of human genes indicating that despite some major physiological differences and evolutionary distance, they share fundamental biological components. They also have orthologues for 82% of human disease-associated genes (as classified in the Online Mendelian Inheritance in Man database), highlighting their value for studying disease (Howe et al., 2013).

It is estimated that the ancestors of teleosts underwent a whole genome duplication (WGD) distinct to mammalian ancestors 320 Mya. Certain teleost species also show evidence of an additional WGD but this is not the case in zebrafish (Ravi and Venkatesh, 2018). The teleost-specific WGD means that zebrafish have many duplicated orthologues of mammalian genes. The zebrafish genome has been fully assembled and many genes have been annotated. This allows for comparisons with other model organisms and for genetic manipulation of target loci, including potential mammalian orthologues. Tools like CRISPR and TALENs are well established in zebrafish making genetic editing accessible and relatively straightforward. In addition, modified antisense DNA oligonucleotides (morpholinos) can be administered to knockdown genes, particularly in zebrafish embryos (Trede et al., 2004).

Zebrafish also offer many practical advantages: they are small organisms that can be easily maintained in large quantities and at much lower cost than mammalian species. They can also be bred easily, with female fish capable of releasing hundreds of eggs at one time (Skinner and Watt, 2007). In addition, their *ex utero* fertilisation and development allows manipulation and monitoring of development from the earliest stages.

Zebrafish are optically translucent during early stages in development. This allows for visualisation of some physiological processes such as blood circulation, intestinal peristalsis and heartbeat. There are also several mutant zebrafish lines which lack pigmented cells and allow *in vivo* visualisation at older stages (Antinucci and Hindges, 2016; White et al., 2008). In addition, many transgenic zebrafish reporter lines have been produced which express fluorescent proteins under control of specific gene promoters. This allows visualisation of different cell types *in vivo,* including immune cells. As a result,

66

many studies have been able to document the dynamics and transcript profiles of immune cells responding to pathogens, tissue injury, and foreign material (Lin et al., 2019; Nguyen-Chi et al., 2015; van Pomeren et al., 2019; Willis et al., 2018). This is a major advantage compared to commonly used mammalian species which require invasive and complex procedures for live *in vivo* imaging. Several microscopy methods have been used for live *in vivo* imaging of zebrafish, each providing different levels of cost, resolution, acquisition speed, and sample handling. For example, stereomicroscopy offers easy sample handling and lower cost, whilst confocal microscopy is more expensive but allows for much higher resolution. Lightsheet microscopy has also been increasingly used for zebrafish imaging as it can achieve high signal to noise ratios and is less toxic for live organisms (Abu-Siniyeh and Al-Zyoud, 2020). Optical projection tomography has also been used to acquire complete 3D images of live zebrafish adult and embryos (Andrews et al., 2016; Kumar et al., 2016)

1.4.2 Zebrafish immunology

With regards to their immunology, zebrafish have most of the same immune cell types (phagocytes, granulocytes, and lymphocytes), genes, and effector functions as mammalian species (Meeker and Trede, 2008). Both innate and adaptive immune systems are present in zebrafish, with the former developing from 1 day post fertilization (dpf) (Herbomel et al., 1999). Components of the adaptive immune system are present in early development but only seem functional from 4-6 weeks post fertilization (Novoa and Figueras, 2012). Zebrafish orthologues of mammalian immune-related genes include major cytokine families (IFNs, chemokines, and interleukins), receptors (PRRs, cytokine receptors, adhesion molecule receptors), antimicrobial genes (ISGs, antimicrobial peptides), and effector molecules (immunoglobulins, perforins, complement proteins) (Novoa and Figueras, 2012; Varela et al., 2016).

Polarisation of immune responses has been extensively described in mammals and is important for appropriate immune responses to different infections and insults (Cosmi et al., 2014; Murray et al., 2014). There has been some investigation of macrophage and T cell polarization in zebrafish but further characterization is needed to determine how far zebrafish cell phenotypes and functions mirror mammalian polarization (Dee et al., 2016; Nguyen-Chi et al., 2015). Several tools are available to investigate zebrafish

immunology, in addition to those previously described. These include flow cytometry and scRNA-Seq which will be reviewed in further detail in Chapter 3.

1.4.2.1 Immune mediators

Molecular pattern recognition, cell activation, and effector functions show some conservation between zebrafish and mammals, but differences also exist. Orthologues of mammalian PRRs have been identified in zebrafish, along with fish-specific receptors (Li et al., 2016). The ligands for some of these receptors have been identified in zebrafish but many receptors still require functional characterisation to fully understand how these compare to proposed mammalian orthologues. Zebrafish can respond to many of the same PAMPs and synthetic TLR agonists as mammalian species with some showing conservation in responses and signaling pathways. These receptors will be covered in more detail in Chapter 4. With regards to TLRs, current research has proposed that zebrafish contain orthologues for 10 of 12 human TLRs, and some fish-specific TLRs (Table 1.1). This partial conservation in TLR genes highlights the importance of this evolutionary ancient arm of immunity, whilst the presence of fish-specific genes emphasises the importance of considering differences in immune pathways between vertebrate species.

Zebrafish gene	Human orthologue	Ligands	Reference
tlr1	Similarities to *TLR1/TLR6/TLR10*	Potential ligand: triacylated lipopeptides	(Jault et al., 2004; Meijer et al., 2004)
tlr2	*TLR2*	Some evidence for Pam3CSK4, a synthetic triacylated lipopeptide	(Yang et al., 2015)
tlr3	*TLR3*	Potential ligand: dsRNA	(Matsuo et al., 2008)
tlr4a/b	*TLR4*	Unknown	(Li et al., 2016; Meijer et al., 2004)
tlr5a/b	*TLR5*	Some evidence for bacterial flagellin	(Yang et al., 2015)
tlr7	*TLR7*	Potential ligand: ssRNA	(Meijer et al., 2004)
tlr8a/b	*TLR8*	Potential ligand: ssRNA	(Meijer et al., 2004)
tlr9	*TLR9*	Unmethylated CpG DNA motifs	(Yeh et al., 2013)
tlr14	*Non-mammalian – some similarities to TLR10/TLR6*	Unknown	(Li et al., 2016)
tlr18	*Non-mammalian - some similarities to TLR1/TLR6/TLR10*	Unknown	(Meijer et al., 2004)
tlr19	*Fish-specific*	Potential ligand: dsRNA	(Ji et al., 2018; Meijer et al., 2004)
tlr20a/b/c/d	*Fish-specific*	Unknown	(Pietretti et al., 2014)
tlr20e/f	*Fish-specific*	Predicted to be pseudogenes	(Pietretti et al., 2014)
tlr21	*Non-mammalian - functional similarities to TLR9*	Unmethylated CpG DNA motifs	(Yeh et al., 2013)
tlr22	*Fish-specific - potentially functionally equivalent to TLR3*	Potential ligand: dsRNA	(Matsuo et al., 2008)

Table 1.1 List of zebrafish TLR genes

Zebrafish contain many cytokines like in mammals but due to low sequence conservation, orthologous relationships between genes can be hard to determine (Huising et al., 2006). It has been proposed that cytokine receptors and signalling components show greater conservation between fish and mammals than the cytokines themselves (Stein et al. 2007; Carradice and Lieschke 2008). However, some key cytokine homologs have been identified in zebrafish, including those associated with infection: TNF-α, IL-1β, IL-6, and IL-10 (Van Der Vaart et al., 2012; Varela et al., 2017).

Interferons are part of the class II helical cytokine family and in mammals form three types: type I IFNs (including α, β, ε, κ, and ω) and type III IFNs (λ), which are induced by viral infection, and type II IFNs (γ) which have more immunomodulatory functions (Schoggins, 2019). In teleosts, orthologues for type I and type II IFNs have been identified but not for type III IFNs. The repertoire of IFNs can vary considerably between fish species highlighting the importance of investigating species-specific differences. In zebrafish there are four type I IFNs: IFNΦ1, IFNΦ2, IFNΦ3, and IFNΦ4, and two type II IFNs: IFNγ1 and IFNγ1rel (Langevin et al., 2013a; Zahradník et al., 2018). Induction and activity of zebrafish type I IFNs during viral infection is well established with some studies clearly demonstrating antiviral effects (Boucontet et al., 2018; López-Muñoz et al., 2010; Palha et al., 2013; Phelan et al., 2005). Type II IFNs can also be induced by viral infection in zebrafish although this is not always the case in zebrafish larvae (Aggad et al., 2010; Novoa et al., 2006). Overexpression of *ifng1* or *ifng1rel* (previously named *ifng2*) in zebrafish larvae was not found to protect against viral infection. However, both IFNs induced upregulation of type I and type II IFNs, ISGs, proinflammatory cytokines and antigen presentation-related genes suggesting that they do play a role in modulating immune responses (López-Muñoz et al., 2011). Zebrafish have many ISGs, including orthologues of mammalian genes, and these are induced type I and II IFNs and during viral infection (Aggad et al., 2009; Briolat et al., 2014; López-Muñoz et al., 2011; Phelan et al., 2005). At least one of these ISGs, ISG15, has antiviral activity *in vivo* (Langevin et al., 2013b). Few studies have investigated the cells responsible for IFN expression in zebrafish but one study revealed that neutrophils and hepatocytes can both produce *ifnphi1* transcripts (Palha et al., 2013). This parallels the expression of type I IFNs in immune and non-immune cells in mammals. Many zebrafish studies use larvae and therefore cannot investigate mature adaptive immune cells, which are known to be a source of IFNs in mammals.

Other immune mediators have been identified in zebrafish including AMPs and complement proteins (Caccia et al., 2017). AMPs are present in the zebrafish gut, skin and gill mucosa indicating similarities with the mammalian mucosa (Shike et al., 2004; Yang et al., 2017). Complement proteins are soluble plasma proteins that induce inflammation and initiate pathogen clearance through lysis and opsonisation (Geller and Yan, 2019). Complement genes in zebrafish are expressed from embryonic stages and can be upregulated by LPS or bacterial challenge and are involved in host defense against *Escherichia coli* bacteria (Lü et al., 2014; Wang et al., 2008a, 2008b).

1.4.2.2 Innate immune cells

Innate immunity is the non-antibody mediated arm of the immune system that relies on recognition of conserved microbial products by germline-encoded receptors. In zebrafish it develops earlier than adaptive immunity. This allows investigation of innate immunity independently from the adaptive immune system in zebrafish embryos and larvae. This is useful to understand the specific contributions the of innate immune system, for example, transcriptome analysis of *Salmonella typhimurium*-infected embryos revealed conserved immune responses to infection in human cell lines, but also enabled identification of genes with novel putative immune function (Stockhammer et al., 2009). In adult fish it would be difficult to link genes with poorly characterised function to the innate immune response. However, for questions involving adaptive immunity, this requires older fish which are larger, providing more material to work with but proving less practical for *in vivo* microscopy.

Multiple types of granulocytes have been identified in zebrafish. Like in mammalian species, zebrafish neutrophils are rapidly recruited to the site of infection or injury (Le Guyader et al., 2008; Renshaw et al., 2006). Some of this recruitment has been linked to the chemokine CXCL8 which is found in both humans and zebrafish (de Oliveira et al., 2013; Sarris et al., 2012). Interestingly, CXCL8 homologs are not present in mice or rats which highlights that humans have more conservation with zebrafish in some cases (Hol et al., 2010). Mast cells and eosinophils/basophils have also been identified in zebrafish based on functional and morphological analysis (Balla et al., 2010; Dobson et al., 2008). It is currently unclear whether eosinophils and basophils are distinct populations in this species.

Multiple studies have characterized different mononuclear phagocytes (DCs and monocytes/macrophages) in zebrafish. Interestingly, some macrophage-like cells in the skin, fins and gills arise from non-haematopoietic lineages in zebrafish (Alemany et al., 2018; Lin et al., 2019). This highlights the heterogeneity of cell populations and the need to perform functional analyses. Characterisation of DCs in zebrafish is limited as transgenic lines have not been developed, specific gene markers have not been identified, and different DCs subsets have not been described (Moyse and Richardson, 2020).

As previously mentioned, NK-cells, ILC-1-, ILC2- and ILC3-like cells have been identified in zebrafish gut and kidney (Hernández et al., 2018; Moore et al., 2016b; Muire et al., 2017; Pereiro et al., 2015; Tang et al., 2017). Further functional, phenotypic and tissue characterisation is needed to determine the distinctions between NCCs and NK cells and the homology between zebrafish and mammalian ILCs.

1.4.2.3 Adaptive immunity

In contrast to innate immunity, adaptive immunity relies on somatic gene rearrangement of lymphocyte receptors. These genetic rearrangements produce diverse repertoires of receptors that allow highly specific recognition of the many pathogens and exogenous materials that organisms encounter in their lifetime. Adaptive immunity is thought to have developed during the emergence of early vertebrates and is present in all extant vertebrates, including teleosts (Boehm and Swann, 2014).

Long-lasting antibody secreting plasma B cells have been described in zebrafish based on transcript analysis but not functional analysis (Page et al., 2013). In contrast to mammalian species, antibody class switching does not occur in zebrafish B cells (Danilova et al., 2005). Affinity maturation and somatic hypermutation does seem to occur but, as measured in other teleost species, this is not to the same extent as in mammals (Lewis et al., 2014).

There has been some characterisation of T cell subsets in zebrafish and evidence currently supports the existence of Th2, Treg, and γ+δ+ cells (Dee et al., 2016; Wan et al., 2017). Some studies have also reported increased transcript levels of Th2, Treg, Th17 and Th1-related genes in zebrafish tissues following vaccine or infection challenges (Zhang et al., 2014). However, these studies did not investigate the cells responsible for these changes. Another study found that CD4.1+ lymphocytes (likely T cells) expressed Th1,

Th2 and Th17 cytokines following antigen challenge, but did not investigate if distinct lymphocyte subsets expressed different cytokines (Yoon et al., 2015). Although CD8+ T cells have been identified, their cytotoxicity has not been functionally investigated (Martins et al., 2019a).

In mammals, initiation of adaptive immune responses takes place in germinal centres in secondary lymphoid tissues like the spleen, lymph nodes and MALT. Although teleosts have spleens and MALT, they appear to lack lymph nodes or germinal centres (Castro et al., 2013; Wittamer et al., 2011). However, melanomacrophage centres in teleosts, including zebrafish, have been hypothesised to function as primitive germinal centres. These structures are aggregates of melanomacrophages – highly pigmented phagocytic cells – and are found in several tissues including haematopoeitic tissues (kidney and spleen) and occasionally in the gills (Agius and Roberts, 2003; Sanders et al., 2003; Vigliano et al., 2006). These melanomacrophages have been found to respond to environmental changes and infection and are capable of trapping antigen long-term (Lamers and De Haas, 1985; Suresh, 2009). They have also been found in close association with lymphocytes, including those positive for immunoglobulin. In addition, both melanomacrophages and lymphocytes can increase in number following immune challenge. However, lack of lymphoid compartmentalization and poor correlation with antibody production levels indicates that melanomacrophage centres may not be directly equivalent to mammalian germinal centres (Steinel and Bolnick, 2017).

One of the hallmarks of adaptive immune responses in mammals is the establishment of immunological memory. It is broadly defined as the ability to respond more rapidly and robustly to a secondary immune challenge following primary exposure. Zebrafish and other teleosts have been found to develop stronger secondary antibody responses following antigen challenge indicating establishment of immunological memory (Lam et al., 2004; Lumsden et al., 1995; O'Dowd et al., 1999). In addition, primary infection or vaccination is protective in zebrafish against a number of pathogens (Gao et al., 2014; von Gersdorff Jørgensen, 2016; Novoa et al., 2006). However, the mechanisms for this are not well understood. There is some evidence that protection may be mediated in part by innate immunity through innate lymphocytes or through enhanced granulopoiesis (Hohn and Petrie-Hanson, 2012; Willis et al., 2018). The role of adaptive responses has not been extensively researched and questions remain about the existence of memory lymphocyte

populations and magnitude of humoral and cytotoxic responses during secondary challenge.

1.4.3 Zebrafish viral infections

Although natural viral infections of zebrafish have been rarely described, this species is susceptible to experimental infection by multiple mammalian and fish viruses. Consequently, responses to viral infections have been studied in zebrafish embryos, larvae and adults. Key aspects of the antiviral response have been investigated including immune cell recruitment, tissue pathology, transcriptional regulation, and activation of signalling pathways (Langevin et al. 2013; Goody, Sullivan, and Kim 2014; Kavaliauskis et al. 2016). Zebrafish viral infection models and the associated immune response will be explored in more detail in Chapter 5. Of particular interest to this project is IAV which has been used to infect zebrafish embryos but has not yet been tested in adult stages (Gabor et al., 2014). Studying viral infection in zebrafish provides an opportunity to interrogate numerous aspects of zebrafish immunology. These included poorly understand concepts such as the mechanisms and nature of adaptive immune responses, the role of lymphocytes, the role of MALT and in the case of this project, of GIALT.

1.4.4 Zebrafish gill models of respiratory inflammation and infection

Several models have been established to study inflammation and infection in the gills. Aside from their previously described immune components, the gills are highly accessible making them easy to work with and allowing non-invasive procedures to be performed. Repeated gill sampling of individual fish can also be performed, reducing inter-individual variability and allowing longitudal analysis. Local infection of the swimbladder has also been used as a model of epithelial or respiratory infection (Ho et al., 2019; Sullivan et al., 2017). Despite developmental and transcriptomic similarities, the zebrafish swimbladder is thought to play a role in buoyancy and sound perception rather than gas exchange and lacks a comparable highly-branched architecture to the lungs (Perrin et al. 1999; Zheng et al. 2011). The zebrafish gills are therefore a more analogous system to study respiratory mucosal immunology.

Previous work in the Dallman lab established cigarette smoke exposure in zebrafish as a useful model to study respiratory tissue inflammation and repair (Progatzky et al., 2015). Following exposure, zebrafish gills mounted an inflammatory response characterised by higher transcript levels of proinflammatory cytokines, a phenomenon also seen in mammals. In addition, early structural changes in smoke exposed gills reflected some of the changes observed in mammals. Notably, structural changes and collagen deposition in the gills were reversible even after several weeks of smoke exposure. This contrasts with human lungs where long-term cigarette smoke exposure has been linked to fibrotic pulmonary disease (Oh et al., 2012).

Further work in the Dallman lab has also focused on establishing a model of gill inflammation more closely related to viral infection. Synthetic agonists resiquimod (R848) and poly(I:C), were used to challenge the gills and assess their immune response. These compounds stimulate nucleic acid-sensing PRRs, TLR7/8 and TLR3, which are involved in viral detection. In collaboration with researchers at Imperial College London, the immune responses to these agonists were also assessed in human and mouse intranasal challenges. R848 induced a robust IFN and pro-inflammatory cytokine response in all three species with strikingly similar kinetics. In contrast, poly(I:C) induced a response in mouse but not in zebrafish or humans. These results demonstrated clear species-differences and therefore the need to expand the selection of respiratory models in immunology research. In addition, the response to R848 showed the potential of the zebrafish gill for further use in viral infection research. As part of this PhD project, the cellular response to R848 was also investigated, part of which is detailed in the study by (Progatzky et al., 2019).

Other research groups have reported on the effects of viral infection in zebrafish gills however, these studies have focused on pathology and rarely examine the immune responses and viral load of this tissue (Bermúdez et al., 2018; Burgos et al., 2008; Cho et al., 2019; Encinas et al., 2013; Gabor et al., 2014; Novoa et al., 2006; Sanders et al., 2003). Studies in other teleosts species have provided slightly more insight into the role of the gills in viral infection (section 1.3.2.3). This highlights a clear gap in zebrafish research which will be addressed in this thesis.

1.5 Aims

The literature review highlights that research on respiratory viral infections would benefit from additional *in vivo* models where the respiratory mucosa can be easily accessed, monitored and manipulated. In this thesis I evaluate the zebrafish gills as one potential model by testing the following hypotheses:

1. Zebrafish gills are immunocompetent tissues that respond to non-infectious stimuli and viruses.
2. The gill immune response is similar to responses observed in respiratory mucosa of human and other mammalian species.

In the following chapters I test these hypotheses by focusing the following aims:

1. Characterising immune cell development, composition, and function in zebrafish gills to understand how this tissue compares to mammalian respiratory mucosa.
2. Assessing the response of zebrafish gills to immunostimulants to interrogate the different immune pathways in the gills.
3. Assessing whether zebrafish gills can be infected with human respiratory viruses or fish-endemic viruses.

2 Chapter 2 – Methods and materials

2.1 Zebrafish maintenance

Zebrafish were reared and maintained at 28.5°C on a 14h light/10 h dark cycle. For zebrafish breeding, eggs from individual or multiple crosses were collected and maintained in methylene blue (MB) solution (0.3 ppm in aquarium system water) until 5 dpf. Larvae were reared in embryo E2 media (15 mM NaCl, 0.5 mM KCl, 1 mM $MgSO_4$, 0.15 mM KH_2PO_4, 0.05 mM Na_2HPO_4, 1 mM $CaCl_2$, 0.7 mM $NaHCO_3$) containing penicillin/streptomyocin (10 U penicillin, 10 μg streptomyocin, GIBCO) from 6-14 dpf and fed on ZM000 (6-8 dpf, ZM Fish Food & Equipment) and ZM100 (9-14 dpf, ZM Fish Food & Equipment) food. Larvae were transferred to a circulating aquarium system at 15 dpf and fed ZM200 (ZM Fish Food & Equipment) food until 2 mpf. From 2 mpf onwards they were fed brine shrimp (ZM Fish Food & Equipment) and Hikari Micro Pellets (ZM Fish Food & Equipment) daily.

All regulated procedures were performed in accordance with UK Home Office requirements (ASPA 1986) under the project license P5D71E9B0 and personal license IA2AC7A94. Zebrafish lines used are detailed in Table 2.1. *Tg(cd4.1:mCherry; lck:GFP) and Tg(IgM:GFP)* lines were kindly provided by Dr Adam Hurlstone (University of Manchester).

For experiments on adult zebrafish, fish at 3-14 months post fertilisation (mpf) were used unless otherwise stated. Both male and female zebrafish were used where possible and in as equal numbers as possible for each experiment. Following most experimental procedures, fish were maintained in static water tanks at 28.5°C unless otherwise stated. For adult viral and temperature challenges, fish that were kept for 24 hours or more were fed daily with Hikari Micro Pellets (ZM Fish Food & Equipment) and water was also replaced daily. Fish were monitored daily for breathing, feeding and swimming behaviour to check for any signs of ill health.

Line	Background	Description	Reference
Wildtype (WT)		Non-genetically modified wildtype zebrafish	
Tra-/-Nac-/- (*TraNac*)		Mutants lack pigment-producing iodophores and melanocytes due to homozygous mutations in the *mpv17* and *mitfa* genes.	(Krauss et al., 2013; Wenz et al., 2020; White et al., 2008)
casper		Mutants lack pigment-producing iodophores and melanocytes due to homozygous mutations in the *mpv17* and *mitfa* genes.	(D'Agati et al., 2017; White et al., 2008)
Tg(fli:GFP)	*casper*	GFP is expressed in endothelial cells.	(Lawson and Weinstein, 2002)
Tg(lyz:GFP)	*TraNac*	GFP is expressed in some neutrophils.	(Hall et al., 2007; Wittamer et al., 2011)
Tg(lyz:dsRed)	*TraNac*	dsRed is expressed in some myeloid cells	(Hall et al., 2007; Wittamer et al., 2011)
Tg(lck:GFP)	*TraNac, tra (mpv17-/-), or nacre (mitfa-/-)*	GFP is expressed in T/NK lymphocytes. Fish used were double or single mutants for *mpv17* and *mitfa* genes.	(Langenau and Zon, 2005)
Tg(mpx:GFP)	*casper*	GFP is expressed in neutrophils	(Renshaw et al., 2006)
Tg(mpeg1:Caspase1biosensor) Referred to as Tg(mpeg1.1:SECFP-YPet) in this thesis	*TraNac*	The fluorescent proteins SECFP and YPet are linked by a YVHDA amino acid motif which can be cleaved by zebrafish caspase A and B.	(Andrews, 2016; Ramel, personal communication)
Tg(cd4-1:mCherry) Tg(cd4-1:mCherry; lck:GFP)	*casper* or WT	mCherry is expressed in certain T cells and myeloid cells; GFP is expressed T, natural killer (NK)-like and innate lymphoid cell (ILC)-like cells.	(Dee et al., 2016)

Tg(cd4-1:mCherry;fli:GFP)	WT x *casper* genetic cross	mCherry is expressed in certain T cells and myeloid cells; GFP is expressed in endothelial cells.	(Dee et al., 2016; Lawson and Weinstein, 2002)
Tg(IgM:GFP) Tg(IgM:GFP; cd4-1:mCherry)	WT	GFP is expressed in a subset of B cells. mCherry is expressed in certain T cells and myeloid cells.	(Dee et al., 2016; Page et al., 2013)

Table 2.1 Zebrafish lines used in this thesis.

2.2 Viruses

Plaque-purified human RSV (grown in human epithelial type 2 (HE-p2 cells), originally from A2 strain, ATCC, US) and uninfected HE-p2 cell supernatant were kindly provided by Dr Cecilia Johansson (National Heart and Lung Institute, Imperial College London).

A/Puerto Rico/8/34 (PR8) and A/X-31 (X31) influenza viral stocks were kindly provided by Professor Wendy Barclay with assistance from Jennifer Shelley and Dr Jay, Jie Zhou (Department of Infectious Disease, Imperial College London).

IPNV (strain CD 975/99) was passaged five times and propagated in chinook salmon embryo cells (CHSE214 cells) from a clinical isolate. The viral stock was kindly provided by Professor Ross Houston with assistance from Dr Jon Pavelin (Roslin Institute, University of Edinburgh)**.**

2.3 Harvesting zebrafish tissues

Fish were culled in 400 mg/L MS-222 followed by brain destruction with a scalpel. For collection of gill tissues, the operculum was removed and gill arches detached from the gill cavity. Contaminating blood or non-gill tissue was removed, and individual arches were separated when necessary. For collection of the gut, the head was removed and the body open along the ventral side. Internal organs were removed and the gut separated. The gut was stretched out and cut into the distal and proximal sections. For collection of (whole kidney marrow) WKM, the head, trunk, and tail kidney tissue on the dorsal side of the body cavity was harvested and any contaminating oocytes, or bones were removed. The dorsal aorta, which runs directly below the kidney, could not be separated and therefore was included with the kidney forming the WKM.

2.4   Flow cytometry

WKM was dissociated into a single cell suspension by passing the tissue through a 40 μm cell strainer with 2% fetal calf serum (FCS) solution in phosphate-buffered saline (PBS). Gill tissue was digested with collagenase (2 mg/ml) for 10 mins at 37°C. Digested tissue was mixed with FCS solution (2% in PBS) and mechanically disrupted by pipetting the mixture up and down. The cell suspension was then centrifuged, supernatant removed, and resuspended in FCS solution (2% in PBS). This suspension was then filtered through a 40 μm cell strainer. 4′,6-diamidino-2-phenylindole (DAPI) was added to samples (final concentration 1 μg/ml) a few minutes prior to processing on 4 or 5-laser BD LSRFortessa analyzers in the Department of Life Sciences Flow Cytometry Facility (Imperial College London) using BDFACSDiva software (BD Biosciences).

For compensation controls, gill or WKM tissue from WT fish (with DAPI, without DAPI or with ovalbumin (OVA)-AF647 or R848-ATTO488 compounds) and from single colour transgenic fish (without DAPI) were processed.

Data was analysed with FlowJo™ software (Becton, Dickinson & Company).

2.5   Cytospinning and staining of gill cells

Gill tissue was processed into single cell suspensions as described above. Samples from all 8 arches of 6 fish were pooled into one sample and processed on a BD FACSAria III cell sorter by Dr Jane Srivastava and Dr Radhika Patel (Department of Life Sciences Flow Cytometry Facility, Imperial College London). Cells were sorted by forward scatter-area (FSC-A) and side scatter-area (SSC-A) into four populations (Figure 2.1). This was performed to enrich samples for different leukocytes so they could be more easily identified following cytospinning. For lymphocyte and myeloid-like populations, enough cells were collected to sort these samples a second time and potentially further enrich populations for cells of interest.

Sorted cell samples were adjusted to a concentration of 50,000 cells/100 μl or less. 100 μl per cell suspensions was cytospun onto glass slides for 3 mins at 300 rpm, using the CytoSpin 3 Cytocentrifuge (Shandon Scientific). Slides were air dried for 1 h then dipped in methanol to fix cells. Slides were further air dried for 5 mins before dipping in Wright-Giemsa stain for 30 seconds. Slides were next dipped in PBS for 1 min and thoroughly

rinsed under running deionized water (dH$_2$O). After overnight drying, glass coverslips were affixed onto the cells using clear nail varnish.
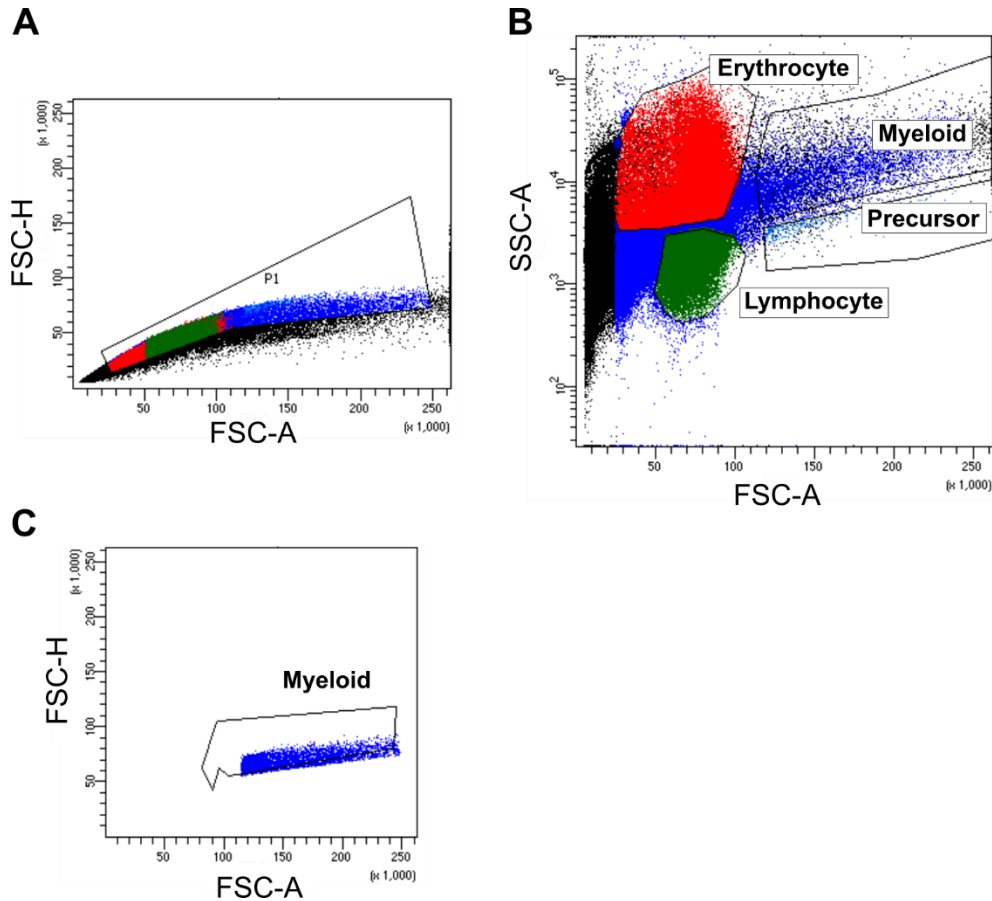
Figure 2.1 Flow cytometry sorting strategy of adult gill tissue.

Gill tissues from WT fish (n = 6) were digested with collagenase into single cell suspensions and pooled. Cells were processed on a BD FACSAria III cell sorter by Dr Jane Srivastava and Dr Radhika Patel (Department of Life Sciences Flow Cytometry Facility, Imperial College London). A) Non-singlet cells were excluded by gating total cells on FSC-area (FSC-A)/FSC-height (FSC-H). B) Cells were then gated on into four populations (erythrocyte, myeloid, precursor and lymphocyte) according to their FSC-A/SSC-A properties. Plot illustrates gates but shows all cells prior to exclusion of non-singlet cells. C) Individual cell populations were further gated to more stringently exclude non-singlet cells. Myeloid cells shown as an example.

2.6   Whole mount immunostaining

Whole larvae, whole fish heads, and dissected gill arches were fixed in 4% paraformaldehyde (PFA) at 4°C for 1-3 days. Gill arches were separated from the fish heads before continuing to further processing. Samples were washed in PBS followed by dH$_2$O before immersing in ice-cold methanol for 10 mins. Samples were further washed

with dH$_2$O then washed twice in PBST (PBS, 0.05% Triton X-100, 0.05% Tween-20). Next samples were incubated in blocking buffer (PBST, 1% DMSO, 5% serum from species of secondary antibody – see Table 2.2) for 30 mins. Following this, samples were incubated with primary antibodies (Table 2.2) overnight at 4°C.

The following day, samples were washed with four times in 20 mins stages with PBST. Samples were subsequently incubated with secondary antibodies (Table 2.2) in the dark at room temperature for 4 hrs. Samples were then washed twice with PBST in 20 mins stages before incubating in DRAQ5™ (5µM in PBS, ThermoFisher Scientific) for 15 mins. Samples were further washed in PBS and PBST before storing in PBST at 4°C.

Antibody	Species	Dilution	Supplier	Transgenic targets
Primary antibodies				
Anti-GFP	Chicken	1:1000	Abcam (ab13970)	*lck*:GFP, *lyz*:GFP, *mpx*:GFP, *IgM*:GFP, *mpeg1.1*:SECFP-YPet
Anti-RFP	Rabbit	1:1000	MBL (PM005)	*Cd4.1:*mCherry
Secondary antibodies				
Anti-chicken AF488	Donkey	1:500	Jackson ImmunoResearch (703-545-155)	N/A
Anti-rabbit AF555	Goat	1:300	ThermoFisher Scientific (A-32737)	N/A

Table 2.2 List of antibodies used for immunostaining

2.7 Microscopy

All confocal and widefield microscopy was performed in the Facility for Imaging by Light Microscopy (Faculty of Medicine, Imperial College London).

2.7.1 Confocal microscopy of fixed immunostained samples

Immunostained and/or fixed gills (4 % PFA) were placed in a glass-bottomed dish in PBST or PBS and imaged with a Leica SP5 inverted confocal microscope with a 10X or 20X air objective.

2.7.2 Widefield microscopy of cytospun cells

Slides with cytospun and stained cells were imaged with a Zeiss Axio Observer inverted widefield microscope with a 40X air objective.

2.7.3 Live intravital microscopy of zebrafish adults and larvae

Fish were anaesthetised in 168 mg/L MS-222. 5-15 dpf larvae were mounted on a glass coverslip in 0.8 % low melt agarose whilst fish 21 dpf or older were placed directly in a glass-bottom dish or plastic Petri dish. Fish 21 dpf or older were returned to tanks on an aquarium system with circulating water following recovery from anaesthesia. Images were acquired with a Zeiss Axiovert 200 widefield microscope with a 10X or 20X objective. Images of 7 dpf *Tg(lyz:GFP)* fish were acquired with a Leica SP5 inverted confocal microscope with a 20X objective.

For intravital imaging of adult *Tg(lyz:dsRed)* fish without the operculum, fish were euthanized in 400 mg/L MS-222 and the operculum was cut off using dissecting scissors. This did not result in any bleeding, or damage to the gills. Images were acquired with a Leica M205 FCA stereomicroscope.

2.7.4 Live microscopy of dissected gill tissue

Gills were dissected from adult zebrafish and separated into individual arches. For imaging with a Leica M205 FCA stereomicroscope arches were placed in a plastic Petri dish in PBS. For imaging with a Leica SP5 inverted confocal microscope, arches were placed on a glass-bottom dish and covered with FCS solution (2% in PBS). Confocal images were acquired with a 20X air objective.

2.7.5 Imaging analysis

Imaging processing and analysis was performed with ImageJ (Rueden et al., 2017) or Icy software (de Chaumont et al., 2012).

Images of cytospun cells were cropped and adjusted for color balance to allow clear representation of cellular features.

Detection and analysis of *lck*:GFP+ cell clusters in the gills were performed with Icy software. Maximum projections were generated from confocal z-stacks of gills at 170X magnification and cropped to focus on the arch region. Binary images of the GFP channel were created using the k-means thresholder plugin. These images were segmented to detect clusters using the HK-means plugin (Dufour et al., 2008). The edges of these

clusters were more precisely defined using the active contours plugin (Dufour et al., 2011). Following identification of clusters, these were compared with the original maximum projection to manually exclude any clusters which were noise rather than GFP signal, exclude portions of the clusters which fell outside of the arch, and determine the location of individual clusters within the arch. Areas of these clusters was calculated using the ROI statistics plugin.

Lck:GFP+, *lyz*:GFP+ and *cd4.1*:mCherry+ cells were counted in maximum projections of the gills using Icy software. Regions of interest were manually defined to identify cells solely in the first 20 secondary lamellae from the arch. Sets of lamellae that are clearly damaged or obstructed were excluded from analysis. Individual cells were detected in these regions using the spot detector plugin (Olivo-Marin, 2002).

2.8   Immunostimulant challenges in zebrafish

2.8.1   Topical gill challenge and intraperitoneal challenge with R848, LPS, Pam3CSK4, or CpG-ODN 2007

For topical gill challenge adult zebrafish were anaesthetised in 168 mg/ml MS-222 and placed laterally on a Petri dish. The operculum and gills were dried with tissue before applying 5 μl of 0.5 mg/ml resiquimod (R848, Sigma), Pam3CSK4 (Invivogen), CpG oligonucleotide (ODN)-2007 (Invivogen), lipopolysaccharide (LPS) from *Pseudomonas aeruginosa* (Sigma) or endotoxin-free water directly on gills for 5 mins. For i.p. challenge adult fish were anaesthetised and placed dorsally in a damp sponge. Fish were injected with 5 μl of the compounds described above. All immunostimulants were dissolved in endotoxin free water. Following challenge fish were recovered from anaesthesia in aquarium system water.

Challenges were performed with *TraNac* zebrafish except i.p. challenges with R848 which were performed with WT fish.

2.8.2   Oxytetracycline and R848 challenges

Adult WT zebrafish were immersed in 50 mg/L of oxytetracycline (OTC) for 10 days. OTC media was replaced daily. Following OTC treatment zebrafish were challenged with 5 μl of 0.5 mg/ml R848 applied to the gills as described above.

2.8.3 Topical gill challenge with fluorescent compounds

Fluorescent R848-ATTO488 was generated by Dr Lindsay Evans (Department of Chemistry, Imperial College London) using a protocol adapted from (Isobe et al., 2011). 5 µl of dissolved R848-ATTO488 [0.15 mg/ml in endotoxin-free water, 0.3% dimethyl sulfoxide (DMSO)] was directly applied to the gills of adult *Tg(cd4.1:mCherry)* zebrafish as described above. Ovalbumin-AF647 (Molecular Probes) was prepared as a 2 mg/ml solution in PBS and 5 µl of this solution was directly applied to the gills of adult *Tg(IgM:GFP; cd4.1:mCherry)* zebrafish.

2.9 Monitoring effects of temperature on adult zebrafish

For assessment of changes in immune gene transcription, adult *TraNac* zebrafish were maintained in static water tanks at 28.5°C or 33°C for 5 days. Water was pre-warmed and replaced daily. Gills were harvested after 5 days and analysed for RNA by qRT-PCR.

2.10 Viral challenges

2.10.1 RSV challenges

Adult *TraNac* fish were challenged by topical gill application with 10 µl of RSV (4.9 x 10^4 FFU) or uninfected HE-p2 cell supernatant. Adult *TraNac* fish were i.p. injected with 5 µl of RSV (2.45 x 10^4 FFU) or uninfected HE-p2 cell supernatant control. Fish were maintained at 28.5°C or 33°C in static water tanks until euthanasia and harvesting at selected timepoints.

2.10.2 RSV plaque assays

HE-p2 cells were seeded as monolayers in 96 well plates in DMEM media with 10% FCS and incubated overnight at 37°C. Next cells were washed with serum-free media. RSV samples (n = 2) were diluted in a 1:2 serial dilution from 1/500 to 1/512,000 in serum-free media and added to the cells. For each RSV sample each dilution was performed in triplicate on the same plate. Cells were incubated at 37°C for 2 hours followed by addition of pyruvate-free DMEM media with 2% FCS. Cells were further incubated at 37°C for 20 hours before being washed with PBS and fixed in methanol with 2% hydrogen peroxide for 20 mins. Next cells were incubated with biotin-conjugated goat anti-RSV antibody (Biogenesis, United Kingdom) at room temperature for 2 hours. This antibody was

detected by incubating cells with extravidin peroxidase for 1 hour followed by addition of diaminobezindine tetrahydrochloride (DAB) substrate (Sigma). Cells were washed in PBS then double distilled water and plaques were visualised and counted using an Olympus CKX41 fluorescent microscope. Viral titre was calculated for RSV aliquots and positive control using the number of plaques at the 1/1000 dilution and 1/4000 dilution respectively.

2.10.3 Influenza A virus challenges

Adult *TraNac* zebrafish were placed in static water tanks and acclimatised to 33°C over 5 days by increasing the temperature by 1°C every day. Fish were then challenged by topical gill application or i.p. injection with 5 µl of PR8 (1.4×10^5 PFU) or PBS. Fish were maintained at 33°C in static water tanks until euthanasia and harvesting at selected timepoints.

For embryo immersion challenges, *TraNac* embryos were spawned and kept in MB solution at 28.5°C until 2 dpf. They were then immersed in 2 ml of MB solution alone (control) or PR8 (2.8×10^5 PFU in MB solution) and maintained at 33°C for 3 days.

For embryo injection challenges, *TraNac* embryos were spawned and kept in E2 solution at 28.5°C until 2 dpf. They were then intravenously (i.v.) injected with 1-3 nl of X31 virus (2.65×10^5 PFU/ml), PR8 virus (1.8×10^2 PFU/ml or 2.8×10^7 PFU/ml) or PBS. Injected fish and uninjected controls were maintained in E2 solution at 33°C for up to 3 days.

2.10.4 Influenza cell growth kinetics

Madin-Darby Canine Kidney (MDCK) cells were seeded in monolayers and incubated at 37°C overnight. X31 and PR8 samples were diluted in serum-free Dulbecco's modified Eagle's medium (DMEM) medium to 1.2×10^4 PFU/ml and added to cells for 1 hour at 37°C. Diluted virus (0 h group) was separately collected for RNA extraction. Cells were then washed in PBS and incubated with serum-free DMEM with 1 µg/µl TPCK-trypsin at 37°C. Supernatant was collected every 24 hours. RNA was extracted using the QIAAmp RNA kit (Qiagen) and analysed for the viral M gene using the AgPathID one-step RT-PCR kit (Applied Biosystems). Samples were run in duplicate on a QuantiFlex PCR machine (Applied Biosystems).

To analyse the relative change in M gene transcripts the difference in cycle threshold (dCT) between each sample and the 0 h group was calculated. The fold change was then obtained by performing 2^-dCT.

2.10.5 IPNV challenges

Adult *TraNac* zebrafish were challenged by i.p. injection or topical gill application with 5 µl of IPNV (1.35×10^5 PFU) or PBS. Fish were recovered from anaesthesia and maintained at 28.5°C in static water tanks until euthanasia and harvesting at selected timepoints.

For challenges at lower temperature fish were gradually acclimatised from 28°C to 15°C over 5 days in static water tanks. Fish were then challenged with IPNV or PBS as described above.

2.11 Real time reverse transcriptase polymerase chain reaction (qRT-PCR) of zebrafish samples

Tissues from zebrafish were homogenized in 200 µl of TRIzol (ThermoFisher Scientific) and total RNA was extracted using the PureLink™ RNA Micro Kit (ThermoFisher Scientific) with DNAse treatment. RNA concentration and quality was measured using the Nanodrop 1000 or NanoDrop One spectrophotometers (ThermoFisher Scientific). For analysis of zebrafish transcripts or RSV genomic RNA, 125ng RNA per sample was used to synthesise complementary DNA (cDNA) using the High-Capacity cDNA Reverse Transcriptase Kit (Applied Biosystems) with random primers. cDNA was diluted 1:5 with water before further use. qPCR reactions for Taqman primer and probe pairs (Applied Biosystems) were prepared using 1 µl cDNA and 9 µl Taqman Fast Universal 2X Mastermix (Applied Biosystems) and water. qPCR reactions using oligonucleotide primers (0.5 µl each of forward and reverse primers) were prepared using 5 µl SyBr Green Mastermix 2X (Applied Biosystems), 1 µl cDNA and water.

For detection of RSV genomic RNA, qPCR reactions were prepared using 1 µl cDNA or L gene plasmid standard at different dilutions, 6.25 µl 2x QuantiTect Probe PCR Master Mix (Applied Biosystems), forward primer (0.9 µM), reverse primer (0.3 µM), probe (0.175 µM) and water. Standards, primers, and probes were kindly provided in part by Dr Cecilia Johansson (National Heart and Lung Institute, Imperial College London).

For detection of IPNV transcripts 500 ng of RNA was used to generate cDNA as described above except cDNA was not diluted. qPCR reactions were prepared 10 µl SyBr Green Mastermix 2X (Applied Biosystems), 1 µl cDNA, oligonucleotide primers (0.9 µM) and water.

For detection of IAV transcripts 500 ng RNA was used to generate cDNA using RevertAid Reverse Transcriptase with oligo(dT) primers (ThermoFisher Scientific). cDNA was diluted 0.8X with water before further use. qPCR reactions were prepared 10 SyBr Green Mastermix 2X (Applied Biosystems), 1 µl cDNA, oligonucleotide primers (0.2 µM) and water.

Reactions were run in duplicate or triplicate on a 7500 Fast Real Time PCR System Machine (Applied Biosystems) and CT threshold was set at 0.2. Any samples with fluorescence below this threshold were listed as 'undetermined' by the software.

2.11.1 qRT-PCR analysis

Transcript levels of zebrafish genes were analysed relative to 18S levels by calculating the -dCT between the gene of interest and 18S for each sample. Detection limits for primer/probe assays per tissue were determined by assessing the CT at which the standard deviation for technical replicates was consistently above 0.3 across many experiments. Any sample with a CT higher than the detection limit (Table 2.3) or with a CT listed as 'undetermined' was assessed as having too few transcripts to reliably detect and was not plotted on graphs or quantitatively analysed. For all other assays used, technical replicates were consistently precise (SD < 0.3) across all CT values obtained and therefore transcripts were considered to be above detection limits.

Assay	Gill	WKM
ifnphi1	34	32
ifng1	33	33
il1b	34	34
tnfa	32.5	33

Table 2.3 CT detection limits for qRT-PCR assays for gill and WKM tissue samples.

Fold change was calculated relative to the median of control groups using the 2-ddCT method (Livak and Schmittgen, 2001) and using 18S CT values to normalise CT values of genes of interest.

Absolute quantification of RSV L gene was performed using a standard curve of a plasmid containing the L gene. Copies of L gene were normalized to CT values of the zebrafish 18S gene and calculated per µg of RNA used in cDNA synthesis.

Transcript levels of IAV M gene were analysed by calculating the -dCT between IAV M gene and zebrafish *act1b* for each sample.

2.12 List of primers and probes

Gene	Taqman primers and probe ID, or oligonucleotide primer and probe sequences
il1b	Dr03114368_m1
ifng1	Dr0381923_m1
ifnphi1	Dr03100938_m1
tnfa	Dr03126850_m1
cxcl18b	Dr03436643_m1
mmp9	Dr03139882_m1
rsad2	Dr03096954
18S	4319413E
act1b	Dr03432610_m1
lyz	Dr03099436_m1
mpx	Dr03075659_m1
mpeg1.1	Dr03439207_g1
lck	F: 5'-ACGCCGAAGAAGATCTC-3' R: 5'-GCTTGGGGCAGTTACA-3'
16S	F: 5'-TCCTACGGGAGGCAGCAGT-3' R: 5'-GGACTACCAGGGTATCTAATCCTGTT-3'
VP2 (IPNV)	F: 5'-GCCAAGATGACCCAGTCCAT-3' R: 5'-TGACAGCTTGACCCTGGTGAT-3'

M (IAV)	F: 5'-CCAATCCTGTCACCTCTGAC-3'
	R: 5'-TGGACAAAGCGTCTACGC-3'
L (RSV)	F: 5' GAACTCAGTGTAGGTAGAATGTTTGCA-3'
	R: 5'-TTCAGCTATCATTTTCTCTGCCAAT-3'
	Probe: 5'-TTTGAACCTGTCTGAACATTCCCGGTT-3'

Table 2.4 qRT-PCR primers and probes

2.13 Statistical analysis

All statistical tests were performed in GraphPad Prism versions 7.03-8.4.2 for Windows, GraphPad Software (CA, USA). Paired or unpaired two-tailed t-tests were performed for parametric comparisons of two groups. Mann-Whitney tests were performed for non-parametric comparisons of two groups. One-way or two-way ANOVA was performed for parametric comparisons of three or more groups followed by Sidak's or Tukey's multiple comparisons test for pairwise comparisons. Welch's ANOVA was used if the data being compared was heteroscedastic.

Significant differences in variance between groups was tested with Brown-Forsythe's test or Spearman's rank correlation test. Normality of data was assessed by plotting a normal QQ plot.

3 Chapter 3 – Characterisation of immune cells in the zebrafish gill at homeostasis

3.1 Introduction

3.1.1 Tools to investigate zebrafish immune cells

3.1.1.1 *Flow cytometry tools*

Flow cytometry is heavily used in human and mouse immunological studies and has also been adopted into the zebrafish toolkit. Flow cytometry allows the detection and quantification of fluorescent cells from transgenic zebrafish and measurement of the level of fluorescence of these cells. Flow cytometry has also been used to measure cellular uptake of fluorescent antigen (Lin et al., 2020; Page et al., 2013). In addition, fluorescent cells can be isolated by fluorescence activated cell sorting (FACS) for downstream analyses such as qPCR or cell staining. Flow cytometry also provides data on the light-scattering properties of cells regardless of fluorescence. Forward scatter (FSC) and side scatter (SSC) correlate with cell size and granularity respectively and therefore provide an indication of cell morphology. In adult zebrafish whole kidney marrow (WKM), FSC/SSC can distinguish major haematopoietic cell lineages (Traver et al., 2003). Cells in other tissues including the spleen, peripheral blood and thymus, have been defined based on the FSC/SSC properties of WKM cells (Langenau et al., 2004; Stachura and Traver, 2011). However, there has been limited work evaluating whether haematopoietic cells have the same light-scattering properties across tissues.

3.1.1.2 *Light microscopy tools*

Intravital live imaging of immune cells in zebrafish larvae is well established and more straightforward than in older stages. Larvae are small, can be immobilized in agarose, and can be anaesthetized for long periods of time as they do not rely on gill ventilation for oxygen uptake (Rombough, 2002). Intravital live imaging of adult zebrafish is more challenging as they cannot be anaesthetized for long periods of time without intubation (Kasheta et al., 2017). In addition, their larger size reduces their optical translucency meaning that light can only penetrate a limited depth of the fish. Although adult fish are immobilized during imaging, movement from the heartbeat can create large fluctuations in surrounding tissue, making it difficult to image fast processes such as cell movement. Live imaging of individual immune cells in adult zebrafish has been demonstrated in external tissues like the skin (Lin et al., 2019). Brightfield imaging of adult zebrafish gills

has been used to monitor gill tissue repair following injury or fluorescent particle uptake but these studies did not visualise immune cells (Borvinskaya et al., 2018; Mierzwa et al., 2020). GFP fluorescence has previously been detected in adult *Tg(mpx:GFP)* transgenic gills using stereomicroscopy, however, the resolution of these images was too low to identify individual GFP+ cells (Progatzky, 2014). Therefore, although live imaging of adult gills is possible, further work is needed to understand how this can be used to investigate different aspects of immune cells.

Alternatively, confocal imaging of dissected tissue has been used with multiple animal tissues including mouse heart and lungs, and zebrafish heart, gut, and retina (Giarmarco et al., 2018; Harrison et al., 2015; Martins et al., 2019b; Pieretti et al., 2014; Sorvina et al., 2018). By placing the tissue in a supportive medium, cells can be kept alive and visualised for several hours. Tissues can also be cultured as explants in specific media conditions and visualised for longer periods, in some cases for several days (Harrison et al., 2015; Pieretti et al., 2014). Live imaging of dissected zebrafish gills was achieved in this PhD project and has since been independently reported highlighting the suitability of this method for studying mucosal immune cells (Lin et al., 2020).

Fluorescent immune cells from transgenic lines can also be imaged in tissues following fixation. Some fluorescent proteins remain fluorescent after fixation however others are impaired by the process. To overcome this, antibodies can be used to detect the fluorescent proteins. Antibodies that recognize endogenous proteins can also be used to detect immune cells, however, many of these are produced in zebrafish research labs and are not commercially available. Alternative options include using cross-reactive antibodies from other species (Miyazawa et al., 2016). Immune cells have been visualized in fixed gills in several studies and since the gill is a thin tissue this can be achieved without sectioning (Progatzky et al., 2015, 2019). This allows visualisation of the cells within the 3D structure of the gills.

3.1.1.3 *Cell markers and transgenic lines*

Immunological studies in mice and humans commonly use antibodies to distinguish cell populations based on the presence of cell surface markers. However, the lack of antibodies for zebrafish proteins has limited the use of similar techniques in this model organism. This has driven the development of many transgenic zebrafish lines where fluorescent proteins are under control of cell-selective promoters. The development of

transgenic lines for zebrafish immune cells has generally relied on approaches based on zebrafish orthologues of mammalian immune cell genes. This requires prior knowledge of genes and identification of promoter elements for each gene. Transgenes are assessed for their ability to recapitulate endogenous gene expression and their selective expression in cell populations of interest. In mice and humans, immune cells are often characterised with multiple markers which allows more precise phenotyping. Zebrafish lines can contain more than one transgene-encoded fluorescent protein although it is difficult to find more than 3 proteins with non-overlapping fluorescence spectra. Many genes in zebrafish have been described as cell-specific markers, however, it is increasingly clear that these markers label more heterogenous cell populations than initially described.

Over the last few years several studies have used scRNA-Seq to identify novel cell populations without the restriction of pre-selected cell markers. Many of these studies have used adult WKM since this haematopoietic tissue contains abundant immune cells reflecting major myeloid and lymphoid lineages. scRNA-Seq has also been performed on spleen, gut, gill and thymus tissue however in some cases this was limited to cells expressing a particular transgene (Carmona et al., 2017; Hernández et al., 2018). There is only one report of scRNA-Seq of whole zebrafish gill tissue but this is from a meeting abstract and the data have not been published (Pan et al., 2020). Furthermore, although scRNA-Seq allows unbiased clustering of cells based on transcriptional profiles, assignment of cell types is still performed manually and therefore subject to the researchers' own judgements.

The following section will discuss the immune cell markers used in this project and the cell populations in which they are expressed.

Myeloperoxidase is an enzyme found in neutrophil granules which catalyses the production of the bactericidal compound, hypochlorous acid (Strzepa et al., 2017). In zebrafish, myeloperoxidase (Mpx), is also produced in polynuclear cells with neutrophilic morphology (Lugo-Villarino et al., 2010). The transgenic *Tg(mpx:GFP)* line was developed to label neutrophils and as expected from previous studies on zebrafish neutrophils, *mpx:*GFP+ cells were found to migrate to sites of injury in larvae (Renshaw et al., 2006). Subsequent scRNA-Seq data revealed that *mpx* was indeed enriched in myeloid cell clusters of adult WKM cells and co-expressed with other myeloid-related genes including

lyz. However, transcript levels were much lower in B cell, T cell and erythroid clusters (Moore et al., 2016a). The data so far indicates that *mpx* transcription is fairly specific for neutrophils in zebrafish.

Lysozyme (Lyz) is an enzyme produced by mammalian monocytes and granulocytes which hydrolyses bacterial cell walls (Haneberg et al., 1984). In zebrafish embryos it was initially described as a macrophage-specific marker (Liu and Wen, 2002). The transgene *lyz*:GFP recapitulates *lyz* transcription and labels cells with myeloid morphology, as assessed by flow cytometry and confirmed by Leishman's staining of fluorescent cells. Some *lyz*:GFP+ cells have also been found to express *mpx* transcripts in zebrafish embryos (Hall et al., 2007). Additional studies have found *lyz* and *mpx* co-expressed in cells from both embryos and adults (Alemany et al., 2018; Meijer et al., 2008; Moore et al., 2016a). More thorough characterisation of myeloid cells using the *mhc2dab*:GFP transgenic line or scRNA-Seq has revealed a lack of *lyz* transcription in mononuclear phagocytes (MNPs) and macrophage populations (Hernández et al., 2018; Wittamer et al., 2011). Collectively this evidence points towards *lyz* being a neutrophil marker rather than a macrophage marker*.*

Macrophage expressed 1.1 (*mpeg1.1*) was also initially described as a zebrafish macrophage marker and several transgenic lines have been generated to label *mpeg1.1*-expressing cells (Ellett et al., 2011; Zakrzewska et al., 2010). The human orthologue *MPEG1* (also termed *Perforin-2*) encodes a transmembrane protein which is predicted to form pores in other cells (Pang et al., 2019). In mammals this protein is expressed in macrophages, other phagocytes, certain B cells and some non-immune cells (Kleiman et al., 2015). Recent studies have revealed that zebrafish *mpeg1.1* is also expressed in cells besides macrophages*.* In one study, *mpeg1.1+cd4-1+cldnh-* cells in the skin were defined as Langerhans cells (skin resident macrophages), whilst *mpeg1.1+cd4-1-cldnh+* cells constituted a distinct non-haematopoietic population termed metaphocytes (Lin et al., 2019). This work was corroborated by (Kuil et al., 2020) who also identified these populations in the skin and gut. Metaphocytes have also been identified in gills although they have a different origin to skin metaphocytes (Lin et al., 2020). Despite non-haematopoietic origins, metaphocytes in all three tissues were capable of antigen sampling. scRNA-Seq data has also revealed *mpeg1.1* transcripts in zebrafish B cells and a novel NK-like (NKL) population in adult WKM, although at lower levels than in

macrophages (Tang et al., 2017). Flow cytometry analysis and imaging of transgenically labelled *mpeg1.1+* cells confirmed the presence of cells with lymphoid and myeloid morphologies (Ferrero et al., 2020). In addition, qPCR analysis revealed that lymphoid cells were enriched for B cell genes such as *ighm* (IgM heavy chain constant region) but not T cell genes like *lck*. Lymphoid cells were also lower in *mpeg1.1* transcript levels supporting scRNA-Seq findings from (Tang et al., 2017). In contrast, *mpeg1.1+* myeloid cells did not express B cell genes or *mpx* but were enriched for *csfr1a* (a marker of MNPs). The B cell identity of *mpeg1.1+* cells was further supported by the presence of a double positive population in the *Tg(IgM:GFP; mpeg1.1:mCherry)* line in tissues including the WKM, skin and gut. Another study has identified lymphoid *mpeg1.1+* cells in the zebrafish adult heart (Moyse and Richardson, 2020). Initial characterisation of *mpeg1.1* largely focused on zebrafish larvae and embryos, before the adaptive system is fully developed. This no doubt contributed to the lack of characterisation of lymphoid cells and highlights the importance of evaluating immune cell markers in different tissues and developmental stages.

Lymphocyte-specific protein tyrosine kinase (Lck) in zebrafish has mainly been used to identify T lymphocytes. In mammalian species, LCK is expressed in T cells and ILCs, including NK cells where it propagates downstream signalling of cell surface receptors (Björklund et al., 2016; Rajasekaran et al., 2016). scRNA-Seq studies have identified multiple *lck+* populations in zebrafish WKM, spleen, or gut which express genes associated with T cells, NK cells or the three types of ILCs (Carmona et al., 2017; Hernández et al., 2018; Tang et al., 2017). One study also reported on a novel NK-like population that expressed cytotoxic markers but not *lck* (Tang et al., 2017). The *Tg(lck*:GFP) transgenic was found to label cells in the thymus and the WKM however only thymic GFP+ cells expressed *rag2*, which encodes a DNA recombinase essential for T and B cell development (Langenau et al., 2004). This indicated that *lck*:GFP+ cells in the WKM did not include immature T cells. *Lck*:GFP+ cells are also present in the gills (Dee et al., 2016) but *rag1* (another recombinase expressed in immature lymphocytes) is not expressed in this population (Dorottya Polos, personal communication). Zebrafish *rag1-/-* mutants lack T cells but contain *lck+* cells with NK cell and ILC transcriptome profiles or morphological properties (Hernández et al., 2018; Muire et al., 2017). This further supports the existence of *lck+* cells with distinct developmental pathways.

There are currently no transgenic lines to distinguish NK cells and ILCs *in situ* however, *cd4-1+* T cells have been identified in zebrafish using the *Tg(cd4-1:mCherry*; *lck:GFP)* line (Dee et al., 2016). scRNA-Seq studies have shown that *cd4-1* is not enriched in NK cells or ILCs (Carmona et al., 2017; Hernández et al., 2018). In mammals, CD4-1 is expressed in both T cells and MNPs and this is also the case in zebrafish. Using flow cytometry (Dee et al., 2016) identified myeloid-like *cd4-1+* cells in the WKM. They also used confocal imaging of *Tg(cd4-1:mCherry*; *mhc2dab:GFP)* fish to identify double positive cells in the skin with MNP morphology. MHCII transgene expression indicated possible antigen-presentation abilities of the *cd4-1+* cells. *Cd4-1+Foxp3a+* cells were also identified in the zebrafish gut indicating presence of a Treg population. In contrast, *cd4-1+* T cells in the gills expressed Th2-associated genes, indicating tissue-specific differences. scRNA-Seq and qPCR data have revealed that *cd4-1* and *cd8* are expressed in different lymphocyte populations paralleling cells in mammals (Carmona et al., 2017; Dee et al., 2016).

B cells in zebrafish, as in mammals, can be identified by expression of IgM. Generation of the *Tg(IgM:GFP)* line has allowed further investigation into zebrafish B cell development (Page et al., 2013). Based on the presence of *pax5*, *rag2* and *ighm* transcripts, 3 populations of B cells were identified in the kidney which resembled different stages of mammalian B cell development. Some *ighm+* cells were also suggested to represent plasma cells based on the presence of plasma cell markers such as *blimp1*. Zebrafish B cells are also likely to express IgD, IgZ, and IgZ-2. Based on the genomic organization of these genes, expression of IgM or IgD is likely to exclude IgZ expression due to excision of the IgZ constant loci during VDJ recombination (Danilova et al., 2005). Indeed, *IgM*:GFP+ cells in the kidney and spleen are *igz-* (Page et al., 2013). The genomic loci of IgZ-2 has not been reported but, IgM+IgZ-2+ cells have been identified in zebrafish blood by immunofluorescence (Hu et al., 2010).

3.1.2 Gill intrabranchial lymphoid tissue

The various immune cells present in fish gills was addressed in the literature review (Chapter 1) and therefore this section will focus on interbranchial lymphoid tissue (ILT). This structure was first identified in salmon and trout (salmonid species) as an accumulation of intraepithelial lymphocytes situated at the interbranchial cleft at the base of the septum (Haugarvoll et al., 2008). It has since been identified in zebrafish (a

cyrprinid species) as part of this project and another recent study (Rességuier et al., 2020). The latter study identified ILT in several other species but revealed that not all teleosts contain this structure. This latest evidence highlights that comparisons between species could shed light on the evolutionary development and shared or divergent features of the ILT.

Lymphocytes in the ILT have been shown to reside within a network of epithelial cells as identified by cytokeratin staining (Haugarvoll et al., 2008). The structure is also surrounded by a mucosal epithelium that is continuous with the gill lamellar epithelium (Dalum et al. 2015). Studies in salmon showed that this intraepithelial lymphoid tissue extends from the interbranchial septum along the filament edges. Intraepithelial lymphoid tissue at the septum has been termed proximal ILT whilst the tissue along the filaments has been termed distal ILT. Distal ILT has an uneven distribution of lymphocytes with a higher density on the afferent edge of filaments than the efferent edge (Dalum et al. 2015). Comparative studies have revealed that a lack of ILT in some species correlates with significantly shortened or absent interbranchial septum or interbranchial cleft (Rességuier et al., 2020). The ILT therefore seems closely related to gill tissue structure.

Further histological characterisation of the ILT in salmon has revealed that this structure consists primarily of CD3+ lymphocytes (T cells) including CD8+ cells (Koppang et al. 2010; Dalum et al. 2015). Transcripts of T cell markers (CD3, TCRα, TCRδ, CD4-1, and CD8) have also been detected in the ILT by qPCR suggesting the presence of diverse T cell populations. MHCII+ cells have also been observed suggesting the presence of APCs (Dalum et al. 2015). Immunoglobulin-producing cells (B cells) have been reported as absent or very few in number in the ILT although transcripts for IgM and IgT have been detected (Austbø et al., 2014; Haugarvoll et al., 2008; Koppang et al., 2010). In addition, proliferating cell nuclear antigen (PCNA)-expressing cells have been identified demonstrating the presence of proliferating cells (Haugarvoll et al., 2008). Some of these cells are CD3+ T cells but the identity of other proliferating cell types has not been investigated (Haugarvoll et al. 2008; Dalum et al. 2016). The efferent edge was found to contain noticeably fewer CD3+, CD8+, and PCNA+ cells than the afferent edge which could indicate functional differences within the distal ILT.

Several studies have also sought to clarify the role of the newly described ILT. The presence of T cells within a network of epithelial cells, alongside MHCII+ cells, was found to bear similarity to the thymus, suggesting that the ILT could function as a primary lymphoid tissue (Haugarvoll et al., 2008). In addition, the ILT is located in close proximity to and develops from the same structure as the thymus (Dalum et al. 2016). However, *rag1* and *rag2* transcripts are absent in the ILT indicating that T cell maturation does not occur in this tissue (Aas et al., 2014). Furthermore, unlike the thymus, the ILT is not vascularised and lacks AIRE transcripts, an important gene in the selection for self-tolerant T cells (Aas et al., 2017). Therefore, the ILT is unlikely to function as a primary lymphoid tissue.

Since there is a lack of highly organised MALT or lymph nodes in teleosts, some have speculated that the ILT could represent a primitive version of these tissues. This is supported by the presence of both lymphocytes and MHCII+ cells, suggesting that antigen-presentation could take place. However, the limited presence of B cells and lack of segregated B/T cell regions are noticeable differences with mammalian secondary lymphoid tissue. Despite these differences, the ILT has been found to respond to gill infection which is an important feature of secondary lymphoid function. In rainbow trout, number of IL-22+ cells were higher in the ILT following bacterial challenge with *Aeromonas salmonicida* (Hu et al. 2019). Furthermore, transcripts for type I and type II IFNs, VIG-1 (an ISG), IgT, and RIG-I (a PRR that recognizes nucleic acids), were higher in the ILT following infectious salmon anaemia virus (ISAV) challenge in salmon. Viral transcripts were not detected in the ILT showing that non-infected cells contributed to the immune response (Austbø et al., 2014). The ILT was also smaller in size following ISAV challenge and this was not due to apoptosis. In addition, the ratio of TCRα/TCRδ transcripts decreased in the ILT but increased in the gill indicating dynamic changes in T cell populations. However, some T cell-associated transcripts were unchanged in the ILT (Aas et al., 2014). These data suggest that the ILT may act as a store of rapidly responsive T cells. In contrast to the changes observed in the ILT, secondary lymphoid tissue usually increases in size during infection, reflecting increased proliferation of lymphocytes. Therefore, further work is needed to determine the proliferation dynamics and the number of leukocytes present in the ILT beyond estimations with transcript levels.

The ILT has also been suggested to play an immunoregulatory role due to its transcription of regulatory cytokine genes and transcription factors such as *Foxp3a*, *IL-10*, *GATA-3*, and *ROR-γ*. These transcripts were unchanged in salmon following ISAV infection except for *GATA-3* (Aas et al., 2017). In addition, *foxp3a*:RFP+ cells were present in *Tg(foxp3a:RFP)* zebrafish gill arches although this was not commented on or investigated further in the study (Hui et al., 2017). Indeed, few studies on the gills report on cells in the arch, except studies directly investigating the ILT. This gap in the literature could be easily addressed by researchers already working on the gills and would provide useful information on this poorly understood lymphoid tissue.

3.1.3   Immune cell populations in developing and ageing respiratory tissue

In humans, immune cells and responses in the respiratory system are known to change across the lifespan with important consequences for disease. Infants and elderly people are more susceptible to RVIs and more likely to develop severe disease. In addition, the incidence of chronic inflammatory respiratory diseases increases with age. It is therefore important to understand these immunological changes, the mechanisms which drive them, and how they influence disease in both humans and experimental models. Mammalian organisms develop *in utero* whilst zebrafish develop *ex utero*, hatching just 2 days post fertilisation. This means that zebrafish are exposed to the external environment much earlier than mammals. This is important to consider when studying how antigen exposure may influence immunological development.

3.1.3.1   Early development

Accessing fetal and infant lungs in humans is understandably difficult to achieve and therefore most studies have focused on mice and other animal models. Mammalian lung development is initiated *in utero* but continues postnatally. In mice, alveolarisation occurs postnatally whilst in humans it starts *in utero* but continues for up to 3 years after birth (Miller and Spence, 2017). After birth the respiratory system faces major physiological and environmental changes including an oxygen-rich environment, mechanical ventilation, commensal microbial colonization, and exposure to exogenous pathogens and particulates. These factors are all likely to impact and interact with the developing immune system.

Macrophages are the predominant immune cell type in embryonic and neonatal lungs. In mouse embryonic lung explants, macrophages were frequently localised at branching points. In addition, macrophages during alveolarisation stages were polarised towards an M2 phenotype which is associated with tissue remodelling (Jones et al., 2013). In neonatal mice, ablation of *Csf1r*-expressing monocyte/macrophages protected mice from hyperoxia-impairment of alveolar development (Kalymbetova et al., 2018). Macrophages are therefore associated with normal and aberrant structural changes in developing lungs. However, scRNA-Seq and immunostaining has revealed that cell composition changes in the respiratory tract within a few weeks of birth. Lymphocytes are only present in very small numbers in fetal airways in mice but increase significantly after birth, becoming the most abundant population within a few weeks (Domingo-Gonzalez et al., 2020; Loffredo et al., 2020). Neutrophils have been found to increase in number between embryonic and postnatal stages in mice, but decrease as a proportion of leukocytes over the first 4-5 weeks of postnatal development, possibly reflecting the increase of lymphocytes (Bry et al., 2007; Loffredo et al., 2020). Other leukocytes including dendritic cells, basophils, eosinophils and mast cells are also present in the postnatal lungs with some showing dynamic changes in abundance (Domingo-Gonzalez et al., 2020; Loffredo et al., 2020).

During early development, lymphocytes and dendritic cells in the respiratory tract are functionally immature for several weeks after birth. Responses to infection challenge are often skewed to type 2 immunity, which is particularly notable in RSV infections in infants (Openshaw et al., 2017). In addition, recruitment of neutrophils is impaired in infancy possibly due to lower expression of PPRs, chemokines and cytokines (Lambert and Culley, 2017). Therefore, although changes in cell composition may be important, they do not always provide an indication of immune cell function and responses to infection.

In addition to immune cells in the lungs, lymphoid tissues also undergo changes following birth. In cattle, NALT is already present in fetal stages but further develops after birth. This involves increased lymphocytes in the interfollicular regions and development of germinal centres in tonsils (Osman et al., 2018). In mice, NALT development occurs postnatally and can be promoted by the microbiota and external antigens (Krege et al., 2009). Species differences are important in lymphoid tissue development and further highlighted by the development of BALT. This tissue develops postnatally in some

species, such as rabbits and mice, but not in others such as dogs (Cesta, 2006). BALT is more commonly found in children and young people but rarely observed in healthy adults. BALT in children does not appear to be related to respiratory disease or pre-existing inflammation indicating clear differences to the development of iBALT (Heier et al., 2011; Hiller et al., 1998; Tschemig et al., 1995). However, few studies have investigated early development of BALT in human and animal models. Understanding the different factors driving iBALT and BALT formation could provide new insights into the immunological environment of developing respiratory tissues.

Despite a common function, teleost gills have a different developmental origin to mammalian lungs. The gills develop from the embryonic pharyngeal arches whereas mammalian lungs develop from the foregut (Hogan et al., 2004; Warburton, 2017). In zebrafish, larvae do not immediately rely on their gills for oxygen uptake but become reliant on the gills from about 14 dpf. Interestingly, this is about 7 days later than when zebrafish become dependent on the gills for ionoregulation (Rombough, 2002). Indeed there are conflicting theories on whether oxygen uptake or ionoregulation have been more important in influencing gill development (Rombough, 2007).

Zebrafish gill arches and filaments are visible at 3 dpf and secondary lamellae from 7 dpf (Jonz and Nurse, 2005). This mirrors lung development where the alveoli are the last structure to form. This sequence of gill structural development is similar in medaka and gilthead seabream showing some consistency across teleosts (Leguen, 2018; Mulero et al., 2007). Taste buds have also been identified from 3 dpf indicating that the gill is likely to sense exogenous material from very early stages (Hansen et al., 2002).

Like in mammals, lymphocyte-driven adaptive immunity matures later in zebrafish than does innate immunity. Antigen challenges in developing zebrafish have revealed that heightened secondary antibody responses only occur from 4-6 weeks post fertilisation (wpf) indicating a functionally mature adaptive system at this stage (Lam et al., 2004). Furthermore *IgM*:GFP+ B cells were only observed from 20 dpf in transgenic zebrafish closely preceding a noticeable increase in *ighm* transcript levels at 4 wpf (Page et al., 2013). There are limited studies on gill immunological development but B cells were clearly identified in carp gills from 6 wpf (Huttenhuis et al., 2005). This study also identified intraepithelial lymphocytes (thought to be T cells) significantly earlier at 7 dpf. Both populations of lymphocytes increased over time however, their functions were not

investigated. CD3+ T cells were identified in the gills of salmon larvae but did not form an ILT structure until in later in development but before adulthood (Dalum et al. 2016). Acidophilic granulocytes have also been detected in early development of gilthead sea bream gills coinciding with the emergence of lamellae and increasing over time (Mulero et al., 2007).

3.1.3.2 *Ageing*

Ageing in humans and other mammals is a complex process associated with many physiological changes. For the respiratory system this includes structural changes, impaired respiratory function, and impaired mucocilliary clearance (Lowery et al., 2013). The immune system also undergoes systemic changes, most notably, increased baseline inflammation known as inflammaging, and impaired immune function known as immunosenescence. Collectively these physiological and immunological changes are thought to be involved with tissue damage, development of chronic inflammatory respiratory conditions and increased susceptibility to respiratory infection.

Within the respiratory tract, changes in immune cell abundance have been observed but there are some discrepancies between studies. This may be explained in part by the method used to quantify cell abundance. One study reported higher levels of NK cells in the lungs of aged mice analysed by flow cytometry (Beli et al., 2011) whilst another reported no change in this population as analysed by bulk tissue RNA-Seq (Angelidis et al., 2019). NK cell levels were found to be lower in older mice by another study (Calvi et al., 2011), in contrast to findings by Beli et al. However, these two studies analysed 12 month old and 22 month old mice respectively, suggesting that there could be considerable cellular changes across the lifespan of an organism.

Ageing-related changes may also vary between different regions of the respiratory tract and tissues outside of the respiratory tract such as peripheral blood and lymph nodes. Indeed, Foxp3a+ Treg cells were greater in aged mouse lymph nodes where they impaired co-stimulatory receptor expression in dendritic cells. However, Treg levels were unchanged in the lungs (Chiu et al., 2007). This lack of change in the lungs was also observed in a study by Birmingham et al. The study additionally showed that Treg levels were higher in the lungs following ovalbumin challenge and this was greater in aged mice than young mice (Birmingham et al., 2013). Based on results from Chiu et al. this could have been due to greater numbers of Tregs in the lymph nodes.

Changes in abundance of myeloid cells and B cells have sometimes been observed in the lungs of older mice (Angelidis et al., 2019; Wansleeben et al., 2014). One study showed that greater levels of B cells in mice was associated with greater levels of immunoglobulin in the airways and this could have contributed to structural changes (Calvi et al., 2011). However, the consequences of altered immune cell abundance are not frequently investigated. On the other hand, numerous studies have highlighted the impaired immune response to RVIs in older animals or patients (Haq and McElhaney, 2014). It will therefore be important to understand how the broad immunological and physiological changes contribute to this impairment.

Data on ageing teleost gills is even more limited. This may be a result of the focus on early and young adult stages of fish in aquaculture and the focus on zebrafish larvae for many research studies. With the increasing use of zebrafish as model organism, it is important to increase our understanding of ageing in teleosts. Studies in salmon have shown that the proportion of ILT decreases between adult and more mature fish mirroring a reduction in volume of the thymus (Dalum et al. 2016). This suggests that T cells may be systemically reduced in the fish. Interestingly, humans also show thymus atrophy during ageing (Majumdar and Nandi, 2018).

3.2 Aims

Evaluating zebrafish gills as a model for respiratory mucosal immunology requires a better understanding of the immunological properties of the gills. In this chapter I hypothesise that:

- The gills contain multiple types of both innate and adaptive immune cells with a similar composition to the mammalian respiratory mucosa.

- Lymphoid tissue in zebrafish gills has some similarities to MALT in mammals.

In order to assess these hypotheses, this chapter addresses the following aims:

1. To validate flow cytometry and microscopy as tools for the investigation of gill immune cells.
2. To determine immune cell composition in the gills from early development to aged stages.

3. To characterise anatomical and immunological properties of lymphoid tissue in the gills.

4. To assess immune cell interactions with exogenous antigen and between individual cells.

3.3 Results

3.3.1 Validation of flow cytometry and microscopy as tools for investigation of immune cells in the gills

3.3.1.1 Analysing immune cell properties using flow cytometry

Zebrafish WKM-derived haematopoietic cell types are easily distinguishable by their forward and side light-scattering properties (Traver et al., 2003). However, to date there is no comprehensive description of FSC/SSC properties of gill haematopoietic cells. The following experiments aimed to determine whether FSC/SSC properties of gill haematopoietic cells are consistent with those of WKM haematopoietic cells. This would confirm whether these are suitable parameters for identifying and characterising different immune cell types in the gills.

WKM and gill tissue (whole arches) from individual adult zebrafish were processed into single cell suspensions and analysed by flow cytometry. Live cells were identified for further analysis by gating to exclude debris, gating to select for singlet cells, and gating to exclude DAPI+ cells (Figure 3.1A). WKM tissue (Figure 3.1B) contained cell populations with FSC/SSC properties reflecting previously described erythrocyte, lymphocyte, myeloid, and haematopoietic precursor populations (Traver et al., 2003).

Gill tissue had a FSC/SSC profile with a similar range to WKM tissue, and therefore similar gates were applied to distinguish four populations (Figure 3.1C). However, some differences to WKM tissue were observed including the lack of a distinct population in the myeloid gate, and a different distribution of cells between the four gates. WKM tissue had a greater proportion of events in the precursor, myeloid, and lymphocyte gates than the gills. On the other hand, gill tissue had a greater proportion of events in the erythrocyte gate. This indicated that further analysis was needed to clarify whether cells gated in the gills represented the same cell types as in the WKM. This analysis would need

to consider that the gills also contain many non-haematopoietic cells such as endothelial and epithelial cells.
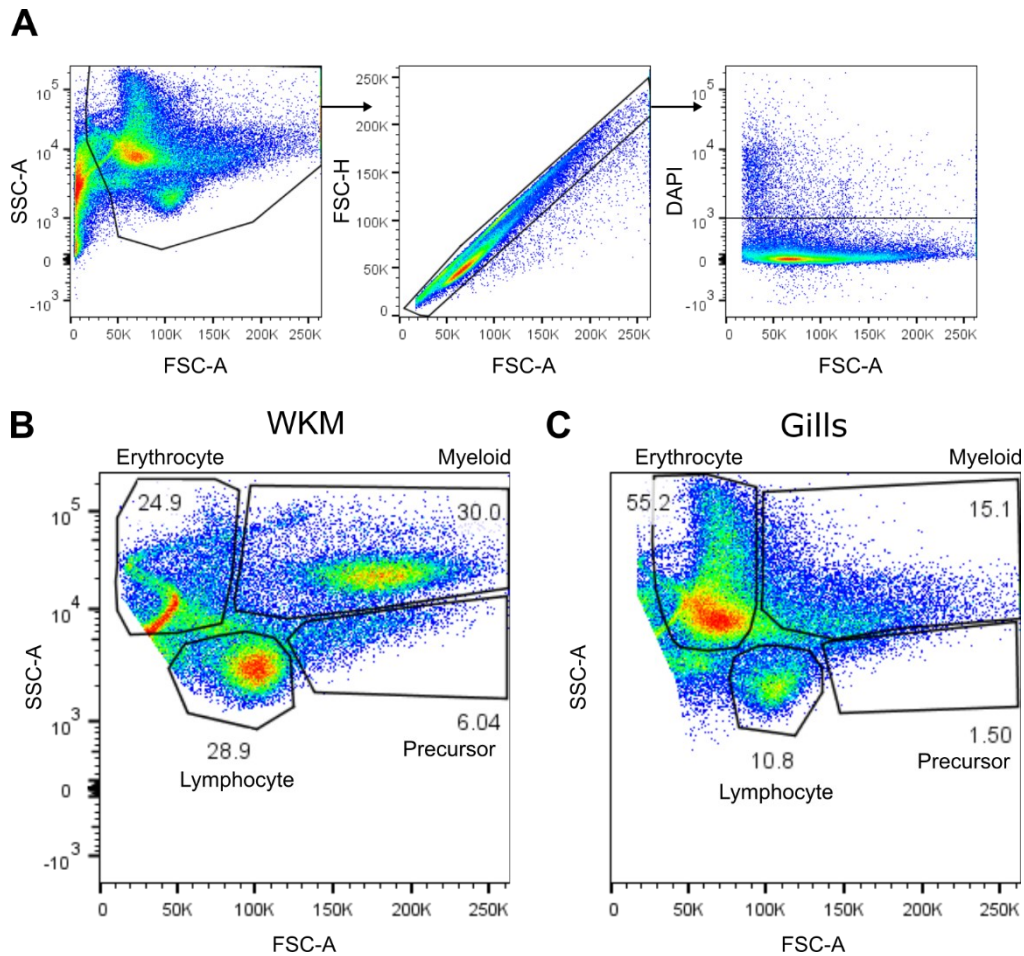
Figure 3.1 Flow cytometry gating strategy and FSC/SSC profiles of adult gill and WKM tissue.

Gill and WKM tissues from *Tg(fli:GFP)* fish (n = 4) were analysed by flow cytometry to identify live cells. WKM was manually triturated and gills were digested with collagenase into single cell suspensions. A) Gill sample showing representative gating strategy to identify live cells. Debris was excluded on FSC-A/SSC-A, singlet cells were selected on FSC-A/FSC-height (FSC-H), and finally DAPI-cells were selected on FSC-A/DAPI. Gates are shown in black outlines. (B, C) Representative WKM and gill samples following live cell gating. Values in plots reflect percentages of events in each gate compared to total events in plot. The samples in this experiment were processed in collaboration with Katie Tsoi (Imperial College London) as part of her Master's thesis on zebrafish gill characterisation (Tsoi, 2019). Analysis of these samples in this PhD thesis was performed by me.

To identify cell types with more precision than using FSC/SSC alone, gill cells from transgenic fluorescent reporter lines were analysed for fluorescence. Adult gills from *Tg(mpx:GFP)* and *Tg(cd4-1:mCherry; lck:GFP)* zebrafish were analysed by flow cytometry to identify neutrophils, and *cd4-1*-expressing lymphocyte and myeloid cells respectively (Dee et al., 2016; Renshaw et al., 2006). *Tg(fli:GFP)* gills were also analysed to assess whether endothelial cells could be distinguished from immune cells by FSC/SSC parameters (Lawson and Weinstein, 2002). These three transgenic lines were chosen not only for the cell types they label, but also because their transgenes are known to be expressed in zebrafish during adulthood and in the gills (Dee et al., 2016; Progatzky et al., 2015).

Fluorescent cells were identified by comparing transgenic samples to WT or *TraNac* gills. *Mpx:*GFP+, *cd4-1:*mCherry+ and *fli:*GFP+ cells were clearly distinguished from non-fluorescent cells and made up on average 0.47% (SD = 0.19), 5.82% (SD = 0.57), and 8.48% (SD = 2.20) of gill cells respectively (Figure 3.2A-F). *Mpx:*GFP+ cells were found primarily in the myeloid gate (M = 66%, SD = 7), with a minority in the three other gates (Figure 3.2G). This corresponded to the expected morphology of neutrophils, that is more granular (greater SSC) and larger (greater FSC) than lymphocytes including T cells, B cells and NK cells.

*Cd4-1:*mCherry+ cells fell mostly in the lymphocyte (M = 50%, SD = 8) and myeloid (M = 27%, SD = 4) gates (Figure 3.2H) likely representing the two previously described *cd4-1*-expressing cell populations: T cells and myeloid cells (Dee et al., 2016). The different *cd4-1*-expressing populations in the gills therefore cannot be distinguished by fluorescence alone.

Although *mpx:*GFP+ and *cd4-1:*mCherry+ cells were found mostly in FSC/SSC gates corresponding to their expected cell types, they were not exclusively confined to these gates. This shows that immune cells have heterogenous FSC/SSC properties and each gate may not capture all the cells of its designated population. It is also possible that a small percentage of fluorescent cells were not neutrophils, lymphocytes or myeloid cells due to leaky transgene expression or lack of specificity of cell markers.

*Fli:*GFP+ endothelial cells had a broad range of FSC/SSC properties with events in all four population gates; the majority of *fli:*GFP+ cells were distributed across the myeloid (M =

29%, SD = 1), erythrocyte (M = 27%, SD = 2), and lymphocyte (M = 15%, SD = 2) gates with a much smaller proportion in the precursor gate (Figure 3.2I). These cells therefore cannot be distinguished by FSC/SSC properties alone. Furthermore, this shows that the four gates do not exclusively contain their designated haematopoeitic cell types.
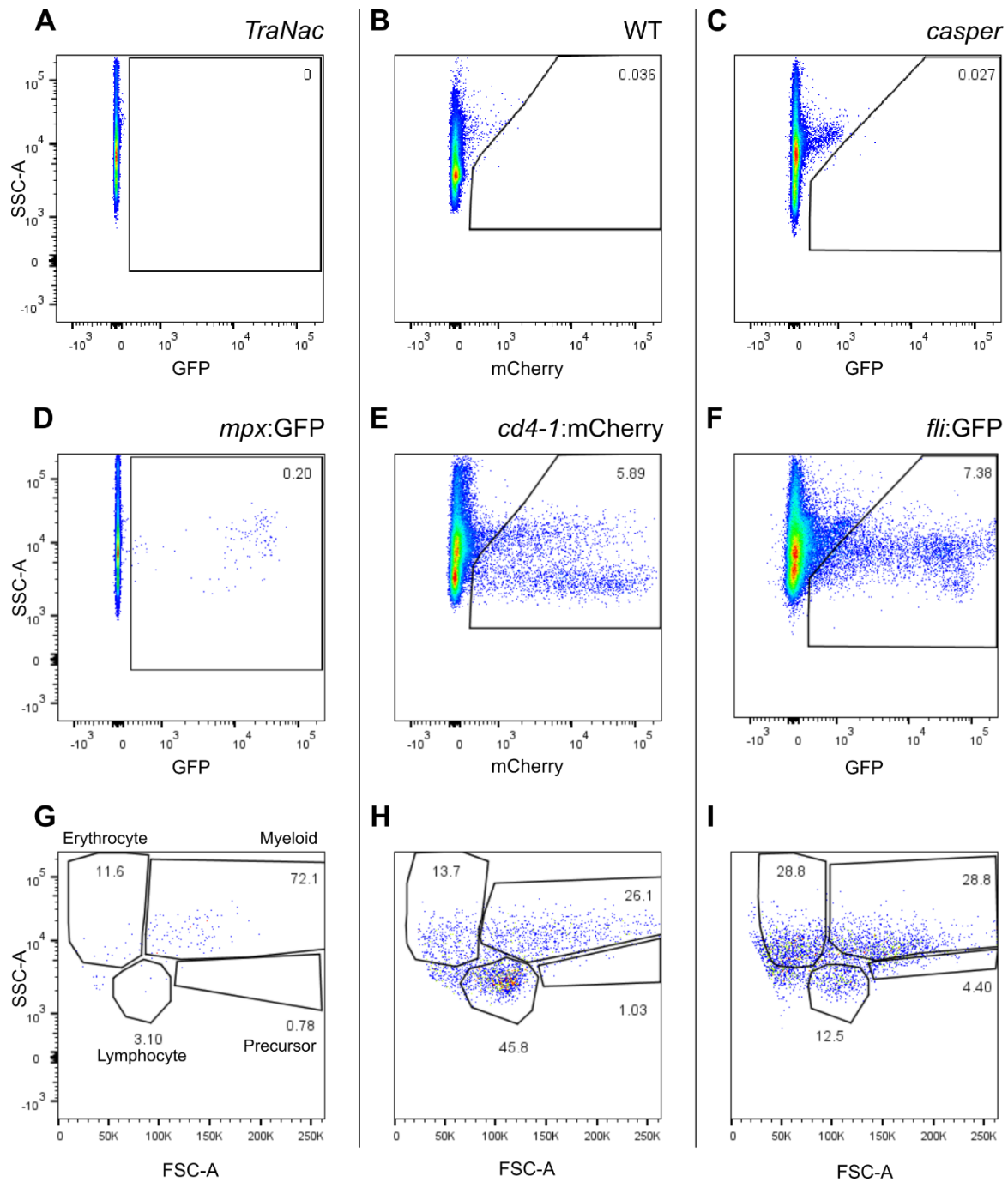
Figure 3.2 Flow cytometry of immune and endothelial gill cells from *Tg(mpx:GFP), Tg(cd4-1:mCherry; lck:GFP)* and *Tg(fli:GFP)* adult zebrafish.

Tg(cd4-1:mCherry; lck:GFP), Tg(fli:GFP), TraNac, *casper* and WT gills were digested with collagenase into single cell suspensions. (A-C) Background fluorescence was identified from WT or *TraNac* control gills and excluded in subsequent gating. (D-F) This gating was used to identify fluorescent cells in transgenic samples for the fluorescent protein of interest. (G-I) FSC/SSC profile for fluorescent cells from (D-F). Erythrocyte, myeloid, lymphocyte and precursor gates were based on FSC/SSC profile of total live cells. Values in (A-I) reflect percentages of events in each gate compared to total events in plot. N = 4. Samples for *Tg(fli:GFP)* are the same samples as shown in Figure 3.1. *Tg(cd4-1:mCherry;*

lck:GFP), *Tg(fli:GFP)*, *casper* and WT samples were processed in collaboration with Katie Tsoi (Imperial College London) as part of her Master's thesis on zebrafish gill characterisation (Tsoi, 2019). Analysis of these samples in this PhD thesis was performed by me.

In addition to flow cytometry, gills from these transgenic lines were visualised by fluorescence microscopy to assess cell morphology *in situ* (Figure 3.3). *Mpx:*GFP+ cells had irregular and heterogenous morphologies (Figure 3.3A). *Cd4-1:*mCherry+ cells were either small and round, indicative of lymphoid lineage, or larger with cytoplasmic projections indicative of myeloid lineage (Figure 3.3B). *Fli:*GFP+ cells were present at known sites of endothelial cells, including in the secondary lamellae (Figure 3.3C) where they appeared to have the morphology of pillar cells (Macirella and Brunelli, 2017). These cells spanned the width of individual secondary lamellae. *Fli:*GFP+ cells were also found in the primary lamellae with thin and elongated morphologies forming what appeared to be vessels.

In summary, gill immune cells have similar FSC/SSC properties to WKM immune cells and gating on these parameters provides a general indication of cell type. However, FSC/SSC alone cannot distinguish all cell populations and therefore fluorescent markers are an important tool for further characterisation of immune cells in the gills. Furthermore, these fluorescent markers allow *in situ* visualisation of cells in the gills, providing additional details on their properties and localisation.
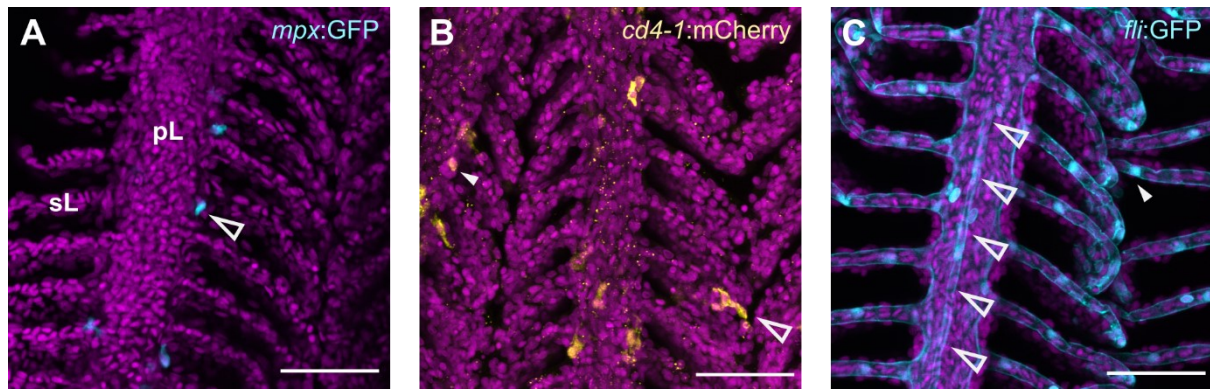
Figure 3.3 Fluorescence microscopy of immune and endothelial gill cells in *Tg(mpx:GFP), Tg(cd4-1:mCherry; lck:GFP)* and *Tg(fli:GFP)* adult zebrafish.

Representative maximum z-stack projections of fixed immunostained gills**.** DRAQ5 nuclear staining in magenta; GFP immunostaining in cyan; mCherry immunostaining in yellow**.** Images were acquired with a Leica SP5 inverted confocal microscope at 800X magnification; scale bar represents 50 μm. A) Arrowhead indicates a GFP+ cell in the primary lamellae (pL). GFP+ cells rarely observed in the secondary lamellae (sL). N = 6. B) Filled arrowhead indicates a rounded mCherry+ cell; unfilled arrowhead indicates a larger mCherry+ cell with cytoplasmic projections. N = 4. C) Filled arrowhead indicates a GFP+ pillar cell; unfilled arrowheads indicate a GFP+ vessel. N = 4. *Tg(cd4-1:mCherry; lck:GFP)* and *Tg(fli:GFP)* samples were processed and imaged in collaboration with Katie Tsoi (Imperial College London) as part of her Master's thesis on zebrafish gill characterisation (Tsoi, 2019). Post-acquisition image processing in this PhD thesis was performed by me.

3.3.1.2 *Visualising immune cells in the gills using microscopy methods*

Microscopy is a powerful technique for gaining information on cell behaviour, properties and localisation *in situ*. Several studies have successfully used fluorescence microscopy to visualise cells and particles in dissected gill tissue, however, there are far fewer examples of live intravital microscopy of fluorescent cells in zebrafish gills. Therefore, a series of experiments was conducted to assess whether detection of fluorescent immune cells was feasible with the microscopy equipment available in this project. *Tg(mpeg1.1:SECFP-YPet), Tg(lyz:dsRed)* and *Tg(cd4-1:mCherry)* transgenic lines were chosen because cells expressing these markers have previously been imaged in dissected adult gills (Dee et al., 2016; Progatzky et al., 2015; Rességuier et al., 2017).

In the first experiment, juvenile *TraNac Tg(mpeg1.1: SECFP-YPet)* fish were imaged by widefield microscopy (Figure 3.4A). This work was part of a pilot experiment investigating the early development of zebrafish gills and therefore no images were

acquired of adult gills. Although these fish were juvenile, they had distinguishable filaments and secondary lamellar structure similar to that observed in adult fish. Individual *mpeg1.1:*SECFP-YPet+ cells were visible in the general gill area and specifically along the edges of primary lamellae.

Later in the project, a new stereomicroscope was acquired and systematically assessed for intravital microscopy of the gills. Compared to the widefield microscope, the stereomicroscope platform allowed manipulation of specimens alongside image acquisition. A single adult *TraNac Tg(lyz:dsRed)* fish was euthanised and subject to intravital imaging using the stereomicroscope. The gills were subsequently dissected, imaged using the stereomicroscope, then fixed and imaged using a confocal microscope.

*Lyz:*dsRed+ cells were clearly identified in the gills using intravital imaging regardless of whether the operculum was intact or removed (Figure 3.4B and C). However, removing the operculum allowed visualisation of cells in the gills without the confusion of cells in the operculum epidermis (Figure 3.4C). It also increased the detectable fluorescent signal and possibly the number of *lyz:*dsRed+ cells visible in the gills. Cells in the filaments were certainly more easily identified. The stereomicroscope used in this project did not have the capability to acquire z-stacks therefore images were taken at single z-positions.

Imaging dissected gills with the stereomicroscope did not greatly improve the resolution, but it did allow imaging of separate arches (Figure 3.4D). This made it easier to see the gill structure and therefore precise localisation of *lyz:*dsRed+ cells (Figure 3.4E). Imaging the gills with confocal microscopy allowed a higher magnification, increased resolution, and z-stack acquisition (Figure 3.4F and G). This allowed cells at different focal positions to be visualised in single image and greater clarity in visualisation of the morphology of individual cells (Figure 3.4F and G).

The confocal microscope was not used for intravital imaging as it requires more time for image acquisition, and it did not allow for manipulation of specimens. This would not be practical for procedures where fish must be recovered from anaesthesia within 15 mins. In addition, movement of the gills due to the heartbeat makes it difficult to acquire z-stacks at high resolution.

Widefield microscopy
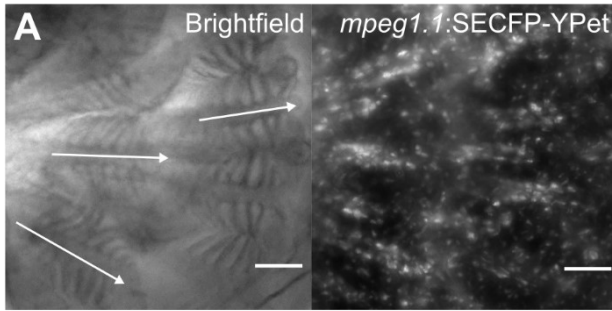
Sample orientation
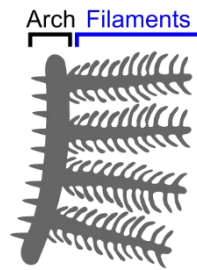
Stereomicroscopy
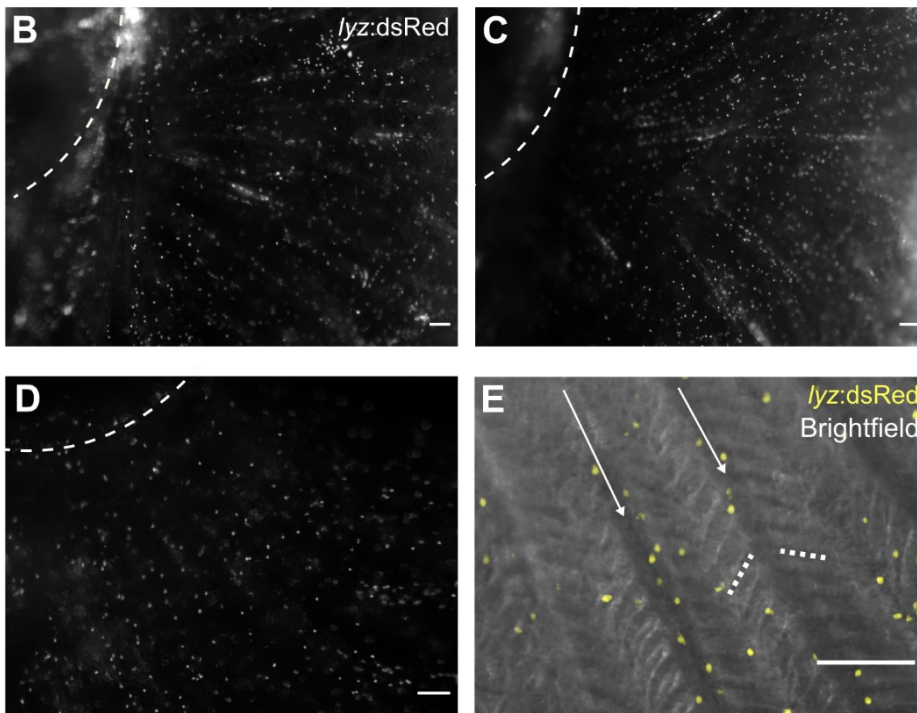
Sample orientation
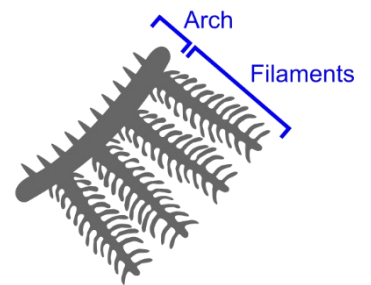
Confocal microscopy
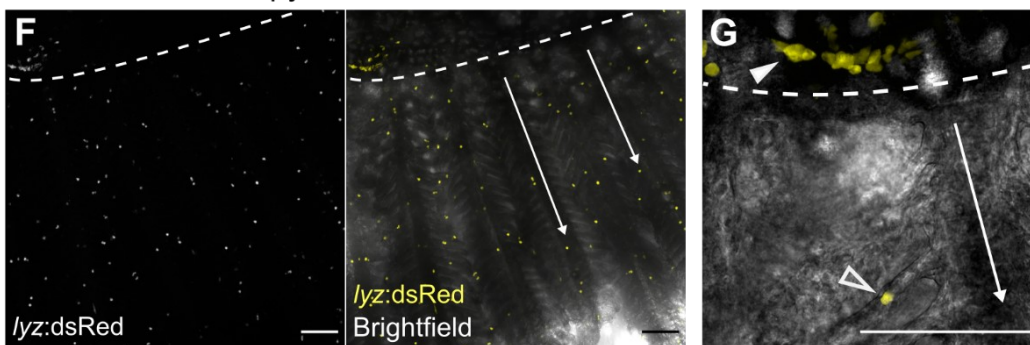
Sample orientation
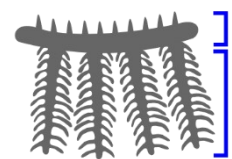
Figure 3.4 Intravital and *ex vivo* imaging of fluorescent immune cells in zebrafish gills.

A) Live intravital brightfield and fluorescence images of 46 dpf *TraNac Tg(mpeg1.1:SECFP-YPet)* fish gills acquired with a Zeiss Axiovert 200 widefield microscope. Brightfield image is a single z slice. *Mpeg1.1*:SECFP-YPet image is a maximum z-stack projection. N = 2 fish, representative image shown. Schematic of the orientation of the gills (right) with imaged region (filaments) highlighted in blue. (B-E) Single plane stereomicroscopy images of *TraNac Tg(lyz:dsRed)* gills acquired with a Leica M205 FCA stereomicroscope, n = 1. Schematic of the orientation of the gills (far right) with imaged region (arch and filaments) highlighted in blue. Live intravital image of fish with intact operculum (B) or with operculum removed (C). D) Image of dissected gill. E) Enlarged region of filaments from (D). (F, G) Maximum z-stack projections of fixed gills at 170X magnification (F) and 800X magnification (G). Images acquired with a Leica SP5 inverted confocal microscope, n = 1. Schematic of the orientation of the gills (right) with imaged region (arch and filaments) highlighted in blue. (A-G) Scale bar represents 100 μm. Curved dashed lines indicate gill arch; arrows indicate primary lamellae; straight dashed line in (E) indicates secondary lamellae; filled arrowhead in (G) indicates *lyz*:dsRed+ cells in arch, unfilled arrowhead in (G) indicates *lyz*:dsRed+ cells in secondary lamellae.

In order to optimise imaging of immune cells in the gills, confocal imaging of freshly dissected, unfixed tissue was investigated (Figure 3.5). Gills from an adult *Tg(cd4-1:mCherry)* fish were dissected, placed in 2% FCS in PBS, and immediately imaged with a confocal microscope for a duration of 30 mins in order to monitor cell motility. FCS is used to maintain dissociated live gill cells for flow cytometry and therefore it was anticipated that this medium would support whole gill tissue for at least the duration of imaging.

*Cd4-1:*mCherry+ cells were detectable in the gills with rounded or dendritic morphologies (Figure 3.5). Both rounded and dendritic-like cells were motile. Dendritic-like cells frequently extended and contracted long cytoplasmic projections whilst travelling within the tissue or whilst staying in one place. Rounded cells on the other hand did not display long cytoplasmic projections but were still found to move around the tissue. The tissue itself moved slightly during imaging however this did not impair the ability to monitor cell motility and may be related to the tissue being placed in a liquid medium. mCherry fluorescence diminished over time suggesting that photobleaching occurred. However, cell motility was observed for the entire duration of imaging suggesting that cells remained alive during this process.

These results demonstrated that widefield microscopy and stereomicroscopy are suitable for visualising individual fluorescent immune cells in the gills intravitally. The operculum does obstruct some fluorescent signal but cells can still be clearly observed in zebrafish with a *TraNac* genetic background. Confocal microscopy is better suited for visualising cellular details in high resolution in dissected live or fixed gill tissue. The combination of

these tools offers a versatile way of investigating immune cell features and behaviours in the gills. It is also important to note that some transgenic lines, such as *Tg(lck:GFP),* have low fluorescent protein expression meaning that fluorescent cells were difficult to detect in the gills using live microscopy techniques described. Cells from these lines were instead visualised by immunostaining of fixed tissues.
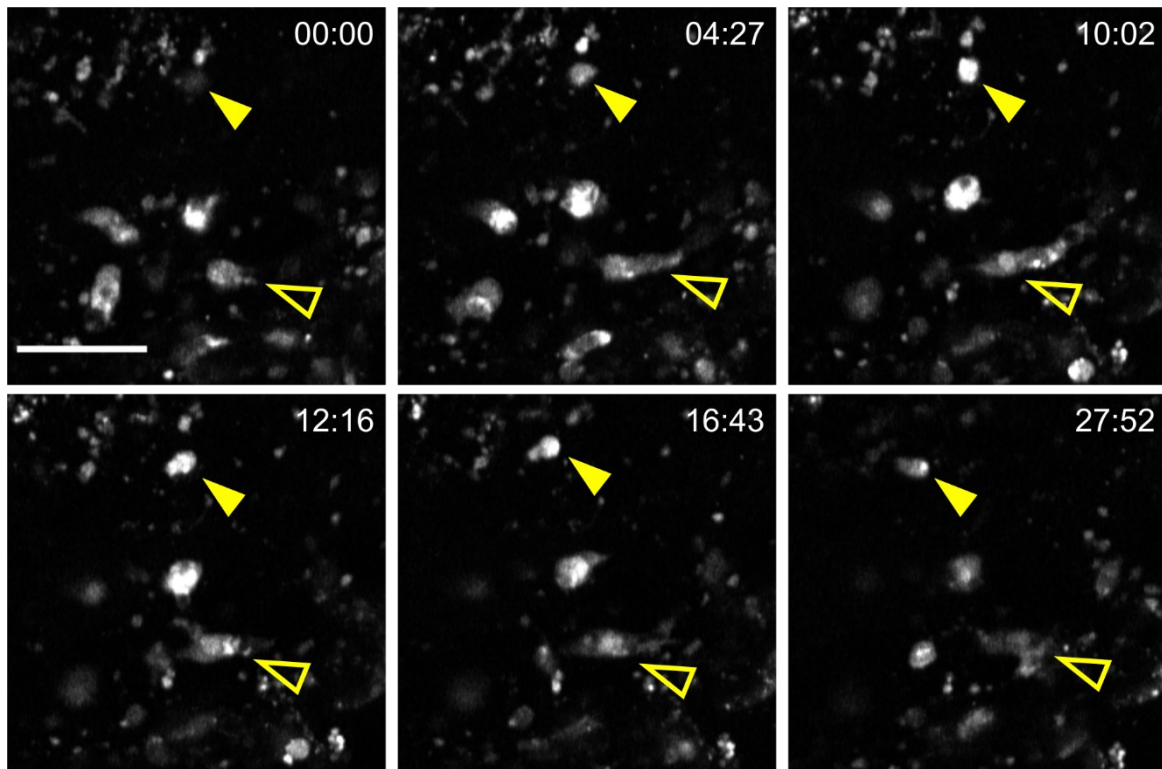
Figure 3.5 Live *ex vivo* confocal imaging of fluorescent immune cells in adult gills.

Maximum z-stack projections of dissected *Tg(cd4-1:mCherry)* gills acquired with a Leica SP5 inverted confocal microscope. *Cd4-1:*mCherry fluorescence is shown in white. Scale bar represents 25 μm. Numbers represent min:sec. Filled arrowhead indicates a rounded cell; unfilled arrowhead indicates a dendritic-like cell with multiple cytoplasmic projections.

3.3.1.3   *Morphological features of adult gill haematopoietic cells*

The data thus far reveals that diverse immune cells in the gills can be identified and characterised using flow cytometry and microscopy methods. However, focusing on transgenic fluorescent reporters limits cell characterisation to cell types for which reporters have been developed. The morphologies and cellular features of zebrafish

haematopoietic and immune cells have been previously described using Wright-Giemsa staining in several tissues including WKM, blood, and intraperitoneal exudate (Balla et al., 2010; Jagadeeswaran et al., 1999; Traver et al., 2003). To my knowledge, descriptions of gill immune cells using similar methods have not been published.

Gill cells from adult fish were first sorted into four fractions based on their FSC/SSC, corresponding to previously described populations (Figure 3.1C). This was performed to enrich populations that normally represent a small proportion of total gill cells, compared to erythrocytes. Sorted cells were then cytospun, stained with Wright-Giemsa, and imaged by widefield microscopy (Figure 3.6). Gills cells with similar features to published description of zebrafish haematopoietic cells were identified and categorised as lymphocyte, myeloid or erythrocyte-like.

Mononuclear cells with a small round shape and small cytoplasm:nucleus ratio were identified and categorised as lymphocyte-like (Figure 3.6A).

Mononuclear cells with a larger shape, large cytoplasm:nucleus ratio, and prominent cytoplasmic vacuoles were identified as myeloid-like cells (Figure 3.6B). These mostly likely represented monocytes and macrophages. Other myeloid-like cells included eosinophil/mast cells which had eosinophilic cytoplasm, large cytoplasm:nucleus ratio, a and polarised nuclear location (Figure 3.6C). Some myeloid-like cells exhibited long cytoplasmic projections suggesting these may have been dendritic cells (Figure 3.6D). Cells with typical neutrophil morphology (bilobed nucleus, granular cytoplasm), were not identified. This may be explained by the low proportion of neutrophils observed in *Tg(mpx:GFP)* gills (Figure 3.11A).

Erythrocytes were clearly identified as small elliptical cells with eosinophilic cytoplasm and a central nucleus (Figure 3.6E). Unlike in mammals, zebrafish erythrocytes are known to be nucleated (Jagadeeswaran et al., 1999).

These results show that gill cells have features consistent with previously described zebrafish haematopoietic cells. The use of Wright-Giemsa staining allowed identification of additional cell types and cellular features not fully captured with flow cytometry or fluorescence microscopy. This is further evidence of a diverse immune environment in the gills*.*
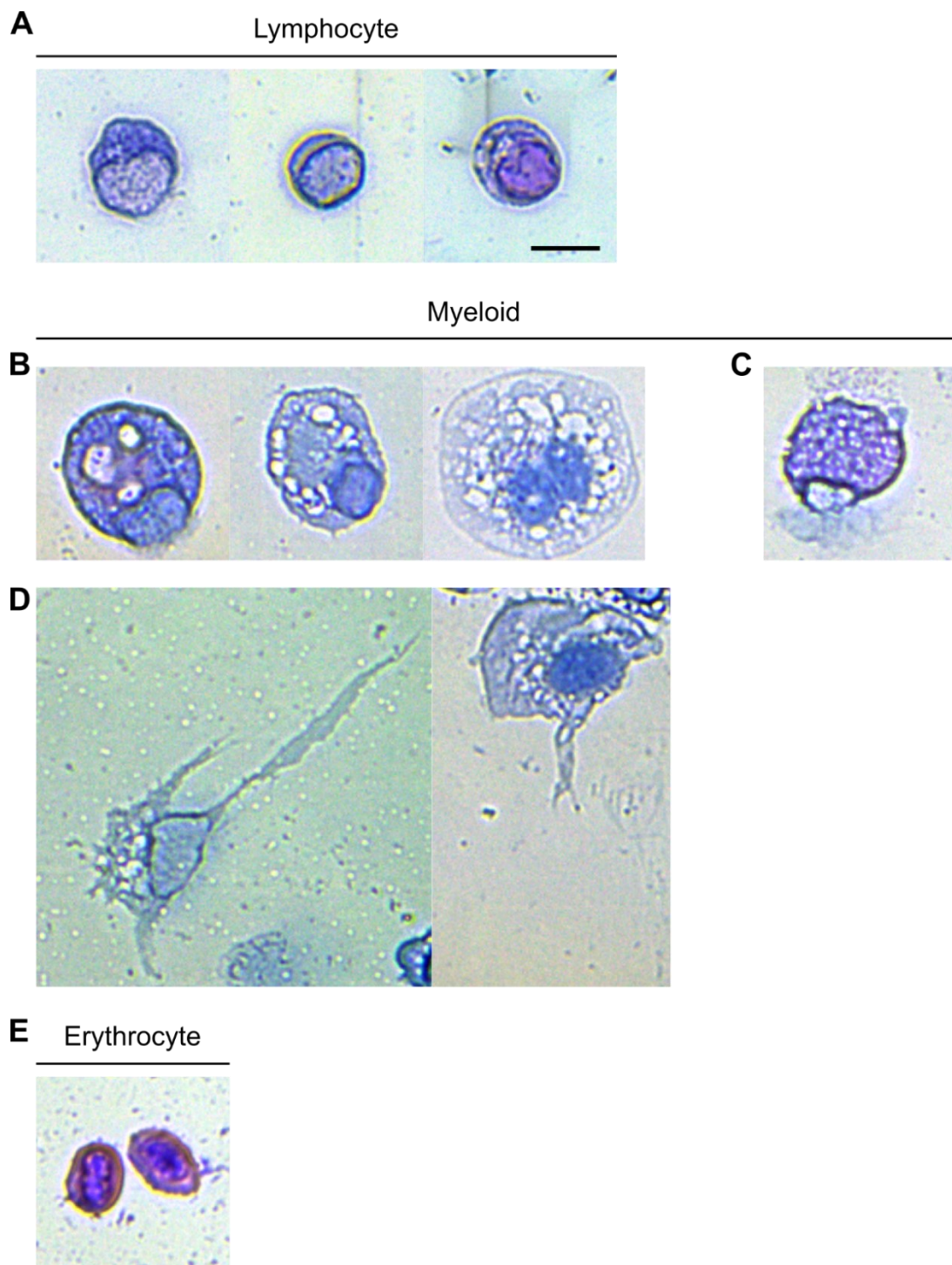
Figure 3.6 Haematopoietic cells from adult zebrafish gills.

Adult zebrafish gill cells were separated into four fractions based on FSC and SSC using a cell sorter. The cells were then cytospun, stained with Wright-Giemsa stain and imaged by widefield microscopy at 400X magnification. Images were cropped to show individual cells. Scale bar represents 10 μm. A) Lymphocyte-like cells. B) Monocyte/macrophage-like cells. C) Eosinophil/mast cell. D) Dendritic-like cells. E) Erythrocytes.

3.3.2 Immune cell composition in the gills from early development to aged stages

The following experiments aimed to determine how the composition of immune cells in the gills changes during early development and as zebrafish age. This would provide new evidence on potential immunological functions of the gills and reveal which aspects of immunology can be studied at different stages of gill development, as well as how this development compares to mammalian respiratory tissue.

3.3.2.1 *Presence and localization of neutrophils and lymphocytes in developing gills*

To visualise cells of the innate and adaptive immune system, gills from *Tg(lyz:GFP)* and *Tg(lck:GFP)* fish were imaged for neutrophils and lymphocytes respectively. *Tg(lyz:GFP)* fish contained brightly fluorescent myeloid cells which were easily identified by widefield and confocal microscopy (Figure 3.7). *Tg(lck:GFP)* fish contained fluorescent lymphocytes which were too dim to be identified by live intravital microscopy. Gills from these fish were therefore fixed, immunostained, and imaged using confocal microscopy (Figure 3.8).

Early development of zebrafish has been extensively characterised with stages defined according to anatomical features (Westerfield, 2000). Therefore, the gills were imaged at developmental stages corresponding to larval (5-21 dpf), juvenile (1-2 months post fertilisation), and adult stages (3 months post fertilisation or older).

The gill structure in both transgenic lines was identified as immature budding filaments at early larval stages (Figure 3.7A and Figure 3.8A). By the early juvenile stage at 21 dpf (Figure 3.7A and Figure 3.8B), the gills had a repeating filament structure more closely reflecting the adult anatomy (Figure 3.7B and Figure 3.8D). Confocal microscopy of the *Tg(lck:GFP)* line showed that secondary lamellae were present at this stage but with less symmetry than adult tissue (Figure 3.8B). Budding rakers were also identified in these samples. By 1 months post fertilisation (mpf), the gill structure was indistinguishable from the adult gills (Figure 3.7B & Figure 3.8C). No further changes in gross structure were observed after 1 mpf besides an increase in size.

Small numbers of individual GFP+ cells were present in and around the gill tissue at the early larval stage for both lines (Figure 3.7A and Figure 3.8A). Confocal imaging of *Tg(lyz:GFP)* (Figure 3.7C) and *Tg(lck:GFP)* (Figure 3.8A) samples showed that GFP+ cells were directly within developing gill tissue. In *Tg(lck:GFP)* samples, a direct connection between the gills and the *lck:*GFP+-cell-rich thymus was also observed. This connection has previously been reported in zebrafish (Lam et al., 2002).

Between 5 - 21 dpf, the number of *lyz:*GFP+ cells in the gill area appeared to increase, however it was not clear whether individual cells were in the gills or in surrounding tissue (Figure 3.7A). There were also more *lck:*GFP+ cells in the gills at this stage (Figure 3.8B). *Lck:*GFP+ cells were present throughout the gill structure, with more appearing to reside in the filaments than in the arch.

At 1 mpf, *lyz:*GFP+ cells remained in the gill area (Figure 3.7B)*.* In contrast to gills at 21 dpf, the majority of *lck:*GFP+ cells at 1 mpf were found in the arch region and few were found in the filaments or the rakers (Figure 3.8C). *Lck:*GFP+ cells were clearly aggregated in the gill arch between the rakers and the filaments, a unique feature not identified in earlier stages which is likely to developing ILT. Beyond 1 mpf, adult gills appeared to have increased numbers of *lck:*GFP+ cells in the filaments but also retained lymphocyte aggregates in the arch (Figure 3.8D).

These results show that immune cells are present from early stages of gill development, before the adaptive immune system has functionally matured. The gills undergo distinctive structural and immunological changes in lymphocytes between 21 dpf and 1 mpf which aligns with this period being an important point of zebrafish anatomical metamorphosis and adaptive immune system maturation (Lam et al., 2004; Parichy et al., 2009). This raises the question of whether immunological changes in the gills contribute to this maturation or are a consequence of more systemic changes.
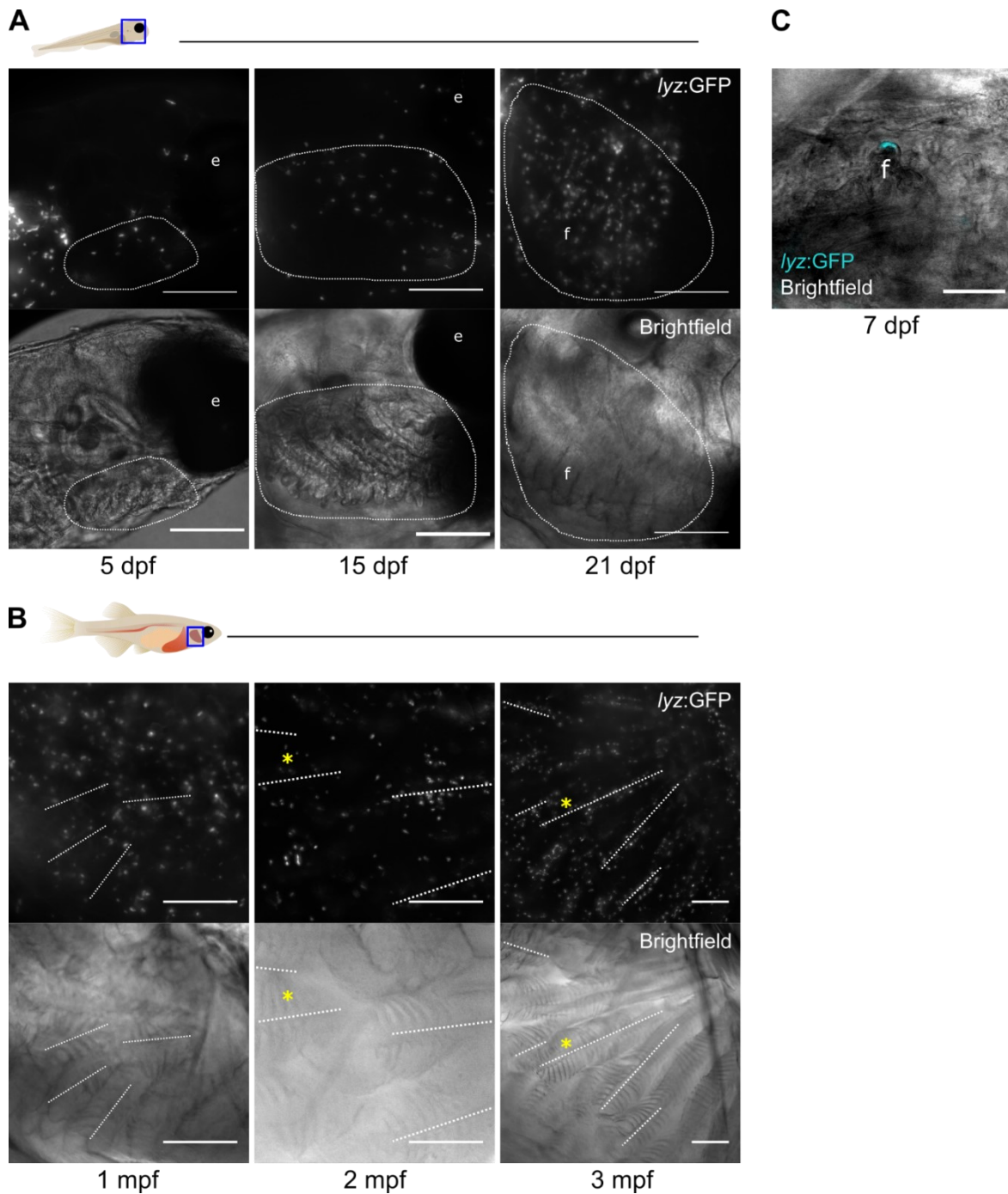
Figure 3.7 Live intravital imaging of neutrophils in developing *TraNac Tg(lyz:GFP)* gills from 5 dpf to 3 mpf.

(A, B) Representative widefield microscopy of the gills showing maximum z-stack projection of GFP+ cells (top image) and single plane image of the gill structure under transmitted light (bottom image). Area imaged is indicated by a blue box on diagrams of fish. Gill area is indicated by round shape. Filaments are indicated with dashed lines. e: eye, f: filaments, asterisk: secondary lamella. Scale bars represent 200 μm. C) Confocal image of developing gill filament (f) under transmitted light containing a GFP+ cell (cyan). Scale bar represents 50 μm.
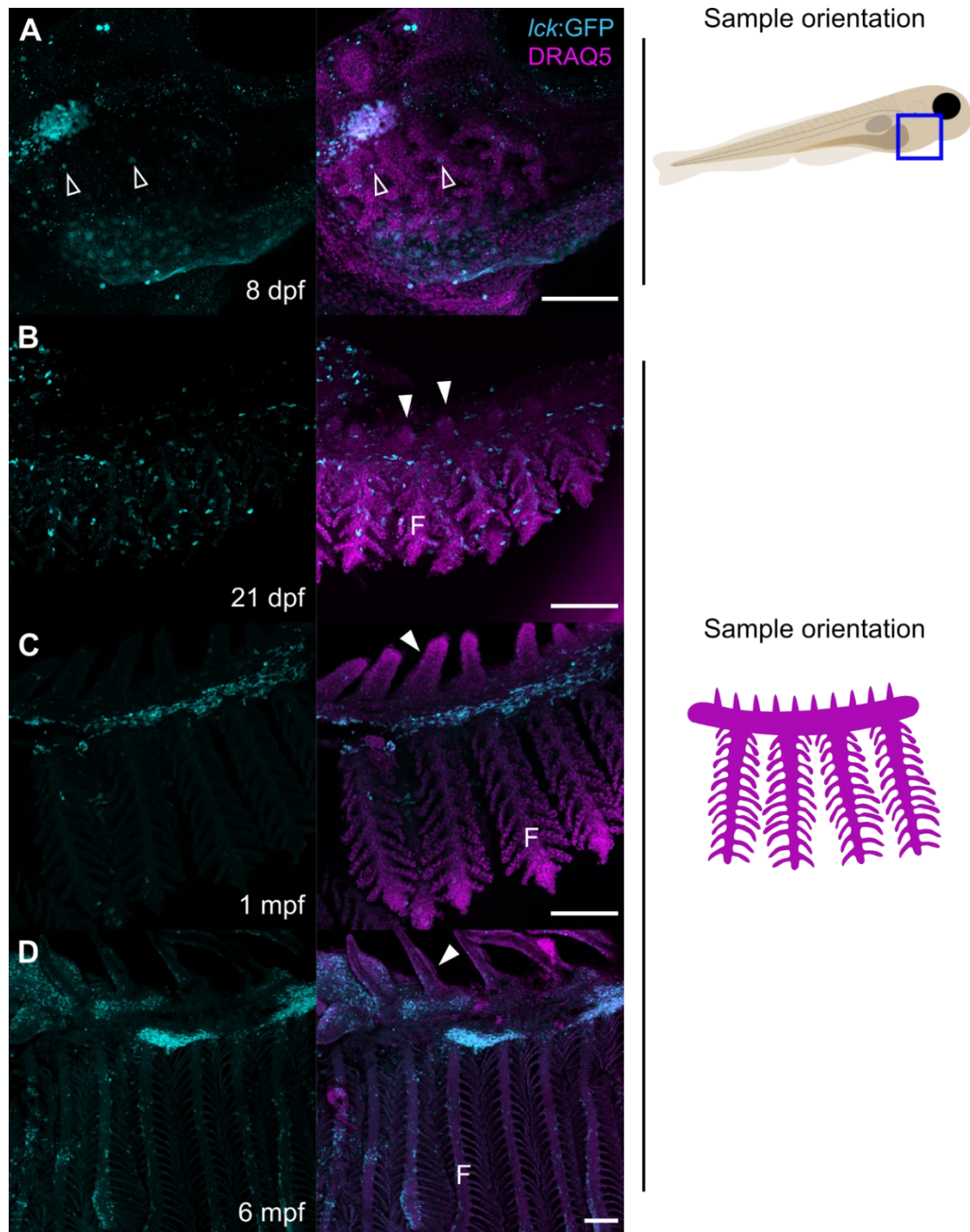
Figure 3.8 Confocal microscopy of lymphocytes in developing *TraNac Tg(lck:GFP)* gills from 8 dpf to 6 mpf.

(A-D) Maximum z-stack projections of fixed and immunostained gills in whole larvae (A) or as dissected tissue (B-D) with corresponding schematic or sample orientation (right). Blue box in schematic of (A) indicates region imaged. GFP immunostaining in cyan; DRAQ5 nuclear staining in magenta. Scale bar represents 100 μm. Unfilled arrowheads indicate GFP+ cells in gill tissue; filled arrowheads indicate rakers; F: filament.

3.3.2.2 *Immune cell composition and distribution in juvenile to adult gills*

To visualise and measure immune cell composition as zebrafish aged, gills from *Tg(mpeg1.1:SECFP-YPet)*, *Tg(lck:GFP)*, and *Tg(mpx:GFP)* fish were chosen to investigate macrophages, T and NK lymphocytes or ILCs, and neutrophils respectively. Recent evidence indicates that *mpeg1.1*-expressing cells also consist of B cells (Ferrero et al., 2020) and non-haematopoeitic metaphocytes (Lin et al., 2020). Gills were dissected and subjected to flow cytometry and fixed in parallel, then immunostained and imaged with confocal microscopy. Gills were analysed at three timepoints corresponding to juvenile (2 mpf), young adult (6-10 mpf), and ageing adult (18-21 mpf) stages. Physiological differences between the two adult stages have previously been reported, therefore it was hypothesised that immunological differences may also exist between these stages (Kishi et al., 2003; Tsai et al., 2007).

3.3.2.3 *Microscopy of juvenile and adult gills*

*Lck:*GFP+ cells formed dense aggregates in the posterior region of the arch close to filaments and sometimes directly between adjacent filaments (Figure 3.9A-C)**.** These dense aggregates were highly variable in size**.** More diffuse aggregates of *lck:*GFP+ cells were found in the anterior region of the arch surrounding the rakers, with much fewer cells appearing in the rakers themselves. *Lck:*GFP+ cells were also distributed through the filaments including in the primary lamellae, secondary lamellae, and interlamellar regions. *Lck:*GFP+ cells appeared as individual cells or as small aggregates in the filaments, however there appeared to be no obvious structural organization to these features. *Lck:*GFP+ cells were small and either round or irregularly shaped (Figure 3.10A). The distribution of *lck:*GFP+ cells was similar across all three developmental stages.

*Mpeg1.1:*SECFP-YPet+ cells formed a diffuse network of dendritic-like cells in the anterior region of the arch around the rakers (Figure 3.9D-F). *Mpeg1.1:*SECFP-YPet+ cells were also found in the posterior region of the arch, however unlike *lck:*GFP+ cells, they did not form dense clusters and appeared to be evenly distributed along the arch. *Mpeg1.1:*SECFP-YPet+ cells were also found in the filaments, in both the primary and secondary lamellae, and in the interlamellar regions with no obvious organization. Most *mpeg1.1:*SECFP-YPet+ cells had extensive cytoplasmic projections and an irregular shape,

however, some were round and smaller in size (Figure 3.10B). Cells of both morphologies were found throughout the arch and filaments. The distribution and morphology of *mpeg1.1:*SECFP-YPet+ cells did not appear to change over time.

Unlike *lck:*GFP+ or *mpeg1.1:*SECFP-YPet+ cells, *mpx:*GFP+ cells were infrequently found in the arch, residing primarily in the filaments (Figure 3.9G-I). Furthermore, they were found mainly as individual cells, forming small clusters only infrequently. Within the filaments, *mpx:*GFP+ cells were found in the primary and secondary lamellae, and in interlamellar regions with no obvious organization. *Mpx:*GFP+ cells throughout the gills showed a range of morphologies with either round or irregular shapes, and with or without cytoplasmic projections (Figure 3.10C). *Mpx:*GFP+ cells were overall less dendritic than *mpeg1.1:*SECFP-YPet+ cells and larger than *lck:*GFP+ cells. Again, cell distribution and morphology appeared unchanged over time.

In addition to cell distribution and morphology, there were no obvious changes in gill structure beyond an increase in size from juvenile to young adult stage.
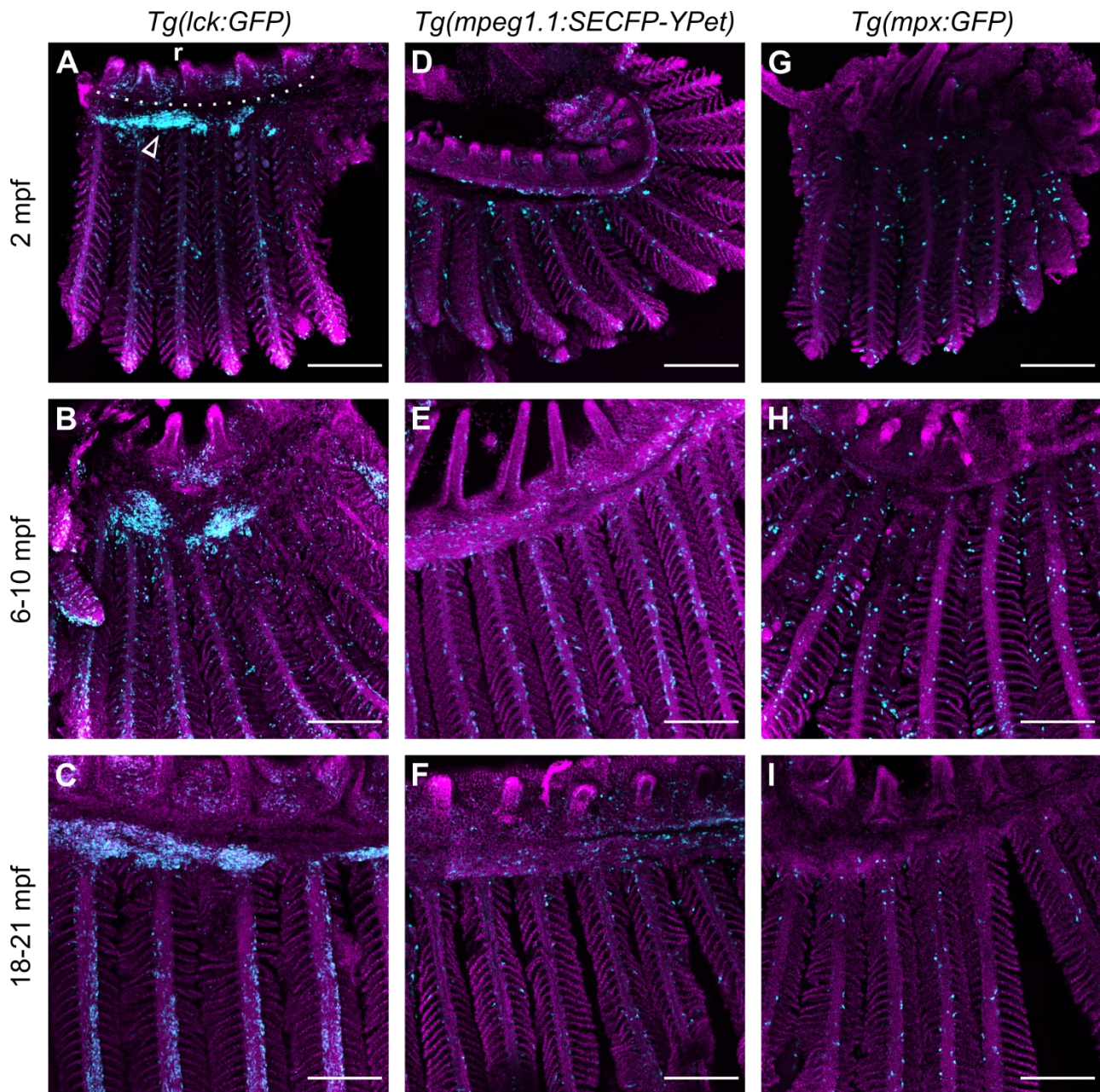
Figure 3.9 Confocal microscopy of immune cells in juvenile (2 mpf), young adult (6-10 mpf), and ageing adult (18-21 mpf) gills.

Tg(lck:GFP), *Tg(mpeg1.1:SECFP-YPet)* and *Tg(mpx:GFP)* transgenic gills were immunostained and imaged to visualise T and innate lymphocytes, myeloid/B/metaphocyte cells, and neutrophils respectively. Representative maximum z-stack projections of confocal microscopy images of immunostained gills at 170X magnification. N = 3-6. GFP and SECFP-YPet immunostaining in cyan; DRAQ5 nuclear staining in magenta. Scale bar represents 200 µm. Dotted line indicates gill arch; r: rakers; arrowhead: GFP+ cell accumulation in posterior arch region.
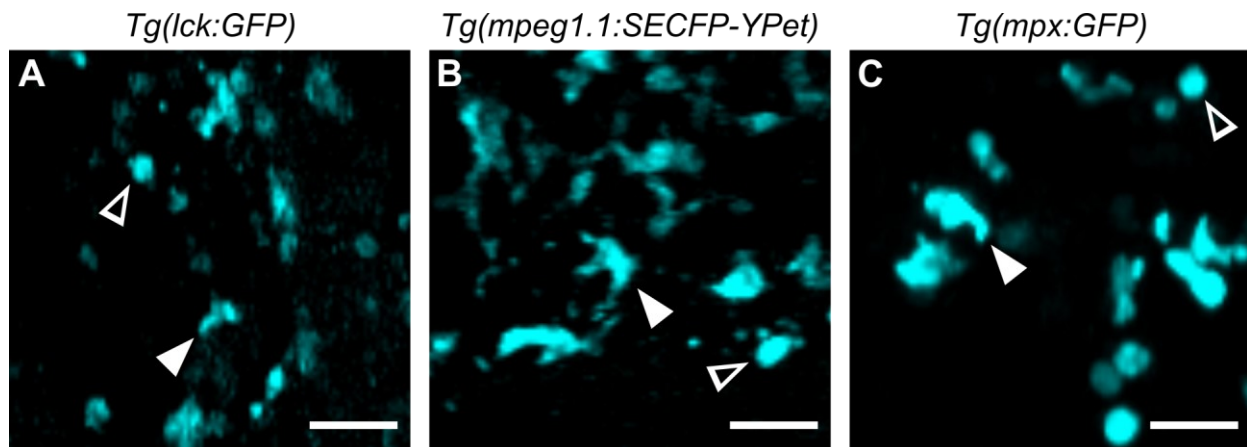
Figure 3.10 Confocal microscopy of immune cell morphology in young adult (6-10 mpf) gills.

A) *Tg(lck:GFP),* B) *Tg(mpeg1.1:SECFP-YPet)* and C) *Tg(mpx:GFP)* transgenic gills were immunostained and imaged to visualise T and innate lymphocytes, myeloid/B/metaphocyte cells, and neutrophils respectively. Representative maximum z-stack projections of confocal microscopy images of immunostained gills at 170X magnification. N = 3-6. GFP and SECFP-YPet immunostaining in cyan; DRAQ5 nuclear staining in magenta. Scale bar represents 20 μm. Unfilled arrowhead indicates irregular cell morphology; filled arrowhead indicates rounded cell morphology.

3.3.3 Flow cytometry of juvenile and adult gills

Analysis by flow cytometry showed that the proportion of fluorescent cells in the gills from each transgenic line did not change over time (Figure 3.11A). However, there were notable differences in the proportion of fluorescent cells between each transgenic line. *Lck:*GFP+ cells comprised a far greater percentage of cells in the gills than *mpeg1.1:*SECFP-YPet+ or *mpx:*GFP+ cells, averaging between 16-21% of total gill cells. *mpeg1.1:*SECFP-YPet+ cells made up 2-3% of gills cells whilst *mpx:*GFP+ cells made up the smallest percentage, averaging less than 1% of total gill cells at each developmental stage.

Furthermore, fluorescent cells showed different FSC/SSC properties in the three different transgenic lines (Figure 3.11B). *Lck:*GFP+ cells were almost entirely found in the lymphocyte gate for all three developmental stages. *Mpeg1.1:*SECFP-YPet+ cells on the other hand showed some differences in FSC/SSC properties between developmental stages. At 2 mpf, the majority of *mpeg1.1:*SECFP-YPet+ cells were found in the lymphocyte gate (M = 71%, SD = 7) with 10% or less found in each of the other three gates. However, in both the young adult and ageing adult stages, *mpeg1.1:*SECFP-YPet+ cells were evenly

126

distributed between the myeloid and lymphocyte gates with a small percentage in the precursor and erythrocyte gates. Using a transgenic *mpeg1.1:*GFP reporter, one study showed that lymphoid *mpeg1.1:*GFP+ cells were significantly lower in fluorescence than *mpeg1.1:*GFP+ myeloid cells (Ferrero et al., 2020). In this project, the median intensity fluorescence (MFI) for *mpeg1.1:*SECFP-YPet was similarly found to be lower in cells in the lymphocyte gate than cells in the myeloid gate (Figure 3.11C). This was true for each developmental stage. However, the fluorescence of cells in the myeloid gate was noticeably lower at 18-21 mpf than at the two other developmental stages. This may indicate reduced expression of Mpeg1.1 although protein or RNA levels were not measured in this experiment. *Mpx:*GFP+ cells exhibited similar FSC/SSC properties at all three developmental stages with fluorescent cells found mainly in the myeloid gate, and smaller percentages found primarily in the erythrocyte and lymphocyte gates (Figure 3.11B).
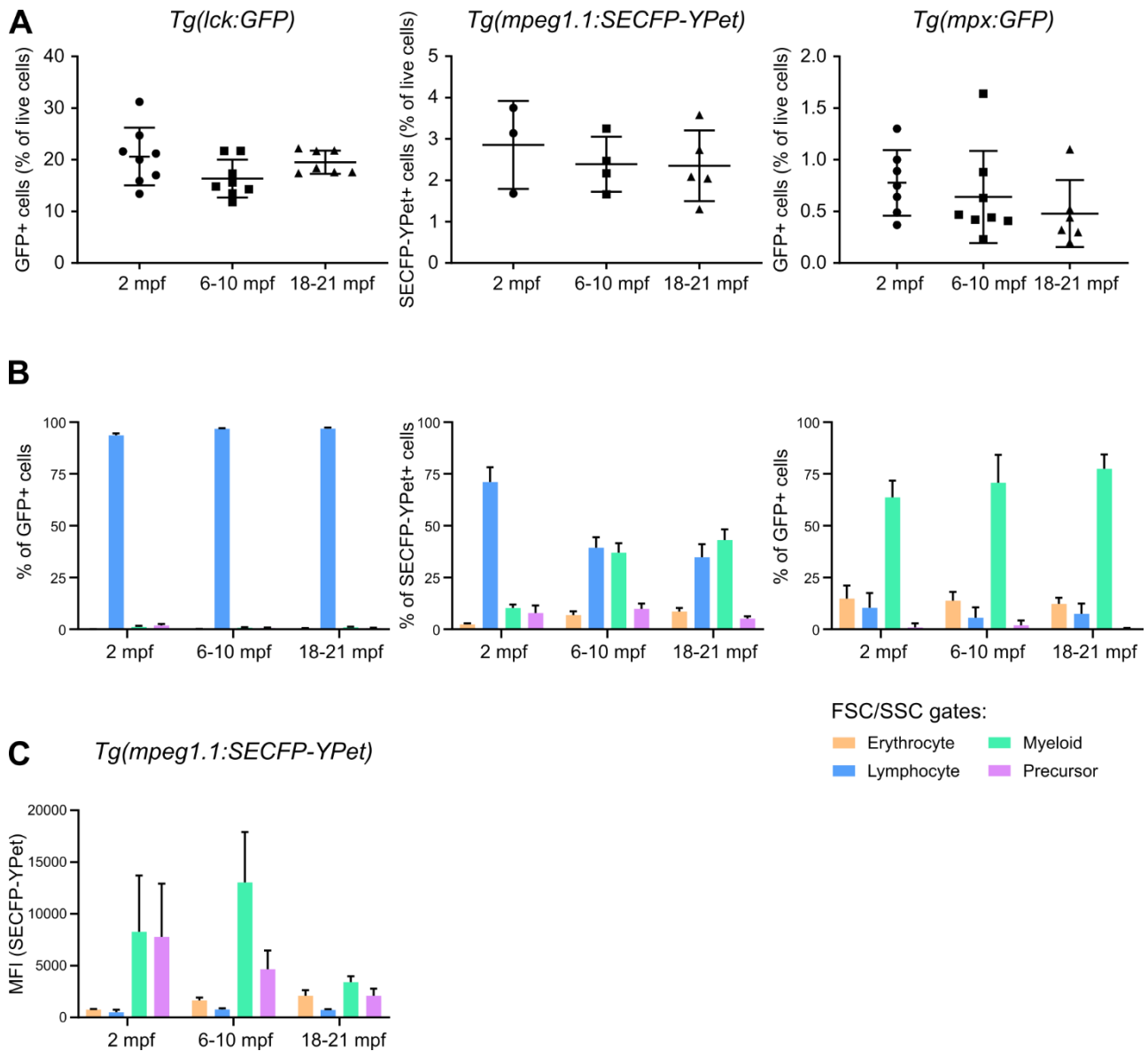
Figure 3.11 Flow cytometry of immune cells in juvenile (2 mpf), young adult (6-10 mpf), and ageing adult (18-21 mpf) gills.

Tg(lck:GFP), *Tg(mpeg1.1:SECFP-YPet)* and *Tg(mpx:GFP)* transgenic gills were used to quantify T and innate lymphocytes, myeloid/B/metaphocyte cells, and neutrophils respectively. N = 3-8. A) Proportion of fluorescent cells as a percentage of total live cells. Each dot represents 1 fish. One-way ANOVA performed with Tukey's multiple comparisons test. No statistically significant differences were identified for any of the datasets. B) Mean proportion of cells in erythrocyte, lymphocyte, myeloid, or precursor gates as a percentage of total fluorescent cells. C) Median fluorescence intensity (MFI) of SECFP-YPet for SECFP-YPet+ cells in the four population gates. Mean and SD shown for (A-C).

3.3.4 Cellular and anatomical properties of lymphocyte clusters in the gills

In this project, imaging of *Tg(lck:GFP)* gills revealed prominent clusters of lymphocytes in the arch (Figure 3.9). *Lck:*GFP+ cells were also found to comprise the largest proportion of immune cells investigated in the gills (Figure 3.11A). The large size of these clusters and general abundance of lymphocytes in the gills suggests that this lymphoid structure may have an important immunological role in the gills. Previous literature has identified lymphocyte-rich tissue in the interbranchial region of salmonids which further extends along filament edges. During the experimental stages of this thesis, literature on the ILT was limited to salmonids species. Investigation of *Tg(lck:GFP)* gills in this thesis revealed the presence of a similar structure in zebrafish. More recently a study has identified ILT in the zebrafish gills by detection of Zap70+ cells (Rességuier et al., 2020). This corroborates the findings in this thesis although additional cellular features were not investigated by Rességuier et al.

It has been suggested that the ILT could function as a secondary lymphoid tissue, however, unlike lymph nodes and other mammalian secondary lymphoid structures, distinct B- and T cell regions have not been described. Having identified ILT in zebrafish the next set of experiments sought to address three questions:

- What are the defining cellular and anatomical features of ILT in zebrafish?
- Does this tissue bear any similarity to mammalian lymphoid tissues?
- From these features can we infer a potential role of this tissue as a secondary lymphoid tissue?

3.3.4.1 *Quantitative analysis of lymphocyte cluster anatomy*

The first step was to define the anatomical features of lymphocyte clusters in the gills. These features are important for comparing zebrafish gill lymphoid tissues to lymphoid tissues in other species, and for informing future studies on this tissue. The main features investigated in this project were the size of clusters, distribution within the arch and variability between fish. Some secondary lymphoid structures in mammalian species, such as lymph nodes, develop in precise anatomical locations, whilst other structures, such as Peyer's patches, are more randomly distributed within particular regions (Cesta, 2006).

For this experiment, gill arches from the right side of *Tg(lck:GFP)* fish were immunostained and imaged by confocal microscopy. Multiple z-stacks of the outermost (1st) and innermost (4th) gill arches (Figure 3.12A) were acquired and stitched together, revealing the entire length and width of the arch for both the external-facing and internal-facing hemibranches (Figure 3.12C-F). All fish displayed *lck:*GFP+ cell clusters in the arch in both hemibranches of the 1st and 4th gill arches.

ILT in salmon gills extends from the arch into the filaments and displays anatomical differences between afferent and efferent edges (Dalum et al., 2015). In teleosts, each hemibranch consists of an afferent edge where deoxygenated blood enters the filaments and an efferent edge where oxygenated blood exits the filaments (Figure 3.12B) (Olson, 2002). The afferent edge contains larger numbers of T cells and a more prominent basement membrane separating the ILT from the underlying gill tissue (Dalum et al., 2015). To assess distribution of *lck:*GFP+ cells in zebrafish filaments, both the afferent and efferent edges of immunostained arches were imaged by confocal microscopy. Whole-mount imaging of gill arches is usually performed in the medio-lateral orientation which mostly obstructs the afferent edge (Figure 3.12B). Arches were therefore cut transversally into sections and orientated in agarose to expose the afferent edge (Figure 3.12G). This allowed visualisation of both edges simultaneously but could not capture the afferent edge of the entire hemibranch.

*Lck:*GFP+ cells were identified on both the efferent and afferent edges of filaments for all fish (Figure 3.12H). The primary lamellae of the afferent edge appeared to be consistently wider than the efferent edge and correspondingly contained a much larger accumulation of *lck:*GFP+ cells. The accumulation on the afferent edge was often continuous from the arch and extended into the intrabranchial region between the two hemibranches.

To quantify *lck:*GFP+ clusters in the arch, the arch area was manually defined and split into two regions: the anterior region covering the tips to the bases of the rakers, and the posterior region, covering the bases of the rakers to the top of filaments (Figure 3.13A). Only anterior or posterior regions with intact rakers or filaments respectively were considered for analysis.

Clusters of *lck:*GFP+ cells were defined as structures with an area ≥ 250 μm², equivalent to around ten times the area of an individual *lck:*GFP+ cell. These clusters were detected

and their areas measured computationally with an automated protocol. Some clusters extended beyond the arch so the portions outside the arch were manually excluded from the analysis. In addition, the protocol occasionally detected areas of high background GFP signal which were identified manually and excluded from analysis.

For quantitative analysis, only samples of the 1st gill arch (Figure 3.12A) were used due to a larger number of biological replicates. Clusters were measured for both the internal and external hemibranches (Figure 3.13A). Clusters covered on average 38% (SD = 7) and 29% (SD = 8) of the total arch area on the external and internal hemibranches respectively (Figure 3.13B). Although clusters covered a slightly larger area in the external hemibranch, this was not statistically significant. Clusters were found along most of the length the arch and this did not seem to differ much between internal and external hemibranches (Figure 3.13C).

The posterior region of the arch was more extensively covered in clusters than the anterior region for both hemibranches (Figure 3.13D). Cluster coverage in anterior regions was similar in both hemibranches, however, coverage in posterior regions appeared to be greater in the external hemibranch. Analysis with two-way ANOVA showed that the differences between hemibranches, and the differences between arch regions were statistically significant overall ($p = 0.04$ and $p = 0.0007$ respectively). However, coverage of the internal and external posterior regions were not found to be significantly different following direct comparison (Sidak's multiple comparison test, $p = 0.12$). These results indicate that cluster distribution is similar between hemibranches but there may be differences which warrant further investigation.

The areas of individual clusters were highly variable ranging from magnitudes of 10^2-10^6 µm^2 (Figure 3.13E). The variation in size was similar between internal and external hemibranches, where the 75% percentiles were 1377 µm^2 and 1108 µm^2 respectively. Clusters that overlapped anterior and posterior regions had the largest range of sizes and a greater median size than clusters found exclusively in anterior or posterior regions (Figure 3.13F). Furthermore, clusters in the anterior regions had a smaller range and lower median size than clusters in posterior regions. This pattern was similar between hemibranches, although the median size of overlapping clusters was greater in the internal hemibranch.

These results show that *lck:*GFP+ clusters are a consistent feature of the gill arch and filaments. Although clusters are distributed throughout the gills, they cover a greater proportion of the posterior arch region and the afferent filaments. These differences in distribution, along with the large variability in cluster sizes, may indicate functional differences within this lymphoid tissue. Internal and external hemibranches may have slight differences in cluster coverage but overall showed similar patterns of distribution. Therefore, further study of this lymphoid tissue could be carried out using either hemibranch, at least at steady state.
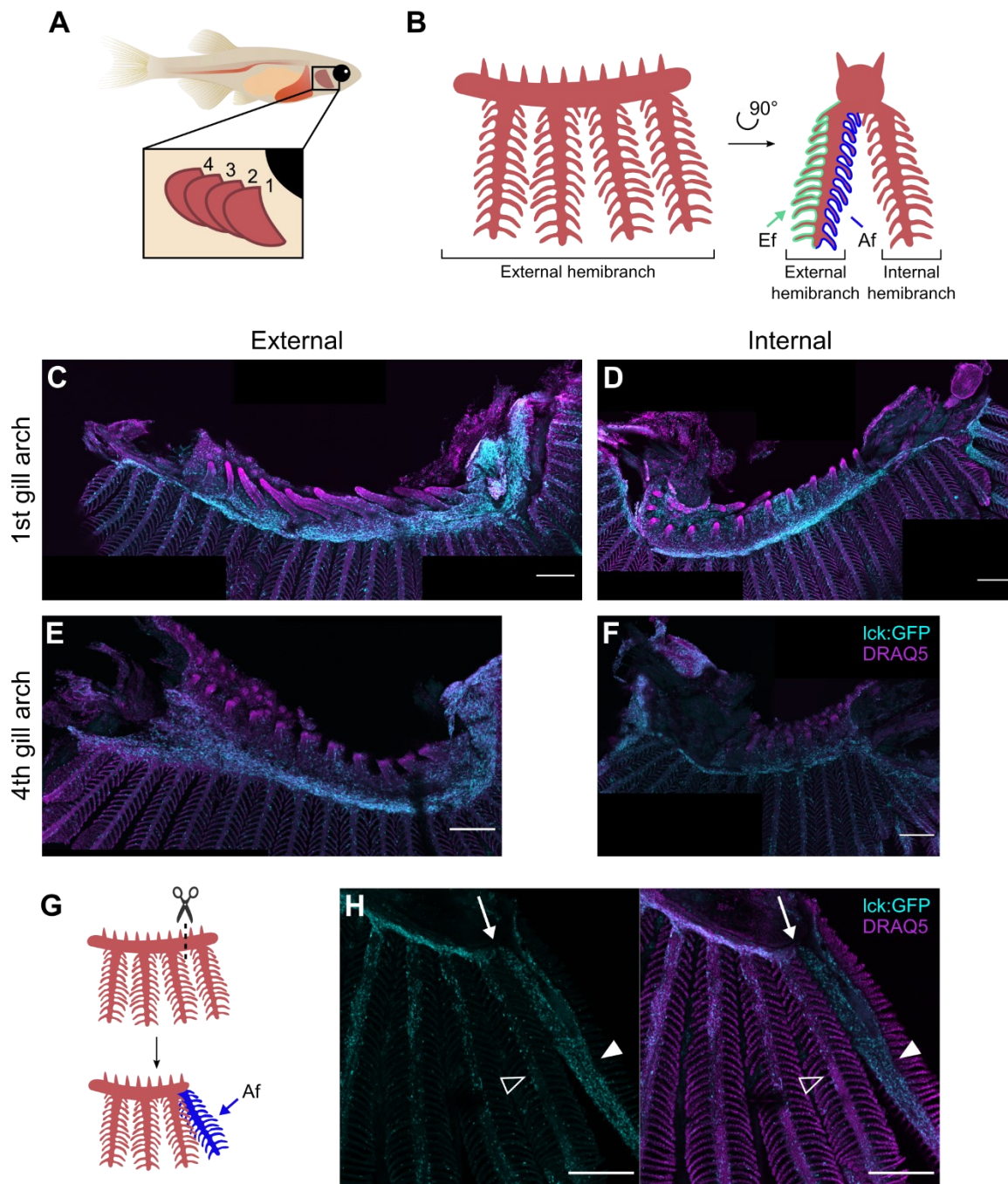
Figure 3.12 Confocal microscopy of arches and afferent filaments of adult *Tg(lck:GFP)* gills.

A) Schematic showing a medio-lateral view of how the gills are arranged in zebrafish. B) Schematic showing the medio-lateral view of a single gill arch (left), and a transverse view of a gill arch showing the two hemibranches (right). The efferent and afferent edge of the external hemibranch are highlighted in green and blue respectively. (C-F) Maximum z-stack projections of immunostained gills from a representative fish. Each image is composed from 2-3 overlapping images. N = 4. G) Schematic showing transverse cut (dotted line) of a gill arch to expose the afferent edge of a filament (blue). H) Representative maximum z-stack projections of an immunostained gill showing the efferent filaments

(unfilled arrowhead), an afferent filament (filled arrowhead) and GFP+ cells extending into the interbranchial region (arrow). N = 4. (C-G) Scale bar represents 200 μm. GFP immunostaining in cyan; DRAQ5 nuclear staining in magenta.
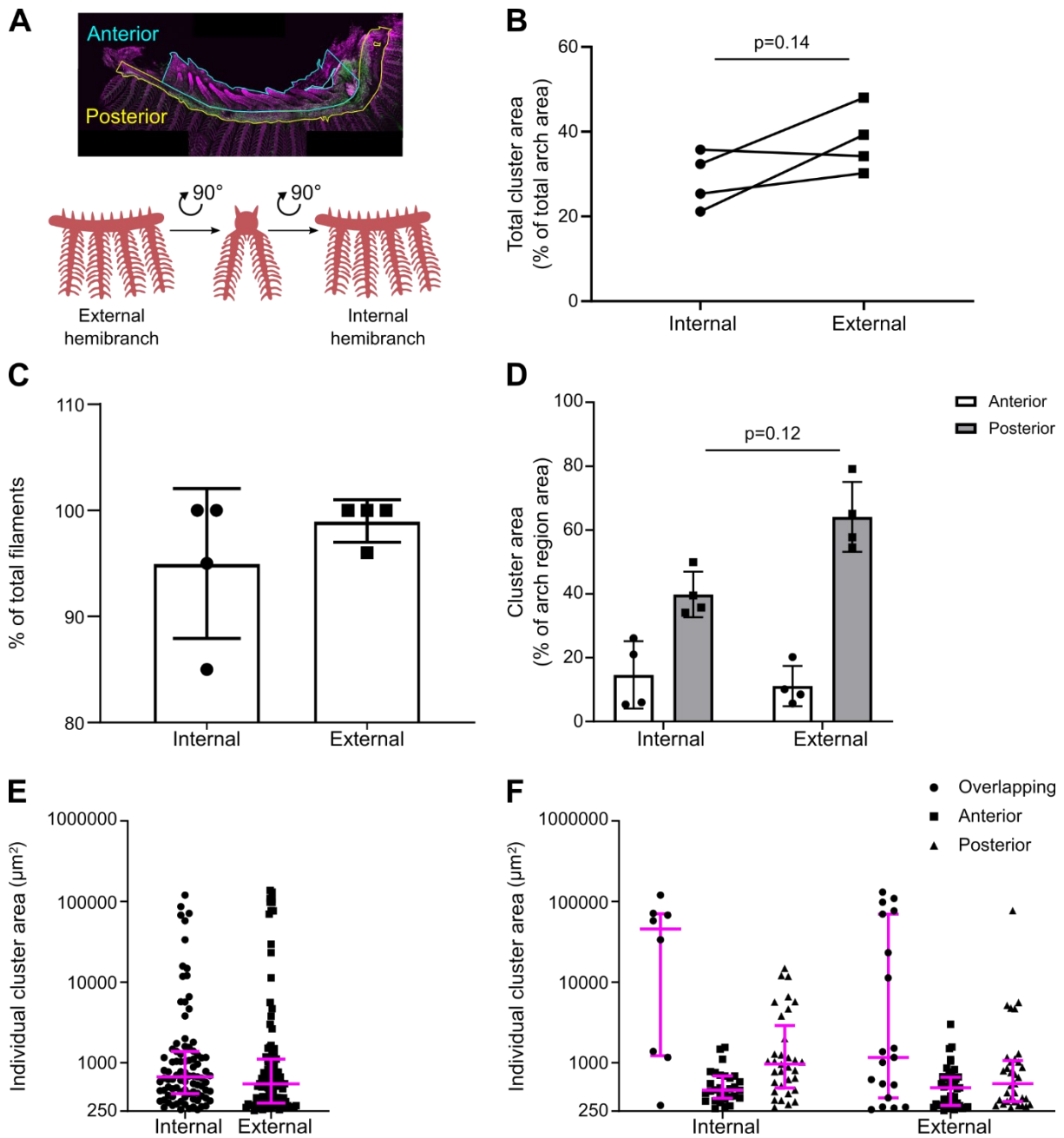
Figure 3.13 Quantitative analysis of *lck:*GFP+ cell clusters in adult gills.

*Lck:*GFP+ cell clusters in the 1st gill arch were detected and measured computationally from maximum z-stack projections as shown in Figure 3.12. A) The arch region in which to detect clusters was manually defined and split into the anterior and posterior region (top). Schematic showing the relationship between external and internal hemibranches (bottom). B) The cumulative area of clusters as a percentage of the total area of the arch region. Paired two-tailed t-test was performed. C) The percentage of filaments directly below clusters in the posterior region. D) The cumulative area of

whole or partial clusters found in the anterior or posterior arch region, as a percentage of the total area of these regions. Two-way ANOVA performed followed by Sidak's multiple comparison test. (B-D) Mean and SD shown. E) The area of individual clusters in the gill arch. F) The area of individual clusters found overlapping the anterior and posterior regions or found exclusively in either region. (E, F) Median and 75 percentiles shown.

3.3.4.2 *Flow cytometry analysis of lymphocyte and myeloid cells in whole gill tissue*

To further characterise the lymphocyte populations in the gills, *Tg(cd4-1:mCherry; lck:GFP)* and *Tg(IgM:GFP; cd4-1:mCherry)* transgenic fish were analysed by flow cytometry and confocal imaging. These lines were chosen to identify cells known to be present in MALT such as, T cells, B cells, and myeloid cells. As detailed in the introduction to this chapter, *cd4-1* expression distinguishes some T cells from *lck*-expressing NK- or ILC-like cells. It is also expressed in some myeloid cells. *IgM*:GFP labels a subset of B cells. *Lck+*, *ighm+*, and *cd4-1+* cells have all been previously identified in zebrafish gills but detailed characterisation of these populations is lacking, especially regarding their spatial distribution within the tissue (Dee et al., 2016; Progatzky et al., 2019; Rességuier et al., 2017). Sample processing and data acquisition of *Tg(cd4-1:mCherry; lck:GFP)* samples was carried out by Katie Tsoi (MRes, Imperial College London).

In this set of flow cytometry experiments, *lck:*GFP+ cells made up 18% (SD = 4.6) of gill cells and were found mostly in the lymphocyte gate (Figure 3.14A, E, J and K). Of *lck:*GFP+ cells, 17% (SD = 4.0) were *cd4-1:*mCherry+ which closely matches previously reported figures from Dee et al. (Figure 3.14B). The scatter of both GFP+mCherry+ and GFP+mCherry- populations was similar to total *lck:*GFP+ cells with most cells falling in the lymphocyte gate (Figure 3.14F, G, and K).

*Cd4-1:*mCherry+ cells made up 5% (SD = 1) of gill cells - a smaller proportion than *lck:*GFP+ cells (Figure 3.14C and J). They also had more heterogenous FSC/SSC properties than *lck:*GFP+ cells; although the majority of *cd4-1:*mCherry+ cells were in the lymphocyte gate (M = 60%, SD = 13), 22% (SD = 7) of cells were in the myeloid gate (Figure 3.14H, I and K). The proportions of *cd4-1:*mCherry+ cells in the precursor and erythrocyte gates were also greater than for the *lck:*GFP+ population. The percentage of *cd4-1:*mCherry+ cells in the lymphocyte gate closely matched the percentage of *cd4-*

*1:*mCherry+ cells which were *lck:*GFP+ (M = 65%, SD = 12), further supporting the use of FSC/SSC properties to distinguish immune cell subsets in the gills.

*Cd4-1:*mCherry+*lck:*GFP- cells had a different scatter profile to total *cd4-1:*mCherry+ cells with the majority of cells in the myeloid gate (M = 59%, SD = 5) (Figure 3.14K). The proportion of cells in the erythrocyte gate was also increased compared to total *cd4-1:*mCherry+ cells.
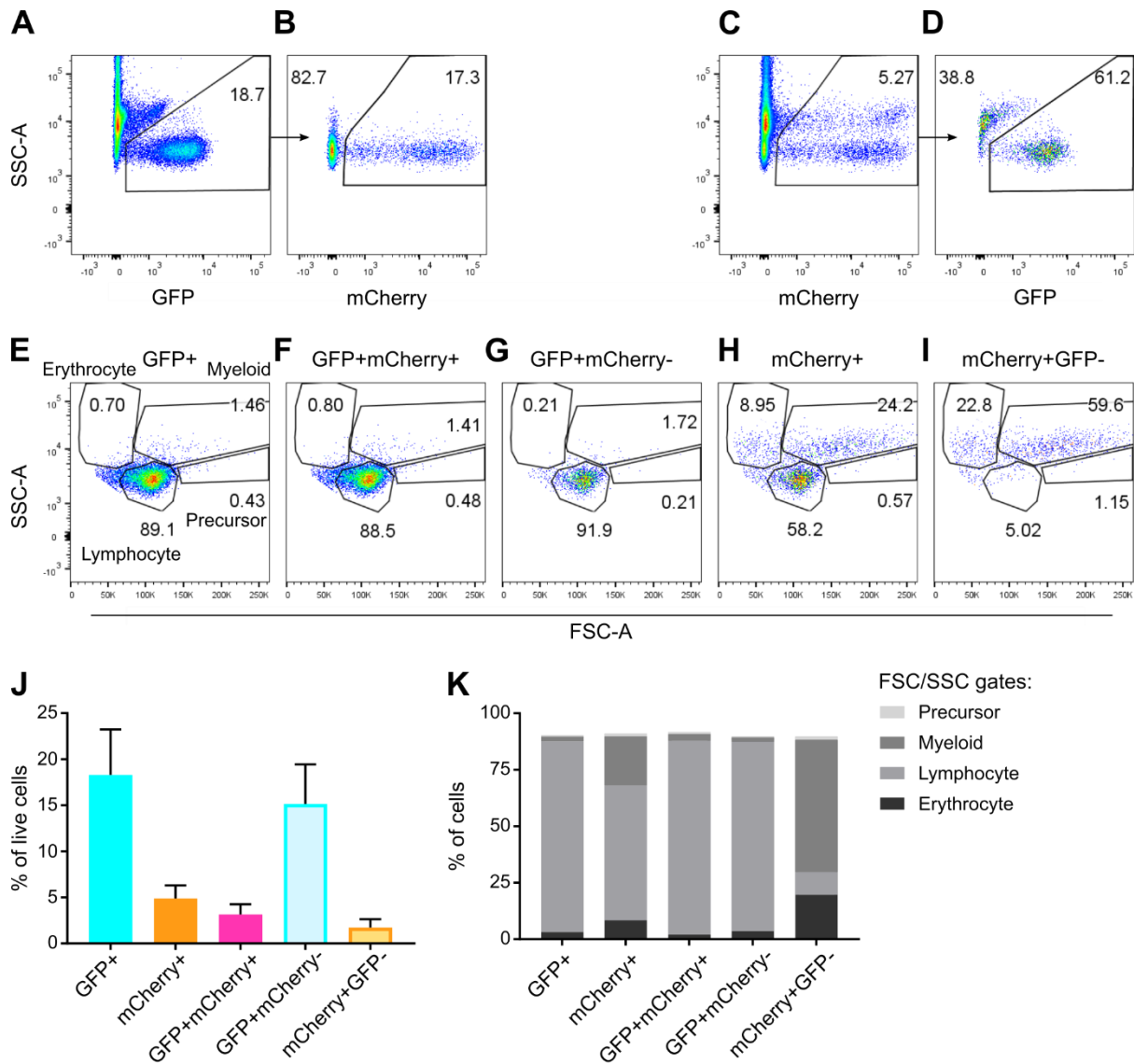
Figure 3.14 Flow cytometry of gills from adult *Tg(cd4-1:mCherry; lck:GFP)* fish.

A) Live cells gated for GFP fluorescence. B) GFP+ population gated for mCherry+ fluorescence. C) Live cells gated for mCherry fluorescence. D) mCherry+ population gated for GFP fluorescence. (A-D) Values inside and outside the gates indicate the respective proportion of events as a percentage of total events in the plot. (E-I) FSC/SSC profile of fluorescent cell populations. Values in plots reflect percentages of events in each of the four gates compared to total events in each plot. (A-I) Representative plots from one fish. N = 4. J) Proportion of fluorescent cells as a percentage of live cells. Mean and SD shown. K) Mean proportion of cells in the four population gates as a percentage of total cells of each fluorescent population. Sample processing and data acquisition was carried out by Katie Tsoi (Imperial College London) as part of her Master's thesis on zebrafish gill characterisation (Tsoi, 2019). Analysis in this PhD thesis was performed by me.

137

*IgM:*GFP+ cells made up 0.6% of total gill cells and the majority were *cd4-1:*mCherry- (Figure 3.15A, B and E). *IgM:*GFP+*cd4-1:*mCherry+ double positive cells made up an even smaller minority, only 0.03% of total gill cells. B cells are not generally expected to express *cd4-1* in zebrafish (Tang et al., 2017) or other species. Therefore, these cells may be false positives; their mCherry expression may not correlate to *cd4-1* expression or they may not truly express mCherry at all. No double positive cells were observed in any gill samples imaged by fluorescence confocal microscopy (n = 5) providing support that these cells may indeed be false positives. The majority of *IgM:*GFP+ cells fell in the lymphocyte gate (M = 82%, SD = 3.5), with fewer cells in the myeloid gate than the *cd4-1:*mCherry+ population (Figure 3.15C, D and F).
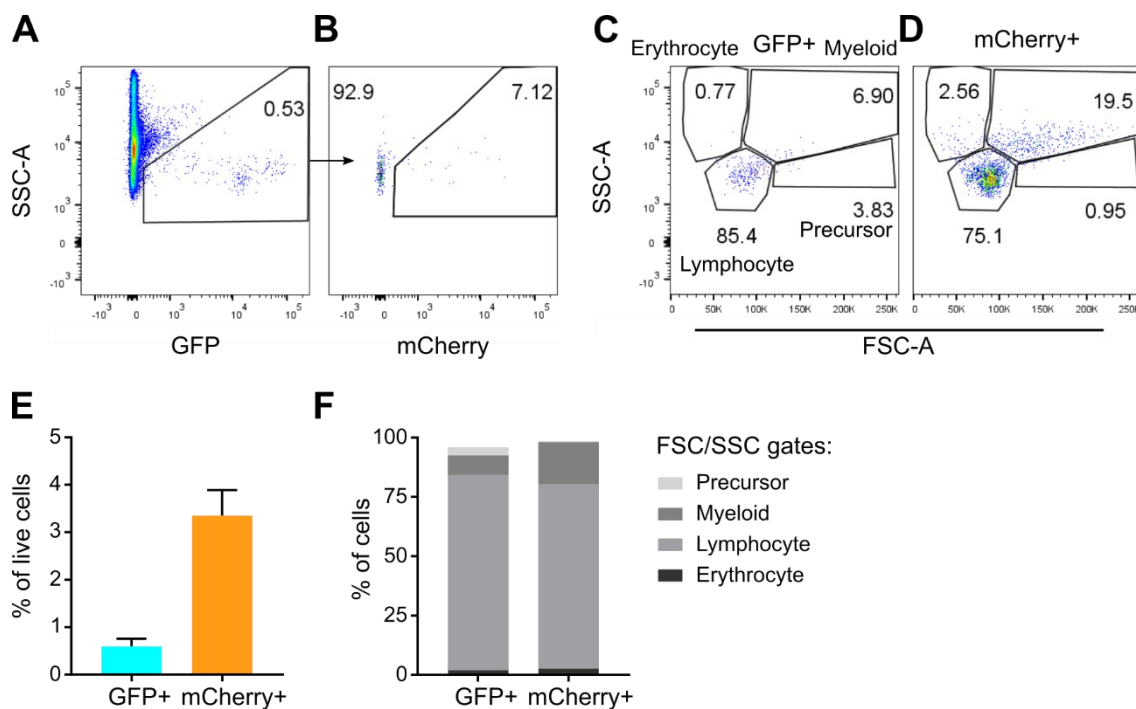
Figure 3.15 Flow cytometry of gills from adult *Tg(IgM:GFP; cd4-1:mCherry)* fish.

A) Live cells gated for GFP fluorescence. B) GFP+ population gated for mCherry+ fluorescence. Values inside and outside the gates indicate the respective proportion of events as a percentage of total events in the plot. (C, D) FSC/SSC profile of GFP+ (C) and mCherry+ (D) cell populations. Values in plots reflect percentages of events in each of the four gates compared to total events in each plot. (A-F) Representative plots from one fish. N = 5. E) Proportion of fluorescent cells as a percentage of live cells. Mean and SD shown. F) Mean proportion of cells in the four population gates as a percentage of total cells for each fluorescent population.

3.3.4.3   *Tissue localisation and cell morphology of immune cells in the gills*

Having quantified the proportion of myeloid and lymphoid cells in adult gills, the distribution of these cells was visualised *in situ*. *Tg(cd4-1:mCherry; lck:GFP), Tg(cd4-1:mCherry; IgM:GFP),* and *Tg(mpeg1.1:SECFP-YPet)* gills were dissected, immunostained and imaged by confocal microscopy. The overall distribution of cells was investigated, in addition to the detailed distribution in the arch.

This work includes contributions from Katie Tsoi and Alisha May (Imperial College London) who I worked with to support experimental design and execution during their Master's projects on gill cell characterisation.

As previously identified in Figure 3.9, *mpeg1.1:*SECFP-YPet+ cells formed a loose network throughout the arch whilst *lck:*GFP+ cells formed denser clusters around the rakers and close to the filaments (Figure 3.16A and B).

*Cd4-1:*mCherry+ cells were found to aggregate in the arch and localise to both the primary and secondary lamellae, showing a similar distribution to *lck:*GFP+ cells (Figure 3.16B). In particular, *cd4-1:*mCherry+ cells were found directly within *lck:*GFP+ lymphocyte clusters in the arch. One fish did not contain any *lck:*GFP+ clusters in the gill arches imaged (n = 2) which is inconsistent with findings shown in Figure 3.12 and Figure 3.13. Only a portion of the arch was imaged in this experiment which may explain this discrepancy. It is also possible that there is more variation in lymphocyte clusters than originally captured from the fish studied in Figure 3.12. In all arch clusters observed, both *lck:*GFP+ and *cd4-1:*mCherry+ cells were identified. This showed that presence of *cd4-1:*mCherry+ clusters correlated to presence of *lck:*GFP+ lymphocyte clusters.

I used this finding to assess the distribution of *IgM:*GFP+ B cells within lymphocyte clusters, as well as within the gill structure more broadly. *IgM:*GFP+ cells were found in proximity to *cd4-1:*mCherry+ cells in the posterior region of the arch, near the filaments (Figure 3.16C). Few *IgM:*GFP+ cells were identified in the filaments or around the rakers, thereby showing a distinct distribution to *mpeg1.1:*SECFP-YPet+ cells which as previously mentioned, are likely to label both macrophages and a subset of B cells (Ferrero et al., 2020). This difference in distribution is most likely explained by the macrophages labelled by the *mpeg1.1* reporter, which likely correspond to the cells loosely aggregated around the rakers (based on their dendritic morphology).
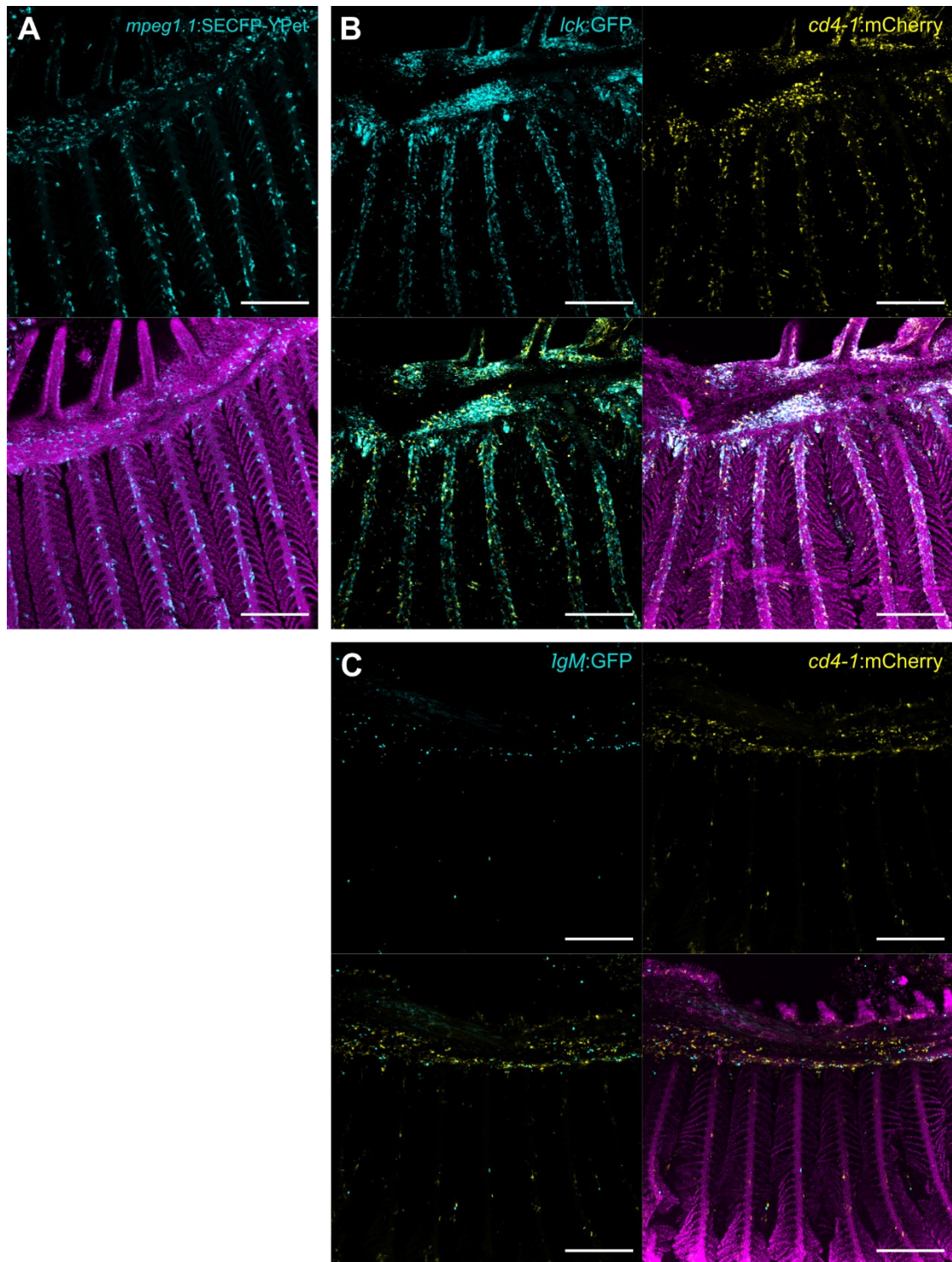
Figure 3.16 Confocal microscopy of immunostained gills from *Tg(mpeg1.1:SECFP-YPet)*, *Tg(cd4-1:mCherry; lck:GFP)*, and *Tg(IgM:GFP; cd4-1:mCherry)* adult fish.

Representative maximum z-stack projections of immunostained gills at 170X magnification. N = 4-5.; GFP and SECFP-YPet immunostaining in cyan; mCherry immunostaining in yellow; DRAQ5 nuclear staining in magenta. Scale bar represents 200 µm. A) *Mpeg1.1:*SECFP-YPet signal (top) and merge of DRAQ5 and *Mpeg1.1:*SECFP-YPet signal (bottom). (B, C) *Lck:*GFP or *IgM:*GFP signal and *cd4-1:*mCherry signal (top), merge of GFP and mCherry signal (bottom left), and merge of GFP, mCherry, and DRAQ5 signal (bottom right). *Tg(mpeg1.1:SECFP-YPet)* sample processing and image acquisition was carried out by Katie Tsoi (Imperial College London) as part of her Master's thesis on zebrafish gill characterisation (Tsoi, 2019); *Tg(cd4-1:mCherry; lck:GFP)* sample processing and image acquisition was carried out by Alisha May (Imperial College London) as part of her Master's thesis on zebrafish gill characterisation (May, 2017). Post-acquisition image processing in this PhD thesis was performed by me.

Visualising the gills at higher magnification revealed further details of the morphology and interactions of cells within the arch (Figure 3.17). Imaging focused on the arch region between the filaments and the rakers (Figure 3.17C). *Mpeg1.1:*SECFP-YPet+ cells were often irregularly shaped with thin cytoplasmic projections (Figure 3.17A). These cells were larger than most *lck:*GFP+ and *IgM:*GFP+ cells in the arch (Figure 3.17B and D). *lck:*GFP+ cells were mainly round with a few cells displaying irregular morphologies. In contrast, *IgM:*GFP+ cells were mostly irregularly shaped with a smaller proportion of round cells. *Cd4-1:*mCherry+ cells displayed a combination of small and round, or larger and dendritic morphologies, with *lck:GFP-* cells generally exhibiting the latter. The morphologies of all these cells were representative of the FSC/SSC properties measured in flow cytometry analyses (Figure 3.14 and Figure 3.15).

Compared to *lck:*GFP+ cells, *cd4-1:*mCherry+ and *IgM:*GFP+ cells were less densely aggregated in the arch. This revealed that within the tissue as a whole (Figure 3.14J and Figure 3.15E), and within lymphocyte clusters specifically (Figure 3.17), *lck:*GFP+ cells form the largest population of the gill leukocytes investigated. Both double positive *cd4-1:*mCherry+*lck:*GFP+ cells (Figure 3.17B) and single positive *cd4-1:*mCherry+*lck:GFP-* cells were identified in the clusters. On the other hand, *cd4-1:*mCherry and *IgM:*GFP did not show overlapping expression in any of the samples investigated.

*Lck:*GFP+, and *cd4-1:*mCherry+ cells were closely associated but distributed within lymphocyte clusters with no obvious pattern of organisation (Figure 3.17B). In comparison, *IgM:*GFP+ cells were often found in direct contact and closely intertwined with *cd4-1:*mCherry+ cells despite being more loosely aggregated (Figure 3.17C). This suggests that *IgM+* and *cd4-1+* cell interactions may not simply be a consequence of physical proximity, but an important part of lymphocyte biology in this tissue.
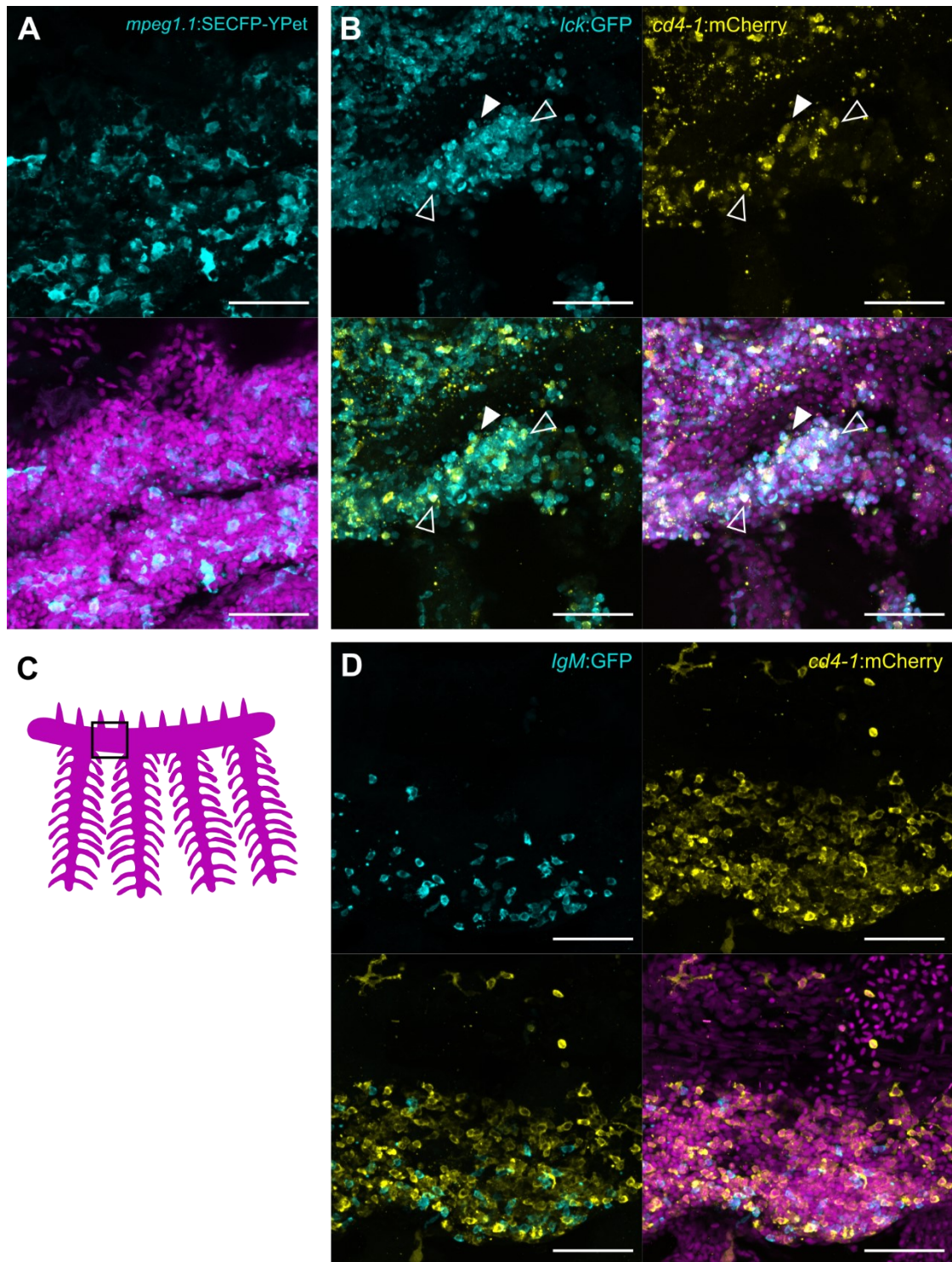
Figure 3.17 Confocal microscopy of the arch region of immunostained gills from *Tg(mpeg1.1:SECFP-YPet)*, *Tg(cd4-1:mCherry; lck:GFP)*, **and** *Tg(IgM:GFP; cd4-1:mCherry)* **adult fish.**

Representative maximum z-stack projections of immunostained gills at 800X magnification. N = 4-5. GFP and SECFP-YPet immunostaining in cyan; mCherry immunostaining in yellow; DRAQ5 nuclear staining in magenta. Scale bar represents 50 μm. A) *Mpeg1.1:*SECFP-YPet signal (top) and merge of DRAQ5 and *Mpeg1.1:*SECFP-YPet signal (bottom). (B, D) *Lck:*GFP or *IgM:*GFP signal and *cd4-1:*mCherry signal (top), merge of GFP and mCherry signal (bottom left), and merge of GFP, mCherry, and DRAQ5 signal (bottom right). Filled arrowhead indicates an mCherry+GFP- cell; unfilled arrowhead indicates an mCherry+GFP+ cell. C) Schematic of a gill arch showing the region imaged in a black square. *Tg(mpeg1.1:SECFP-YPet)* and *Tg(IgM:GFP::cd4-1:mCherry)* sample processing and image acquisition was carried out by Katie Tsoi (Imperial College London) as part of her Master's thesis on zebrafish gill characterisation (Tsoi, 2019). Post-acquisition image processing in this PhD thesis was performed by me.

3.3.4.4 Distribution of gill vasculature in relation to lymphocyte clusters

In addition to various leukocytes, MALT in mammals is associated with lymphatic vessels and specialised blood vessels known as HEVs (Ruddle and Akirav, 2009). In order to investigate this in lymphoid tissue in the gills, the *Tg(fli:GFP)* line was crossed with the *Tg(cd4-1:mCherry)* line. *Fli:*GFP expression has been reported to label endothelial cells of both blood and lymphatic vessels in zebrafish (Okuda et al., 2012). The gills are known to be highly vascularised, an important feature for their respiratory function, but they have also been reported to contain lymphatic vessels (Harrison et al., 2019; Okuda et al., 2012).

Immunostaining and confocal microscopy of *Tg(fli:GFP; cd4-1:mCherry)* fish revealed that endothelial cells formed vessels along the arch and primary lamellae (Figure 3.18A). Endothelial cells were also identified spanning the two epithelial layers of the secondary lamellae, corresponding to pillar cells (Figure 3.18B). The distribution of endothelial cells matched previous descriptions of zebrafish gills from electron microscopy and immunofluorescence studies (Harrison et al., 2019; Macirella and Brunelli, 2017; Rességuier et al., 2017).

Within the arch, a large vessel was consistently identified between the rakers and the filaments (Figure 3.18A). This corresponds to the afferent or efferent branchial arteries which connect the gills to the general circulation via the heart and dorsal aorta (Holden

et al., 2013). Smaller vessels, either separate from, or branching from, the larger vessel were also identified in the arch. These vessels were located close to *cd4-1:*mCherry+ cell clusters in the posterior arch but did not generally infiltrate clusters. Vasculature was less abundant in the anterior arch with *fli:*GFP+ cells located towards the bottom of rakers.

Some *cd4-1:*mCherry+ cells had highly dendritic morphology and appeared to form a network over the large vessel in the arch (Figure 3.18B). Individual z-slices and 3D rendering of these images revealed that these cells were located around the surface of the posterior arch, slightly above the vessel, hence not directly interacting with it (Figure 3.18C and E). *cd4-1:*mCherry+ cells within clusters were rounder and appeared to be directly below the vessel, albeit with a slight gap (Figure 3.18D). These results identify at least two distinct populations of *cd4-1:*mCherry+ cells in the posterior arch, both of which are found close to vessels. However, unlike in mammalian lymphoid tissues, these vessels do not infiltrate the area of tissue in which the immune cells reside.
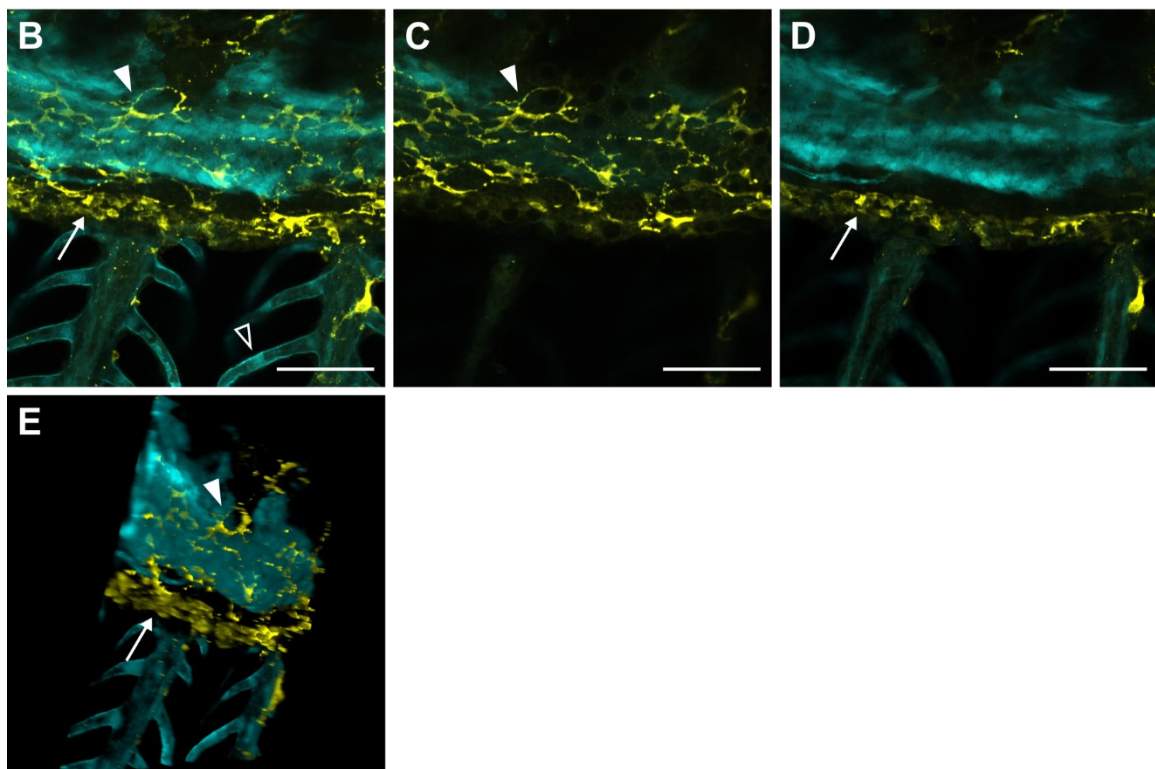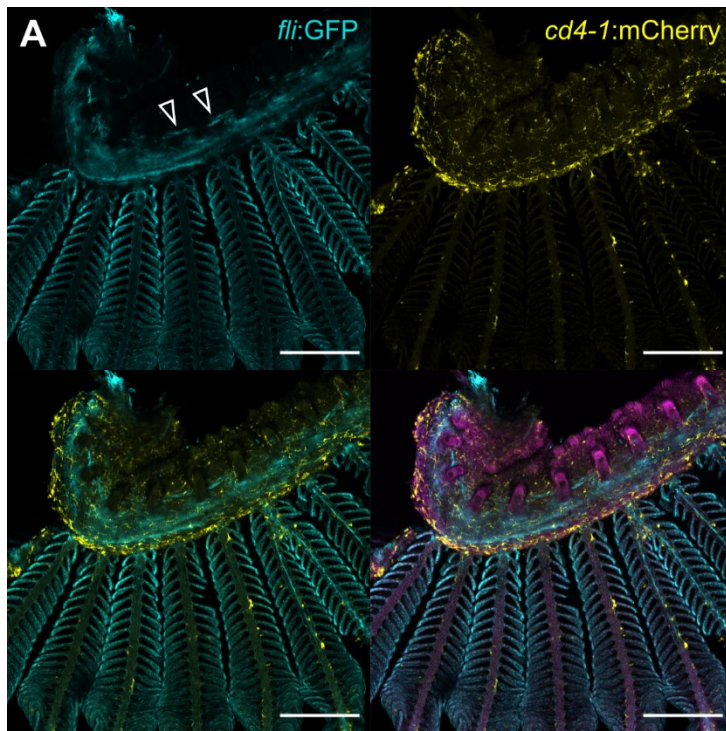
Figure 3.18 Confocal microscopy of immunostained gills from *Tg(fli:GFP; cd4-1:mCherry)* adult fish.

GFP immunostaining in cyan; mCherry immunostaining in yellow; DRAQ5 nuclear staining in magenta. A) Representative maximum z-stack projection of immunostained gill at 170X magnification. N = 5. GFP signal and mCherry signal (top), merge of GFP and mCherry signal (bottom left), and merge of GFP, mCherry, and DRAQ5 signal (bottom right). Arrowheads indicate smaller vessels. Scale bar represents 200 μm. B) Representative maximum z-stack projection of immunostained gill at 800X magnification. Unfilled arrowhead indicates a GFP+ pillar cell. Filled arrowheads indicate mCherry+ cell with dendritic morphology. Arrows indicate a cluster of mCherry+ cells below a major vessel. (C, D) Single z-slices of (B) showing GFP and mCherry signal at two different planes in the gills. E) 3D rendering of (B), rotated to show relative positions of *cd4-1:*mCherry+ cells compared to *fli:*GFP+ cells.

3.3.5   Investigation of gill immune cell function via ovalbumin uptake

Having defined cellular components and anatomical features of gill lymphoid tissue, the functions of gill leukocytes were then addressed. One of the key functions of mucosal leukocytes is sampling of the external environment for antigens. In mammalian MALT, antigens are sampled from the environment by specialized cells, such as M cells, or delivered to the tissue by afferent lymphatic vessels (Randall, 2015). These antigens are then processed by professional phagocytes and presented to T helper cells, initiating adaptive immune responses. Cd4-1+ T helper cells present antigen to B cells leading to B cell activation, proliferation and plasma cell differentiation.

The presence and close association of lymphocytes and myeloid cells in the gill arch suggests that gill lymphoid tissue is capable of both antigen sampling and antigen presentation. Macrophages, IgZ+ B cells, and dendritic cells in zebrafish gills have all been found to take up nanoparticles following immersion exposure (Rességuier et al., 2017). Furthermore, antigen uptake has been reported in *cd4-1+* myeloid cells in zebrafish skin and in *mpeg1.1+* cells in the gills (Lin et al., 2019, 2020). However, it is not known if *cd4-1+* cells in the gills are also capable of antigen uptake. Both studies by Lin et al. used fluorescent ovalbumin (OVA-AF647, henceforth shortened to OVA) to challenge adult zebrafish by immersion. In this thesis OVA was topically applied to the gills of adult *Tg(cd4-1:mCherry; IgM:GFP)* fish and gills were harvested at 0.5 h, 5 h, or 24 hours post treatment (hpt). Samples were subjected to flow cytometry or live confocal imaging to assess antigen uptake and cell behaviour.

OVA+ cells were identified in challenged samples by using unchallenged wildtype gills as a negative control for flow cytometry analysis (Figure 3.19A). OVA+ cells made up a minority of total gill cells, indicating that only a subset of cells was responsible for OVA uptake. The proportion of OVA+ cells was similar at 0.5 hpt and 5 hpt but decreased at 24 hpt (Figure 3.19B). Conversely, OVA+ cells displayed a wide range of fluorescent signal (Figure 3.19A) and the median fluorescent intensity of these cells was similar at 0.5 hpt and 5 hpt but increased at 24 hpt (Figure 3.19C). These results indicated that although fewer cells were associated with OVA at 24 hpt, overall these cells were associated with a greater amount of the compound.

The morphology of OVA+ cells was investigated by analysing their FSC/SSC properties. Compared to total gill cells which are composed mainly of cells in the erythrocyte gate (Figure 3.19D), OVA+ cells were enriched for cells in the myeloid gate (Figure 3.19E).
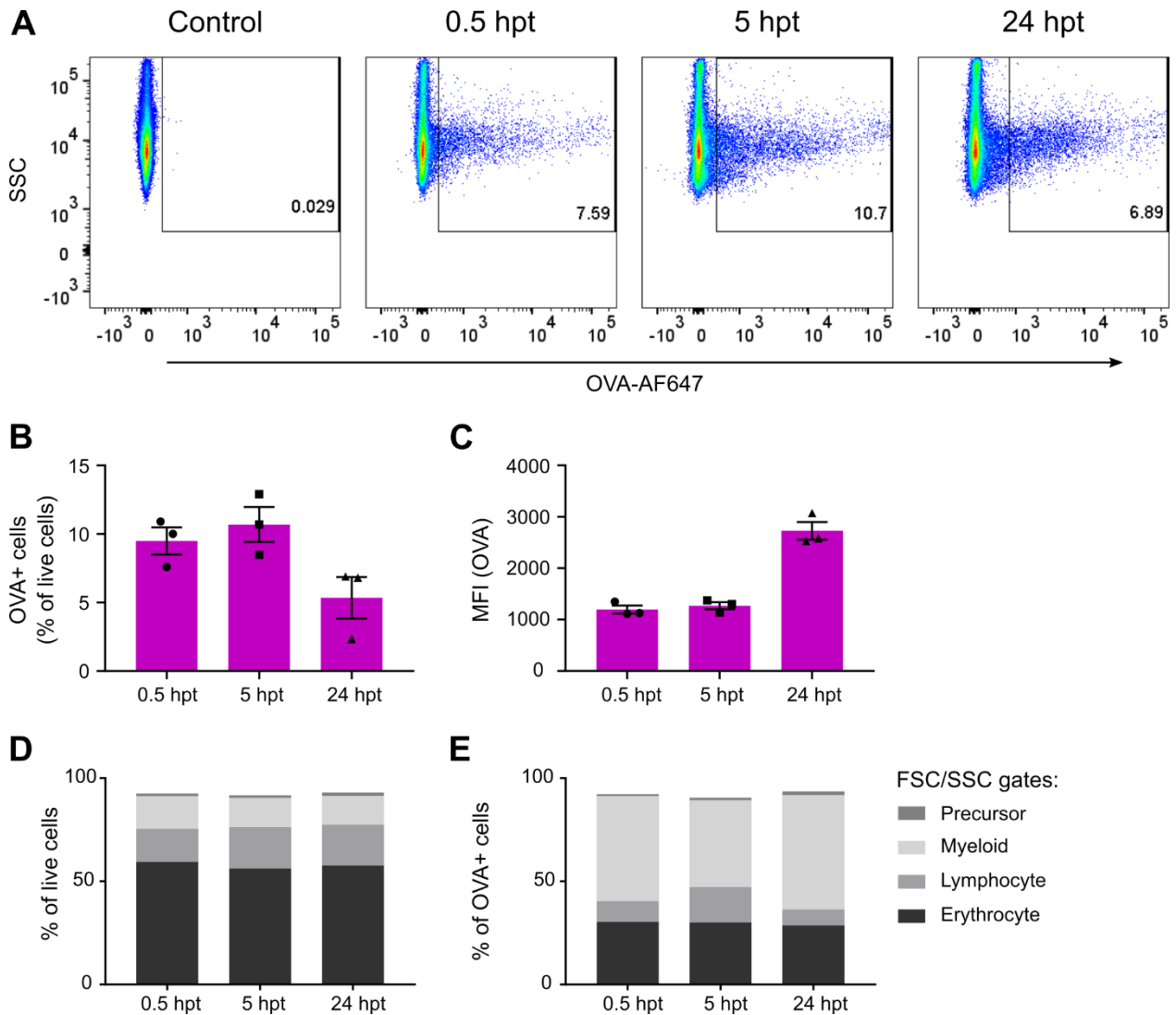
Figure 3.19 Flow cytometry analysis of gills topically challenged with OVA-AF647.

OVA-AF647 was topically applied to the gills of *Tg(IgM:GFP; cd4-1:mCherry)* fish and gills were harvested 0.5, 5, or 24 hpt and analysed by flow cytometry. N = 3. A) Live cells gated for OVA-AF647 fluorescence. Control is unchallenged WT gill. Representative plots shown. B) Proportion of OVA+ cells as a percentage of live cells. Mean and SEM shown. C) Median fluorescence intensity (MFI) of OVA-AF647 for OVA+ cells. Mean and SEM shown. (D, E) Mean proportion of cells in erythrocyte, lymphocyte, myeloid, or precursor gates as a percentage of total live (D) or OVA+ (E) cells.

Use of the *Tg(cd4-1:mCherry; IgM:GFP)* line allowed further interrogation of the types of cells associated with OVA. Firstly, the proportion of total *IgM:*GFP+ and *cd4-1:*mCherry+ cells was consistent over time and roughly in line with proportions previously identified in steady state (Figure 3.20 and Figure 3.14). Of the OVA+ cells, less than 1% were *IgM:*GFP+ and this remained consistent over time (Figure 3.20B). *cd4-1:*mCherry+ cells comprised a larger proportion of OVA+ cells than *IgM:*GFP+ cells but still made up less than 10% of OVA+ cells (Figure 3.20B). Although the proportion of *cd4-1:*mCherry+ cells was increased slightly at 24 hpt, the biological replicates showed considerable variation.

Within the total *IgM:*GFP+ and *cd4-1:*mCherry+ populations, OVA+ cells made up a sizeable minority of cells (Figure 3.20C). This indicated that although capable of antigen uptake, *IgM:*GFP+ and *cd4-1:*mCherry+ populations each consist of functionally heterogenous cells. The percentage of OVA+ cells was greater in the *cd4-1:*mCherry+ population, indicating that these cells are more capable of OVA uptake than *IgM:*GFP+ cells. The proportion of OVA+ cells in GFP+ and mCherry+ populations remained consistent over time.

*Cd4-1:*mCherry+ cells in the gills are known to consist of both lymphocytes and myeloid cells, therefore light-scattering properties were used to help identify which subsets of cell were responsible for OVA uptake. Compared to total *cd4-1:*mCherry+ cells, *cd4-1:*mCherry+*OVA+* cells were enriched for cells in the myeloid gate and contained a much smaller proportion of cells in the lymphocyte gate (Figure 3.20D and E). Furthermore 63-75% of mCherry+ myeloid-like cells were OVA+ compared to only 2-9% of mCherry+ lymphocyte-like cells across the three timepoints (Figure 3.20F). This indicated that *cd4-1+* lymphocytes are less capable of antigen uptake than *cd4-1+* myeloid cells in this context.
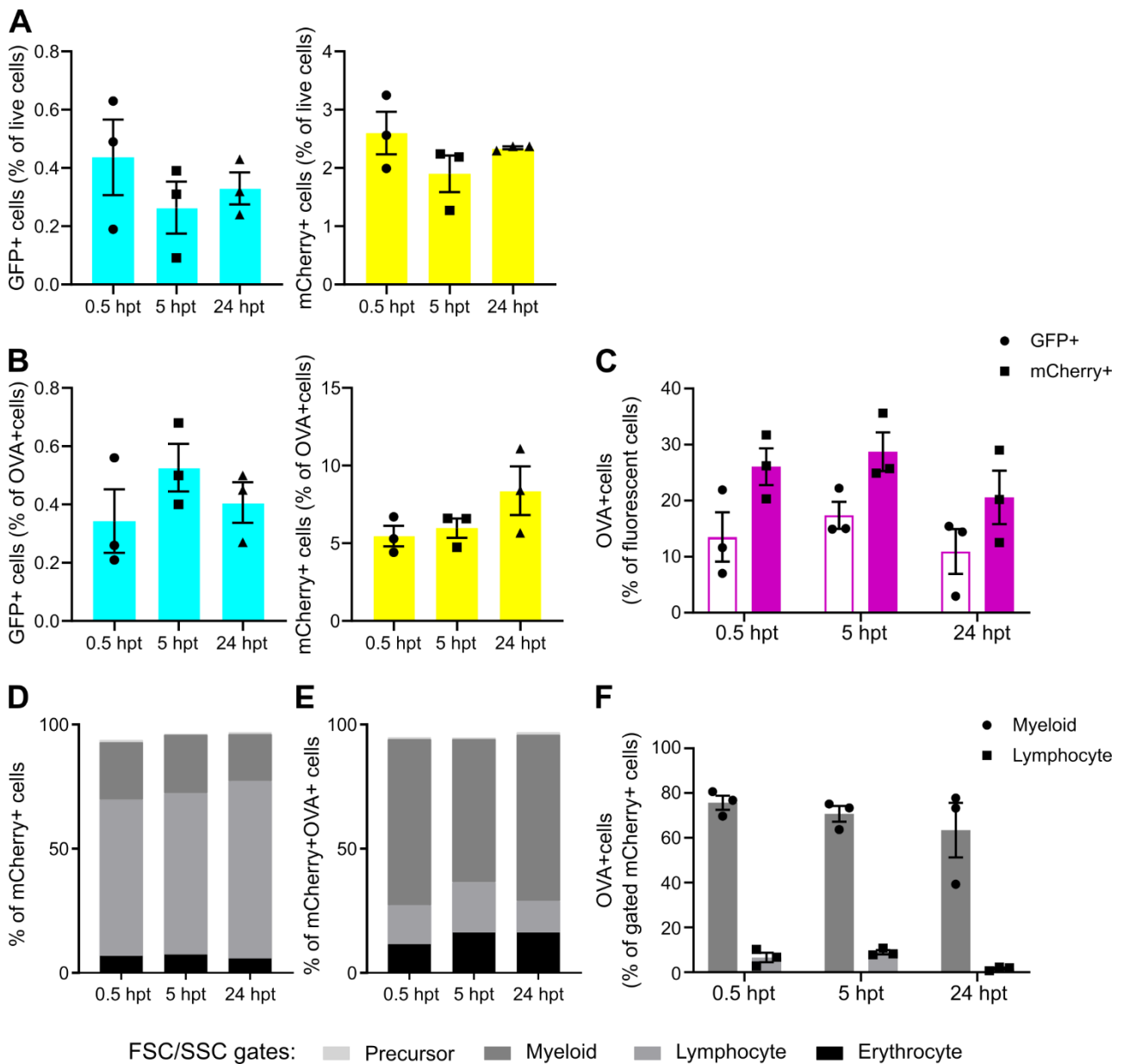
Figure 3.20 Flow cytometry analysis of *cd4-1:*mCherry+ and *IgM:*GFP+ cells in gills topically challenged with OVA-AF647.

OVA-AF647 was topically applied to the gills of *Tg(IgM:GFP; cd4-1:mCherry)* fish and gills were harvested 0.5, 5, or 24 hpt and analysed by flow cytometry. N = 3. A) Proportion of *IgM:*GFP+ (cyan) or *cd4-1:*mCherry+ (yellow) cells as a percentage of total live cells. B) The proportion of *IgM:*GFP+OVA+ (cyan) or *cd4-1:*mCherry+OVA+ (yellow) cells as a percentage of total OVA+ cells. C) The proportion of OVA+ cells as a percentage of total *IgM:*GFP+ (unfilled bar) or *cd4-1:*mCherry+ (filled bar) cells. Mean and SEM shown. (D, E) Mean proportion of cells in erythrocyte, lymphocyte, myeloid, or precursor gates as a percentage of total *cd4-1:*mCherry+ (D) or *cd4-1:*mCherry+OVA+ (E) cells. F) The proportion of OVA+ cells in FSC/SSC gated *cd4-1:*mCherry+ cell populations. Mean and SEM shown.

In order to assess cell behaviour *in situ*, gills challenged with OVA were imaged live by confocal microscopy. Z-stacks of the external side of the outermost arch were acquired for 16-19 mins and a region of the arch selected for further analysis; this region extended from the base of the filaments, up to the area around the base of the rakers and is expected to contain ILT (Figure 3.21A).

*IgM:*GFP+ cells were identified in this region and assessed for at least one physical contact with a *cd4-1:*mCherry+ cell (Figure 3.21B). Both *IgM:*GFP+ and *cd4-1:*mCherry+ cells were motile within the arch. OVA was identified within fluorescent cells, moving independently of GFP or mCherry fluorescence, or static within the tissue.
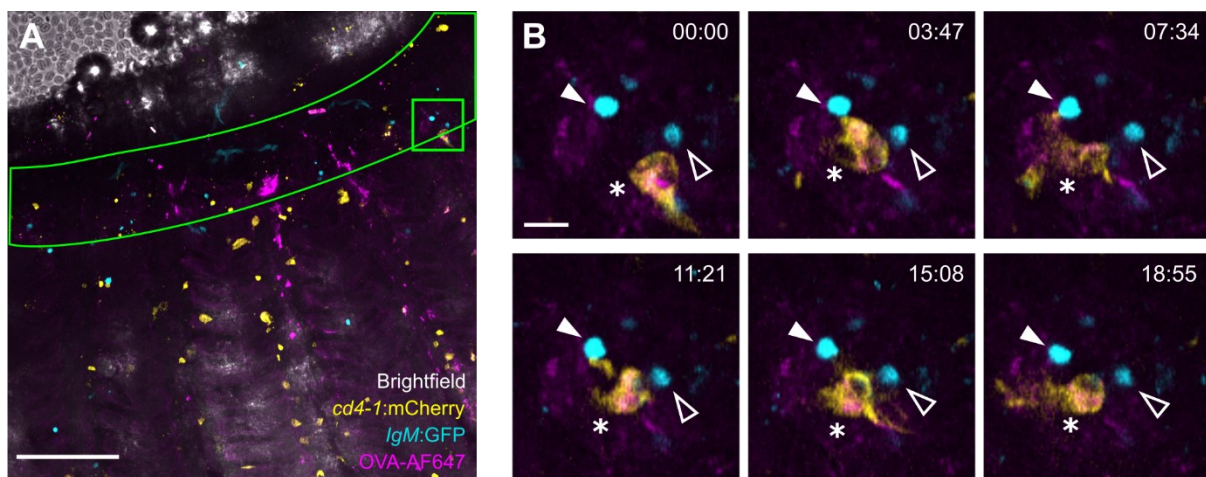
Figure 3.21 Live confocal imaging of *Tg(IgM:GFP::cd4-1:mCherry)* gills topically challenged with OVA-AF647.

Videos of *Tg(IgM:GFP::cd4-1:mCherry)* gills were acquired by confocal microscopy 0.5, 5, or 24 h following OVA-647 challenge. Videos lasted 16 -19 mins per sample. (A, B) Examples of the gill region and cell behaviours analysed from live gill videos. A) Maximum z-stack projection of a gill at 340X magnification. Single timepoint shown. Merge of brightfield (black and white), *cd4-1*:mCherry (yellow), *IgM*:GFP (cyan), and OVA-AF647 (magenta) signal. Scale bar 100 μm. Arch region used for quantitative analysis defined by green polygon. Region shown in (B) indicated by green square. B) Example of GFP+ cell (filled arrowhead) that contacts an mCherry+OVA+ cell (asterisk) and GFP+ cell on a different plane that does not contact any mCherry+ cells (unfilled arrowhead). Times are from the start of image acquisition (mins:sec). Scale bar 10 μm.

The total number of *IgM:*GFP+ cells showed considerable variation within groups, even when normalised with the area of the region for each sample (Figure 3.22A and B). The average number of cells was lower at 5 hpt but the large variation within groups indicates that a larger number of samples is needed to accurately assess this parameter.

*IgM:*GFP+ and *cd4-1:*mCherry+ cell contacts were identified at all timepoints (Figure 3.22C). The percentage of cells with contacts was highly variable at 0.5 hpt but more consistent at 5 and 24 hpt. In addition, it appeared that a greater percentage of cells formed contacts at 5 hpt. These results suggest that *IgM+* B cell and *cd4-1+* cell interactions are dynamic, changing over time. Furthermore, in each group, over 50% of *IgM:*GFP+ cells, on average, formed *cd4-1:*mCherry+ cell contacts, further supporting the conclusion that *IgM+* B cells are closely associated with *cd4-1+* cells in the gill arch. Cells outside of this region were not analysed. Therefore, it is unknown whether the frequency of these interactions is different outside the arch.

OVA was detected in mCherry+ cells in the arch region (Figure 3.21B). Of the GFP+ cells that interacted with mCherry+ cells, 53% (SEM = 4) interacted with at least one mCherry+OVA+ cell at 0.5 hpt. This proportion decreased at 5 and 24 hpt. From flow cytometry we know that neither the proportion of total mCherry+OVA+ cells (Figure 3.20C), nor the MFI of OVA in this population (Figure 3.22E), changed between 0.5-5 hpt. Therefore, the reduction in these interactions was not due to whole tissue changes in OVA uptake. However, it could have been due to specific changes in OVA uptake in the arch or a specific feature of *cd4-1:*mCherry+, *IgM:*GFP+ interaction kinetics.

No OVA+GFP+ cells were identified in the videos. This is likely because OVA fluorescence was much lower in GFP+ cells than mCherry+ cells (Figure 3.22E). MFI of OVA in GFP+ cells did not change over time.

This experiment was performed at the end of the project resulting in strict time constraints. Investigating the kinetics of potential antigen uptake was prioritised and therefore sham challenges were not performed in this experiment. Therefore, although changes in *IgM:*GFP+ and *cd4-1:*mCherry+ interactions were identified, the possibility of these changes occurring in response to the topical challenge procedure alone cannot be excluded.
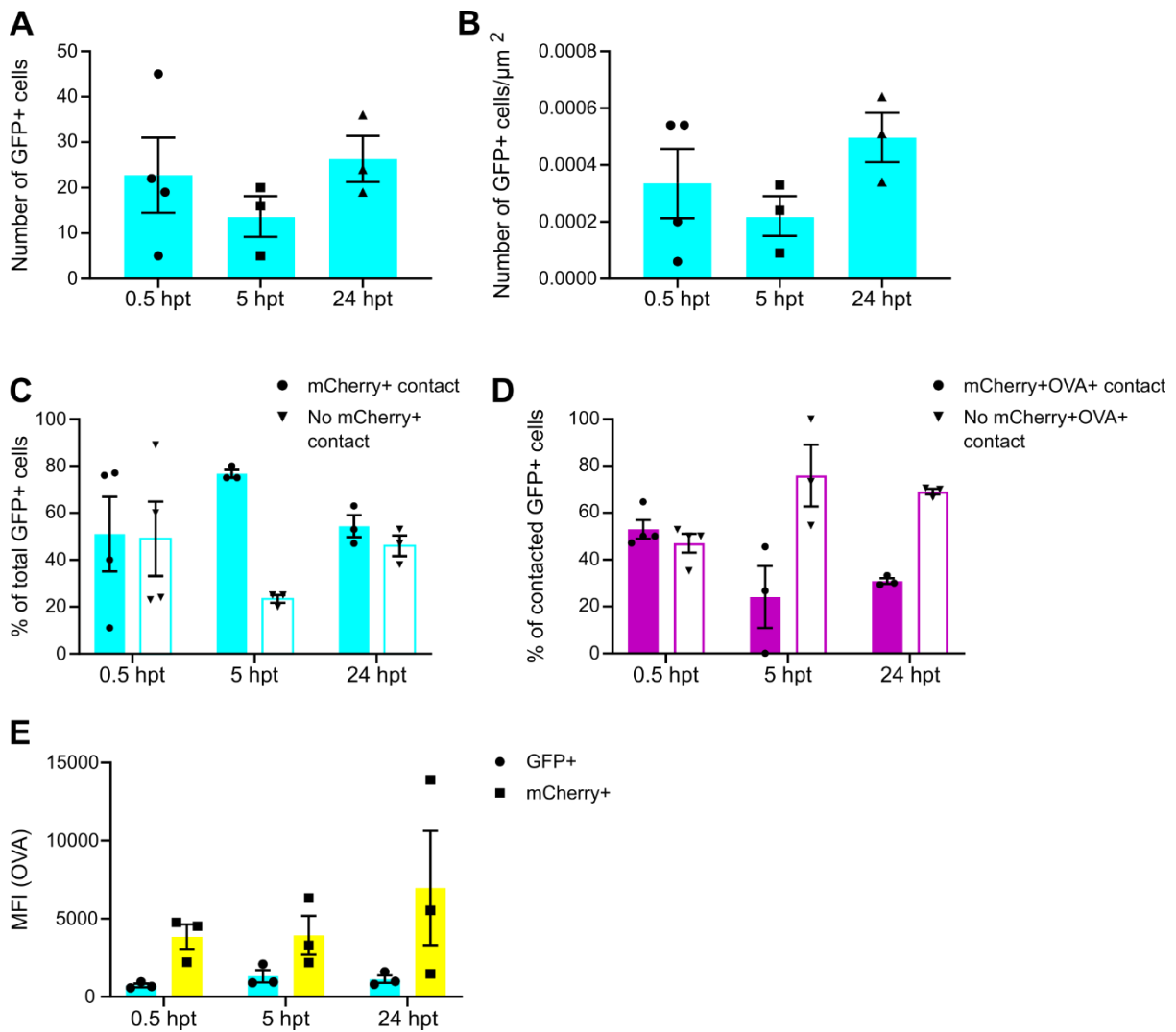
Figure 3.22 Quantitative analysis of *IgM:*GFP+ and *cd4-1:*mCherry+ cell interactions in gills topically challenged with OVA-AF647.

Videos of *Tg(IgM:GFP::cd4-1:mCherry)* gills were acquired by confocal microscopy 0.5, 5, or 24 h following OVA-647 challenge. Videos lasted 16 -19 mins per sample. A) Absolute number of GFP+ cells in the arch region over course of the video. B) Number of GFP+ cells in arch normalised to arch area. C) Proportion of *IgM*:GFP+ cells that form contacts with *cd4-1*:mCherry+ cells (filled bar) or do not form any contacts (unfilled bar). D) Proportion of contacted GFP+ cells that contact at least one mCherry+OVA+ cell (filled bar) or do no contact any mCherry+OVA+ cells. E) Median fluorescence intensity of OVA in GFP+OVA+ (cyan) or mCherry+OVA+ (yellow) populations from flow cytometry analysis. Mean and SEM shown. N = 3-4.

3.4 Summary

1. **Validation of flow cytometry and microscopy tools.** Gill leukocytes have similar light-scattering properties to leukocytes in WKM, allowing some characterisation of these cell types by flow cytometry. Combining this approach with fluorescent transgenic lines allows more specific interrogation and quantification of both immune and non-immune cells in the gills. In parallel, fluorescent cells can be visualised by a range of microscopy tools including widefield microscopy, stereomicroscopy, and confocal microscopy. This includes visualisation in live adult fish, dissected gills, and fixed and immunostained gills. The combination of flow cytometry and microscopy tools therefore provides a platform to investigate multiple aspects of leukocyte biology and tissue physiology within the gills.

2. **Development of zebrafish gills.** Like mammalian respiratory tissue, the gills undergo both structural and immunological changes during early development. Neutrophils and *lck*:GFP+ lymphocytes are present in the gills from early larval stages, increasing in population and in changing distribution over time. The gills appear to undergo a structural and immunological transition at 1 mpf, showing that gill development coincides with broader metamorphological changes and adaptive immune system maturation in the fish. Major changes in immune cell composition during ageing do not seem to occur.

3. **Composition of immune cells in the gills.** Adult zebrafish gills contain a multitude of immune cell types dispersed throughout the tissue. These cells belong to both the innate and adaptive immune system suggesting that the gills have the potential for both inductive and effector functions of the immune response. The most abundant leukocytes are *lck*:GFP+ lymphocytes which form distinct clusters in the arch region corresponding to the gill-specific ILT. The abundance and distribution of lymphocytes indicates a potentially important role for the gills with regards to zebrafish immunity.

4. **Distribution and composition of gill lymphoid tissue.** The gills contain multiple clusters of *lck:*GFP+ lymphocytes which are found on both hemibranches of the gills and dispersed across the width of the arch. The distribution of clusters may differ between hemibranches but is consistently more prominent around the posterior region of the arch, near the base of the filaments. Within the filaments, lymphoid tissue is more prominent on the afferent edge. This lymphoid tissue

colocalises with multiple cell types including *cd4-1*:mCherry+ cells, *IgM*:GFP+ B cells, and *mpeg1.1*:SECFP-YPet+ cells, but it is not vascularised.

5. **Functional characterisation of gill immune cells.** Zebrafish gills can take up antigen (OVA) following topical challenge. The cells associated with OVA uptake appear to be mostly myeloid-like and specifically include *cd4-1*:mCherry+ and *IgM*:GFP+ cells. These two cells types are closely associated in the gill arch, forming interactions which change over time following topical gill treatment. These interactions can involve but do not seem dependent on OVA uptake in *cd4-1*:mCherry+ cells.

3.5 Discussion

3.5.1 Flow cytometry and microscopy enable multi-faceted investigation of immune cells in the gill respiratory mucosa

3.5.1.1 *Flow cytometry tools*

Light-scattering properties of haematopoietic cells have been well described in zebrafish WKM but not in the gills. In this project gill cells exhibited broadly similar FSC/SSC properties to WKM cells and reflected expected properties of fluorescent myeloid and lymphoid immune cells from transgenic fish. There were some obvious differences to WKM cells including the lack of a distinct population in the precursor gate and a population with slightly different FSC/SSC properties in the myeloid gate. This may reflect differences in cellular composition which could be tested with analysis of additional transgenic lines. *Tg(cd41:GFP)* fish contain GFPlo haematopoietic stem and progenitor cells (HSPCs) in the WKM and preliminary analysis revealed the absence of this population in the gills (Appendix 1). *Runx1*:mCherry+ HSPCs have been described in *Tg(runx1:mCherry)* WKM, and whilst the gills also contain mCherry+ cells these lack *cmyb* transcripts – a key HSPC transcription factor (Dorottya Polos, personal communication). In this PhD project eosinophils were detected in the gills by Wright-Giemsa staining, but flow cytometry did not reveal a distinct FSChiSSChi population expected for this cell type possibly reflecting a low abundance. This could be tested by quantifying GFP+ gill cells from the *Tg(gata2:GFP)* line (Balla et al., 2010).

Analysis of endothelial cells with *Tg(fli:GFP)* fish revealed that the selected FSC/SSC gates were not exclusive for haematopoietic cells. Endothelial cells in teleost gills form populations with different morphologies including pillar cells, squamous vascular cells, and heightened vascular cells as observed in salmon (Dalum et al., 2016). This may explain the broad FSC/SSC profile of *fli:*GFP+ cells, however, distinct populations were not identified by flow cytometry highlighting one of the limitations of this technique. In the mammalian respiratory tract, scRNA-Seq analysis has shown that epithelial and mesenchymal cells make up a large portion of total cells (Reyfman et al., 2019; Vieira Braga et al., 2019). As a tissue with a large epithelial surface area, the gills are likely to contain substantial non-immune cell populations which share some FSC/SSC properties with immune cells. FSC/SSC is therefore a useful starting point for assessing cell morphology but not enough to define immune cell types in the gills. scRNA-Seq analysis of zebrafish gills has been reported and publication of these data should provide quantitative and phenotypic information on these non-immune populations (Pan et al., 2020). Further work is also needed to assess whether collagenase digestion and cell isolation from gill tissue enriches or excludes any cell populations. Studies in other models have shown that enzymatic digestion can alter sample cell composition leading to discrepancies with true tissue composition (Quatromoni et al., 2015).

The presence of 8 gill arches per fish is major advantage of this model as it allows multiple analyses to be performed on a single fish. In this project whole-mount immunofluorescence in parallel with flow cytometry provided insights into gill cell morphology and localisation alongside high-throughput quantification. In the case of *fli*:GFP+ cells, this allowed identification of pillar cell and vascular cells which was not possible with flow cytometry alone. However, differences between gill arches have been reported, including differences in the proportion of ILT tissue and gill size, (Dalum et al., 2016; Stolper et al., 2019). This may limit generalisations of results from individual gills to the entire gill system. Future work could utilise imaging flow cytometry to analyse cells from single gill arches by microscopy and flow cytometry simultaneously. This technique has already been used to assess nanoparticle uptake in zebrafish gill cells (Rességuier et al., 2017).

3.5.1.2 Microscopy tools

In other animal models, intravital microscopy of cells in respiratory tissue requires invasive, technically complicated procedures and highly specialised equipment. Results from this project showed that individual immune cells can be visualised non-invasively in adult zebrafish gills using commercially available stereomicroscopes or widefield microscopes. This expands on previous studies that visualise fluorescent cells in zebrafish larvae or adult external organs and provides an opportunity for longitudal monitoring of immune responses through repeated sampling. The method used in this project is restricted to short-term imaging due to the anaesthesia protocol, but intubation of adult zebrafish has been developed allowing long-term imaging for up to 2 days (Xu et al., 2015). However, this involves passing water over the gills to maintain gill movement for respiratory function and is likely to interfere with visualisation of the tissue. Several acquisition or post-processing methods have been developed to account for movement of cardiac and lung tissue during intravital microscopy and some of these could provide solutions for imaging gills in intubated fish (Fiole and Tournier, 2016; Kavanagh and Kalia, 2019).

The resolution of images acquired by intravital microscopy was high enough to visualise the localisation of individual cells in the primary lamellae. However, the resolution was not high enough to accurately to assess cell morphology. Resolution could be improved by computational tools such as deconvolution which mathematically removes out-of-focus light (Bueno et al., 2019; Sarder and Nehorai, 2006). Alternatively, confocal, multi-photon and light sheet microscopy can produce higher resolution images than stereomicroscopy or widefield microscopy. Multiphoton microscopy is most favoured for intravital imaging as it allows deeper penetration into the specimens and the lower energy photons are less phototoxic to live samples. However, these alternative microscopes are also highly sensitive to sample movement. Removal of the operculum in adult fish has also been shown to increase resolution but further work is needed to assess if the procedure induces any inflammation. If inflammation is observed, removal could be performed ahead of any experimental interventions and imaging with enough time for inflammation to subside. The operculum regenerates over several months and therefore removal would not be ideal for long-term studies on the same fish (Marie-Christine Ramel, personal communication).

Given these challenges, live imaging of dissected gills offers a straightforward method to gain high resolution time-lapse images of this tissue. This is a similar system to precision cut lung slices but due to the thin structure of the gills, it can be used with intact gill arches. Furthermore, submerging the gills in media more closely reflects the physiological conditions of this tissue, avoiding the need for air-liquid interface conditions. In this project dissected gills were maintained for up to 30 mins of imaging allowing monitoring of immune cell movement and interactions. Live imaging of dissected gill tissue for up to 5 hours was recently achieved by (Lin et al., 2020) whilst precision cut lung slices have been maintained for up to two weeks highlighting the potential of this system for longer-term gill imaging (Liu et al., 2019a). Changes such as apoptosis and gene expression, should be measured to ensure conditions do not significantly alter gill physiology. As with all explant systems, this cannot be used to study migration of cells in and out of the tissue.

Neither the mucus layer nor the commensal microbiota – both important features of the mucosa – was visualised with the imaging protocols used in this study. Mucus has previously been visualised in live imaging of tissue sections or cell cultures using fluorescent nanospheres or fluorophore-conjugated dextran (Button et al., 2012; Hoegger et al., 2014). Further research would be needed to determine if these compounds can diffuse through zebrafish gill mucus and if the mucus layer is affected in *ex vivo* culture conditions. Live imaging of bacteria has been achieved by introducing of exogenous fluorescent bacteria in germ-free or wildtype animals (Jemielita et al., 2014; Rakhilin et al., 2019; Wiles et al., 2016). However, this does not provide information on existing bacterial populations. Alternatively, bacteria can be visualised in fixed tissue samples using fluorescence *in situ* hybridisation (FISH) probes against bacterial ribosomal RNA (Hasegawa et al., 2017).

3.5.2 Immune cell composition changes during early gill development but stabilises in later life

3.5.2.1 *Early presence and development of immune cells in the gills*

The mammalian respiratory mucosa is known to undergo considerable changes in immune cell presence and composition during postnatal stages of development. Few studies have investigated immunological development of the teleost respiratory mucosa

and this project reveals that zebrafish gills undergo similar changes. Both neutrophils and lymphocytes were identified at early larval stages before the gills were structurally mature. This parallels mammalian development where immune cells are present in the lungs during fetal stages before alveolarisation has fully occurred (Domingo-Gonzalez et al., 2020; Mjösberg et al., 2011). The presence of immune cells suggests that antigen sensing may be an important function of the gills at these early stages of development. Further work would be needed to address whether these early immune cells are functionally mature given that mammals show immunological immaturity during early development. Indeed, evidence in zebrafish indicates that systemic adaptive immune responses are not mature until 4-6 wpf (Lam et al., 2004). However, neutrophils can protect zebrafish from bacterial infection within 4 dpf suggesting that innate cells in the gills would be functional at early stages (Phan et al., 2018).

Lck:GFP+ lymphocytes identified in early gill development could consist of T cells, NK-like cells or ILC-like cells and further work would be needed to assess this. In zebrafish the thymus is directly connected to the gills for at least 15 wpf suggesting that T lymphocytes could migrate to the gills during early development (Lam et al., 2002). *Lck*:GFP+ cells have been reported to egress from the thymus as early as 10 dpf but since *lck*:GFP+ cells were present in the gills at 8 dpf, it is possible that egress occurs even earlier. In salmon, CD3+ T cells were identified in the gills of larvae and the thymus was closely associated with the gills until juvenile stages highlighting some conservation between teleost species (Dalum et al., 2016). In both zebrafish and medaka, lymphoid precursor cells have been shown to utilise Cxcr4 and Ccr9 chemokine receptors to home to the thymus in response to chemokine gradients (Bajoghli et al., 2009). This poses the question of whether similar pathways exist for lymphocyte recruitment to the gills. Interestingly lymphoid homing to the thymus relies on the same receptors in mice highlighting that some of these homing pathways are well conserved within vertebrates (Calderón and Boehm, 2011).

In salmon, ILT was not observed in larval tissue despite the presence of individual CD3+ T cells (Dalum et al., 2016). This PhD project expands on these previous findings by identifying the specific transition in which lymphocytes accumulate in the zebrafish gill arch at 3-4 wpf. The consistent timing and location of lymphoid tissue development in zebrafish indicates that the ILT is not an ectopic lymphoid tissue. Rather, it appears to be

part of the normal process of development. This hypothesis is further supported by the emergence of ILT coinciding with the emergence of an adult-like gill structure. This suggests that structural and lymphoid tissue development may be governed by similar pathways in the gills. The sequence of gill structural development is well conserved between teleost species and similar to zebrafish, medaka gills develop an adult-like structure around 40 days post fertilisation (Leguen, 2018). However, medaka lack ILT indicating that this lymphoid tissue is unlikely to affect gross structural development of the gills (Rességuier et al., 2020).

The development of ILT in zebrafish parallels the large increase in lymphocytes in mammalian lungs during postnatal stages (Loffredo et al., 2020). However, questions remain on the functions of ILT lymphocytes compared to lymphocytes present earlier in the gills. The emergence of ILT and maturation of adaptive immunity occurs at similar times suggesting that these phenomena may be linked (Lam et al., 2004). The major shift in the cellular microenvironment of lymphocytes residing mostly individually in the gill filaments, to lymphocytes residing in close proximity to each other in the arch could lead to significant functional differences. Indeed, disruption of CD4-1+ lymphocyte spatial organization in mouse lymph nodes was found to impair adaptive immune responses (Baptista et al., 2019). Furthermore, expression of cytokines, such as IL-17 and lymphotoxin, by lymphocytes has been found to promote lymphoid tissue development in mice (Endres et al., 1999; Rangel-Moreno et al., 2011). Homeostatic maintenance of lymphoid tissue could therefore be one function of ILT lymphocytes that differs from earlier stages development.

3.5.2.2 *Immune cell composition in juvenile to aged gills*

Quantification of *mpx*:GFP+ neutrophils, *lck*:GFP+ lymphocytes and *mpeg1.1*:SECFP-YPet+ cells revealed no differences in immune cell abundance during later stages of gill development and ageing. Similarly, beyond an increase in gill size, there were no obvious structural changes in aged gills. In mice, airspace enlargement in ageing lungs has been associated with higher B cell and macrophage abundance (Calvi et al., 2011). IL10 deficiency has also been found to enhance ageing-related airspace enlargement and immune cell accumulation in mice indicating that regulation of inflammation is important for respiratory tissue homeostasis (Malinina et al., 2020). In zebrafish, Il10 deficiency has been found to induce structural changes to the adult gill respiratory mucosa. Gene set

enrichment analysis revealed that these changes are likely to be associated with persistent inflammation and greater immune cell presence (Bottiglione et al., 2020). The lack of structural changes in ageing zebrafish gills may therefore be explained by the lack of change in immune cell presence, and potentially a lack of inflammation. This highlights the ability of the gills to regulate inflammation long-term. This is supported by previous work in the Dallman group which showed that long-term cigarette smoke exposure did not result in chronic inflammation and observed structural changes were reversible following cessation of smoke exposure (Progatzky et al., 2015).

Although changes in immune cell abundance were not observed in ageing zebrafish gills, this does not exclude the possibility of changes in the immune response. Ageing in mice and humans has been consistently associated with impaired responses to RVIs and vaccination which involves many changes including excessive neutrophil recruitment, delayed immune cell recruitment and reduced B cell responses (Frasca et al., 2010; Kulkarni et al., 2019; Toapanta and Ross, 2009). Ageing-related changes in the gills may also be more obvious in certain compartments; in salmon, the ILT was reduced in size between adult and mature fish despite an increase in gill volume (Dalum et al., 2016). This study estimated the volume of ILT through histological measurements and weighing of whole gill tissue. 3D imaging methods, such as multiphoton imaging, may provide a more accurate way to measure ILT in zebrafish gills. Dalum et al. found that the thymus was also reduced in volume and showed significant reductions in *Rag1* and *Rag2* expression. This raises the possibility that ageing in fish induces global changes in T cell populations and that the thymus influences gill immunity.

3.5.3 Cellular and structural features of the ILT suggest a significant role in gill immunity and bear some similarities to secondary lymphoid tissue

Studies on teleost gills have mostly visualised the ILT in gill sections and therefore lack a complete 3D overview of this structure. Whole-mount confocal imaging in this project has provided a partial 3D visualisation of the ILT, showing that it is more extensive than previously described (Dalum et al., 2015; Rességuier et al., 2020). Although the full interbranchial region could not be visualised, imaging revealed that the ILT extends continuously from the interbranchial region, across both efferent and afferent edges along the arch and the filaments. This highlights the ILT as a prominent immunological

but also physical barrier to underlying gill tissue. In comparison to the mammalian respiratory system, the ILT is structurally most similar to NALT or BALT which consist of structures distinct from the gas-exchange regions but which are connected to the mucosal epithelium, as opposed to lymph nodes which are entirely separate from the mucosa. Given the spread of lymphoid tissue beyond the interbranchial region, the term *interbranchial lymphoid tissue* may be misleading. The presence of lymphoid tissue at the base and afferent sides of filaments in European perch, despite of lack of ILT, further supports re-evaluation of this term (Rességuier et al., 2020). However, it is unclear what functional similarities and differences exist between these lymphoid structures. For simplicity lymphoid aggregates in zebrafish gills will continue to be referred to as ILT in this thesis.

The presence of ILT across numerous gill compartments raises the question of whether functional and cellular differences exist within this tissue. Indeed, the greater prominence of ILT on the afferent edge of filaments has been reported in several species including zebrafish, which was similarly observed in this PhD project (Dalum et al., 2015; Rességuier et al., 2020). In this project, lymphocytes clusters also showed a striking difference in distribution between the posterior and anterior arch regions. The reduced presence of lymphocyte clusters and *IgM*:GFP+ B cells in the anterior regions suggests that cellular responses may indeed differ from the posterior region. In salmon, ILT is separated from underlying tissue by the basal lamina so it is not clear whether distinct anterior clusters are part of the ILT or form part of broader GIALT (Haugarvoll et al., 2008). Furthermore, it is unclear whether anterior clusters reside within a network of epithelial cells as observed in the interbranchial region. This highlights a limitation of immunofluorescence in visualising different structural features compared to histological methods.

The function of ILT is not well understood and therefore the cellular composition of this tissue was further investigated. CD4-1+ helper T cells are important activators of B cells in mammalian secondary lymphoid tissues and both *cd4-1*:mCherry+ and *IgM*:GFP+ B cells were identified in the ILT. These cells were closely associated in the arch which could indicate that the ILT functions as an inductive site of mucosal immune responses. However, unlike mammalian lymphoid tissues, B cells were few in number and not segregated into distinct regions from T cells, mirroring observations in salmon ILT

(Koppang et al., 2010). Lymphocyte segregation in mammals allows for the generation of germinal centres (GCs) and efficient B cell responses whilst the loss of lymphoid architecture has been associated with impaired immune responses in a mouse model of kidney injury (Allen et al., 2007; Maarouf et al., 2018). The lack of segregation in zebrafish ILT could therefore be associated with less efficient adaptive immune responses. However, in this project only *IgM+* B cells were investigated, and it is possible that *IgZ+* cells have a different spatial distribution. Similarly, the interbranchial region was unexplored and this region could have a different lymphocyte architecture, although studies in salmon suggest that this is unlikely to be the case (Koppang et al., 2010). To elucidate ILT function, future work could involve stimulating adaptive responses by infection or immunisation and monitoring cell proliferation and distribution in the ILT. FISH could also be used to explore the expression of chemokine factors known to be important in the maintenance of secondary lymphoid tissues (Gentek and Bajénoff, 2017).

ILT in the zebrafish gill arch was not directly vascularised but was found in close proximity to vessels. This has also been described in salmon ILT highlighting conservation between teleosts and indicating a possible route for antigen transport and cell recruitment (Aas et al., 2017; Dalum et al., 2016). Indeed, smaller vessels near salmon ILT were characterized with electron microscopy and found to consist of heightened endothelial cells and often associated with immune cells, bearing similarities to HEVs in mammalian lymphoid tissues (Dalum et al., 2016). Zebrafish gill vasculature was not characterized in such detail in this project but *cd4-1*:mCherry+ cells with dendritic morphology formed a network near the vessels and ILT in the arch. The ability of motile *cd4-1+* cells to take up OVA in the arch supports a role for these cells in antigen transport. Furthermore, *mhc2dab* expression has been reported in *cd4-1+* cells in the zebrafish skin epidermis suggesting that these cells may be involved in antigen presentation (Dee et al., 2016; Lin et al., 2019). MHCII+ cells have also been directly identified in salmon ILT although the lineage of these cells was not characterised (Dalum et al., 2015; Haugarvoll et al., 2008). Some *cd4-1+* cells in the zebrafish epidermis are resident macrophages (Langerhans cells) which co-express *mpeg1.1* (Lin et al., 2019). Given the presence of *mpeg1.1*:SECFP-YPet+ cells throughout the gills, it is possible that similar gill-resident macrophages also exist. This could be easily tested by crossing the *Tg(cd4-1:mCherry)* and *Tg(mpeg1.1:SECFP-YPet)*. One study showed that some *mpeg1.1+* cells could

phagocytose *E.coli* bacteria *in vitro* although they did not address potential differences between myeloid-like and lymphoid-like *mpeg1.1+* cells which were distinguished by flow cytometry in this project (Lin et al., 2020). Furthermore, the authors identified non-haematopoieitic *mpeg1.1+* cells (metaphocytes) in the gills which were highly capable of soluble antigen sampling but not bacterial phagocytosis (Lin et al., 2020). However, the study did not report on cells in the arch, a common gap in zebrafish gill studies. Similar cells have not yet been identified in mammals. Overall, current evidence suggests that antigen uptake, transport, and presentation are likely to be features of the ILT although these may be achieved by slightly different populations to mammalian lymphoid tissues.

3.5.4 Immune cells in the gills take up antigen and form dynamic cellular interactions

Teleost gills are known to take up external antigens although the cells and mechanisms driving this are not well understood. In this project, fluorescently labelled OVA was topically applied to zebrafish gills to monitor uptake. Similar experiments by Lin et al. showed that non-haematopoietic *mpeg1.1+* cells could take up OVA following bath immersion but the authors did not investigate other cell types (Lin et al., 2020). This PhD project analysed antigen uptake in whole gill tissue revealing a wider range of cells that take up OVA following topical application including *cd4-1*:mCherry+ cells, *IgM*:GFP+ cells, and many unidentified cells. These unidentified OVA+ cells in the gills could include lamellar epithelial cells which have been found to take up formalin inactivated bacteria in rainbow trout (Kato et al., 2018). The latter study also identified antigen-sampling epithelial cells with similar gene expression and lectin staining properties to mammalian M-cells. Given the role of mammalian M cells in transferring antigen to underlying immune cells, it would be of interest to investigate whether these cells are also present in zebrafish gills.

In this PhD project, OVA was rapidly taken up by gill cells within 30 mins of exposure. This suggests that cells sampled antigen directly or obtained antigen through rapid transfer from other cells. Live imaging of Peyer's patches (intestinal lymphoid structures) in mice has shown that M cells can bind antigen within 5 mins and transport it to the basolateral membrane within 30 mins (Fischer et al., 2020). It is therefore feasible that similar epithelial cells in the gills could transport antigen to underlying immune cells

within this timeframe. Alternatively, OVA+ cells could extend transepithelial protrusions (TEPs) to directly sample antigen from the gill surface. This process has been visualised by live imaging of mouse intestinal mucosa and shown to be important in antigen uptake in DCs. In this study cx3cr1-deficient mice had reduced TEPs and consequently reduced bacterial uptake in DCs. TEPs have also been visualised by live imaging of *mpeg1.1*+ cells in the zebrafish skin epidermis (Lin et al., 2019). In this PhD project, *cd4-1*+ cells in the gills extended long dendrites although it is unknown if these extended through the gill epithelium. Lymphocytes are not expected to form TEPs and live imaging showed that *IgM*+ cells did not exhibit extended dendrites. This suggests that these cells acquire antigen through other means.

OVA+ cells were detected in the gills for at least 24 hours indicating some level of antigen retention. In the study by (Lin et al., 2020), OVA uptake in *mpeg1.1*+ cells increased from 5-12 hours post immersion but rapidly decreased once fish were no longer exposed to OVA. This contrasts with OVA uptake in this PhD project which was stable in *cd4-1*+ and *IgM*+ cells between 30 mins to 24 hours post treatment. These differences could be due to the differences in cell type or method of antigen exposure, specifically immersion with more dilute OVA by (Lin et al., 2020) compared to topical application with more concentrated OVA in this project. Antigen retention in mammals is an important feature of immune functions, including follicular dendritic cell stimulation of GC B cells and accumulation of memory T cells after IAV infection (Heesters et al., 2013; Kim et al., 2010). Understanding the mechanisms of antigen retention in zebrafish gills will allow a better understanding of the immunological role of this tissue.

Immune cell interactions in OVA-challenged gills were investigated to further our understanding of antigen transport and potential immune cell functions. Live imaging analysis of these interactions focused on the arch region to capture ILT cells. Movement of *cd4-1*+ and *IgM*+ cells in and out of the arch region suggested that cells may migrate in and out of the ILT. This provides new insight on the dynamics of a structure which has previously been imaged in fixed samples (Dalum et al., 2015; Rességuier et al., 2020). However, due to the small region visualised, the lack of tissue structure markers, and lack of *cd4-1*+ cell clusters in some samples, it was not possible to identify the ILT in every sample. Additional vehicle controls would be needed to assess whether OVA affects the cellular composition of the ILT.

Within the arch, *cd4-1+* and *IgM+* cells formed close, sometimes transient, interactions which became more consistent between samples 30 mins post OVA challenge. Live imaging in mice has shown that lymph node B cells are less motile and more confined to the subcapsular sinus region when acquiring cognate antigen from macrophages (Carrasco and Batista, 2007). However, B cells are more motile and can form multiple transient interactions with T cells following migration to the T/B cell regions (Carrasco and Batista, 2007; Shulman et al., 2014). These T cell interactions are also longer-lasting in the presence of cognate antigen (Shulman et al., 2014). The reduced variability in *IgM+/cd4-1+* cell interactions after 30 mins suggests that the types of interactions may have become more consistent over time. Since the proportion of interactions involving *cd4-1*+OVA+ cells decreased over time, it is possible that the interactions involved fewer *cd4-1+* myeloid cells and more *cd4-1+* lymphoid cells which had lower OVA uptake. This hypothesis is supported by studies in mice, where lymph node B cells have been visualised migrating to T cell regions following initial antigen uptake from macrophages (Carrasco and Batista, 2007). Studies on lymphocyte interactions often use adoptive transfer of transgenic antigen-specific cells in combination with immunization to assess the effect of cognate interactions. Although cellular interactions in the gills were assessed in the presence of antigen, prior immunization was not performed therefore OVA-specific lymphocytes were likely to be rare. In addition, since vehicle controls were not performed, the effect of OVA on these interactions cannot be separated from the effect of gill manipulation during topical application.

4 Chapter 4 – The gill immune response to pathogen mimetics and derivatives

4.1 Introduction

4.1.1 Pattern recognition receptors pathways

Recognition of pathogens is essential to initiate immune responses, and this is achieved in part by PRRs which recognise PAMPs. These receptors are an ancient arm of defense with PRR genes found in vertebrates and invertebrates. In vertebrates, PRRs are expressed on immune and non-immune cells although the expression profile varies between cell types. There are also species differences in the presence and functions of certain PRRs. Zebrafish have orthologues for many mammalian PRRs but the ligand specificity and signalling pathways of these genes are still being determined.

4.1.1.1 *Toll-like receptors*

TLRs are transmembrane proteins with contain multiple extracellular leucine-rich repeat (LRR) domains that mediate ligand binding. For certain ligands this also requires the involvement of cell surface co-receptors (Botos et al., 2011). Upon ligand binding, TLRs form hetero- or homodimers leading to recruitment of signalling adaptor proteins through their intracellular Toll/interleukin-1 (TIR) domains. This leads to further downstream signalling and activation and nuclear translocation of transcription factors such as nuclear factor kappa B (NF-κB), interferon regulatory factor (IRF) 3 and IRF7. These transcription factors induce expression of cytokines, interferons as well as proteins that negatively regulate TLR signalling (Kawai and Akira, 2010). Signalling pathways differ between TLRs but rely on either myeloid differentiation primary response 88 (MyD88) or TIR-domain-containing adapter-inducing IFN-β (TRIF) adaptor proteins.

There are 10 TLR genes in humans, several of which have a clear zebrafish orthologue. Zebrafish also contain some TLR genes not found in mammals. Although TLR pathways in teleosts are still being elucidated, signalling adaptor genes are well conserved between humans and mammals (Li et al., 2016).

TLRs that recognize nucleic acids

In humans TLR3, TLR7, TLR8 and TLR9 recognize different forms of nucleic acids including bacterial and viral nucleic acids. These TLRs are expressed in endosomal

compartments which prevents recognition of self-nucleic acids during normal cellular processes.

TLR3 recognises double-stranded RNA (dsRNA) including viral RNAs, self-RNA from cellular damage (Bernard et al., 2012), small interfering RNAs (Cho et al., 2009) and a synthetic analogue of dsRNA, poly(I:C). TLR3 is also present in teleosts, and fugu TLR3 has been shown to mediate responses to poly(I:C) and short dsRNA fragments (Matsuo et al., 2008). The same study found that a teleost-specific TLR, TLR22, also mediated responses to poly(I:C) and longer dsRNA fragments (1000 bp). This indicates that multiple teleost TLRs may fulfil the function of individual human orthologues. The zebrafish genome encodes both Tlr3 and Tlr22 although the ligand specificities of these receptors have not been determined. Upregulation of *TLR3* was observed in the gills of virus-infected rare minnow (Su et al., 2009) whilst *tlr3* and *tlr22* were reported to be expressed in zebrafish gill metaphocytes suggesting roles in gill immunity (Lin et al., 2020).

TLR7 and TLR8 in humans recognize viral single-stranded RNA (ssRNA) viral and synthetic agonists such as R848 and poly(U) RNA (Kawai and Akira, 2010). TLR7 can also recognise bacterial RNA from streptococcus B bacteria (Mancuso et al., 2009). TLR7 and TLR8 signal through the MyD88 pathway leading to type I IFN and cytokine production (Cervantes et al., 2012). TLR8 was initially thought to be non-functional in mice since it does not respond to R848 and is not required for the response to ssRNA *in vitro* (Heil et al., 2004; Jurk et al., 2002). However, murine TLR8 has since been shown to respond to a combination of poly(T) ODN and a synthetic TLR8 agonist (Gorden et al., 2006). Orthologues of *TLR7* and *TLR8* are present in teleost genomes and in zebrafish there are two *TLR8* orthologues, *tlr8a* and *tlr8b*. There is no definitive evidence that teleost TLR7/8 recognize the same ligands as their mammalian counterparts but one study found that R848 failed to induce an IFN response in salmon cell lines which had low or absent expression of these receptors (Svingerud et al., 2012).

TLR9 recognises unmethylated CpG motif-containing single-stranded DNA (ssDNA) which is found much more commonly in bacteria and viruses than mammalian cells (Kawai and Akira, 2010). Synthetic CpG-ODN can also be used to stimulate TLR9 leading type I IFN and cytokine expression. Orthologues for TLR9 have been identified in several teleost genomes including zebrafish, and some work has investigated their functional

properties. Zebrafish Tlr9 and a fish-specific receptor, Tlr21, were both found to recognise CpG-ODNs although they had different ligand preferences (Yeh et al., 2013). *Tlr9* seems to be involved in gill immunity as it was upregulated by *Edwardsiella tarda* bacterial infection in Japanese flounder, leading to an accumulation of TLR9+ cells in the primary lamellae (Takano et al., 2007).

TLRs that recognize lipid, glycan and protein PAMPs

In humans, TLR1, TLR2, TLR4, TLR5, TLR6, and TLR10 recognize various lipid, glycan and protein PAMPs. They are expressed on the cell surface allowing detection of extracellular PAMPs which is particularly relevant for sensing of bacteria.

TLR2 can form heterodimers with several other TLRs to recognize a wide range of PAMPs. TLR2-TLR1 dimers can recognize triacylated lipopeptides including the synthetic lipopeptide, Pam3CSK4. TLR2-TLR6 dimers on the other hand recognize diacylated lipopeptides, lipoteichoic acid and beta-glucan, a component of fungal cells walls or cereals (Oliveira-Nascimento et al., 2012). TLR2 has also been found to mediate responses to LPS, an element of Gram-negative bacterial cell walls, in some contexts and this is likely through interaction with TLR4 (Good et al., 2012). Peptidoglycan, an element of Gram-positive bacteria cell walls, is also reported to activate TLR2 although this does not seem to be the case with all types of peptidoglycan molecules (Inamura et al., 2006; Müller-Anstett et al., 2010; Travassos et al., 2004). TLR2 can also be activated by the hemagglutinin protein of measles virus highlighting the ability of this PRR to respond to structurally dissimilar ligands (Bieback et al., 2002). TLR2 signaling is mediated through MyD88 and leads to the cytokine expression. Type I IFNs have also been detected in some cases of TLR2 signaling, such as in inflammatory monocytes responding to vaccinia virus (Barbalat et al., 2009).

Human *TLR2* has a zebrafish orthologue which has been detected in the gills and found to be downregulated in the kidney of virus-infected fish (Encinas et al., 2013; Liu et al., 2014). The zebrafish genome also encodes a gene designated *tlr1* however this gene has been named after the fugu gene *TLR1* and has similarities with human *TLR1*, *TLR6* and *TLR10* (Jault et al., 2004; Meijer et al., 2004). TLR6 is absent in teleosts although in Japanese flounder *TLR14* was found to bear some genetic similarities to *TLR1*, *2*, *6* and *10* (Hwang et al., 2011). Morpholino-mediated knockdown of *tlr2* in zebrafish embryos impaired cytokine responses to Pam3CSK4 suggesting that this gene has similar functions

to its human counterpart (Yang et al. 2015). The lack of direct TLR1 and TLR6 orthologues indicates that there are likely to be differences in the mechanism of recognition for ligands of these TLRs.

The recognition of LPS by TLR4 has been well characterized and requires several co-receptors: LBP, CD14 and MD2 (Lizundia et al., 2008). TLR4 can also recognize RSV F protein although the role of this interaction in RSV infection *in vivo* is debated (Kurt-Jones et al., 2000; Marr and Turvey, 2012). TLR signaling can occur either through MyD88 or through TRIF pathways, a unique feature of this TLR. This leads to expression of cytokines or type I IFNs respectively (Mukherjee et al., 2016). Although two orthologues of human *TLR4* have been identified in zebrafish (*tlr4a* and *tlr4b*), orthologues for co-receptors have not been identified (Li et al. 2016). This initially suggested that zebrafish Tlr4a/b may not have the same LPS binding capacity as human TLR4. Indeed cell lines transfected with *tlr4a* or *tlr4b* did not respond to LPS and morpholino-mediated knockdown of these genes did not affect the response to LPS in zebrafish embryos (Sepulcre et al. 2009). Further studies have shown that zebrafish caspase-B (caspy2) can bind LPS leading to caspase oligomerisation and pyroptosis – a form of inflammatory cell death (Yang et al. 2018). This appears to be mediated through NLRP3, resembling the non-canonical NLRP3 inflammasome pathway in humans which is activated by capsase-4/5 and also leads to pyroptosis (Li et al. 2020). However, it is not clear if additional pathways for LPS recognition exist in zebrafish or what ligands Tlr4a and Tlr4b may bind.

TLR5 recognises bacterial flagellin proteins and has two zebrafish orthologues which are expressed in the gills (Hayashi et al., 2001; Liu et al., 2014). TLR10 has been found to mediate an inflammatory response to *Listeria monocytes* bacteria in cooperation with TLR2, and a response to IAV, possibly through intracellular sensing of viral ribonucleoproteins (Regan et al. 2013; Lee et al. 2014). However, signaling pathways and ligand recognition for TLR10 is still poorly understood. In mice, *TLR10* is nonfunctional due to a retrovirus insertion whilst teleosts lack an orthologous gene – although teleost *TLR14* does bear some similarities (Hasan et al. 2005; Li et al. 2016). In addition to the TLRs already mentioned, mice contain TLR11, TLR12, and TLR13 which are not present in the human or zebrafish genome. These receptors recognize various ligands from bacteria, toxoplasma gondii parasites, and vesicular stomatitis virus (Kawasaki and Kawai, 2014). The remaining zebrafish TLRs are TLR18, which has similarities to TLR1,

6 and 10 in humans, TLR19, which recognises dsRNA in grass carp, and four paralogues of TLR20 whose ligands are currently unknown (Ji et al., 2018; Meijer et al., 2004; Pietretti et al., 2014).

4.1.1.2 RLRs, NLRs, ALRs and CLRs

Aside from TLRs, RLRs can recognize ssRNA and dsRNA from viruses. RIG-I, melanoma differentiation-associated factor 5 (MDA5) and laboratory of genetics and physiology 2 (LGP2) are all RNA helicases localised in the cytosol and orthologues have been identified in many teleosts including zebrafish (Varela et al., 2017). Stimulation of RLRs induces type I IFN and proinflammatory cytokine expression which promotes antiviral responses. RIG-I was detected in salmon gills, including the ILT, and the kidney and was found to be upregulated during viral infection (Austbø et al., 2014). LGP2 was similarly detected in zebrafish gills and kidney and upregulated during viral infection (Zhang et al., 2018). This shows that RLRs are involved in mucosal and systemic immune responses in teleosts.

NLRs are a family of cytosolic proteins that detect PAMPs and DAMPs. Activation of NLRs through ligand binding, caspase-4/5 (or caspase-11 in mice) interaction, or as of yet unknown mechanisms, induces oligomerisation and formation of large protein complexes known as inflammasomes. These complexes recruit and activate caspase-1 which cleaves pro-IL-1β and pro-IL-18 to their active forms, and induce pyroptosis (Man and Kanneganti, 2015). Clear zebrafish orthologues have been identified for human NLRs NOD1, NOD2, NOD3, and recently NLRP3 (Li et al., 2020, 2016). However, the NLR family in zebrafish contains around 400 members, in contrast to around 20 observed in humans (Harton et al., 2002; Howe et al., 2016).

ALRs are cytosolic DNA sensors and this family of proteins is absent in teleosts (Li et al., 2016). CLRs are a group of soluble serum proteins and transmembrane proteins which bind carbohydrates, including some from pathogens (Geijtenbeek and Gringhuis, 2009). CLRs have not been extensively studied in zebrafish but several orthologues have been identified or proposed (Van Der Vaart et al., 2012).

4.1.2 TLR agonists in vaccines, therapeutics and experimental models for respiratory disease

Due to their immunostimulatory and immunomodulatory properties, TLR agonists continue to be investigated as vaccine adjuvants. Use of TLR agonists in some RSV vaccine candidates has been found to promote Th1-responses and dampen Th2-responses thus reducing pathology from live RSV exposure (Cyr et al., 2009; Huang et al., 2009). In African green monkeys, R848-conjugated vaccines induced protective responses against influenza infection and this was unchanged with the addition of the TLR5 agonist flagellin (Holbrook et al., 2016). These studies highlight both the potential of TLR agonists as adjuvants and the need to understand the pathways and cells affected as these can have significant consequences on vaccine safety and efficacy.

In addition to their potential as vaccine adjuvants, TLR agonists are being investigated as therapeutics for various diseases including cancer, viral infections and inflammatory respiratory diseases (Anwar et al., 2019). Imiquimod, a TLR7 agonist is currently approved to be used as a topical treatment for various skin conditions (Lebold et al., 2016). In addition, the therapeutic effects of TLR agonists have also been demonstrated in the respiratory tract for allergic rhinitis and viral infection (Greiff et al., 2015; Rosewich, 2010; Wali et al., 2020).

Besides their clinical use, TLR agonists are useful tools for investigating the genes, cells and molecules involved in immune responses. Both synthetic and pathogen-derived agonists can be used to induce and investigate acute or chronic inflammation *in vitro* and *in vivo*. Furthermore, by stimulating specific TLRs, pathways relevant to specific types of pathogens can be investigated. This approach was used to stimulate and compare innate responses to R848 – a TLR7/8 agonist and viral mimic – in zebrafish gill and human and mouse nasal mucosa (Progatzky et al., 2019). The resulting IFN and proinflammatory responses were transient and showed strong similarities between species. In contrast, poly(I:C) treatment only induced a response in mice highlighting important species-specific differences. My contributions to this study began during my Masters' project (Imperial College London) and continued as part of this PhD. I later contributed to a collaboration with Federica Bottiglione (School of Biological Sciences, University of Manchester) where this novel model using R848 stimulation was used to investigate the

roles of *il10*, *il4/13a*, and *il4/13b* in regulating inflammation in zebrafish gills (Bottiglione et al., 2020).

4.1.2.1 Zebrafish responses to TLR agonists

In the experimental results of this chapter four TLR agonists will be compared for their ability to induce an immune response in the zebrafish gills. This section will therefore review the current understanding on the teleost response to the four agonists used: R848, LPS, Pam3CSK4, and CpG-ODN 2007.

R848

As previously mentioned, R848, a TLR7/8 agonist, was found to induce an inflammatory response in zebrafish gills following topical application (Progatzky et al., 2019). Both type I and type II IFNs were upregulated in addition to *il1b*, *tnfa* and *il6* cytokines. Type I IFNs were also upregulated in salmon gills and in the kidney following i.p. injection with R848 (Svingerud et al., 2012). Fluorescence *in situ* hybridisation (FISH) revealed that IFN-expressing cells were present in the primary lamellae of the gills.

Japanese flounder peripheral blood cells and rainbow trout cells kidney leukocytes have been found to respond to R848 *in vitro* through higher cytokine expression or NF-κB activity (Palti et al., 2010; Zhou and Sun, 2015). Inhibition of endosomal acidification or MyD88 impaired this response in flounder cells but inhibition of endosomal acidification did not alter the response in rainbow trout cells. This could be due to species- or cell-specific differences or the experimental conditions since neither study included positive controls for the inhibitors used. In addition, R848 did not increase IFN expression in rainbow trout leukocytes indicating differences in IFN regulation. The ability of R848 to stimulate TLR7/8 in teleosts has not yet been investigated however it does not stimulate zebrafish TLR9 or TLR21 *in vitro* (Yeh et al., 2013). These studies indicate that some elements of the R848 response pathway are conserved with mammals but further study is needed to clarify discrepancies and remaining gaps.

LPS

Fish are known to be less susceptible to LPS toxicity than mammals, but they are still able to recognize this PAMP (Sepulcre et al. 2009). Studies in zebrafish consistently report that LPS upregulates the inflammatory cytokines *il1b*, *tnfa*, *il6* and *il10* (Sepulcre et al. 2009; Varela et al. 2012; Forn-Cuní et al. 2017). The transcriptional response in adult zebrafish

correlates well with the response in mice despite the lack of involvement of *tlr4a/b* in zebrafish (Forn-Cuní et al., 2017). The similarities in response indicate that downstream signalling pathways are likely to be similar between the two species. LPS can also upregulate chemokines like *cxcl18b* and some ISGs including *mxa* and *mxf* in zebrafish (Sepulcre et al. 2009; Forn-Cuní et al. 2017). Upregulation of IFN genes has been observed in some LPS challenges but this is not always the case suggesting that some ISGs may be induced through IFN-independent pathways (Lepiller et al., 2009; Reyes-Cerpa et al., 2012; Sullivan et al., 2009). Injection of adult zebrafish with LPS results in a transient inflammatory response that is usually resolved within 24 h (Sepulcre et al. 2009; Varela et al. 2012). However, bath immersion of LPS has not been found to induce a response in the gills suggesting that mucosal tissues may act as a barrier to certain immunostimulants (Lin et al., 2020).

Pam3CSK4

Intravenous (i.v.) injection of Pam3CSK4, a TLR2/6 agonist, in zebrafish embryos upregulated cytokines and chemokines including *il1b*, *tnfa*, *il6*, *il10* and *il8* revealing a transient inflammatory response (Yang et al. 2015). However, like LPS, bath immersion with Pam3CSK4 did not induce a response in the gills of adult zebrafish (Lin et al., 2020). No other Pam3CSK4 challenges have been reported in zebrafish and therefore it is not clear if these differences are due to the route of administration or the developmental stage of the fish.

Pam3CSK4 challenge of leukocytes *in vitro* have been performed in other fish species. Pam3CSK4 induced a small increase in *TNFα* transcript levels in acidophilic granulocytes and macrophages of gilthead seabream but did not alter transcript levels of *IL-1β* or *COX2* (Sepulcre et al. 2007). In contrast, *IL-1β* but no other genes were upregulated in carp macrophages treated with the agonist (Ribeiro et al., 2010). In rainbow trout primary macrophage cells, Pam3CSK4 did not alter *IL-1β* or *IL-6* transcript levels (MacKenzie et al., 2010). Overall, these studies and those in zebrafish indicate that Pam3CSK4 is not particularly stimulatory in fish. However, few studies have investigated the *in vivo* response to this compound.

CpG-ODN 2007

In vitro challenges of cells transfected with zebrafish *tlr9* and *tlr21* have shown that these receptors are most strongly stimulated by CpG-ODN 2007 compared to other CpG-ODNs

(Yeh et al., 2013). In this study, i.p. injection of CpG-ODN 2007 in adult zebrafish increased *il1b*, *tnfb*, and *ifng* transcript levels in the kidney and gut however, the timing of this response was not described. I.p. injection with CpG-ODN 2007 increased *tlr9* but decreased *il1b* and *myd88* transcript levels in the gills during *Vibrio vulnificus* infection in zebrafish (Chen et al., 2020). In addition, CpG-ODN treatment reduced infection-associated mortality. I.p. injection challenges with a different compound, CpG-ODN 2006, increased *IL-1β* transcript levels in yellowtail fish gills (Angulo et al., 2018). These studies highlight the immunomodulatory and protective effects of CpG-ODNs in peripheral and mucosal tissues. However, bath immersion with CpG-ODN 2007 did not induce a response in zebrafish gills further supporting the hypothesis of a barrier role of the gill mucosa (Lin et al., 2020). *In vitro* studies have also reported that NF-κB or MyD88 inhibitors can suppress the response to CpG-ODNs revealing some similarities with humans and mice (Gao et al., 2013; Yeh et al., 2013).

4.1.3 Effects of antibiotics on immune responses in aquaculture and human health

Although antibiotics are used to combat pathogenic bacteria, they can often alter the commensal microbiota of mucosal tissues, including the respiratory systems in mammals and fish (Ferrer et al., 2017; Rosado et al., 2019). Dysregulation of the microbiota can in turn impact the immune system and its response to challenges (Ni et al., 2012; Yonar, 2012). Antibiotics are heavily used in aquaculture and in human medicine therefore it is important to understand their wider impacts on mucosal immunity. In aquaculture their effects are important not just for the animal being treated, but also those in the wider environment exposed to residual levels of antibiotics (Santos and Ramos, 2018).

4.1.3.1 Effects of antibiotics on respiratory viral infections

The disruption of the respiratory microbiota by antibiotics has been shown to impair both humoral and cellular responses to viral infections leading to greater pathology. In mice, neomycin impaired T cells responses which were characterised by lower IFN-γ secretion and lower levels of antigen-specific cells (Ichinohe et al., 2011). This was associated with lower migration of DCs to the lymph nodes. These impairments seemed to be linked to lower inflammasome activation since antibiotic-treated mice had lower levels of *IL-1β* and *IL-18* mRNA. Furthermore, these impairments were rescued by LPS

suggesting that commensal bacteria stimulate TLR signalling that promotes antiviral responses. This is supported by another study which showed that poly(I:C) administration improved survival following influenza infection in antibiotic-treated mice (Abt et al., 2012). In this study, antibiotic treatment impaired T cell responses but also reduced transcript levels of antiviral genes in macrophages demonstrating effects on innate immunity. Antibiotic treatment was also shown to impair immunoregulatory cytokine production and reduce Treg levels during RSV infection in mice, which coincided with development of airway hyperresponsiveness (Ni et al., 2012).

However, not all antibiotics impair antiviral responses and some have been described to exert antiviral properties (Gopinath et al., 2018; Rausch et al., 2017; Retallack et al., 2016). Some of these antiviral effects are independent of the microbiota and caused by induction of ISGs, cytokines or chemokines (Bawage et al., 2019; Gopinath et al., 2018). Some antibiotics have also been reported to suppress cytokine production during RSV and influenza infection *in vitro* or in hospitalised patients (Lee et al., 2017; Yamamoto et al., 2016). Anti-inflammatory effects could be beneficial in reducing immunopathology, and understanding the underlying mechanisms could reveal new therapeutic targets. This could guide design of new immunomodulators whilst avoiding the use of antibiotics which are associated with microbial dysbiosis and antimicrobial resistance. With the vast range of antibiotics available, more work is needed to understand both the beneficial and detrimental effects on RVIs.

4.1.3.2 *Effects of antibiotics on baseline inflammation or immune responses*

Some studies have used TLR agonists to investigate the effects of antibiotics on specific immune pathways. The tetracycline and macrolide classes of antibiotics have well-established anti-inflammatory effects (Voils et al., 2005) and this has also been investigated *in vitro*. Clarithromycin, a macrolide antibiotic, was found to suppress cytokine and IFN production in immortalised A549 epithelial cells following poly(I:C) or Pam3CSK4 stimulation (Yamamoto et al., 2016). This was linked to disruption of the IFN-signalling pathways and evidence from TLR-null HEK293 cells suggested this effect was independent of TLR signalling. Azithromycin, another macrolide, was found to suppress stimulatory effects of R848 in human peripheral or cord blood (Speer et al., 2018).

Anti-inflammatory effects of antibiotics have also been reported in fish. Florfenicol reduced cytokine transcript levels in LPS-challenged grass carp kidney cells *in vitro* and

in vivo (Li et al., 2019). It also reduced transcript levels of TLR genes and components of the signalling pathways suggesting negative regulation of TLR signalling. However, the level of activation of these components was not investigated. In rainbow trout, two-week oxytetracycline (OTC) treatment reduced numbers of blood leukocytes, plasma immunoglobulin levels, and level of bacterial phagocytosis, indicating a general reduction in immune function (Yonar, 2012). However, these parameters were not investigated in the context of an immune challenge. In contrast, 10-day OTC treatment of gilthead sea bream induced transient increases in erythrocytes, leukocytes and neutrophils (nitro blue tetrazolium+ cells) in the blood (Serezlí, 2005). No additional markers of inflammation were investigated but other studies have observed clear inflammatory effects of OTC. In zebrafish larvae, OTC induced an increase in neutrophils in the tail region and an increase in *il1b* and *mpx* transcripts after 48 hours of treatment (Barros-Becker et al., 2012). Higher cytokine transcript levels was also observed in the liver and gut of Nile tilapia treated with OTC, although the length of treatment was not reported (Limbu et al., 2018). OTC has also been found to affect cellular and humoral responses to infection in fish, and in some cases increase mortality (Van Der Heijden et al., 1996; Lundén et al., 1998; Zhou et al., 2018). These data indicate that OTC has an immunomodulatory effect in fish although the varied species, tissues, and experimental conditions used makes it difficult to compare between studies. In addition, more research is needed to understand whether OTC affects antiviral responses.

4.2 Aims

Characterisation of the gills in Chapter 3 revealed the presence of diverse and abundant immune cell populations suggesting that this tissue is highly capable of responding to immune challenges. This chapter focuses on understanding how the gills respond when different immune pathways are stimulated, and how this compares to systemic immune responses in the fish. This is important for understanding the role of the gills in zebrafish immunity and comparing it the mammalian respiratory immunology. Furthermore, this work helps identify tools that can be used to further interrogate gill immunology. This chapter focuses on the following aims:

- To determine transcriptional response of the gills to different types of immunuostimulatory compounds.

- To evaluate how the type of compound and route of administration influences the transcriptional response.

- To compare the response in the gills to other peripheral tissues.

- To determine which leukocytes are involved in immune responses in the gills.

- To assess whether antibiotic treatment can modulate immune responses in the gills.

4.3 Results

4.3.1 Gill immune responses to immunostimulatory compounds

4.3.1.1 Transcriptional and cellular responses to immunostimulatory compounds

To investigate the gill response to pathogen mimetics and derivatives, this project focused on four compounds known to activate different TLRs in mammalian species: R848 which activates TLR7/8, synthetic CpG-ODNs which activate TLR9, Pam3CSK4, which activates TLR2/TLR1, and LPS which activates TLR4 (Kawai and Akira, 2010). R848 and CpG-ODN mimic viral genetic material, and Pam3CSK4 mimics bacterial lipopeptides which would be recognised by the aforementioned receptors. LPS is a bacteria-derived PAMP itself. Therefore, these compounds can be used to interrogate different PAMP recognition pathways and responses to different types of pathogens.

All four compounds have been previously used to challenge zebrafish adults or embryos and shown to induce varying levels of inflammation (Varela et al. 2012; Yeh et al. 2013; Yang et al. 2015; Forn-Cuní et al. 2017; Progatzky et al. 2019). Zebrafish contain orthologues of all the mentioned TLRs and CpG-ODN and PamC3SK4 have been confirmed to act through the same receptor as mammals, TLR9 and TLR2 respectively (Yeh et al. 2013; Yang et al. 2015; Li et al. 2016). Zebrafish also express TLR21, which is not found in mammalian species but also recognises CpG-ODNs (Yeh et al., 2013). Recognition pathways for R848 have not been identified. Unlike in mammals, LPS is not thought to act through TLR4, but instead through caspase-B (Yang et al. 2018). These compounds are therefore ideal for investigating different PAMP recognition pathways in zebrafish. Of the four compounds, only R848 has been used to challenge zebrafish gills (Progatzky et al., 2019).

In this project, the compounds were topically applied to adult zebrafish gills or i.p. injected to assess the impact of the route of administration on the immune response (n = 3-4 fish). Control fish were challenged with endotoxin-free water. Gill and WKM tissue were collected from the challenged fish at different time points and analysed by qRT-PCR for transcript levels, and by whole-mount immunofluorescence and flow cytometry for cellular changes.

To measure the magnitude, kinetics and nature of the response to these compounds, gill (Figure 4.1) and WKM tissue (Figure 4.2) were analysed at 1 and 8 hpt by qRT-PCR for proinflammatory cytokines *il1b* and *tnfa*, chemokine *cxcl18b*, and interferons *ifnphi1* (type I) and *ifng1* (type II). These genes were chosen to reflect previously observed responses to R848 in the gills, but also to assess different aspects of the immune response (Progatzky et al., 2019).

This work was performed in part by Sabrina Hoong (BSc, Imperial College London) who assisted during the animal challenges and harvesting and performed some of the sample processing and qRT-PCR for CpG-ODN and Pam3CSK4 challenges.

For some samples, transcript levels were not detected above the detection limit indicating low or absent expression of the gene. Although statistical tests could not be performed for datasets with undetected values, the general trend between groups could still be described.

Responses in the gills

Topical R848 challenge increased transcript levels of all the genes studied in the gills (Figure 4.1). The response was characterised by an early increase in *il1b* and *tnfa* levels, which returned to baseline by 8 hpt. This early response also involved an increase in *ifnphi*. The response to R848 was further characterised by a later increase in *cxcl18b* levels, which were already higher than controls at 1 hpt, but even greater at 8 hpt. The late response also included an increase in *ifng1* levels at 8 hpt.

I.p. injection of R848 similarly increased transcript levels for all five genes in the gills. The response had similar kinetics to the topical challenge, with *il1b* and *tnfa* increased at 1 hpt and *cxcl18b* and *ifng1* increased to a greater extent at 8 hpt. However, *ifnphi1* levels were similar at both timepoints indicating a less transient response than in topical challenges.

Unlike R848, topical challenge with LPS did not induce any changes in the gills for the genes studied. However, i.p. challenge with LPS did increase *il1b* and *cxcl18b* levels at 1 hpt. No changes were measured for *tnfa*, *ifnphi1* or *ifng1* indicating that LPS i.p. challenge induced a different type of immune response than R848. The response to LPS declined by 8 hpt, indicating that it was more transient than the response to R848.

In contrast to R848 and LPS, CpG-ODN and Pam3CSK4 challenges did not induce a robust immune response in the gills either through topical or i.p. routes. CpG-ODN did not induce any detectable changes in transcript levels for either challenge whilst Pam3CSK4 induced only small increases in *il1b* at 1 and 8 hpt following topical challenge. These increases were generally smaller than R848 indicating a minimal immune response in the gills. In Pam3CSK4 i.p. challenged fish, there was a statistically significant decrease in *ifnphi1* at 8 hpt however, the magnitude of this change was small in comparison to increases observed in R848-challenged fish. No other changes in transcript levels were detected.
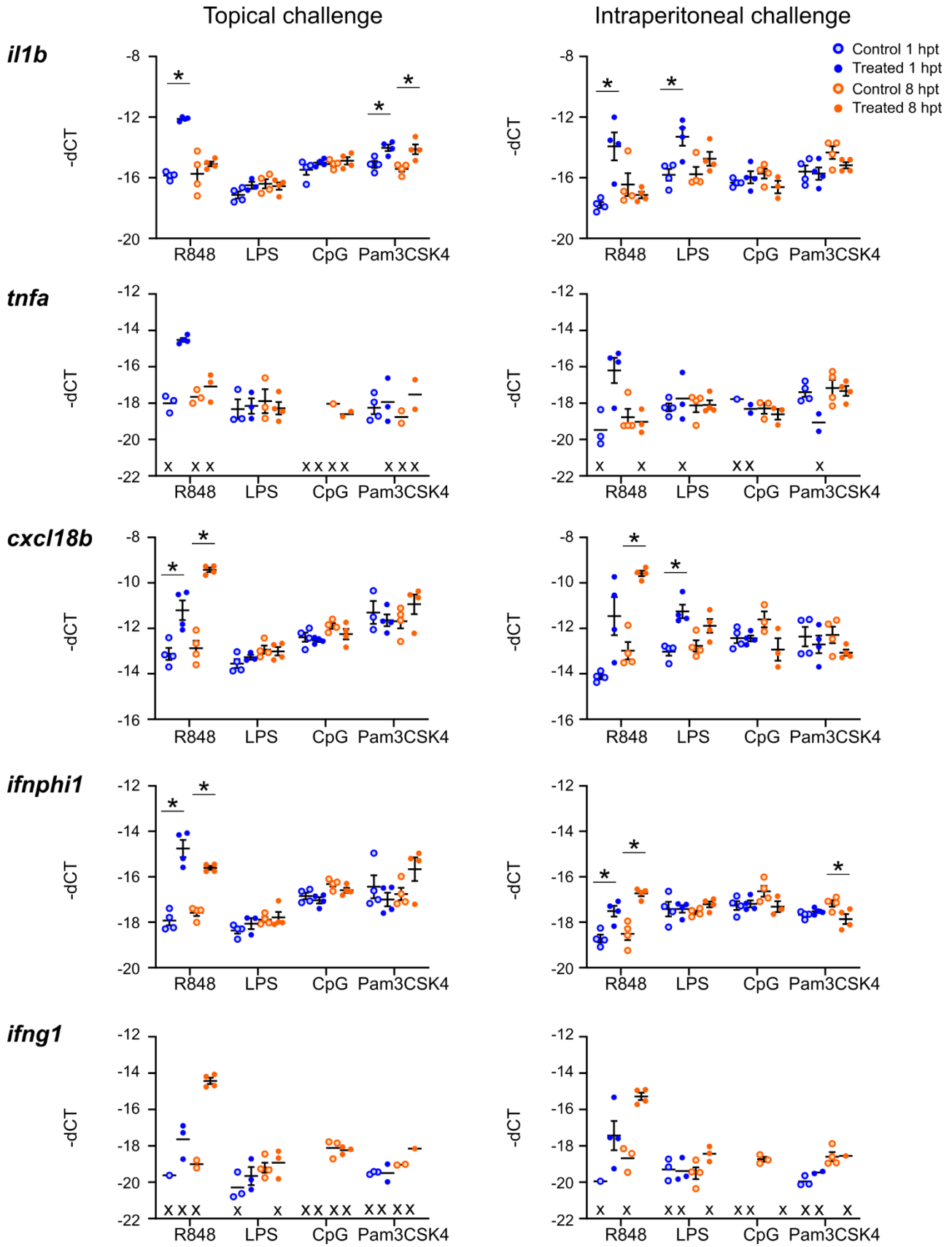
Figure 4.1 Gene transcript analysis of the gills from R848-, LPS-, CpG-ODN (CpG)-, or Pam3CSK4-challenged fish or control (water-challenged) fish.

Compounds (5 µl at 0.5 mg/ml) or endotoxin-free water were topically applied to the gills (left) or intraperitoneally injected (right). Transcripts were measured by qRT-PCR and are shown relative to 18S transcript levels. Data represents one experiment (n = 3-4 per group, samples with detectable transcripts plotted). Mean and SEM shown. One-way ANOVA, or Welch's ANOVA (for datasets with unequal variances), was performed for the four groups of each compound per gene, followed by Sidak's multiple comparison test. *: $p \leq 0.05$. X on the chart indicates ≥ 1 sample in the group had undetected transcripts (SEM not calculated), and therefore statistical testing was not performed for these groups. Processing of Pam3CSK4 and CpG-ODN-challenged samples was performed by Sabrina Hoong (Imperial College London). Certain qRT-PCR analyses for these samples were also performed by Sabrina Hoong as part of her Bachelor's thesis on zebrafish gill characterisation (Hoong, 2018). Processing and analysis for all other samples in this PhD thesis was performed by me.

Responses in the WKM

Transcript levels were measured in the WKM to determine whether challenges induced a purely local response (in the gills), or a more systemic response. Topical R848 challenge increased transcript levels for all five genes in the WKM indicating a systemic response despite local application of the compound (Figure 4.2). The changes in transcript levels followed similar kinetics to changes in the gills (Figure 4.1) where *il1b*, *tnfa*, and *ifnphi1* levels were highest at 1 hpt, and where *cxcl18b* and *ifng1* levels were highest at 8 hpt.

I.p. challenge with R848 also induced upregulation of all fives genes in the WKM. The kinetics of *il1b*, *tnfa*, and *ifng1* regulation was similar in topically and i.p. challenged fish with early upregulation of *il1b* and *tnfa*, and late upregulation of *ifng1*. The kinetics of *cxcl18b* and *ifnphi1* regulation were different between topically and i.p. challenged fish; in i.p. challenged fish, *cxcl18b* levels were highest at 1 hpt, and by 8 hpt showed large variability between samples. *Ifnphi1* was upregulated to similar levels at both time points in i.p. challenged fish. This contrasts with topically challenged fish where *ifnphi1* was highest at 1 hpt.

Topical LPS challenge did not result in any changes in transcript levels in the WKM, and together with data from the gills, this indicates a lack of local and systemic responses. On the other hand, *il1b*, *tnfa*, and *cxcl18b* were all higher in the WKM at 1 h following i.p. LPS challenge. Transcript levels for these genes were similar compared to samples from R848 i.p. challenged fish indicating a similar magnitude in the immune response. *Il1b* and *tnfa* were no longer upregulated at 8 hpt, showing similar kinetics as the response to R848.

Cxcl18b was also higher at 1 hpt but not at 8 hpt. However, no changes in *ifnphi1* or *ifng1* were detected in LPS challenged fish – a clear contrast to the interferon response to R848.

The kinetics of the response to LPS was similar in the gills (Figure 4.1) and WKM (Figure 4.2), however, *tnfa* was not upregulated in the gills indicating tissue-specific differences.

No changes in transcript levels were detected in the WKM following CpG-ODN topical challenge (Figure 4.2). Similarly, minimal changes were detected following i.p. CpG-ODN challenge. Although *il1b* was slightly higher at 1 hpt, the considerable variation between samples suggests this was not a consistent feature of the response to CpG-ODN. Pam3CSK4 did not induce consistent changes in transcript levels in either topically or i.p. challenged fish.

These results support previous work identifying R848 as a potent immunostimulant in zebrafish gills (Progatzky et al., 2019). This additionally shows that topical gill application can induce systemic immune responses (in the WKM), and conversely that i.p. injection can induce responses in the gills. The gill response to LPS following i.p. challenge adds further evidence that LPS can indeed act as an immunostimulant in zebrafish gills. However, the lack of response to topical LPS challenge highlights that exposure through the gills is not always capable of inducing a gill immune response. The lack of response could be a result of the gills acting as a selective barrier to some compounds, influencing both local and systemic responses. Although both LPS and R848 induced immune responses in some of the challenges, only R848 induced changes in interferon genes indicating that adult zebrafish respond differently to different agonists, suggesting differences in downstream pathways. CpG-ODN and Pam3CSK4 induced few, if any, changes in the genes analysed which contradicts previous work studying these agonists in zebrafish (Yeh et al. 2013; Yang et al. 2015).
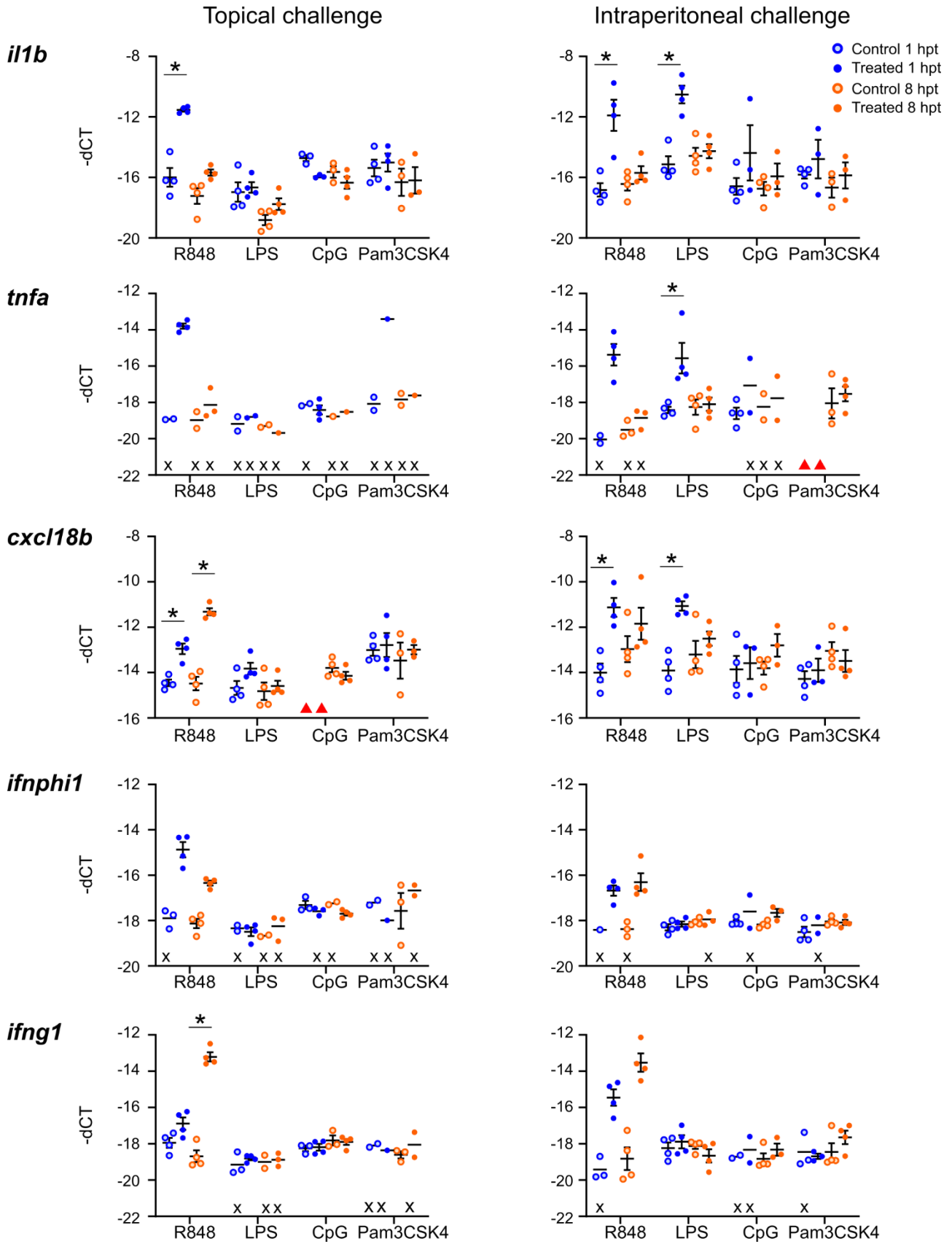
Figure 4.2 Gene transcript analysis of the WKM from R848-, LPS-, CpG-ODN (CpG)-, or Pam3CSK4-challenged fish or control (water-challenged) fish.

Compounds (5 µl at 0.5 mg/ml) or endotoxin-free water were topically applied to the gills (left) or intraperitoneally injected (right). Transcripts were measured by qRT-PCR and are shown relative to 18S transcript levels. Data represents one experiment (n = 3-4 per group, samples with detectable transcripts plotted). Mean and SEM shown. One-way ANOVA, or Welch's ANOVA (for datasets with unequal variances), was performed for the four groups of each compound per gene, followed by Sidak's multiple comparison test. *: p ≤ 0.05. X on the chart indicates ≥ 1 sample in the group had undetected transcripts (SEM not calculated), and therefore statistical testing was not performed for these groups. Red triangles indicate n < 3 in the group and therefore these data were omitted. Processing of Pam3CSK4 and CpG-ODN-challenged samples was performed by Sabrina Hoong (Imperial College London). Certain qRT-PCR analyses for these samples were also performed by Sabrina Hoong as part of her Bachelor's thesis on zebrafish gill characterisation (Hoong, 2018). Processing and analysis for all other samples in this PhD thesis was performed by me.

4.3.1.2 Immune cell responses to topical gill challenge with R848

Measuring transcriptional changes in response to immunostimulatory compounds revealed broad changes in the gill tissue but did not address the involvement of specific immune cell populations. Changes in transcription of immune cell-related genes and immune cell numbers have previously been reported in zebrafish gills during the inflammatory response to cigarette smoke or silica (Progatzky, 2014; Progatzky et al., 2015). Changes in immune cell-related genes have also been observed in the gills of other fish species in response to viral infection (Aquilino et al., 2014; Austbø et al., 2014). It was therefore hypothesised that cellular changes would also occur during the immune response to R848.

Flow cytometry and whole-mount immunofluorescence were used to measure changes in the proportion and localisation of immune cells following topical R848 challenge. R848 was used to induce a robust immune response and, as a viral mimic, provide insight into the response to viral-like components. Immune cells were identified using the following transgenics: *Tg(lyz:GFP)* for neutrophils, *Tg(lck:GFP)* for T and innate lymphocytes, and *Tg(cd4-1:mCherry; lck:GFP)* for cd4-1-expressing T cells and myeloid cells.

This work includes experimental contributions from Morgan Heycock and Alisha May (Imperial College London) who I worked with to support experimental design and execution during their Bachelor's (Heycock, 2017) and Master's (May, 2017) projects on gill immune characterisation. Some of the sample processing and image acquisition for *Tg(lck:GFP)* and *Tg(lyz:GFP)* challenges was performed by Morgan Heycock who also

assisted with the animal challenges. Harvesting of tissues, sample processing and image acquisition for *Tg(cd4-1:mCherry; lck:GFP)* challenges was performed by Alisha May who also assisted with the animal challenges and flow cytometry.

Adult zebrafish gills were challenged topically with endotoxin-free water or R848 and harvested 3 or 8 hpt. These timepoints were chosen to reflect the early and late response as identified by transcriptional analysis (Figure 4.1). 3 hpt was chosen instead of 1 hpt as it was expected that cellular changes may occur more slowly than transcriptional changes. Immune cells in the gills were visualised by confocal microscopy and measured by flow cytometry (*Tg(cd4-1:mCherry; lck:GFP)* only). From confocal images of the gills, the number of fluorescent cells in the secondary lamellae (20 lamellae most proximal to the arch) were counted computationally (Figure 4.3A). These regions were chosen because individual cells were more easily distinguished compared to the primary lamellae which often contained large aggregates of *lck:*GFP+ cells.

*Lyz:*GFP+ cells were identified throughout the gills in control and R848-challenged conditions and at both time points (Figure 4.3B-E). *Lyz:*GFP+ cell numbers were higher in the secondary lamellae of R848-challenged gills at 3 hpt but did not form clusters (Figure 4.3C, F). This was not observed at 8 hpt suggesting that R848 induces a transient change in neutrophil localisation in the gills.
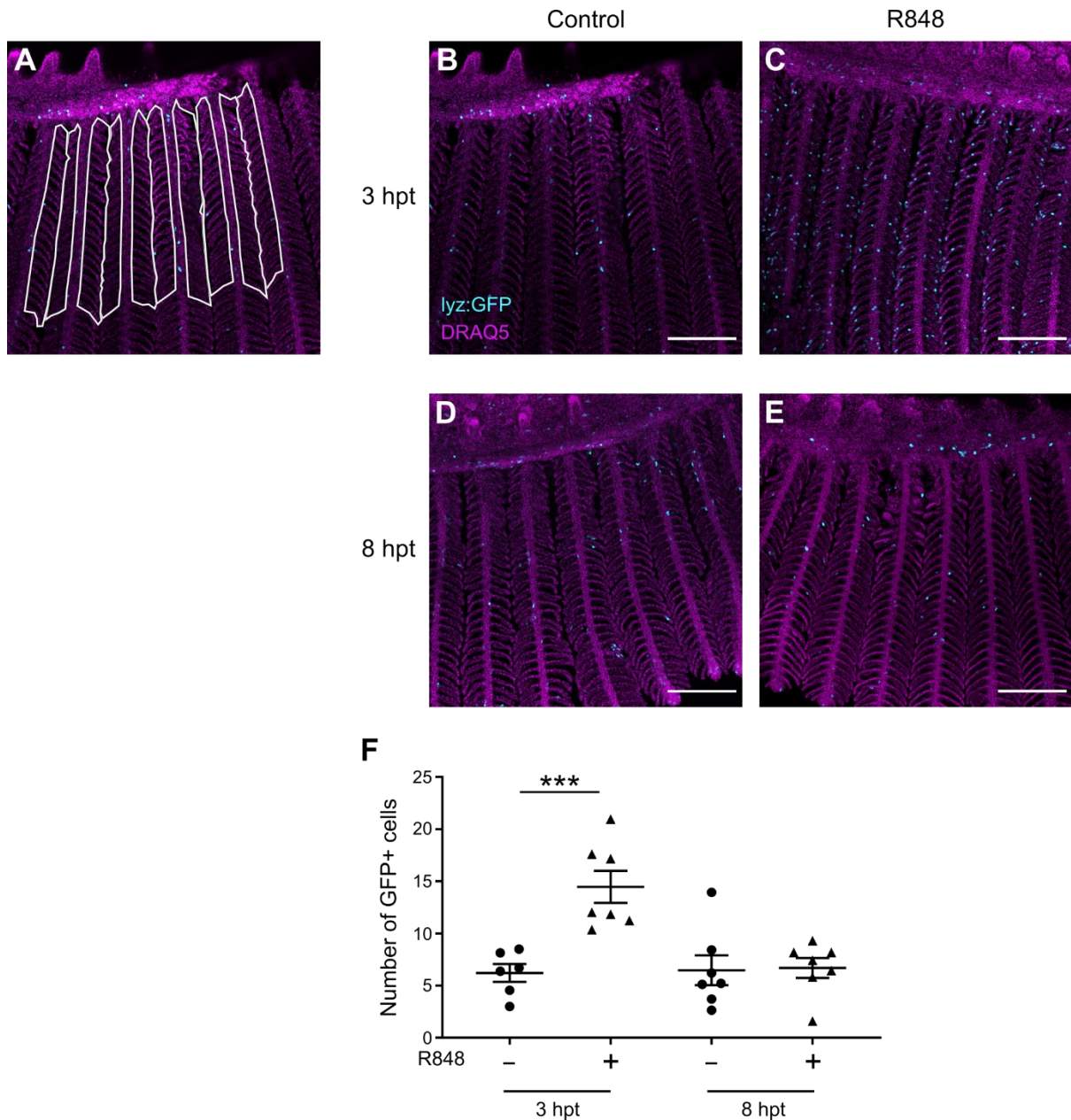
Figure 4.3 Fluorescence microscopy and counting of neutrophils in R848-challenged (5μl at 0.5 mg/ml) or control (water treated) adult *Tg(lyz:GFP)* gills.

A) Example of the regions (white polygons) used for cell counting. Each white polygon delineates the 20 most proximal secondary lamellae from the arch. (B-E) Representative maximum z-stack projections of gills immunostained for GFP (cyan) and counter-stained with DRAQ5 (magenta). F) Average computational counts of GFP+ cells in the 20 most proximal lamellae from the arch. Each point corresponds to one fish, n = 6-7, pooled from two independent experiments. Mean and SEM shown. Two-way ANOVA performed followed by Sidak's multiple comparison test, ***: $p \leq 0.001$. Sample processing and image acquisition was performed alongside Morgan Heycock (Imperial College London). Post-acquisition image processing and analysis in this PhD thesis was performed by me. Image adapted and reproduced with permission of the rights holder, authors of the article (Progatzky et al., 2019).

*Lck:*GFP+ cells were also present in the gills in both control and R848-treated conditions, distributed in the filaments as individual cells or as clusters in the arch (Figure 4.4A-D). Like *lyz:*GFP+ cells, *lck:*GFP+ cell numbers were significantly higher in the secondary lamellae at 3 hpt (Figure 4.4E). However, unlike *lyz:*GFP+ cells, they remained significantly higher at 8 hpt compared to controls.

These results show that both neutrophil and lymphocyte cell distribution is altered by R848 challenge in the gills. The early and transient increase of neutrophils, and more persistent increase of lymphocytes, highlight the temporal regulation of the response to R848, as reflected in the transcriptional response. This suggests that neutrophils and lymphocytes may respond to different cues and/or contribute to different aspects of the transcriptional response to R848. Furthermore, this data aligns with the well-established understanding of neutrophils as first responders to inflammation, including in respiratory tissues (Camp et al., 2015; Tate et al., 2008).
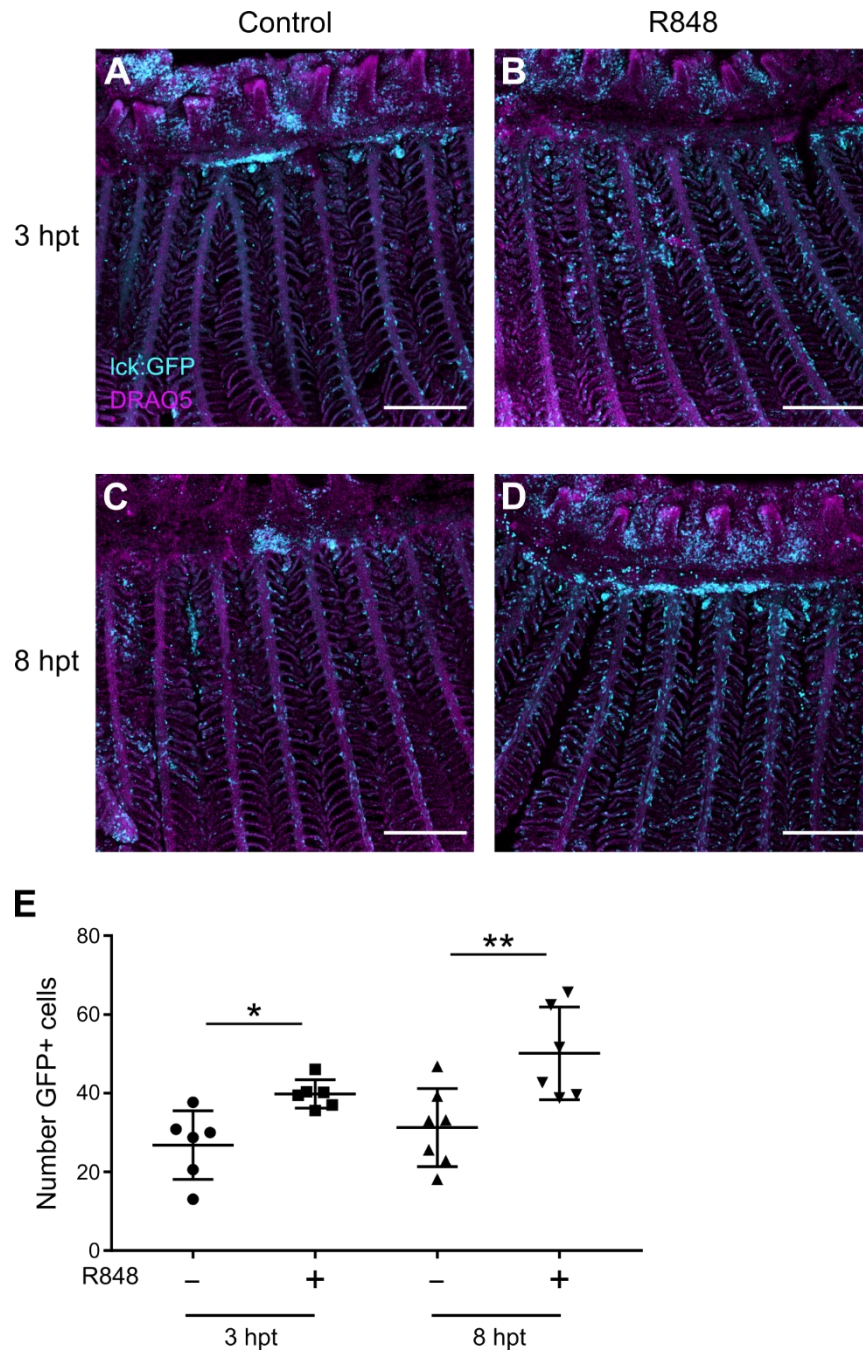
Figure 4.4 Fluorescence microscopy and counting of lymphocytes in R848-challenged (5μl at 0.5 mg/ml) or control (water treated) adult *Tg(lck:GFP)* gills.

(A-D) Representative maximum z-stack projections of gills immunostained for GFP (cyan) and counter-stained with DRAQ5 (magenta). E) Average computational counts of GFP+ cells in the 20 most proximal lamellae from the arch. Each point corresponds to one fish, n = 6-7, pooled from two independent experiments. Mean and SEM shown. Two-way ANOVA performed followed by Sidak's multiple comparison test, *: $p \leq 0.05$, **: $p \leq 0.01$. Sample processing and image acquisition was performed alongside Morgan Heycock (Imperial College London). Post-acquisition image processing and analysis in this PhD thesis was performed by me. Image adapted and reproduced with permission of the rights holder, authors of the article (Progatzky et al., 2019).

To determine whether the *cd4-1:*mCherry+ subset of *lck:*GFP+ lymphocytes (*cd4-1*+ T cells) also responded to R848, *Tg(cd4-1:mCherry; lck:GFP)* gills were analysed with confocal microscopy (Figure 4.5). This double transgenic additionally allowed investigation of how *cd4-1:*mCherry+*lck:*GFP- myeloid cells responded to R848.

GFP+ and mCherry+ cells were identified throughout the gill structure (Figure 4.5A-D). Although most fish exhibited *lck:*GFP+ lymphocyte clusters in the gill arch, 2/8 fish lacked these structures in the 3 hpt control, 8 hpt control, and 8 hpt R848-challenged groups. *Lck:*GFP+ clusters were identified in all 6 fish in the 3 hpt R848-challenged group. This further supports variability and potentially dynamic changes in gill lymphoid tissue regardless of treatment as observed in single transgenic *Tg(lck:GFP)* fish (Figure 4.4).

The number of *lck:*GFP+ cells in the secondary lamellae was unchanged following R848 challenge at either time point (Figure 4.5E). This is inconsistent with results from *Tg(lck:GFP)* fish (Figure 4.4E). However, the number of GFP+ cells in control gills in *Tg(cd4-1:mCherry; lck:GFP)* fish (Figure 4.5E) were higher than in *Tg(lck:GFP)* control gills (Figure 4.4E) suggesting that the double transgenic gills had a higher baseline level of inflammation. In fact, the number of GFP+ cells in *Tg(cd4-1:mCherry; lck:GFP)* gills was more similar to R848-challenged *Tg(lck:GFP)* gills at 8 hpt. The gills are known to have immunoregulatory mechanisms to avoid excessive inflammation, so it is possible that the greater presence of lymphocytes inhibited further increases by R848 (Bottiglione et al., 2020). The reasons for greater immune cell presence in these gills were not investigated but could be related to unidentified and uncontrolled differences in tank conditions or the genetic background of the fish. RNA analysis for one of the experiments showed that *ifng1* transcripts were upregulated in the gills following R848 challenge (Figure 4.5H) Therefore, the lack of change in immune cells was not due to a general lack of responsiveness to R848.

The number of *cd4-1:*mCherry+ cells in the lamellae were also unchanged by R848 challenge and fewer in number than GFP+ cells (Figure 4.5F). *Lck:*GFP+*cd4-1:*mCherry+ cells (*cd4-1*+ T cells) comprised the smallest numbers of cells in the lamellae and were similarly unchanged between control and R848-challenged fish.
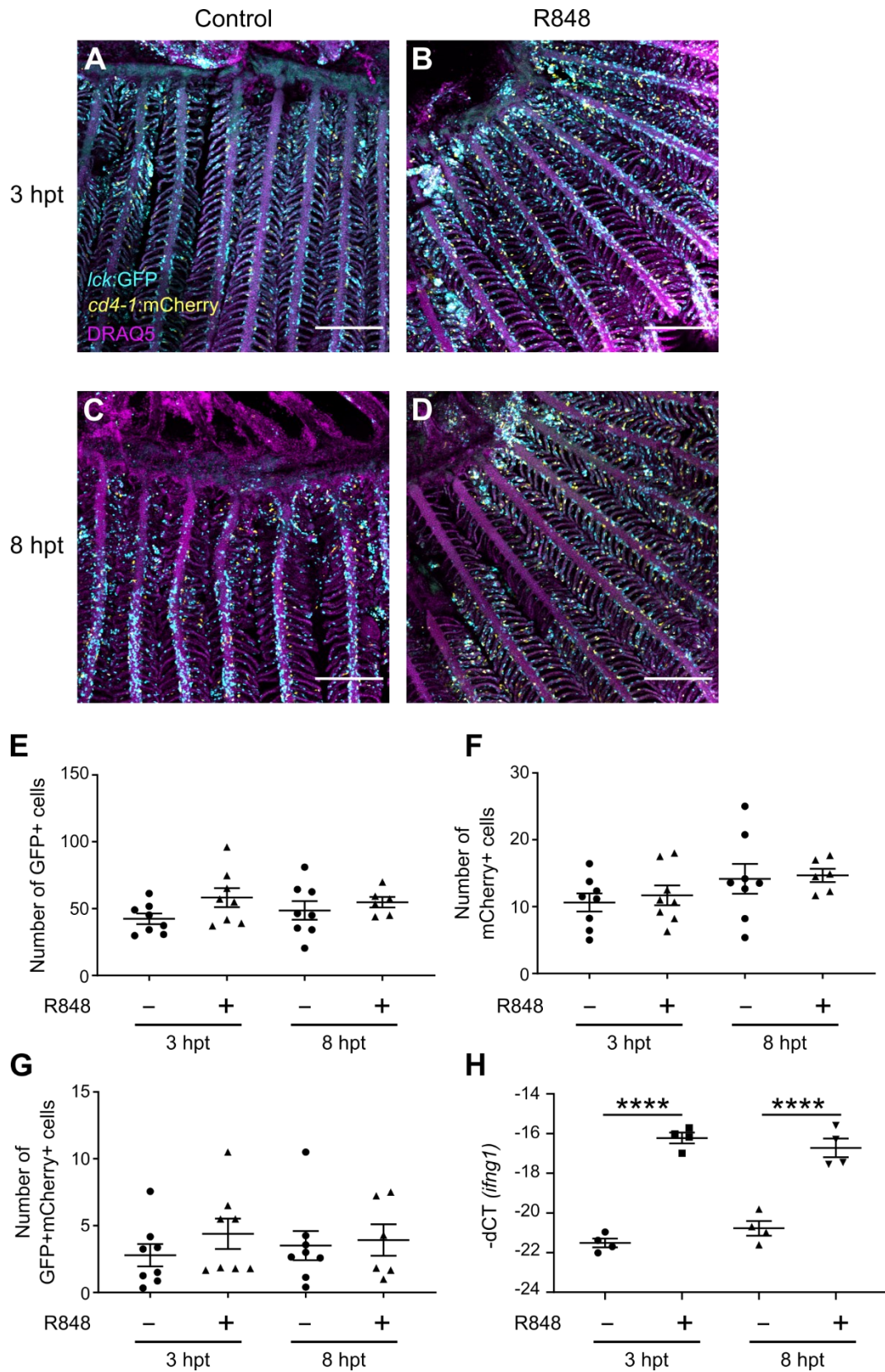
Figure 4.5 Fluorescence microscopy and counting of *lck:*GFP+ and *cd4-1:*mCherry+ cells in R848-challenged (5µl at 0.5 mg/ml) or control (water treated) adult *Tg(cd4-1:mCherry; lck:GFP)* gills.

(A-D) Representative maximum z-stack projections of gills immunostained for GFP (cyan) and mCherry (yellow) and counter-stained with DRAQ5 (magenta). (E-G) Average computational counts of GFP+ cells (E), mCherry+ cells (F), and GFP+mCherry+ cells (G) in the 20 most proximal lamellae from the arch. Each point corresponds to one fish, n = 6-8, pooled from two independent experiments. Mean and SEM shown. Two-way ANOVA performed followed by Sidak's multiple comparison test. All comparisons performed were not significant (p > 0.05). H) *ifng1* transcripts in the gills were measured by qRT-PCR and are shown relative to 18S transcript levels. Data represents one experiment (n = 4). Mean and SEM shown. One-way ANOVA was performed followed by Sidak's multiple comparisons test, ****: p ≤ 0.0001. Sample processing, image acquisition and qRT-PCR procedure were performed by Alisha May (Imperial College London) as part of her Master's thesis (May, 2017). Post-acquisition image processing and analysis in this PhD thesis was performed by me.

Flow cytometry was used to interrogate the morphologies of GFP+ and mCherry+ cells in the gills from the same fish that were analysed by confocal microscopy. As previously described, cells were gated on their FSC/SSC properties with 4 gates reflecting different haematopoietic cell populations (Figure 4.6A). GFP+mCherry- and GFP+mCherry+ cells were found almost entirely within the lymphocyte gate and did not change following R848 treatment after either timepoint (Figure 4.6B and C). mCherry+GFP- cells were more hetereogenous; they were found mainly in the myeloid gate but also in the erythrocyte gate (Figure 4.6D). Again, this did not change following R848 challenge. These results indicate that R848 did not appear to alter the morphology of fluorescent lymphocytes and myeloid cells, nor induce expression of GFP or mCherry in other cell populations.

Next the proportion of the different fluorescent populations was investigated. As expected from gill tissue at homeostasis and observed from cell counts in the lamellae (Figure 4.5E-G), GFP+mCherry- cells were more abundant in the gills than the mCherry+ populations (Figure 4.6E). The proportions of the three fluorescent populations were unchanged following R848 treatment at either timepoint.

GFP+mCherry+ cells made up nearly 15% of the total GFP+ population in all treatment groups (Figure 4.6F). This was higher than the proportion of double positive cells in the lamellae, which formed only 6-8**%** of GFP+ cells (Figure 4.5E and G). This suggests that either the computational counting method underestimated the number for mCherry+ cells, or that the *cd4-1:*mCherry+*lck:*GFP+ T cell subset may reside more prominently in

193

other regions of the gill. GFP+mCherry+ cells made up nearly 60% of the total mCherry+ population in all treatment groups (Figure 4.6G). Therefore, R848 did not affect the proportion of *cd4-1:*mCherry+ T cells within the lymphocyte population, or the proportion of lymphocytes within the *cd4-1*:mCherry+ cell population.

Overall, the flow cytometry analysis shows that topical R848 challenge did not alter induce global changes in the composition or proportion of lymphocytes and *cd4-1+* leukocytes in the gills. However, this does not rule out the possibility of global changes in gills with a lower initial presence of immune cells (Figure 4.4).
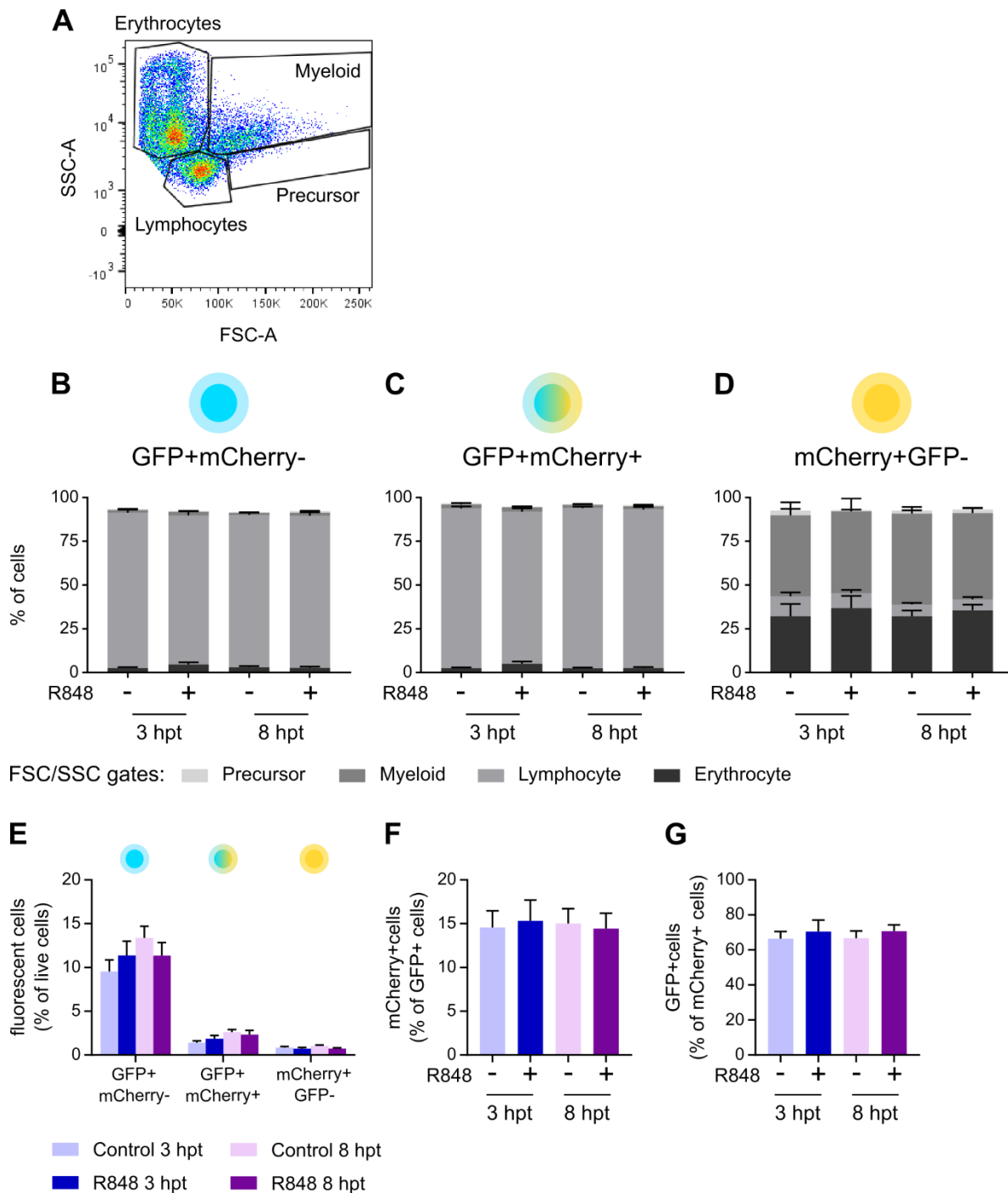
Figure 4.6 Flow cytometry analysis of *lck:*GFP+ and *cd4-1:*mCherry+ cells in R848-challenged (5µl at 0.5 mg/ml) or control (water treated) adult *Tg(cd4-1:mCherry; lck:GFP)* gills.

Fluorescent cells in *Tg(cd4-1:mCherry; lck:GFP)* samples were identified by comparing to an unchallenged non-transgenic *TraNac* gill sample. A) Example of the FSC/SSC profile for live single cells in a gill sample. Gates for the major haematopoietic populations are shown with black polygons. (B-D) Mean proportion of cells in the four FSC/SSC gates as a percentage of total cells for each fluorescent population. Error bars represent SEM. E) Proportion of fluorescent cells as a percentage of live cells. Mean and SEM shown. F) Proportion of mCherry+ cells in the GFP+ population. Mean and SEM shown. G) Proportion of GFP+ cells in the mCherry+ population. Mean and SEM shown. Data shown pooled from two independent experiments, n = 7-8. Sample processing was performed alongside Alisha May (Imperial College London) as part of her Master's thesis (May, 2017). Analysis in this PhD thesis was performed by me.

195

4.3.1.3   *Flow cytometry and imaging of gills challenged with fluorescent R848*

Changes in neutrophil and lymphocyte cell distribution (Figure 4.3 and Figure 4.4) do not on their own reveal the mechanisms by which these cells respond to R848. In order to start addressing this and further study immune cell function in the gills, the interaction between R848 itself and immune cells was studied.

Fluorescent R848-ATTO488 (R848-F) was generated by Dr Lindsay Evans (Department of Chemistry, Imperial College London) and 0.15 mg/ml was topically applied to adult *Tg(cd4-1:mCherry)* gills (right side). This dose is equivalent to 0.05 mg/ml of unlabelled R848. Gill cells were analysed 30 mins post challenge by flow cytometry. This allowed simultaneous detection of R848-F and *cd4-1:*mCherry in gill cells. *Cd4-1:*mCherry+ cells are known to interact with antigen in the skin and were expected to behave similarly in response to R848-F in the gills (Lin et al., 2019).

Fish were challenged whilst being observed with a fluorescence stereomicroscope allowing visualisation of R848-F during the procedure (Figure 4.7A). Fish were recovered from anaesthesia and kept in water for 30 mins following challenge before being euthanised for gill dissection. R848-F was much dimmer after 30 mins and difficult to detect in gills *in vivo* (Figure 4.7B). R848-F signal was detected in the dissected gill filaments of the treated side (Figure 4.7C). Imaging DMSO-treated negative control gills revealed that gills were dimly auto-fluorescent in the arch region. However, fluorescent signal in the filaments appeared to be R848-F specific. The 2 branches containing the brightest R848-F signal were collected for flow cytometry.
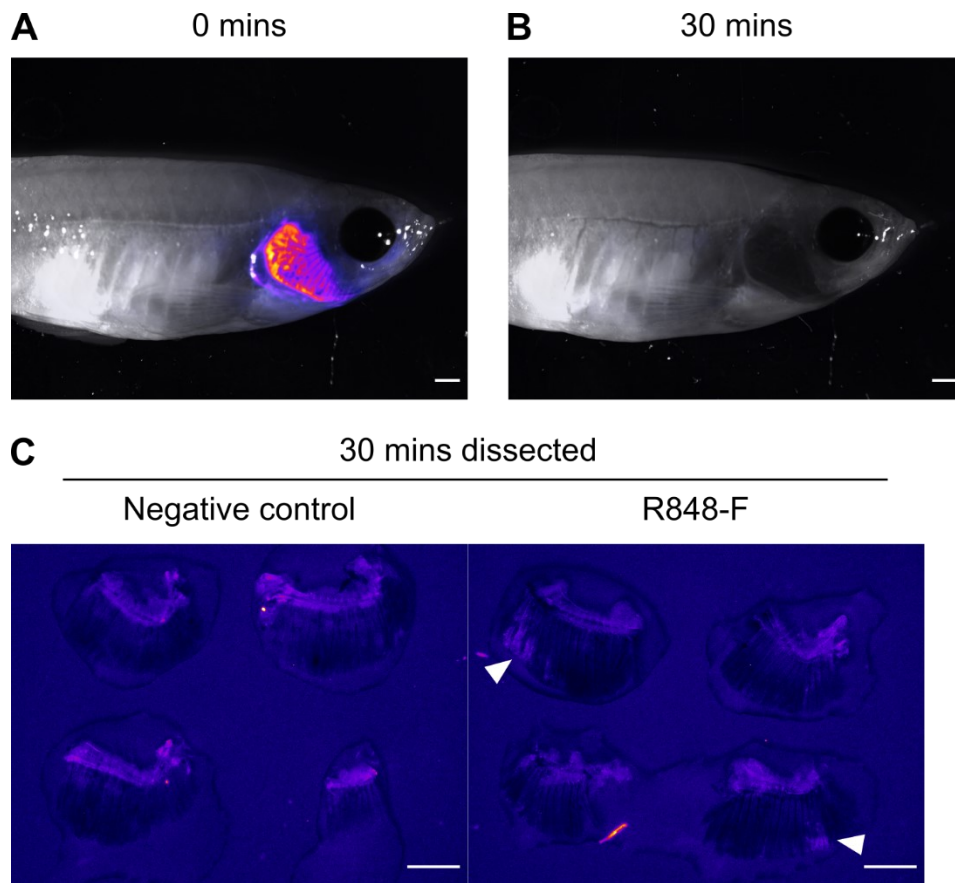
Figure 4.7 Imaging of R848-F in the gills of a topically challenged zebrafish.

R848-F (5µl at 0.15 mg/ml) or 0.3% DMSO (5µl) was topically applied to the gills of *TraNac* fish and imaged immediately following application (A), 30 mins post treatment (B), and following dissection of individual branches from the treated side (C). (A-B) Merge of brightfield (grey) and fluorescent (purple-yellow spectrum) images. Fluorescent images were acquired with 100ms exposure. C) Fluorescent images of dissected gill branches acquired with 500 ms exposure. Left: DMSO-treated gills (negative control); right: R848-F-treated gills. N=1 per group. White arrowheads indicate R848-F signal in the filaments. Scale bar represents 1 mm in all images (A-C)

Only 0.4% (SEM = 0.1) of total gill cells were positive for R848-F (Figure 4.8A). This suggests that only a small proportion of cells need to interact directly with R848 to induce a robust immune response. In pilot experiments R848-F did not alter transcript levels in the gills suggesting a lack of response to this compound (Fränze Progatzky, personal communication). However, competitive challenges with both R848 and R848-F abrogated R848-F uptake which suggests that the molecules compete for the same receptor (Fränze Progatzky, personal communication). The lack of response may result from the low dose of R848-F used, but other possibilities will be addressed in the chapter discussion including potential differences between R848-F and R848.

The majority of R848-F+ cells were found in the myeloid FSC/SSC gate (62%, SEM = 4), however a sizeable minority were also found in the erythrocyte (15%, SEM = 2) and lymphocyte (14%, SEM = 2) gates. R848-F+ cells were therefore enriched for cells in the myeloid gate compared to total live gill cells (Figure 4.8E). Of the R848-F+ cells, 30% (SEM = 5) were *cd4-1:*mCherry+. These R848-F+mCherry+ cells were predominately in the myeloid gate (82%, SEM = 3) in contrast to total mCherry+ cells which were mostly in the lymphocyte gate (Figure 4.8E). The enrichment of myeloid-like cells in the R848-F+ and R848-F+*cd4-1:*mCherry+ populations supports the hypothesis that myeloid cells are more capable of antigen uptake than other immune cells in the gills. This shows that zebrafish myeloid cells in the gills have functional similarities to mammalian myeloid cells in the respiratory system.

Of the total *cd4-1:*mCherry+ population, only 2% (SEM = 0.07) of cells were R848-F+. More specifically, of the *cd4-1:*mCherry+ cells in the myeloid gate, 12% (SEM = 2) were R848-F+ showing that not all *cd4-1:*mCherry+ cells in this gate interacted with the compound. This is further evidence that *cd4-1*-expressing cells in the gills are functionally heterogeneous, even within the myeloid FSC/SSC gate.

In summary, this flow cytometry analysis indicates that initial recognition of R848 may involve a small but heterogenous population of gill cells, particularly cells with myeloid-like morphology. This includes *cd4-1:*mCherry+ myeloid cells but is also likely to include other *cd4-1-* cells. This suggests that initiation of the response to R848 is likely to involve interaction of the compound with myeloid cells. However, the involvement of non-immune cells cannot be excluded as FSC/SSC cannot precisely distinguish these cells from leukocytes.
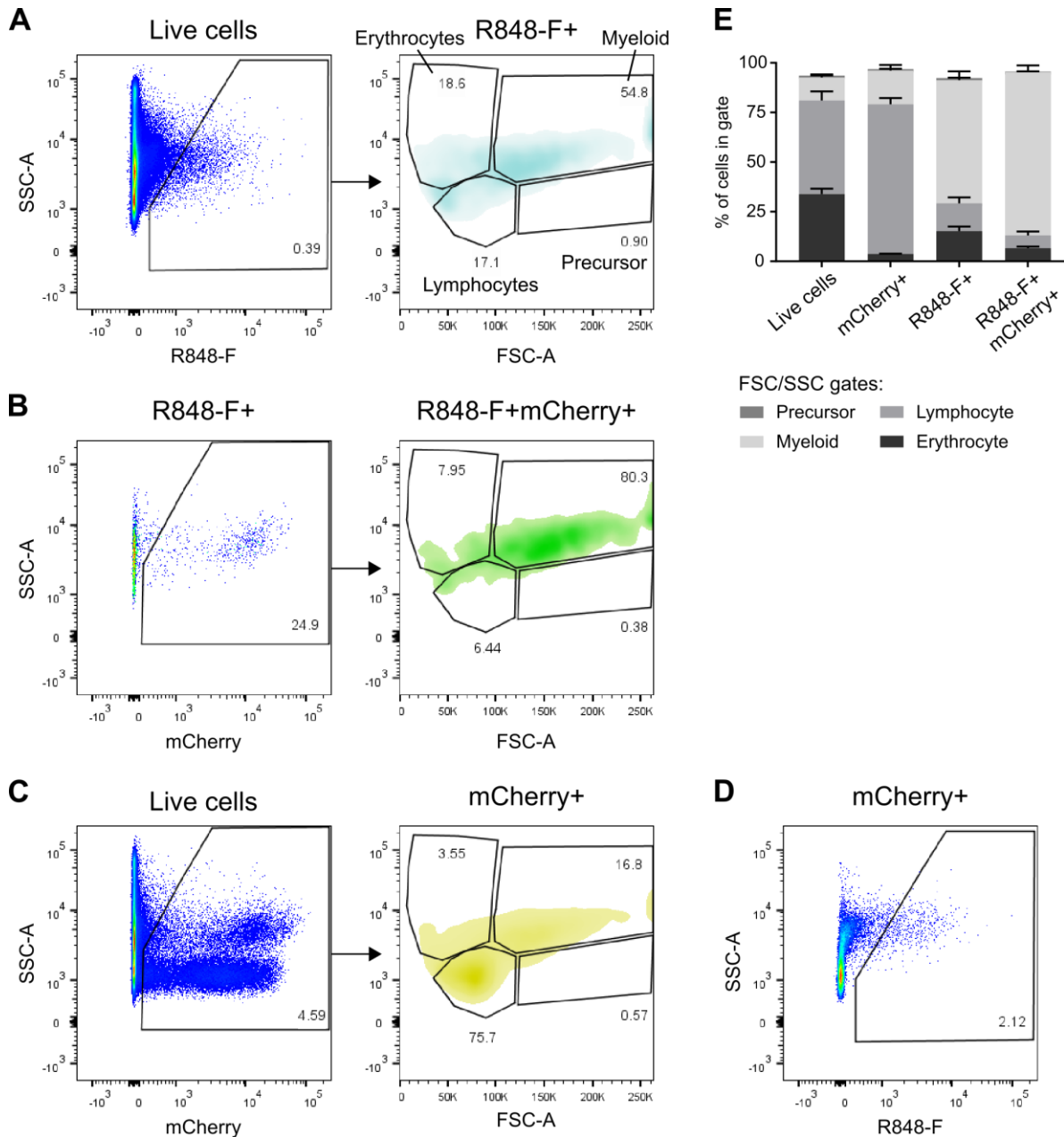
Figure 4.8 Flow cytometry of R848-F challenged gills of *Tg(cd4-1:mCherry)* fish.

R848-F (5µl at 0.15 mg/ml) was topically applied to the gills of *Tg(cd4-1:mCherry)* fish (n = 3), which were dissected 30 mpt. Gills were digested into single cell suspensions and analysed by flow cytometry. Fluorescent cells in *Tg(cd4-1:mCherry)* samples were identified by comparing to an unchallenged non-transgenic WT gill sample. A) Live cells (DAPI-) gated for R848-F+ cells (left). Density plot showing FSC/SSC profile of R848-F+ cells gated for different cell populations (right). B) R848-F+ cells gated for mCherry (left). Density plot showing FSC/SSC profile of R848-F+mCherry+ cells gated for different cell populations (right). C) Live cells (DAPI-) gated for mCherry+ cells (left). Density plot showing FSC/SSC profile of mCherry+ cells gated for different cell populations (right). D) mCherry+ cells gated for R848-F+ cells. (A-D) Numbers in or directly next to gates indicates the percentage of cells within that gate. Representative plots shown. E) Mean proportion of cells in the four FSC/SSC gates as a percentage of total cells for each fluorescent population. Error bars represent SEM.

4.3.2 Effect of antibiotics on the immune responses to R848

In order to test the effect of antibiotics on immune responses in zebrafish gills, adult fish were treated with oxytetracycline (OTC) then challenged with R848. OTC is a broad-spectrum antibiotic which inhibits bacterial growth by interfering with the 30S ribosomal subunit (Zhang, Cheng, and Xin 2015). It is approved for use in human and veterinary medicine and is widely used in aquaculture (Joint Formulary Committee, 2020; Rigos and Troisi, 2005). In rainbow trout and gilt-head bream gills, OTC has been reported to induce histopathological effects, however no inflammatory markers were investigated in those studies (Rodrigues et al., 2017, 2019).

In this project, adult zebrafish were immersed in 50 mg/L of OTC (or water only) for 10 days, with fresh medium replaced every day. This dose was previously used in rainbow trout and found to induce pathological changes in the gills (Rodrigues et al., 2017). Therefore, it was hypothesised that this dose of OTC would induce inflammation in zebrafish gills. The fish were treated for 10 days to reflect acute antibiotic treatments in fish aquaculture (Zhou et al., 2018). Following the 10-day treatment, R848 (or water) was topically applied to the gills and tissues were harvested 1 or 8 hpt for RNA analysis.

This work was performed with Katie Tsoi (Imperial College London) as part of her Master's thesis (Tsoi, 2019). I worked with Katie to support experimental design and execution and she performed some of the animal maintenance (in accordance with ASPA guidelines) and tissue harvesting, and all the qRT-PCR experimental procedures. Data analysis in this PhD thesis was performed by me.

4.3.2.1 *Transcript levels of immune mediators following OTC and R848 treatment*

As previously described, R848 induces upregulation of pro-inflammatory and interferon genes in the gills and WKM in a time-specific manner (Figure 4.1 and Figure 4.2). Therefore, transcript levels for *il1b*, *tnfa*, *cxcl18b*, *infphi1* and *ifng1* were measured in these tissues to assess whether the kinetics or magnitude of the immune response was altered in OTC-treated fish.

Exposure to OTC alone (water-challenged fish) had little effect on transcript levels in the gills except for a very small but statistically significant increase in *ifnphi1* and an increase in *ifng1* at 1 hpt (Figure 4.9A-J). However, both OTC-treated and control fish exhibited

increased transcript levels at 1 hpt for several genes following R848 challenge (Figure 4.9A-E). OTC treatment did not increase this response and did not affect the pattern of the response, with *il1b* and *tnfa* still being the most strongly upregulated of the five genes at this timepoint.

At 8 hpt, *il1b* and *tnfa* levels were similar between R848 and water-challenged gills in the control group (Figure 4.9F and G). However, OTC-treated fish had more variable *il1b* and *tnfa* levels following R848 challenge, with some samples noticeably higher than water-challenged or R848-control samples. OTC may have impaired resolution of the early immune response in some fish however, overall it did not seem to induce persistent inflammation.

Cxcl18b, *ifnphi1* and *ifng12* were upregulated at 8 hpt following R848 challenge in both OTC-treated and control groups (Figure 4.9H-J). Increases in these transcripts were similar between the control and OTC-treated groups. This indicates that OTC did not alter the progression of the late immune response in the gills.

Gills - 1 hpt
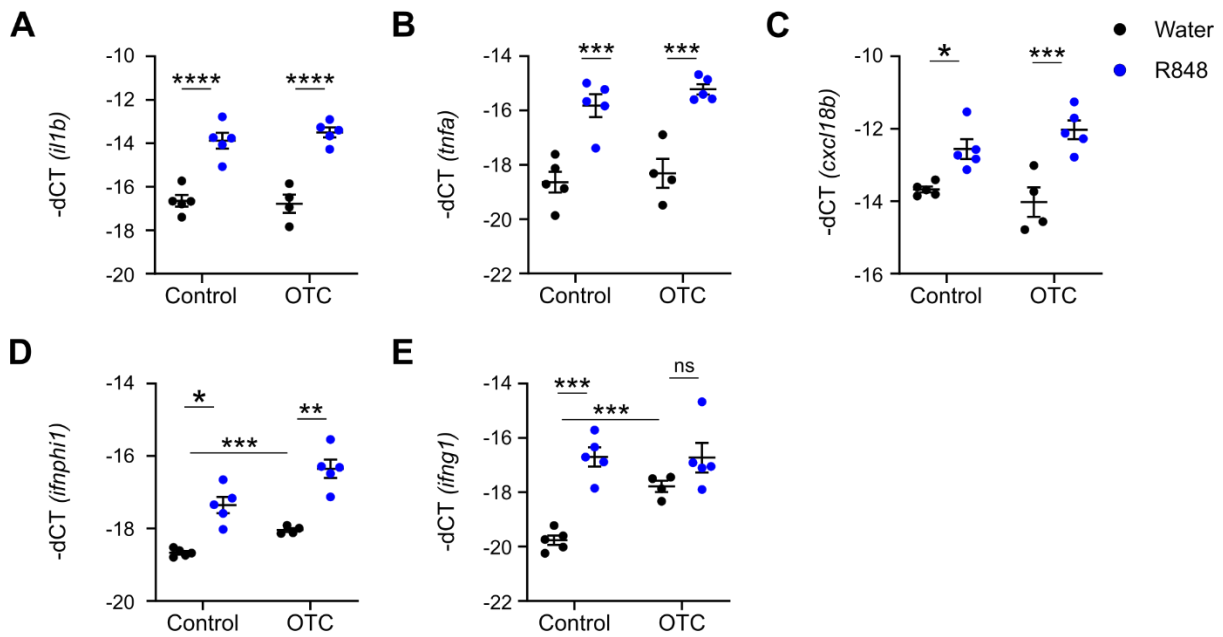
Gills - 8 hpt
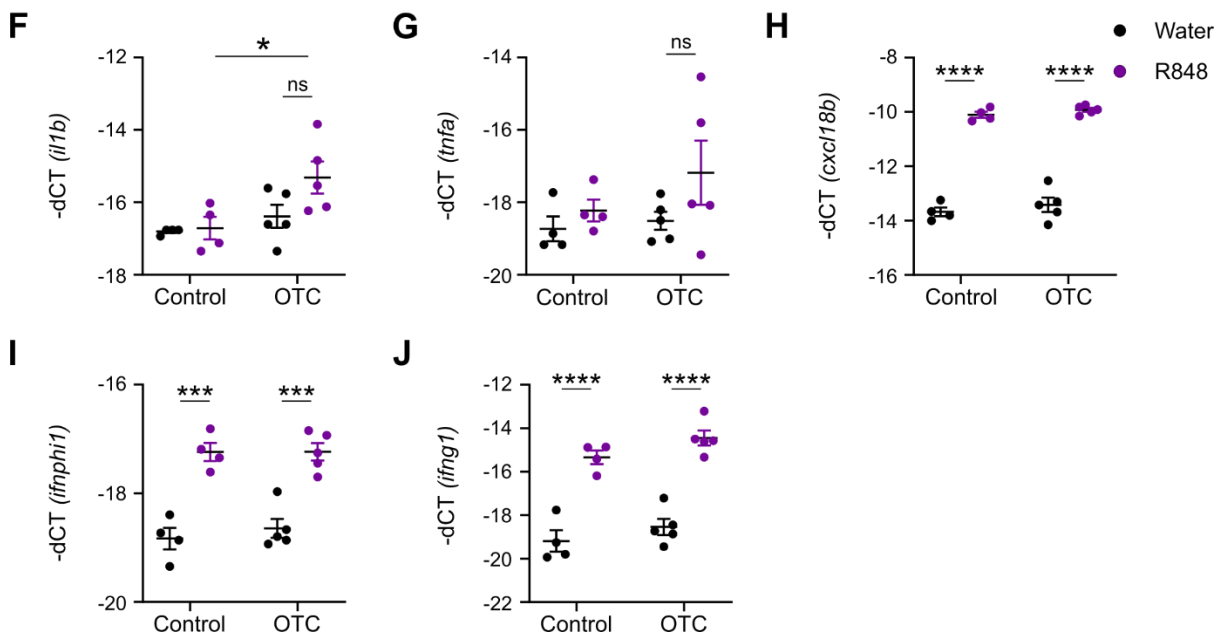
Figure 4.9 Transcript levels of cytokines, chemokines, and interferons in the gills following R848 challenge of OTC-treated fish.

WT fish were immersed in 50 mg/ml of OTC or system water (control) for 10 days followed by topical gill challenge with R848 (5 μl at 0.5 mg/ml) or endotoxin-free water. Transcripts were measured by qRT-PCR and are shown relative to 18S transcript levels. N = 4-5 from one experiment. Two-way ANOVA or Welch's ANOVA (for datasets with unequal variances) was performed followed by Tukey's or Sidak's multiple comparison test. ns: p > 0.05 (not significant), *: p ≤ 0.05, **: p ≤ 0.01, ***: p ≤ 0.001, ****: p ≤ 0.0001. qRT-PCR and some sample processing was performed by Katie Tsoi (Imperial College London) as part of her Master's thesis (Tsoi, 2019). *Il1b* (A), *tnfa* (B), *cxcl18b* (C), *infphi1* (D), *ifng1* (E) transcript levels in the gills at 1 hpt. *Il1b* (F), *tnfa* (G), *cxcl18b* (H), *infphi1* (I), *ifng1* (J) transcript levels in the gills at 8 hpt.

202

Within the WKM, OTC alone did not increase transcript levels at any timepoint showing that this antibiotic did not induce systemic inflammation in the fish (Figure 4.10A-J). All five genes were upregulated at 1 hpt following R848 challenge for both control and OTC-treated groups (Figure 4.10A-E). No significant differences in the upregulation of *il1b* or *cxcl18b* were observed between control and OTC-treated groups. The upregulation of *ifng1* appeared to be slightly greater in the OTC group however, due to undetectable transcripts in this dataset, quantitative statistical analysis could not be reliably performed. As in the gills, *il1b* and *tnfa* were the most strongly upregulated genes in response to R848 at this timepoint. These data indicate that OTC has no significant impact on the early systemic response to R848.

At 8 hpt in the WKM, *il1b* and *tnfa* were not significantly different between water and R848-challenged fish, although some groups exhibited large variation (Figure 4.10F and G). No differences were observed between control and OTC-treated groups indicating that the antibiotic did not alter resolution of the early immune response in this tissue.

Cxcl18b, *ifnphi1* and *ifng1* were elevated in the WKM of R848-treated fish at 8 hpt, in both control and OTC-treated groups. Similar upregulation was observed in both groups confirming that OTC did not have an inflammatory or inhibitory effect on this particular immune response.

Although inflammatory and immunosuppressive effects of OTC have been described in fish, in this setup, acute treatment of OTC alone did not induce major changes in the gill mucosa or in the WKM. Furthermore, OTC did not greatly alter the kinetics of the response to R848.

WKM - 1 hpt
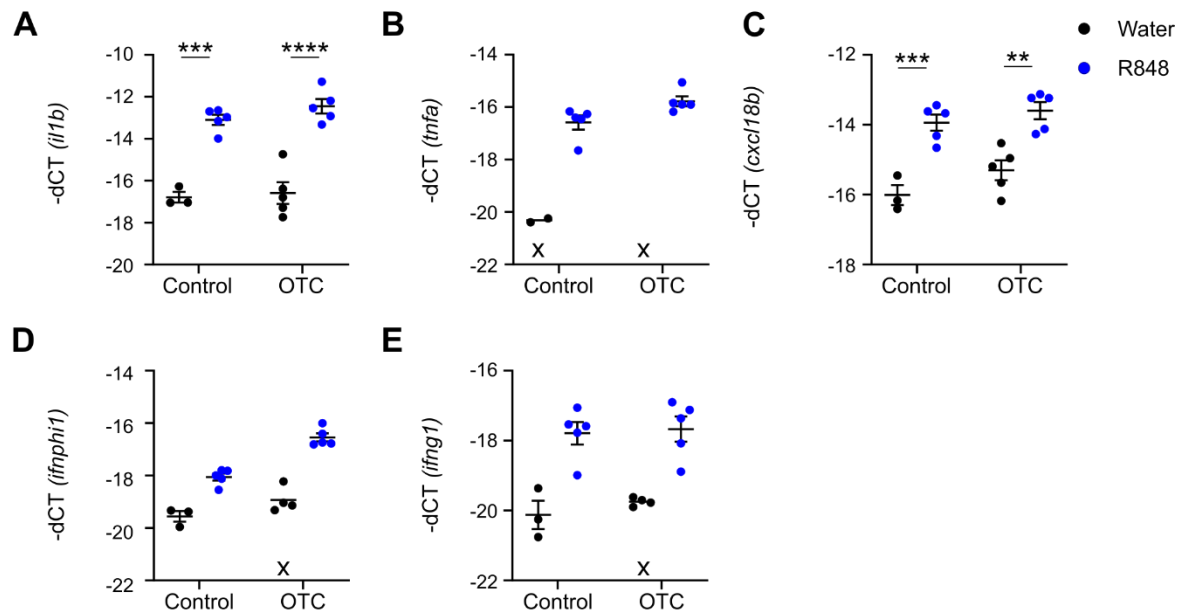
WKM - 8 hpt
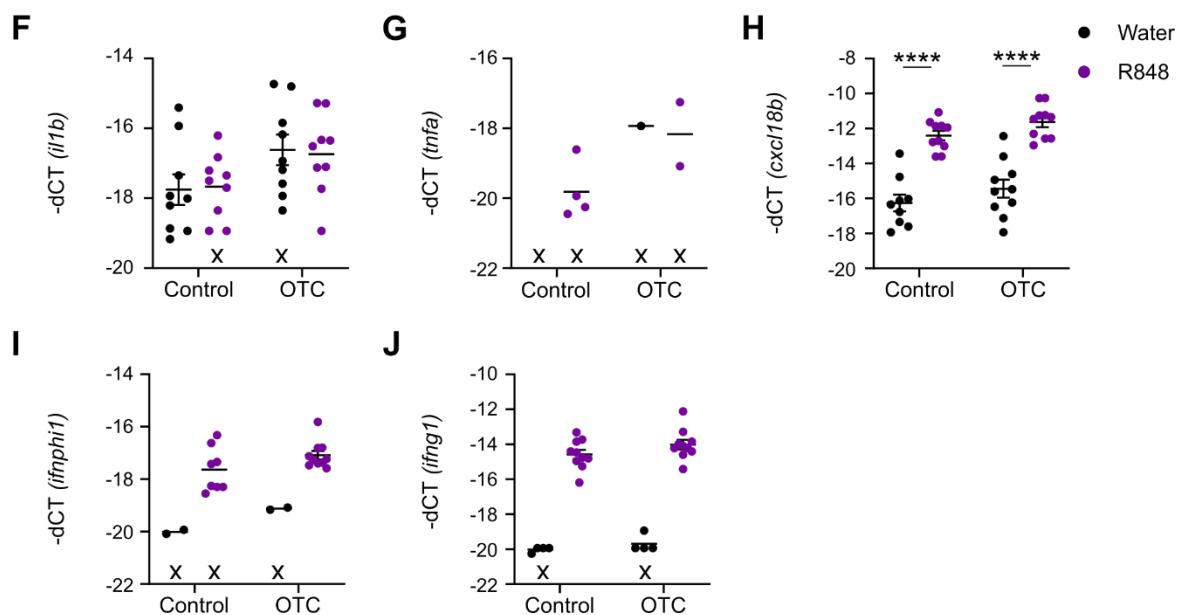
Figure 4.10 Transcript levels of cytokines, chemokines, and interferons in the WKM following R848 challenge of OTC-treated fish.

WT fish were immersed in 50 mg/ml of OTC or system water (control) for 10 days followed by topical gill challenge with R848 (5 μl at 0.5 mg/ml) or endotoxin-free water. Transcripts were measured by qRT-PCR and are shown relative to 18S transcript levels. Mean and SEM shown. X on the chart indicates ≥ 1 sample in the group had undetected transcripts (SEM not calculated), and therefore statistical testing was not performed for these groups. qRT-PCR and some sample processing were performed by Katie Tsoi (Imperial College London) as part of her Master's thesis (Tsoi, 2019). *Il1b* (A), *tnfa* (B), *cxcl18b* (C), *infphi1* (D), *ifng1* (E) transcript levels in the WKM at 1 hpt. N = 4-5 from one experiment. *Il1b* (F), *tnfa* (G), *cxcl18b* (H), *infphi1* (I), *ifng1* (J) transcript levels in the WKM at 8 hpt. N = 8-10 pooled from two independent experiments. Two-way ANOVA or Welch's ANOVA (for datasets with unequal variances) was performed followed by Tukey's or Sidak's multiple comparison test. **: $p \leq 0.01$, ***: $p \leq 0.001$, ****: $p \leq 0.0001$.

4.3.2.2   Transcript levels of immune cell genes following OTC and R848 treatment

In order to assess changes in immune cell presence or activity, transcript levels of cell marker genes were also measured. These included *lyz* and *mpx* (expressed in neutrophils), *mpeg1.1* (expressed highly in macrophages and at a lower level in B cells), and *lck* (expressed in T and NK-like lymphocytes) (Ferrero et al., 2020; Tang et al., 2017). Transcript levels were assessed at 8 hpt as it was anticipated that cellular changes would be more pronounced than at 1 hpt (Figure 4.11).

Lyz levels in the gills were unchanged by OTC alone and slightly but not statistically significantly decreased following R848 challenge (Figure 4.11A). *mpx* and *mpeg1.1* levels appeared to be unchanged between all groups (Figure 4.11B and C). *Lck* levels were unchanged by R848 or OTC alone but slightly increased by R848 in the OTC-treated group (Figure 4.11D). However, due to some undetected transcripts in this dataset, this difference was not statistically tested.

Cell marker transcript levels were mostly unchanged in the WKM (Figure 4.11E-H), except for *mpx* and *mpeg1.1* which were upregulated following R848-challenge in the OTC-treated groups (Figure 4.11G). This suggests that OTC may have a small effect on immune cells in non-mucosal tissue.

Overall, these results indicate that R848 or OTC alone do not induce broad effects on immune cell presence in the gills or in the WKM. This was similar for OTC and R848 in combination except for some increases in *mpx* and *mpeg1.1* transcripts. This suggests that OTC may affect myeloid and macrophage/B cell populations in the context of systemic inflammation, and more specifically during the response to R848.

Gills - 8 hpt

WKM - 8 hpt
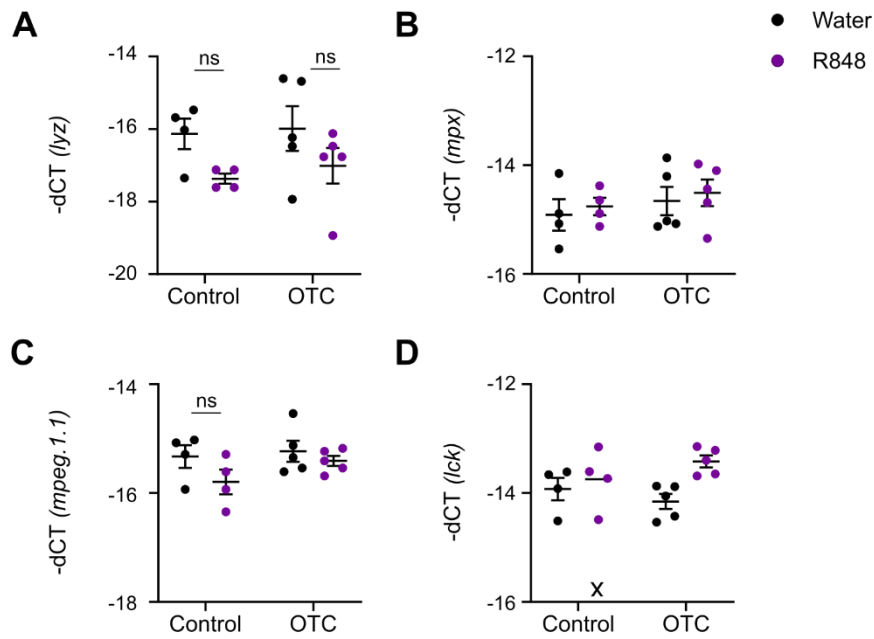
Figure 4.11 Transcript levels of leukocyte-associated genes in the gills and WKM following R848 challenge of OTC-treated fish.

WT fish were immersed in 50 mg/ml of OTC or system water (control) for 10 days followed by topical gill challenge with R848 (5 μl at 0.5 mg/ml) or endotoxin-free water. Transcripts were measured by qRT-PCR and are shown relative to 18S transcript levels. Mean and SEM shown. X on the chart indicates ≥ 1 sample in the group had undetected transcripts (SEM not calculated), and therefore statistical testing was not performed for these groups. qRT-PCR and some sample processing were performed by Katie Tsoi (Imperial College London) as part of her Master's thesis (Tsoi, 2019). *Lyz* (A), *mpx* (B), *mpeg1.1* (C), and *lck* (D) transcript levels in the gills at 8 hpt. N = 4-5 from one experiment. *Lyz* (A), *mpx* (B), *mpeg1.1* (C), and *lck* (D) transcript levels in the WKM at 8 hpt. N = 8-10 pooled from two independent experiments. Two-way ANOVA was performed followed by Tukey's multiple comparison test. ns: $p > 0.05$ (not significant), *: $p \leq 0.05$.

4.3.2.3 Effects of OTC and R848 on the zebrafish microbiota

Antibiotics are known to affect the microbiota, and OTC specifically has been shown to alter microbial composition in the gills or other tissues of several fish species, including zebrafish (López Nadal et al., 2018; Rosado et al., 2019; Zhou et al., 2018). To address whether OTC affected zebrafish microbiota, bacterial 16S rRNA was measured by qRT-PCR 8 hours following topical gill challenge (Figure 4.12).

OTC alone (water-challenged fish) reduced 16S levels in the gills but did not affect 16S levels in the WKM. 16S levels in the gut did not appear to be greatly affected, although lack of detection of in some samples limited reliable statistical testing. This data suggests that compared to the WKM, the gill microbiota is more susceptible to OTC, perhaps because it is more exposed to the antibiotic. In contrast, the gut, a microbial-rich environment also exposed to the environment, was not affected by OTC in the same way suggesting tissue-specific differences between mucosal surfaces.

Lower 16S levels were no longer observed following R848-challenge in the gills (Figure 4.12A). This may indicate some effect of R848 on the microbiota but it is important to note that 16S rRNA levels only provide an estimate of microbial presence or activity. More precise tools, such as bacterial culture or sequencing, would be needed to accurately measure changes in bacterial load and composition. Furthermore, R848 did not affect 16S levels in the WKM or gut further highlighting tissue-specific differences.
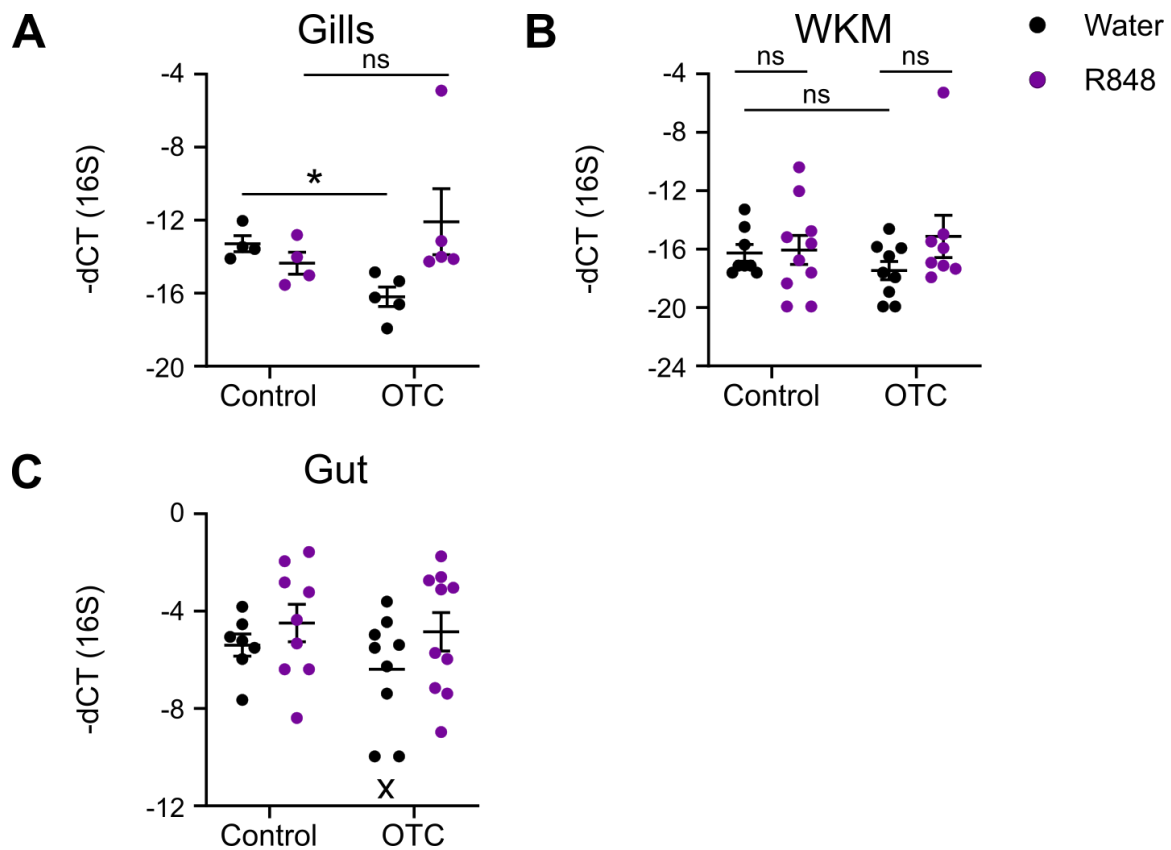
Figure 4.12 Transcript levels of bacterial 16S rRNA in the gills, WKM and gut following R848 challenge of OTC-treated fish.

WT fish were immersed in 50 mg/ml of OTC or system water (control) for 10 days followed by topical gill challenge with R848 (5 μl at 0.5 mg/ml) or endotoxin-free water. Transcripts were measured by qRT-PCR at 8 hpt. Mean and SEM shown. X on the chart indicates ≥ 1 sample in the group had undetected transcripts (SEM not calculated), and therefore statistical testing was not performed for these groups. qRT-PCR and some sample processing were performed by Katie Tsoi (Imperial College London) as part of her Master's thesis (Tsoi, 2019). (A) Transcript levels at 8 hpt in the gills, n = 4-5 from one experiment. Two Mann-Whitney tests performed on two separate groups. (B-C) Transcript levels at 8 hpt in the WKM (B) and distal gut (C), n = 8-10 pooled from two independent experiments. Two-way ANOVA was performed on (B) followed by Tukey's multiple comparison test. ns: $p > 0.05$ (not significant), *: $p ≤ 0.05$.

4.4 Summary

1. **Transcriptional response of the gills to different types of immunuostimulatory compounds.** R848 and LPS induced upregulation of inflammatory mediators in the gills. This was not observed for CpG-ODN or Pam3CSK4.

2. **Impact of the type of compound and route of administration on the immune response.** The immune response to R848 was observed following either topical application or i.p. injection however, the response to LPS only observed following injection. Furthermore, R848 induced an interferon response not observed with LPS challenge.

3. **Comparisons of immune responses in the gills to responses in other peripheral tissues.** For both R848 and LPS, responses in the gills were associated with a similar immune response in the WKM, both in terms of the genes upregulated and the kinetics of the response.

4. **Leukocytes involved in immune responses in the gills.** R848 induced increases in neutrophils and lymphocytes in the secondary lamellae of the gills. Inconsistencies in the lymphocyte response to R848 were observed between experiments which may be linked to differences in the presence of immune cells prior to challenge. R848 directly interacted primarily with myeloid-like cells, including *cd4-1:*mCherry+ myeloid cells.

5. **Effects of antibiotic treatment on immune responses in the gills.** OTC antibiotic treatment did not induce robust inflammation in the gills on its own and had little effect on the transcriptional response to R848 in both the gills and WKM.

4.5 Discussion

4.5.1 Immunostimulatory compounds induce specific pathways in zebrafish and may be selectively taken up through the gill mucosa

RNA analysis was used to compare the responses to different immunostimulants in the gills and WKM. Both R848 and LPS induced increased cytokine transcript levels following

i.p. injection but, only R848 induced IFN transcript levels. In humans and mice, LPS can induce type I IFN expression through the TLR4-TRIF pathway, but in zebrafish, recognition of LPS is not mediated by TLR4 orthologues (Sepulcre et al. 2009). Nevertheless, IFN transcription (Lepiller et al., 2009) and induction of IRF7 (Xiang et al., 2010), a transcription factor upstream of IFN, has been reported following LPS challenge in zebrafish. This suggests that some components downstream of TLR4 may be conserved between zebrafish and humans. The lack of change in IFN transcripts in this study suggests that LPS-induced cytokine production is independent of IFN production, and that the IFN signaling pathway was not stimulated in the gills or WKM. The difference in these findings to those of Lepiller et al. may be explained by the differences in the tissues analysed or the LPS used. The LPS used in this thesis was derived from *Pseudomonas aeruginosa* whilst the LPS used by Lepiller et al. was derived from *Salmonella typhimurium*. LPS molecules from different bacteria are known to have different toxicities in zebrafish larvae and therefore may activate different signalling pathways (Novoa et al. 2009).

The lack of response to CpG-ODN 2007 following i.p. injection was unexpected since this was previously reported to increase cytokine and IFN transcript levels in the kidney (Yeh et al., 2013). Furthermore, the dose used in this study was 2.5 times greater than that used by Yeh et al. However, the timing of the response was not reported in the study by Yeh et al, and it is possible that changes only occurred after 8 hours, the latest time point analysed in this PhD project. Pam3CSK4 similarly failed to induce an inflammatory response in the gills or WKM, adding to the evidence that this compound is not highly stimulatory in fish (Lin et al., 2020; MacKenzie et al., 2010; Ribeiro et al., 2010; Sepulcre et al., 2007). This is in contrast to the inflammation observed in Pam3CSK4-treated zebrafish embryos, which may indicate that younger stages are more sensitive to this compound (Yang et al., 2015). The lack of response to CpG-ODN 2007 and Pam3CSK4 in adult zebrafish is unlikely to be explained by lack of receptors since both *tlr2* and *tlr9* have been detected in the gills and kidney (Novoa et al. 2006; Liu et al. 2014; Chen et al. 2020).

Of the four compounds used, only R848 induced an inflammatory response through the topical gill route. Similar results were observed following bath immersion of adult zebrafish where poly(I:C) but not Pam3CSK4, CpG-ODN 2007 or LPS induced an

inflammatory response in the gills (Lin et al., 2020). These findings suggest that the gill mucosa acts as a selective barrier to exogenous compounds. Interestingly, poly(I:C) was not found to induce a response following topical application despite a more concentrated dose being used (Progatzky et al., 2019). This may be due to the gills only being exposed to poly(I:C) for 5 mins, compared to 12 h in immersion challenges. As observed in Japanese flounder, uptake of bacteria in the gills increased with longer periods of exposure (Du et al., 2017). The ability of compounds to penetrate mucus is governed by many factors including the size of the compound and the pore size of the mucus. In human mucus, including respiratory mucus, pore size has been measured in the range of tens of nanometres to several micrometres (Leal et al., 2017). Pore size in gill mucus has not been clearly reported but is likely to be in the same range of human mucus since fish produce similar mucin proteins (Van Der Marel et al., 2012). LPS, Pam3CSK4 and CpG-ODN 2007 are all estimated to be less than 50 nm therefore size exclusion in unlikely to explain their inability to induce a response in the gills (Arimura, 1975; Hamley et al., 2014; Strauss et al., 2009). Electrostatic forces can also influence adhesion of molecules to mucus. Mucus is negatively charged due to the presence of oligosaccharides and has been found to interact more strongly with cationic (positively charged) materials in gills (Kitiyodom et al., 2019). LPS and CpG-ODNs are negatively charged which suggests that they may adhere poorly to mucosal surfaces. This could explain their inability to induce a response in topical gill application. However, Pam3CSK4 is positively charged therefore other factors are likely to account for the lack of response to this compound. Studying the interactions between exogenous compounds and mucus will be important for designing effective mucosal vaccines, both in humans and in animals.

Topical gill application of R848 induced a local response in the gills as well as a systemic response observed in the WKM. In Japanese flounder immersed in inactivated *Edwardsiella tarda* bacteria, uptake peaked in the gills and skin at 30 mins but continued increasing in the kidney beyond this time (Gao et al., 2016). This suggested that in fish, internal organs obtain antigen from mucosal tissues. Nanoparticles administered to zebrafish by immersion were detected in the gill vasculature suggesting that internal organs are likely to obtain this antigen from the bloodstream (Rességuier et al., 2017). Alternatively, immune responses in the WKM could have been due to peripheral blood cells that were stimulated in the gill vasculature and subsequently migrated to the kidney. Similarly, gill-resident immune cells could have migrated to the kidney following local

stimulation in the gills. However, in mice, migration of DCs to the lymph nodes can take several hours to days (Itano et al., 2003; Kissenpfennig et al., 2005; Lukens et al., 2009b). If similar cellular dynamics occur in zebrafish, migrating gill cells would be unlikely to account for the early responses observed in the WKM of R848-challenged fish. The relative contributions of gill-resident and circulating cells could not be determined in this study, in part because attempts to exsanguinate the gills were unsuccessful (experiments performed by Katie Tsoi). However, future studies could use transgenic zebrafish expressing photoactivatable fluorescent proteins to label cells in the gills and monitor their movements (Nguyen-Chi et al., 2015; Yoo and Huttenlocher, 2011).

4.5.2 Myeloid cells and lymphocytes in the gills are responsive to R848

In addition to transcriptional changes in the gills, neutrophils and *lck*:GFP+ lymphocytes were increased in the secondary lamellae following R848 challenge. An increase in lymphocytes was not observed in a second set of experiments however this may have been inhibited by high levels of immune cells prior to challenge. The early increase in neutrophils is a common feature of many models of inflammation and has been measured in the skin of adult mice and lungs of neonatal mice challenged with R848 (Epaulard et al., 2014; Makris and Johansson, 2020). It is also a feature in the respiratory tract during infection with viruses such as influenza and RSV (Dakhama et al., 2005; Perrone et al., 2008). Macaque neutrophils produce IL-1β and TNF-α following R848 treatment (Epaulard et al., 2014) suggesting that these cells may contribute to the early increase in pro-inflammatory cytokines in the gills. Zebrafish neutrophils produce *ifnphi1* following chikungunya virus infection suggesting that they may also contribute to the IFN response in R848 challenges (Palha et al., 2013). The increase in lymphocytes in R848-challenged gills was greater at later timepoints, again reflecting the kinetics of RVIs (Dakhama et al., 2005; Tate et al., 2012). Human CD4+ T cells and NK cells both produce IFNγ upon R848 challenge and these cell types may be the source of this cytokine in the gills (Caron et al., 2005; Smith et al., 2019). *Rag1-/-* zebrafish, which lack T and B cells, still express increased levels of *ifng1* in response to R848 showing that T cells are not essential for this response (Muire et al., 2017). Due to the limitation of NK cell markers in zebrafish, it was not possible to determine the contributions of different lymphocytes to the gill IFN

response. Overall, these findings add to the limited literature on immune cell dynamics in the gills and provide potential links to cell function.

Cd4-1:mCherry+ myeloid-like cells were found to interact with R848-F which indicates that other immune cells are involved in the gill response to this compound. Furthermore, this finding complements the data on OVA uptake in the gills and previous data in the skin (Lin et al., 2019) showing that *cd4-1+* cells in mucosal tissues can interact with structurally different antigens. These cells may be responsible for initiating the response to R848. In humans, monocytes and DCs both express CD4 and respond directly to R848 (Hart et al., 2005; Jardine et al., 2013; Smith et al., 2019). In fact, monocytes were found to be responsible for stimulating NK cell-derived IFNγ in response to R848 (Hart et al., 2005). Although these cell subsets are poorly understood in zebrafish, it is possible that similar cell interactions exist in this species. However, unlike unlabelled R848, R848-F was not found to induce a transcriptional response in the gills (Fränze Progatzky, personal communication). Therefore, it is important to consider that R848 uptake and responses may occur through different pathways from R848-F. The lack of response could have been due to the lower dose of R848-F used, but prior experiments showed that an equivalent low dose (0.05 mg/ml) of unlabelled R848 still induced a response (Madina Wane, data not shown). Alternatively, the lack of response to R848-F could have been due to the conjugated fluorophore inhibiting receptor binding or downstream signalling. Further work is needed to understand whether R848 binds zebrafish TLR7/8 or other receptors as this is currently unknown.

4.5.3 Acute oxytetracycline treatment is not strongly inflammatory in zebrafish

Administration of OTC for 10 days did not induce inflammation or reduce inflammatory markers in adult zebrafish. This lack of inflammation suggests that significant pathology in the gills or kidney was not present in these fish. However, histological analyses would be needed to assess this. In rainbow trout, bath immersion with OTC resulted in gill pathology within 96 h however, after 28 days this pathology was no longer observed (Rodrigues et al., 2017). It is possible that inflammation developed in earlier timepoints in zebrafish but had resolved by 10 days post treatment. OTC exposure in zebrafish larvae induced increased cytokine transcript levels and neutrophil migration within 72 h

supporting early initiation of inflammation (Barros-Becker et al., 2012). Smoke exposure in adult zebrafish similarly induced increased cytokine transcript levels within 6 hours which had resolved by 6 weeks despite continued smoke exposure (Progatzky et al., 2015). OTC may have slightly delayed resolution to R848-induced inflammation in the gills of some fish, but to a much lesser extent than in *il10-/-* or *il4/13ab-/-* mutants (Bottiglione et al., 2020). Collectively, this shows that OTC does not have a strongly inflammatory effect in adult gills. It appears that zebrafish gills are resistant to various insults previously shown to have immunomodulatory effects in other models. Future investigations could use mutants such as those generated by Bottiglione et al. to assess whether this is due to immunoregulatory mechanisms in the gills.

There were a few cases of increased immune gene transcripts observed in OTC-treated fish in this study. This could have resulted from impaired induction of anti-inflammatory cytokines. In Nile tilapia, OTC treatment reduced *il10* transcript levels in the liver and intestine whilst in zebrafish larvae, *il10* transcript levels were unchanged despite increased expression of pro-inflammatory cytokines (Barros-Becker et al., 2012; Limbu et al., 2018). It is also possible that OTC increased expression of the receptors that recognise R848 or other signalling proteins involved in the response pathways. In mice treated with a combination of antibiotics, several TLR genes were upregulated in the gut (Grasa et al., 2015). In zebrafish, transcript levels of immune cell markers were mostly unchanged by combined OTC-R848 treatment except for *mpx* and *mpeg1.1* in the WKM. This suggests that immune cell presence was largely unchanged in the gills. However, the activation level of immune cells was not investigated and may have differed between conditions. Furthermore, gene expression does not always correlate with cell abundance since some markers, like *mpeg1.1*, are known to be affected during inflammatory conditions (Walton et al., 2015). Overall, there are many remaining gaps in our understanding of the immunomodulatory mechanisms of antibiotics. Further focus on this would help us understand why individual antibiotics have anti-inflammatory effects in some contexts and pro-inflammatory effects in others.

One area that has received more attention is the effect of antibiotics on the microbiota and the resulting consequences on immune responses. In this project, bacterial load and activity was estimated by measuring 16S rRNA levels which were lower in OTC-treated gills. Studies in seabass found that development of disease and subsequent OTC

treatment induced changes in gill microbiome composition as measured by 16S rRNA gene sequencing (Rosado et al., 2019). However, it is not known if bacterial composition was altered as this was not measured. OTC treatment in zebrafish may have similarly induced microbial dysbiosis in the gills in addition to reducing bacteria load. Although 16S levels were unchanged by OTC in the kidney and gut, microbiome composition could have been altered in these tissues, without affecting bacterial load. In another study, 6-week OTC treatment in zebrafish reduced microbial richness in the gut (Zhou et al., 2018). This was associated with higher *tnfa* transcript levels and greater mortality following *Aeromonas hydrophila* infection. This suggests that enhanced inflammatory responses by OTC could be detrimental in some infections.

Although OTC reduced 16S transcript levels in the gills this was no longer observed following R848 challenge. In the gut and kidney tissue 16S levels were more variable than control groups. It is unlikely that R848 induced significant changes in bacterial load within 8 h, but it may have altered bacterial metabolic activity. In ampicillin-treated mice, R848 was found to affect bacterial populations through its immunomodulatory effects (Abt et al., 2016). Ampicillin-treated mice are normally susceptible to intestinal colonisation by vancomycin-resistant *Enterococcus faecium* bacteria however, R848 made mice more resistant to colonisation. This was associated with greater production of Reg3γ, an antimicrobial protein, and was dependent on IL-22. This change in bacterial growth could have been associated with changes in metabolic activity. The data from zebrafish supports the idea that TLR agonists, specifically R848, can alter microbial populations. However, although 16S transcripts indicate the presence of metabolically active bacteria, they do not always correlate well with bacterial growth rate or level of activity. Furthermore, 16S transcripts can vary considerably between taxa, which as previously mentioned may be altered by antibiotic treatment (Blazewicz et al., 2013). Therefore, additional methods such as metabolomics and 16S rRNA gene sequencing should be considered to gain further insight into microbiota activity and composition in future studies.

5 Chapter 5 – Assessing the ability of viruses to infect zebrafish gills

5.1 Introduction

5.1.1 Current zebrafish models of viral infection

Zebrafish are susceptible to different types of DNA and RNA viruses from fish, human and other vertebrate hosts. Infection cases vary from fish with no obvious pathology, those with pathology that eventually recover, and those with major and fatal pathology. Several models of experimental viral infections in zebrafish have been developed, particularly in the last 15 years (Table 5.1). Natural virus infection in zebrafish have also been recently reported although there are few examples of this (Altan et al., 2019; Balla et al., 2020; Bermúdez et al., 2018).

Studies on experimental infections in zebrafish can include descriptions of the viral load, immune response, disease pathology, and mortality in infected fish. Viruses are usually detected by RNA or DNA analysis, cell culture, use of fluorescent viruses, electron microscopy or immunohistochemistry. Only a few studies have investigated viral transmission but these have revealed that both horizontal and vertical transmission are possible in zebrafish (Balla et al., 2020; Seeley et al., 1977). Some viruses, most notably SVCV, have been frequently used to investigate different aspects of antiviral responses in zebrafish.

Host	Virus	Developmental stage infected	Reference
Human	IAV	Embryonic – larval	(Gabor et al., 2014; Sullivan et al., 2017)
	Herpes simplex virus-1 (HSV-1)	Adult	(Burgos et al., 2008)
	Hepatitis C virus (HCV) sub-replicon	Larval	(Ding et al., 2011)
	Chikungunya virus (CHIKV)	Larval	(Palha et al., 2013)
	Human norovirus (HuNoV) GI and GII	Larval	(Van Dycke et al., 2019)

Mammals, insects	Vesicular Somatitis Virus (VSV)	Larval	(Guerra-Varela et al., 2018)
Fish	Viral haemorrhagic septicaemia virus (VHSV)	Adult	(Novoa et al., 2006)
	Snakehead rhabdovirus (SHRV)	Larval-juvenile Adult	(Phelan et al., 2005)
	Spring viremia of carp virus (SVCV)	Larval	(López-Muñoz et al., 2010; Pereiro et al., 2017)
		Adult	(López-Muñoz et al., 2009; Sanders et al., 2003)
	Infectious Hematopoietic Necrosis Virus (IHNV)	Adult Embryonic	(Lapatra et al., 2000) (Aggad et al., 2009)
	Infectious spleen and kidney necrosis virus (ISKNV)	Adult	(Xu et al., 2008)
	Infectious pancreatic necrosis virus (IPNV)	Adult	(Lapatra et al., 2000; Seeley et al., 1977)
	Tilapia lake virus (TiLV)	Adult	(Rakus et al., 2020)
	Nervous necrosis virus (NNV)	Adult	(Lu et al., 2008)
		Larval	(Morick et al., 2015)
	European sheatfish virus (ESV)	Adult Larval	(Martín et al., 2015)
	Sindbis virus (SINV)	Larval	(Boucontet et al., 2018; Passoni et al., 2017)
	Chum salmon reovirus (CSV)	Adult Larval	(Rakus et al., 2019)
	Cyprinid herpesvirus 3 (CyHV-3)	Adult	(Rakus et al., 2019)
	Grass carp reovirus (GCRV)	Adult	(Zhu et al., 2020)

Table 5.1 Viruses used in experimental infections of zebrafish.

5.1.1.1 Key features of the zebrafish immune response

The interferon response

Type I IFNs, type II IFNs and ISGs can all be induced by a range of viruses in zebrafish adults, larvae and embryos (Aggad et al., 2009; Gabor et al., 2014; López-Muñoz et al., 2009, 2010; Palha et al., 2013). This upregulation is consistently observed at 24-48 hours post infection (hpi) but has also been observed several hours earlier and later. Different IFN genes can also show differences in kinetics as exemplified with *ifnphi1* which is induced later than *ifnphi2* in SVCV-infected larvae (Varela et al., 2014). Using recombinant zebrafish IFN proteins or overexpression of IFN genes, studies have revealed that both type I and type II IFNs stimulate ISGs and proinflammatory genes *in vivo* (Aggad et al., 2009; López-Muñoz et al., 2009, 2011). In adult zebrafish, recombinant IFNφ1, IFNφ2, and IFNφ3 (type I) induced ISGs and proinflammatory genes much more strongly than recombinant (type II) IFNγ1 (López-Muñoz et al., 2009). Furthermore, only type I IFNs protected the zebrafish from SVCV infection, whereas IFNγ1 did not improve mortality indicating different roles for these IFNs. Similar results have been found in IHNV-infected embryos (Aggad et al., 2009). Overexpression of *ifng1* has also been found to increase mortality in SVCV-infected larvae further supporting the detrimental effect of this IFN in viral infections (López-Muñoz et al., 2011). However, these studies did not investigate the absence of IFNγ so it is possible that this IFN supports antiviral responses at certain levels.

The inflammatory response

Similarly to IFNs, proinflammatory cytokines are consistently upregulated in response to viral infection in zebrafish. These include *il1b*, *tnfa*, *il6* and *il8* although the specific genes vary with the virus used and experimental design (Boucontet et al., 2018; Rakus et al., 2020; Varela et al., 2014). In SVCV-infected larvae, *il1b* was rapidly upregulated showing two distinct peaks whereas *il6* was upregulated later showing temporal differences between genes (Varela et al., 2014). Again, these kinetics vary between experiments but proinflammatory genes are generally upregulated for several days after infection (Boucontet et al., 2018; Rakus et al., 2020). The inflammatory responses in infected zebrafish are not always enough to protect against disease. This was observed in SVCV-infected larvae which showed high mortality despite induction of proinflammatory genes (López-Muñoz et al., 2010). Overexpression of *ifnphi1, 2* or *3* improved survival in these

fish and this was associated with higher IFN and ISG but also *il1b* transcript levels. In SVCV-infected adult zebrafish, recombinant Tnfa impaired survival and increased transcripts of *il8* and the chemokine *ccl4*. This shows that excessive inflammation can also be detrimental in viral infections.

As expected in the inflammatory environment of viral infections, increases and involvement of immune cells has also been reported. In CHIKV-infected larvae, neutrophils were increased from 48 hpi and contributed to *ifnphi1* expression (Palha et al., 2013). Depletion of neutrophils using a *csf3r* morpholino increased mortality and disease severity indicating the importance of these cells in antiviral immunity. In SVCV-infected larvae, virus-infected macrophages showed significantly lower ll-1β production than uninfected macrophages suggesting this cytokine may contribute to viral resistance (Varela et al., 2014). Some ll-1β+ macrophages also underwent cell death suggesting that this process contributes to inflammation.

5.1.1.2 Involvement of the gills during viral infection

So far at least two viruses used in experimental challenges (ISKNV and TiLV), and one zebrafish picornavirus (ZfPV) identified in natural infections have been detected in zebrafish gills by immunohistochemistry or RNA analysis (Balla et al., 2020; Rakus et al., 2020; Xu et al., 2008). Gill pathology has also been reported during SVCV, IAV and HSV-1 infection, but not during VHSV infection (Burgos et al., 2008; Gabor et al., 2014; Kavaliauskis et al., 2016; Sanders et al., 2003). Responses to SVCV infection have included melanomacrophage proliferation and increased transcript levels of Fin tripartite motif genes in the gills (Liu et al., 2019b; Sanders et al., 2003). However, the functions of these changes have not been investigated. IFNφ1 has also been shown to induce transgenic *isg15*:GFP expression in larval gills although this was not in an infection setting (Balla et al., 2020). No further reports on zebrafish gill antiviral responses have been identified. Furthermore, none of the current reports link gill pathology with viral presence or the response to infection highlighting a major gap in our understanding of zebrafish gill immunity.

5.1.1.3 Models using human viruses

Studies using human viruses have reported similar tissues tropisms or pathologies between humans and zebrafish. IAV infection in embryos/larvae led to gill pathology and viral presence in the swimbladder, two tissues that have been used to mimic respiratory

responses (Gabor et al., 2014). IAV also induced muscle damage which is consistent with the muscle weakness reported in human IAV infections (Goody et al., 2017). CHIKV was shown to infect a wide range of zebrafish cells including endothelial cells, fibroblasts, and muscle fibers, all targets in human CHIKV infection (Palha et al., 2013). In addition, virus was found in the zebrafish brain which is consistent with the neuropathologies associated with human CHIKV disease (Mehta et al., 2018). Similarly HSV-1, which has been confirmed to infect the brain in humans, also infected the brains in zebrafish (Burgos et al., 2008). NoV, an enteric human pathogen, was strongly detected in the zebrafish larval gut (Van Dycke et al., 2019). These studies highlight the potential of zebrafish viral models to reflect human tropisms. However, it is important to note that the route of administration in zebrafish does not always reflect that natural route of infection in humans and may lead to differences in disease progression and immune response.

Like fish viruses, human viruses also induce IFN responses in zebrafish. By comparing microarray data of CHIKV-infected larvae and HCV-infected human liver cells treated with IFNα, one study showed that zebrafish and human samples upregulated some of the same ISGs (Langevin et al., 2013a). Another study reported that the IFN/ISG response in NoV-infected zebrafish involved some of the same genes as mouse and cattle NoV models (Van Dycke et al., 2019). IAV infection also upregulated *ifnphi1* and *mxa* (an ISG) transcripts in zebrafish (Gabor et al., 2014). However, it is unclear if mortality in zebrafish is associated with excessive inflammation as observed in severe IAV infection in humans.

Several studies have used well-established antiviral drugs in infected zebrafish. Zanamivir, a neuraminidase inhibitor, improved pathology and survival in IAV-infected larvae however its effect on viral load was not reported (Gabor et al., 2014). Acyclovir, a drug used to treat herpes infections, did not improve survival in HSV-1-infected zebrafish but it did reduce viral load (Burgos et al., 2008). 2'-C-methylcytidine, a viral polymerase inhibitor, also reduced viral load in NoV-infected zebrafish (Van Dycke et al., 2019). These studies show that zebrafish are responsive to human antivirals and therefore may be useful as models for drug screens.

5.1.1.4 *Considerations for developing new zebrafish models*

When developing a new viral infection model several factors must be considered: the biology of the host and whether this is compatible with the biology of the virus, and the practical requirements of working with the chosen model. Some of these factors were

addressed in the literature review (Chapter 1). The temperature of the host is important as most viruses will only replicate within a certain temperature range. Several studies have maintained zebrafish at cooler or warmer temperatures to promote viral infection. Zebrafish can tolerate a large range of temperatures (López-Olmeda and Sánchez-Vázquez, 2011; Spence et al., 2007), however, changes in environmental temperature are known to affect the zebrafish immune system. For example, *il1b*, *tnfa* and *il6* were upregulated in the liver of zebrafish maintained at 34°C for 4 days (Zheng et al., 2017). Similarly, infection with VHSV at 25°C reduced viral load compared to infection at 15°C (Cho et al., 2019). This was associated with an altered proteomic profile indicating increased immune response and lymphocyte production. This is supported by a study showing that adult zebrafish had greater preference for warmer conditions when stimulated with poly(I:C), a phenomenon known as a 'behavioural fever' (Boltana et al., 2013). This was associated with higher transcript levels of several antiviral genes. In addition, increased temperature reduced the frequency of clinical symptoms following SVCV infection. Increased temperature has also been found to alter gill physiology in other fish species (Sollid et al., 2005; Vargas-Chacoff et al., 2018).

As zebrafish develop, their immune response to viral infection also changes. Adult zebrafish have been reported to express higher levels of IFNs and ISGs both at baseline levels and in response to viral infection (Aggad et al., 2010; Lu et al., 2008). During NNV infection, this was associated with a lack of in mortality and much lower viral load in adults (Lu et al., 2008). In other fish species, juvenile fish are often more susceptible to viral infection than older stages (Office International des Épizooties, 2003).

For this project, two human viruses, RSV and IAV, were used to assess the effect of respiratory viruses relevant to human health. RSV has not been reported to infect fish species but IAV has recently been used in zebrafish (Gabor et al., 2014; Goody et al., 2017). IPNV, a fish virus, was also chosen to assess viral infection with an aquatic pathogen.

5.1.2 Respiratory syncytial virus

5.1.2.1 *Virus structure, tropism and life cycle*

Human RSV is an enveloped, negative sense ssRNA virus with an unsegmented genome. Its genome encodes 10 genes which produce 11 proteins due to 2 overlapping open

reading frames in the M gene. RSV infects the respiratory tract and is rarely found outside of this system (Collins et al., 2013). More specifically, RSV infects ciliated epithelial cells *in vivo* in addition to type I and type II alveolar epithelial cells in the lower airways. Basal epithelial cells do not appear susceptible showing that the RSV does not infect epithelial cells indiscriminately (Johnson et al., 2007a).

Several host receptors have been suggested to mediate virus entry although the exact process is still unclear. These receptors include CX3 chemokine receptor 1, nucleolin, heparan sulfate proteoglycans, TLR4, intercellular adhesion molecule 1, epidermal growth factor receptor, annexin II and calcium-dependent lectins (Griffiths et al., 2017). Some of these receptors have been identified from *in vitro* experiments and it is not clear if they reflect the *in vivo* situation. For example, studies showing that nucleolin interacts with RSV have been primarily performed *in vitro* (Griffiths et al., 2020; Tayyari et al., 2011). Furthermore, nucleolin is primarily localized in the nucleus and it is not known if it is expressed on the cell surface of human respiratory epithelium.

Following viral entry, the RSV genome is transcribed and replicated in the cytoplasm by the viral-encoded RNA-dependent RNA polymerase. The negative sense RNA must be transcribed into positive sense mRNA prior to translation (Griffiths et al., 2017). The full genome is produced through a complementary anti-genome intermediary which is subsequently used as template for genome replication (Noton et al., 2019). This genome is then assembled into new particles continuing the infection cycle.

5.1.2.2 *Notable features of RSV disease and immune responses*

Like most respiratory viruses in humans, RSV mainly causes upper respiratory infection, although this can progress to more severe lower respiratory tract infection particularly in infants. RSV induces IFN production however the viral nonstructural (NS) proteins NS1 and NS2 have both been found to inhibit type I IFN signalling (Ling et al., 2009; Lo et al., 2005). This is thought to contribute to the polarisation towards a type 2 immune response rather than a type 1 response – particularly in infants (Hancock et al., 2003; Lay et al., 2015; Legg et al., 2003). These type 2 responses are associated with greater pathology possibly due to impaired short-term antiviral responses. Although RSV only causes mild disease in healthy adults, its ability to reinfect individuals points towards poor establishment of immunological memory. The inhibition of IFN may also play a role here by impairing development of memory CD8+ T cells (Bueno et al., 2008).

RSV infection also leads to immune cell recruitment to the lungs and circulation, although the roles of some cell types are not well understood. Early neutrophil recruitment to is a key feature of RSV infections in humans and mice, and large numbers have been observed in cases of severe disease (Goritzka et al., 2015; Johnson et al., 2007b; Lukens et al., 2010). In mice neutrophils did not contribute to viral clearance or disease-induced weight loss suggesting a redundant role in infection (Kirsebom et al., 2020). Other studies have indicated that neutrophils can exacerbate epithelial cell damage *in vitro* (Deng et al., 2020). The role of neutrophils in humans is still unclear and may differ from either animal or *in vitro* models.

5.1.3 Influenza A virus

5.1.3.1 Virus structure, tropism and life cycle

IAV is an enveloped virus with 8 negative sense ssRNA segments, each encoding one protein. Each segment forms a complex with nucleoproteins and the viral polymerase heterotrimer. Within the virus envelope the viral-encoded protein haemagglutinin (HA) binds sialic acid residues including those on the host cell surface, mediating viral entry. Another envelope protein, neuraminidase (NA) cleaves these sialic acid residues and this is essential for viral exit from host cells following replication (Dou et al., 2018). HA proteins from different viruses have different preferences for α2,3-sialic acid linkages or α2,6-sialic acid linkages which influence the tropism of these viruses. The A/Puerto Rico/8/34 (PR8) strain has been extensively passaged since its initial isolation from a human patient in 1934 and has a preference for α2,3-sialic acid linkages. The A/X-31 (X31) strain has the same genetic backbone as PR8 except for its HA and NA genes and as a result shows a preference for α2,6-sialic acid linkages. Despite the low level of α2,6-sialic acids in mouse epithelial cells, X31 can still infect this species although it is less pathogenic than PR8 (Bouvier and Lowen, 2010; Ibricevic et al., 2006). This shows that sialic acid preference is not a strict determinant of viral tropism. Anion-exchange chromatography analysis revealed that zebrafish embryos contained α2,6-sialic acids but α2,3-sialic acids were undetected (Gabor et al., 2014). However, both PR8 and X31 appear to infect zebrafish embryos. Older stages or specific tissues were not investigated.

IAV initially infects epithelial cells of the respiratory tract but is also thought to infect macrophages in a process that leads to abortive replication (Meischel et al., 2020). Contrary to most RNA viruses, influenza transcription and replication occurs in the nucleus (York and Fodor, 2013). The nuclear localization signal of viral proteins targets the viral genome segments to the cell nucleus (Samji, 2009). This viral RNA (vRNA) is transcribed by the RNA-dependent RNA polymerase into polyadenylated mRNA or used to produce a complementary RNA (cRNA) strand. This cRNA is used as a template to reproduce new copies of vRNA required for new virions.

5.1.3.2   *Notable features of IAV disease and innate immune responses*

Infection of respiratory epithelial cells leads to rapid and robust induction of type I and type III IFNs. This has been observed *in vitro* in both alveolar and bronchial human epithelial cells (Hsu et al., 2012; Wang et al., 2011). Dendritic cells also produce IFNs and these proteins promote antiviral responses *in vivo* but can contribute to immunopathology when produced at high levels (Crotta et al., 2013; Davidson et al., 2014; Jewell et al., 2010; Mordstein et al., 2008). Current evidence suggests that type III IFNs predominate the response against IAV which is of particularly interest since zebrafish lack this family (Jewell et al., 2010).

In response to IAV, alveolar macrophages (AMs) produce large quantities of cytokines, including IL-1β through inflammasome activation (Ichinohe et al., 2009). They also produce various chemokines which stimulate immune cell recruitment (Matikainen et al., 2000; Wareing et al., 2004). Activated macrophages phagocytose IAV-infected cells and are crucial in limiting viral spread (Hashimoto et al., 2007; Tate et al., 2010). Following initial proinflammatory activation *in vitro*, AMs have been found to adopt an immunosuppressive M2b phenotype suggesting that they may also be involved in resolution of inflammation (Zhao et al., 2014).

Severe influenza infections are associated with high levels of cytokines and immune cell recruitment known as a 'cytokine storm'. This excessive inflammation leads to tissue damage and thus contributes to pathology. Even in milder disease proinflammatory cytokine levels correlate with symptom severity (Kaiser et al., 2001). However, experiments in mice lacking functional IL-1 receptor show that lower levels of inflammation may improve pathology but it can also increase mortality (Schmitz et al.,

2005). There is therefore a fine balance between controlling viral load and limiting immunopathology.

5.1.3.3 *Zebrafish model of IAV infection*

Characterisation of IAV infection in zebrafish was first published in 2014 (Gabor et al., 2014). The authors of this study injected the PR8 or X31 strain into 2 dpf zebrafish embryos and showed that infectious virus was maintained for at least 3 days. Viral load was 10-20 fold higher within the first 24 h, but the lack of additional increase in viral load suggest that the level of viral replication was low. Despite this, infected embryos showed gross pathology, particularly oedemas, and necrosis in the gills, liver and kidney. By 3 days, survival of infected fish was around 50%. Another study showed that PR8 also induced muscle damage in embryos (Goody et al., 2017).

IAV also induced upregulation of *ifnphi1, mxa, il1b* and *il8* transcripts within 24 h and for the first two genes this was sustained until at least 72 hpi (Gabor et al., 2014; Goody et al., 2017). Another study has shown that injection of virus into the larval swimbladder induces recruitment of neutrophils (Sullivan et al., 2017). This work indicates that zebrafish are susceptible to IAV *in vivo* and respond with typical signs of antiviral responses. This model may therefore be a suitable candidate to establish a gill viral infection model. Additional characterisation of the gills during infection are needed to assess this.

5.1.4 Infectious pancreatic necrosis virus

To decide which fish virus to investigate in this project, several criteria were considered to increase the likelihood of gill infection or improve practicality of experimental procedures:

- Virus can infect adult zebrafish

- Virus can infect the gills or causes gill pathology

- Virus can infect by immersion

- Virus can infect at standard zebrafish maintenance temperature (28.5°C)

- Virus causes infection without high mortality

- Virus is not easily transmitted through the water to other fish

With these criteria in mind, the top candidate was SVCV which induces gill pathology in zebrafish (Encinas et al., 2013; Sanders et al., 2003). However, inquiry with the Fish Health Inspectorate revealed that use of this virus for *in vivo* research in the UK is restricted to designated UK government disease laboratories. IPNV was suggested as an alternative virus with permitted use for *in vivo* research. This virus was therefore investigated further. IPNV naturally infects salmonid species including Atlantic salmon and rainbow trout. It is therefore of importance to the aquaculture industry and has been studied both experimentally and in natural settings.

5.1.4.1 Virus structure and life cycle

IPNV is an unenveloped birnavirus with a dsRNA genome consisting of two segments. These segments collectively encode 5 proteins, VP1-VP5. A putative sixth protein has also been detected in some strains of IPNV (Shivappa et al., 2004). The viral-encoded proteins include an RNA-dependent RNA polymerase (VP3) and a protein which makes up the viral capsid (V2) and thus interacts with host cells to mediate cell entry (Dopazo, 2020). The receptor that facilitates viral entry is still unknown (Levican et al., 2017). Upon cell entry, the dsRNA genome first undergoes RNA transcription and later protein synthesis and genome replication (Dopazo, 2020).

5.1.4.2 Disease and transmission

In natural settings, IPNV is thought to infect fish through the gills, skin and gut. The virus spreads to many tissues including the brain, kidney, and spleen and is also detected in circulating leukocytes (Novoa et al., 1995). The resulting infection leads to a variety of symptoms including skin darkening, abnormal swimming behaviour and petechial haemorrhages. Internal pathology also includes damage and necrosis in the liver, gut and pancreas (Dopazo, 2020; Office International des Épizooties, 2003). Some studies have reported gill pathology but also report a lack of viral presence in the gills (Ellis et al., 2010; Zhu et al., 2017).

Mortality in IPNV-infected fish varies considerably depending on the fish age, level of stress of the fish, viral strain, environmental conditions and host genetics (Gadan et al., 2013; Houston et al., 2010; Skjesol et al., 2011). Although both juveniles and adults can be infected, juveniles are more susceptible to infection and disease. In addition, the water

temperature has a large impact with warmer temperatures associated with lower infection rates (Bang Jensen and Kristoffersen, 2015).

IPNV can be transmitted both horizontally through the water, and vertically through eggs of infected fish. Some fish do not show clinical symptoms, but are still positive for the virus, acting as asymptomatic carriers (Office International des Épizooties, 2003; Seeley et al., 1977). The virus is able to persist long-term in these fish, but also in the water as it is very stable under different pH and temperature conditions (Torgersen and Håstein, 1995). This persistence appears to be related to the immune response.

5.1.4.3 Immune response

Induction of IFNs and ISGs has been observed in IPNV-infected fish however this varies with the susceptibility of the host and the pathogenicity of the virus strain. Pre-treatment of cells with recombinant IFNα *in vitro* revealed that IFN has antiviral activities against IPNV but this is dependent on the timing of treatment (Skjesol et al., 2009). Antiviral effects were diminished when IFN was applied after IPNV infection indicating inhibitory effects of the virus. IPNV proteins have been shown to inhibit IFNα promoter activation *in vitro* further supporting mechanisms of immune evasion by the virus (Lauksund et al., 2015). This inhibition of IFN responses is thought to contribute to viral persistence *in vivo* by allowing low levels of viral replication to occur. This is supported by studies where more resistant fish or less pathogenic virus strains exhibit lower mortality, lower viral loads, and lower IFN responses (Reyes-López et al., 2015; Robledo et al., 2016; Skjesol et al., 2011). In contrast, more susceptible fish and more pathogenic virus strains exhibit high levels of IFNs/ISGs but this transient response fails to protect fish from disease. This suggests that the virus may use additional mechanisms to overcome the antiviral effects of IFNs and maintain an environment favourable for replication. Similarly, although inflammatory cytokines are induced during IPNV infection, lower levels are associated with lower mortality (Reyes-López et al., 2015). Higher transcript levels of the anti-inflammatory cytokine TGF-β has been found in resistant and asymptomatic fish supporting the role of a less inflammatory environment in viral persistence (Reyes-Cerpa et al., 2012, 2014).

5.1.4.4 Zebrafish infections with IPNV

IPNV has been used to challenge adult zebrafish adults in three studies (Bello-Perez et al., 2019; Lapatra et al., 2000; Seeley et al., 1977). The study by Seely et al. explored the use

of i.p. injection to infect adult zebrafish at 24-27°C. Eggs spawned from injected fish contained infectious particles for up to 40 days. Furthermore, the progeny of infected females contained virus for at least 21 weeks showing viral persistence and vertical transmission. The study by Lapatra et al. similarly used i.p. injection to infect adult zebrafish although the temperature used was not reported. Infectious particles were detected at 1-10 days post infection (dpi) however the exact viral titres were not provided. In contrast, the authors reported a lack of infection following bath immersion with the virus. IPNV infection by injection resulted in a transient reduction of erythrocytes in the kidney that was no longer observed by 6 dpi. The study by Bello-Perez et al. found that i.p. challenged adults (at 21°C) contained IPNV RNA at 2-30 dpi suggesting viral persistence. Transcript levels of cytokine (*il1b*) or antiviral genes (*mxa* and *gig2l*) were unchanged at 2 or 30 dpi compared to controls indicating the lack of an immune response. Despite this, IPNV improved survival and enhanced immune responses during SVCV challenges. This indicates that IPNV does not persist passively in the fish. None of the studies reported significant mortality or gross pathology with IPNV indicating that zebrafish are resistant to severe disease, at least with the viral strains used. There is currently no evidence on the effects of IPNV in zebrafish gills.

5.2 Aims

The work presented so far provides insight into the diverse immune environment of zebrafish gills and the ability of this tissue to respond to non-infectious immune stimuli. To further interrogate gill immunology in the context of viral infection, this chapter focused on testing several viral pathogens in zebrafish. Multiple zebrafish viral infection models have already been established, including some with human pathogens. However, there has been a lack of investigation into the pathology or immune responses of the gills. The aims of this chapter are therefore:

- To assess the ability of human respiratory viruses (RSV and IAV) and a fish-endemic virus (IPNV) to infect zebrafish by monitoring:
    - o Viral load and kinetics in the gills and WKM
    - o Gross pathology as a sign of disease
- To determine the host immune response to viral challenge in the gills and WKM

5.3 Results

5.3.1 RSV challenges in adult zebrafish

This part of the project built on an existing collaboration with Dr Cecilia Johansson (National Heart and Lung Institute, Imperial College London) to investigate human RSV exposure in zebrafish. Dr Johansson provided RSV viral stocks and materials for assessing viral presence, as well as protocols for working with the virus. In this project the A2 strain of RSV was used to challenge adult zebrafish and pathology, viral load, and immune responses were assessed. This human-derived strain of RSV was isolated in 1961 from the lower respiratory tract of an infant and is now commonly used in several animal models including mice and non-human primates (Cameron et al., 2003; Taylor, 2017).

The viral stock provided by Dr Johansson had a viral titre of 10^7 FFU/ml. This stock was thawed and distributed into single-use aliquots. RSV is unstable during handling so to check that the aliquoting process did not abolish viral infectivity, plaque assays were performed in HE-p2 cells (Collins et al., 2013). These immortalized human epithelial cells are derived from human laryngeal carcinoma and commonly used to propagate RSV. Two RSV aliquots and a non-aliquoted RSV sample (positive control) were tested. The plaque assay materials were prepared by Dr Freja Kirsebom (National Heart and Lung Institute, Imperial College London) who also supervised and assisted throughout the procedures.

From the plaque assay, the viral titre was calculated for each RSV sample used. The two aliquots had a viral titre of 5.6 x 10^6 FFU/ml and 4.2 x 10^6 FFU/ml respectively. The positive control had a viral titre of 1.5 x 10^7 FFU/ml, which was similar to the viral stock used to generate the aliquots. This shows that viral titre in the aliquots was 2 to 3-fold lower but the viruses were still infectious. The viral titre of RSV aliquots in subsequent experiments was therefore estimated to be 4.9 x 10^6 FFU/ml.

5.3.1.1 *Investigating the effects of increased environmental temperature on immune-related genes in the gills*

In humans, RSV generally infects and replicates in the upper respiratory tract which has a temperature of up to 34°C (Keck et al., 2000). It was therefore hypothesised that increasing the incubation temperature of RSV-challenged fish might promote viral

replication. This method has been successfully used in a zebrafish model of influenza infection (Gabor et al., 2014).

Zebrafish can tolerate a large range of temperatures (López-Olmeda and Sánchez-Vázquez, 2011; Spence et al., 2007), however, increases in environmental temperature are known to have some physiological effects on the zebrafish immune system. For example, *il1b*, *tnfa* and *il6* were upregulated in the liver of zebrafish maintained at 34°C for 4 days (Zheng et al., 2017). Increased temperature has also been found to alter gill physiology in other fish species (Sollid et al., 2005; Vargas-Chacoff et al., 2018).

To assess whether increased temperatures altered levels of immune-related gene transcripts, unchallenged adult *TraNac* fish were maintained at 28.5°C or 33°C for 5 days and the gills analysed for changes in transcript levels (Figure 5.1). Specifically, the pro-inflammatory cytokine *tnfa*, type I and type II interferons *ifnphi1* and *ifng1*, and *mmp9*, a metalloproteinase involved in tissue remodelling, were investigated. Higher levels of *mmp9* transcripts have been observed in zebrafish larvae at 34°C and in adult gills exposed to cigarette smoke (Long et al., 2012; Progatzky et al., 2015). The experiment in this thesis was performed on fish without exogenous immune stimuli and therefore, the transcription of immune-related genes was likely to be low or undetectable.

Tnfa transcripts were mostly undetected in fish at 33°C and undetected in one fish at 28.5°C (Figure 5.1A). This suggests overall low *tnfa* expression at either temperature. *Ifnphi1* was similar at both temperatures and the minor increase at 33°C was not statistically significant (Figure 5.1B). *Ifny12* was mostly undetected at either temperature (Figure 5.1C). Levels of *mmp9* transcripts were significantly lower at 33°C (Figure 5.1D) which contrasts with a study which reported higher levels at 34°C (Long et al., 2012). However, the latter study investigated zebrafish larvae, which may explain the difference observed here with adult gills.

The fish in this experiment did not show any behavioural signs of respiratory impairment such as increased opercular ventilation rate or swimming at the surface of the water, at any point. This suggests that increased temperature did not significantly impact gill respiratory function. No other behavioural signs of significant stress were observed.

Overall, maintaining the fish at 33°C did not appear to have a major impact on immune-related gene transcription. Although the *mmp9* transcripts were lower which indicates

that the gills did respond to this environmental change, it does not appear that gill respiratory function was significantly impaired. From this, it was concluded that gills at 33°C were unlikely to have major inflammation or immunosuppression, at least at homeostasis. It was therefore decided that 33°C was a suitable temperature for assessing immune responses to viruses.
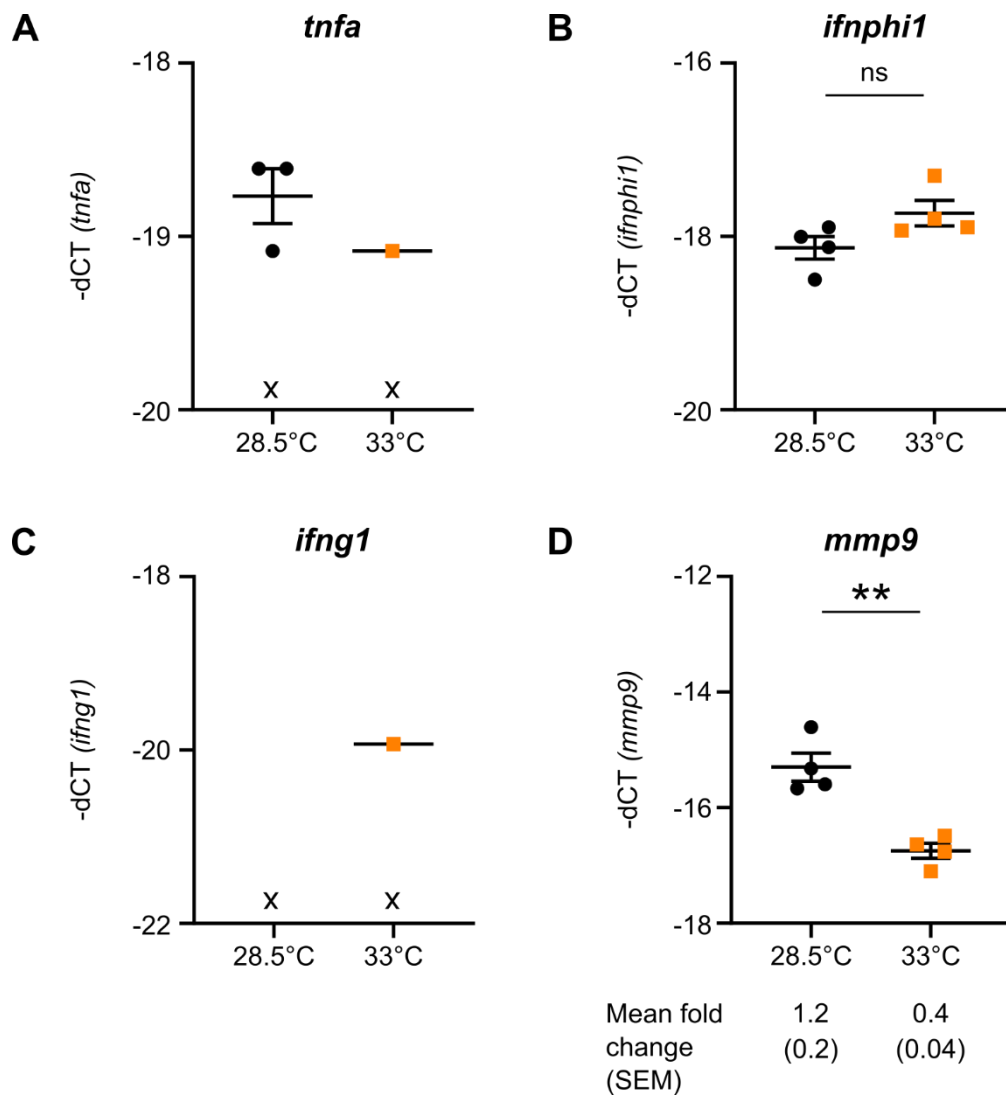
Figure 5.1 Gene transcript analysis in the gills at 28.5°C or 33°C.

Adult *TraNac* zebrafish were maintained at 28.5°C or 33°C for 5 days. Gill tissue was harvested and transcript levels of (A) *tnfa*, (B) *ifnphi1*, (C) *ifng1* and (D) *mmp9* were measured by qRT-PCR. Transcript levels are shown relative to 18S transcript levels. Data represents one experiment and each dot represents one fish (n = 4). Mean and SEM shown. Unpaired t-test performed, *: p ≤ 0.05, ns: non-significant (p > 0.05). X on the chart indicates ≥ 1 sample in the group had undetected transcripts (SEM not calculated), and therefore statistical testing was not performed for these groups. D) Fold change relative to median control sample was calculated using the ΔΔCT method.

5.3.1.2 Topical gill challenges with RSV at 28.5°C and 33°C

Next, the effects of topical gill challenge with live RSV were assessed at both 28.5°C and 33°C. Although 33°C was expected to be more permissive for RSV replication, infection at 28.5°C was also tested because this is a more practical approach that does not require prior acclimatisation. For challenges at 28.5°C, adult *TraNac* fish were challenged by topical gill application with 10 µl of RSV suspension or uninfected HE-p2 cell supernatant (negative control). Based on results from the plaque assay, the viral dose was estimated to be 4.9×10^4 FFU per fish. The viral dose was undiluted thus representing the maximum concentration possible from the materials available. Gills of challenged fish were harvested at 1 h, 24 h, and 96 hours post challenge (hpc). These timepoints reflect the period of increasing and peak immune response and viral load in mice infections (Goritzka et al., 2016). Fish showed no behavioural or gross pathologies over the course of the experiment.

The immune response was assessed in the gills by measuring *tnfa*, *ifnphi1* and *ifng1* transcript levels (Figure 5.2A-C). *Tnfa* levels were generally low, with a possible small increase in RSV-challenged fish at 24 hpc, followed by a decrease at 96 hpc (Figure 5.2A). *Ifnphi1* levels were not significantly different between RSV and control samples at any timepoint (Figure 5.2B). *Ifng1* was possibly increased at 24 hpc but mostly undetectable at 1 hpc and 96 hpc (Figure 5.2C). These results indicate that although some changes were observed in RSV-challenged fish, transcript levels were still low and changes were much smaller than those observed in other gill immune responses, for example following R848 challenge (Figure 4.1).

Next, RSV gill challenges were performed at 33°C. Adult *TraNac* fish were maintained at 33°C for 5 days before being challenged with 10 µl of RSV (4.9×10^4 FFU) or uninfected HE-p2 cell supernatant (negative control). Gills were harvested at 4 days post challenge (dpc) and analysed for *tnfa and ifnphi1* transcript levels (Figure 5.2D-E).

Tnfa and *ifnphi1* were unchanged in RSV-challenged fish relative to controls indicating a lack of response in the gills. It is possible that a response occurred at earlier timepoints, as seen in 28.5°C challenges (Figure 5.2A-C). However, the next aim focused on assessing viral load rather than earlier timepoints.
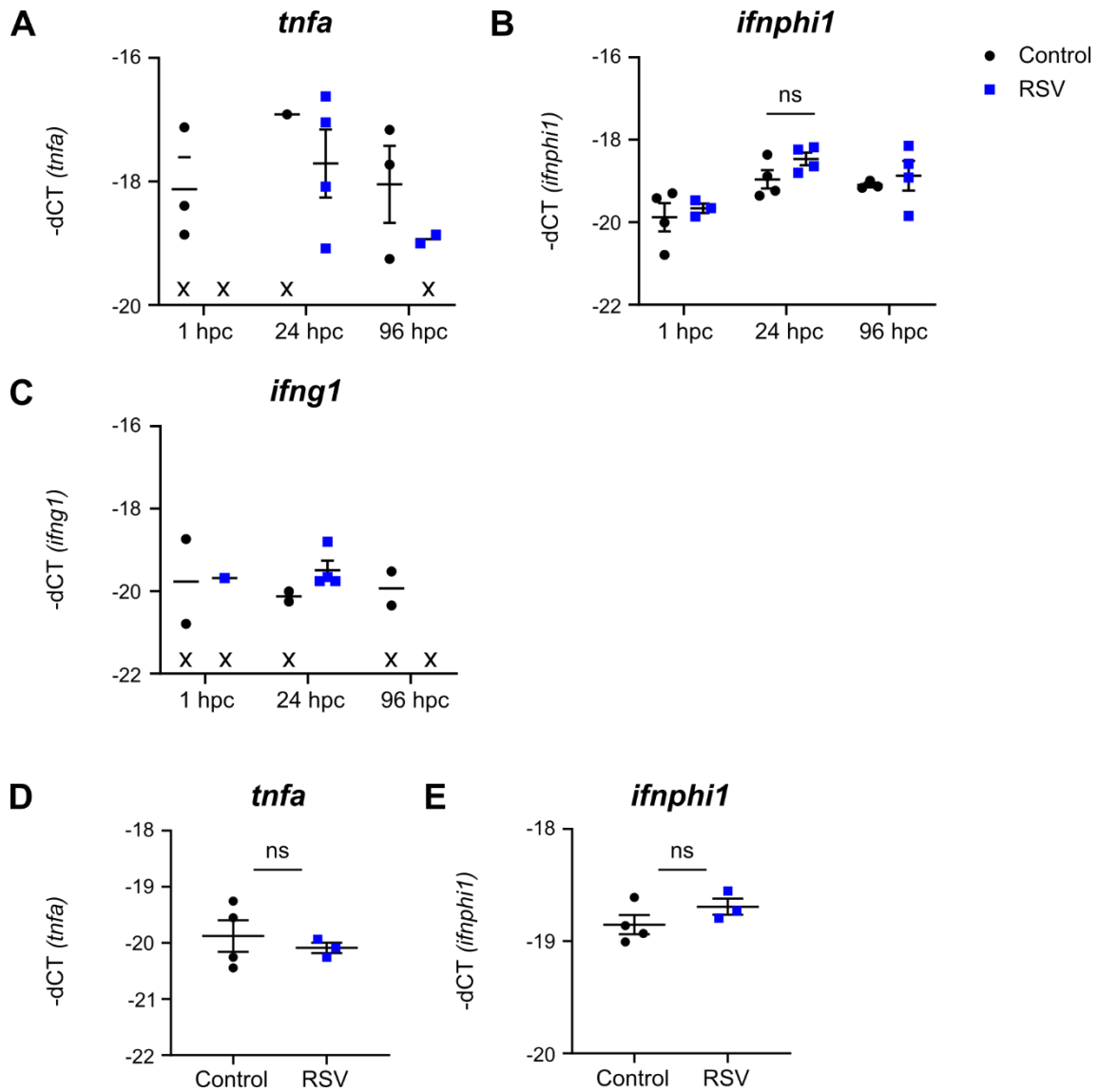
Figure 5.2 Immune gene transcript analysis of RSV-challenged fish.

Transcript levels in the gills were measured by qRT-PCR and are shown relative to 18S transcript levels. (A-C) Adult *TraNac* fish were challenged by topical gill application with 10 µl of RSV (4.9 x 10^4 FFU) or uninfected HE-p2 cell supernatant (negative control). Fish were maintained at 28.5°C and gills harvested at 1, 24 and 96 hpc. Data represents one experiment and each dot represents one fish (n = 3-4). Mean and SEM shown. Two-way ANOVA was performed on (B) followed by Tukey's multiple comparison test. X on the chart indicates ≥ 1 sample in the group had undetected transcripts (SEM not calculated), and therefore statistical testing was not performed for these groups. (D-E) Adult *TraNac* fish were challenged by topical gill application with 10 µl of RSV (4.9 x 10^4 FFU) or uninfected HE-p2 cell supernatant (negative control). Fish were maintained at 33°C and gills harvested at 4 dpc. Data represents one experiment and each dot represents one fish (n = 3-4). Mean and SEM shown. Unpaired t-test performed. *: $p \leq 0.05$, ns: non-significant ($p > 0.05$).

Viral load was measured for both experiments by qRT-PCR for the RSV L gene. The amounts of L gene were calculated from standard curves of a plasmid encoding the RSV L gene (Figure 5.3A, C and E). Known amounts of this plasmid were used which allowed quantification of absolute copies of L gene in experimental samples. To evaluate the use of this assay with zebrafish tissue, dissected gills from unchallenged fish were mixed with 10 µl of RSV and analysed by qRT-PCR. Results showed that this type of sample could be used as a positive control for viral load (Figure 5.3B).

In challenges at 28.5°C, RSV L gene was clearly detected in the positive control but completely undetected in gill samples challenged with uninfected HE-p2 supernatant or live RSV (Figure 5.3B). The positive control showed that L gene was present in large quantities in the initial 10 µl dose. The standard curve shows that RSV L gene should have been detectable even if the amount of L gene decreased $1x10^4$-fold in challenged gills (Figure 5.3A). Lack of detectable L gene even at the earliest timepoint (1 hpc) suggests that the virus did not remain in the gills following topical application and was unlikely to have replicated. One explanation may be that the virus was unable to cross the mucus barrier and was washed out during gill ventilation following the gill challenge.

In gill challenges at 33°C, RSV L gene was similarly undetectable at 4 dpc (Figure 5.3D).

These results show that although small transient changes were observed in immune-related genes in RSV challenges at 28.5°C, substantial viral replication did not occur at either temperature. The changes in immune gene transcripts may have been caused by recognition of viral antigens rather than productive viral infection.
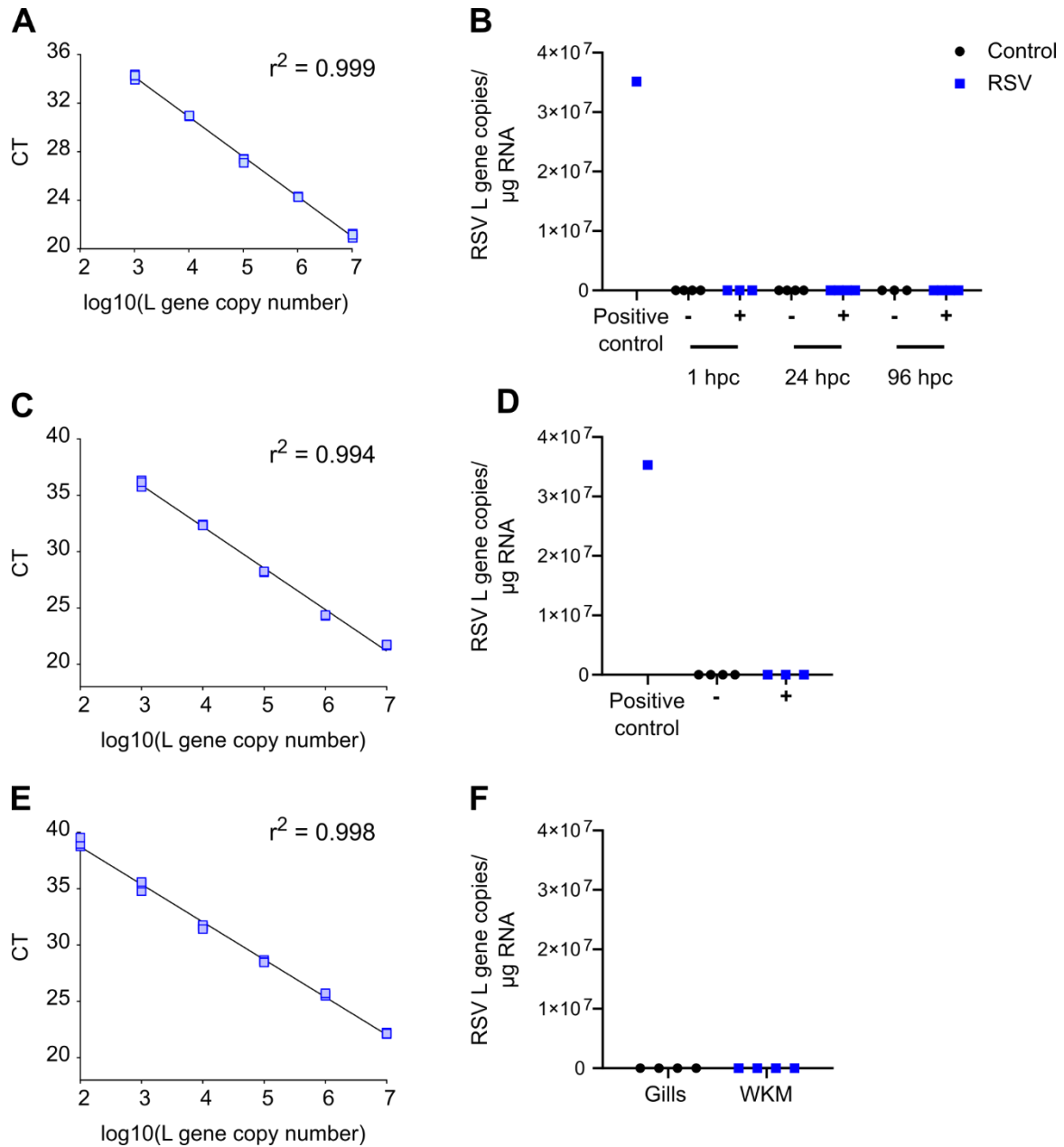
Figure 5.3 Viral load in RSV-challenged fish.

Viral load was measured by qRT-PCR analysis of the RSV L gene. (A, C and E) A plasmid encoding the L gene was used to generate a standard curve for each qRT-PCR run. Simple linear regression was performed for each dataset. (B, D and F) Absolute numbers of L gene copies in zebrafish samples were calculated from the standard curve and normalised to 18S transcript levels. Positive control (n = 1) represents unchallenged gill tissue mixed with 10 µl of RSV (4.9 x 10^4 FFU). B) Gills from fish challenged by topical gill application with 10 µl of RSV (4.9 x 10^4 FFU) or uninfected HE-p2 cell supernatant control at 28.5°C (n =3-4). D) Gills from fish challenged by topical gill application with 10 µl of RSV (4.9 x 10^4 FFU) or uninfected HE-p2 cell supernatant control at 33°C (n = 3-4). Gills were harvested at 4 dpc. F) Gills and WKM from fish challenged by i.p. injection with 5 µl of RSV (2.45 x 10^4 FFU) or uninfected HE-p2 cell supernatant control at 33°C (n = 4). Tissues were harvested at 4 dpc.

5.3.1.3 *Intraperitoneal challenge with RSV at 33°C*

As previously observed in LPS challenges (Figure 4.1), exposure through the gill route will not always induce an immune response. To check if the route of administration also affects the response to RSV, 5 µl of virus (2.45 x 10⁴ FFU) or HE-p2 supernatant was injected intraperitoneally in adult *TraNac* fish acclimatised at 33°C. For this experiment fish were acclimatised more gradually by increasing the temperature by 1°C for the first 3 days of acclimatisation. Fish were then kept at 33°C for last 2 days of acclimatisation. The acclimatisation process was changed from previous experiments as it was thought that a gradual approach was more suitable for a range of different experiments, both in this project and beyond. This is because a gradual approach is more likely to prevent changes in genes beyond those investigated in Figure 5.1.

Gills and WKM of challenged fish were harvested at 4 dpc. The standard curve indicated that L gene was detectable from as little as 100 copies but no L gene was detected in any of the control or RSV-challenged samples (Figure 5.3F). Due to the lack of viral presence, analysis of immune-related host genes was not pursued.

In summary, despite using a large viral dose, neither topical gill application nor i.p. injection resulted in RSV infection in adult *TraNac* fish. The immune response to the topical challenge was minimal further supporting a lack of viral replication. This also suggests that even the initial exposure to RSV particles was not very inflammatory.

5.3.2 IAV challenges in embryonic and adult zebrafish

IAV was chosen for additional viral challenges because of its importance as a human respiratory pathogen and its prior use in zebrafish embryos (Gabor et al., 2014). There are currently no published reports of IAV infection in zebrafish adults, and more specifically few reports of its effect on the gills. The aims of the next set of experiments were therefore to check the infectivity of IAV in zebrafish embryos as previously described and to check the infectivity in adult fish. The PR8 (H1N1) and X31 (H3N2) strains of IAV were chosen for investigation based on their previous use in zebrafish (Gabor et al., 2014). These experimental strains are human-derived and commonly used in mammalian models of IAV (Bouvier and Lowen, 2010).

5.3.2.1 Infection kinetics of IAV in vitro

The PR8 and X31 viral stocks were provided by Professor Wendy Barclay (Department of Infectious Disease, Imperial College London). To confirm that that the viruses in these stocks were infectious, they were used to infect mammalian MDCK cells. The supernatant of infected cells was harvested every 24 h in triplicate. RNA was extracted from these samples and viral load measured by qRT-PCR analysis of viral M gene mRNA (Figure 5.4A).

This experiment was designed in collaboration with Professor Wendy Barclay and Dr Jay, Jie Zhou (Department of Infectious Disease, Imperial College London). Experimental procedures were performed in collaboration with Dr Jay, Jie Zhou.

qRT-PCR analysis revealed that viral load increased exponentially up to 48 h for both PR8 and X31 (Figure 5.4A). Viral load continued to increase after 48h in PR8 infected cells but declined in X31 infected cells. These results confirmed that the viral stocks in this project contained infectious particles.

A

B

C

D

E
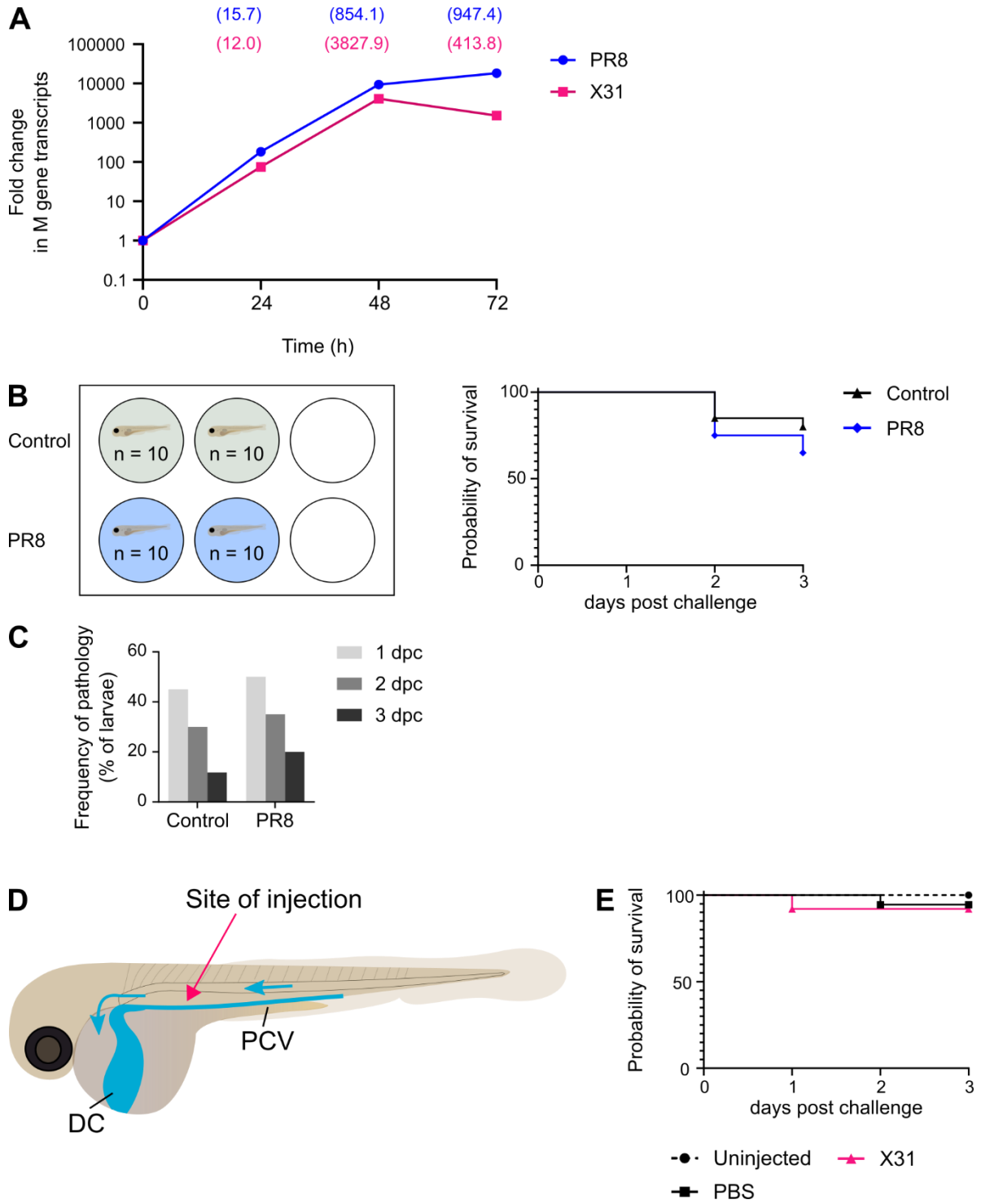
Figure 5.4 IAV infection challenges in MDCK cell culture and zebrafish embryos.

A) MDCK cells were infected in triplicate with PR8 or X31 and supernatant was harvested 24-72 hours post infection. IAV M transcript levels were measured by qRT-PCR and compared to M gene levels at 0 h by the ΔΔCT method. Each dot represents the mean fold change and SEM is shown in brackets. Protocols were performed in collaboration with Dr Jay, Jie Zhou (Imperial College London). B) Experimental setup (left) of zebrafish immersion challenges with PR8. 2 dpf *TraNac* embryos (n = 10 per well) were immersed in MB solution alone (control) or with PR8 [2.8 x 10^5 plaque forming units (PFU)] and maintained at 33°C. Percentage of fish alive at 0-3 dpc (right). Each group represents 20 fish pooled from two wells. Survival curves were compared using the logrank (Mantel-Cox) test and not found to be significantly different. C) Percentage of surviving fish exhibiting pathologies at each timepoint. Each group presents fish pooled from two wells. D) Schematic of a 2 dpf embryo with the posterior cardinal vein (PCV) and Duct of Cuvier (DoC) blood vessels in blow. Blue arrows indicate direction of blood flow. Pink arrow indicates the site of injection for PR8 or X31 challenges (1-3nl at 2.65 x 10^5 PFU/ml). Fish were maintained at 33°C following injections. E) Percentage of fish alive after no injection (n = 24), PBS injection (n = 18), or X31 injection (n = 25). Injections were performed by Håkon Hogset (Imperial College London). Survival curves were compared using the logrank (Mantel-Cox) test and not found to be significantly different.

5.3.2.2 *Immersion challenge of zebrafish embryos with PR8 virus*

For challenges in zebrafish, this project focused mostly on the PR8 strain which appears to be more virulent than X31 in embryos (Gabor et al., 2014). PR8 also replicated to higher levels than X31 in cell culture experiments (Figure 5.4A).

To check if PR8 was infectious in zebrafish, embryos were exposed to the virus by immersion. Immersion is a simple, high-throughput, and physiologically relevant route of administration and can therefore be a useful approach for zebrafish infection studies. Although a previous study reported a lack of infection by immersion, it was important to verify this.

2 dpf *TraNac* embryos were immersed in 2.8 x 10^5 PFU of PR8 virus (in MB solution) or in MB solution alone. Embryos were maintained for 3 days at 33°C and monitored daily for mortality and pathology (Figure 5.4B). Average survival rate in immersed embryos was 80% in the control group and 65% in the PR8 group which was not found to be significantly different (Figure 5.4B). Pathologies (mainly oedemas but also some spine curvature) were observed at all timepoints in both control and PR8 groups at a similar level (Figure 5.4C). These pathologies therefore did not appear to be a specific effect of virus exposure. Overall, PR8 immersion did not induce pathological infection in embryos which aligns with reports from (Gabor et al., 2014).

5.3.2.3 Injection challenges of zebrafish embryos with PR8 or X31

Next, the effects of viral exposure by injection was investigated in zebrafish embryos. Experiments were designed in collaboration with Håkon Hogset (Department of Materials, Imperial College London) who also performed the injections. 2 dpf *TraNac* zebrafish were intravenously injected (in the posterior cardinal vein) with 1-3 nl of PR8 at a titre of 1.8×10^2 PFU/ml (Figure 5.4D). This titre was estimated to be equivalent to the 2.55×10^2 $TCID_{50}$/ml titre used by (Gabor et al., 2014). This was based on the estimate that 1×10 $TCID_{50}$/ml is equivalent to 0.7 PFU/ml for viruses grown in the same cell culture systems (ATCC, 2012). In addition, a higher dose of PR8 (2.8×10^7 PFU/ml) was used for a second group to assess the effect of different doses.

Intravenous injection was chosen as a more practical route than the Duct of Cuvier used by (Gabor et al., 2014). However, the site of injection was close to the Duct of Cuvier with blood flow in the same direction (Figure 5.4D). Uninjected and PBS-injected embryos were used as control groups.

Embryos were maintained at 33°C and mortality and pathology was monitored for up to 3 dpc. At 1 dpc, only 1 death was recorded across all groups. This death was in the high dose PR8 group. Unfortunately, exact numbers of survival for fish at 2-3 dpc are no longer available. However, it was previously noted that the survival rate was similar between control and virus-challenged groups and was higher than the 54% survival rate described for PR8-injected fish by Gabor et al.

Next, 2 dpf embryos were injected with X31 virus to check if a different IAV strain would result in infection. This time only the maximum viral dose (2.65×10^5 PFU/ml) was used. The survival rate was high in all three groups (≥ 80%) and not significantly different between any of the groups (Figure 5.4E). Furthermore, no gross pathology was observed in any group.

The results of these challenges are in clear contrast with results from (Gabor et al., 2014) who reported significantly higher mortality and pathology following virus injection. This discrepancy suggests that the infection phenotype is highly sensitive to differences in experimental procedures, virus materials, zebrafish clutch, or environmental factors. Furthermore, the results reported by Gabor et al. may need to be more carefully interpreted to understand the specific factors that could influence the infection

phenotype. These factors will be discussed in more detail in the discussion section of this chapter.

5.3.2.4 Topical gill challenge of adult zebrafish with PR8

Although disease phenotype was not observed in embryos in this project, it was still important to assess the effects of IAV in adult zebrafish. Unlike embryos, adult fish have structurally and immunologically mature gills and are therefore the most appropriate stage to interrogate the effects of viral exposure on this tissue. Adult challenges were not attempted in the first influenza study by Gabor et al. and have not been reported since in other studies. All adult IAV challenges were performed at 33°C to increase the likelihood of infection.

Adult *TraNac* zebrafish were gradually acclimatised to 33°C over 5 days before being challenged with 5 µl of PR8 (1.4 x 10^5 PFU) or PBS by topical gill application. In PR8 infections in mice, viral load in the lungs peaks between 3-6 days post infection and immune responses are also elevated at this time (Al-Garawi et al., 2009; Ivinson et al., 2017). Zebrafish gills and WKM were therefore harvested at 1 and 4 dpc to identify potential changes in viral load and immune responses. Gills and WKM were analysed for changes in transcripts of proinflammatory cytokines (*il1b* and *tnfa*), a chemokine (*cxcl18b*), interferons (*ifnphi1* and *ifng1*), and an interferon-stimulated gene (*rsad2*) by qRT-PCR. *Rsad2* is upregulated during viral infection in zebrafish (Briolat et al., 2014; Ge et al., 2015). In this project, *rsad2* was also found to be highly upregulated in the gills and WKM in response to the viral mimic, R848 (Figure 5.5A-B). This panel of genes therefore reflects genes expected to be involved in antiviral responses. Viral load was assessed by measuring transcript levels of the viral M gene mRNA by qRT-PCR.
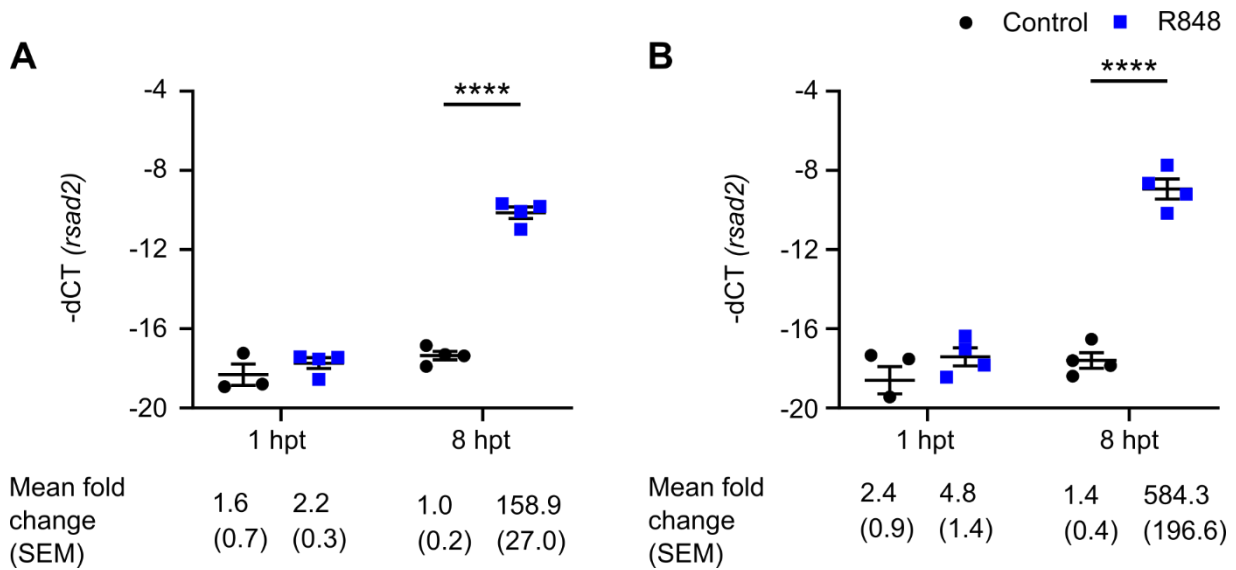
Figure 5.5 *Rsad2* transcript levels in the gills and WKM following R848 i.p. injection.

R848 (5 µl at 0.5 mg/ml) or endotoxin-free water was injected into adult WT zebrafish. Transcripts in the gills (A) and WKM (B) were measured by qRT-PCR and are shown relative to 18S transcript levels. Data represents one experiment and each dot represent one fish (n = 4). Mean and SEM shown. Two-way ANOVA was performed followed by Tukey's multiple comparisons test, ****: $p \leq 0.0001$. The ΔΔCT method was also used to calculate the fold change relative to time-matched controls. Mean fold change for each group is shown underneath each bar with SEM shown in brackets.

No gross pathologies were observed in the fish at any timepoint of this experiment. Furthermore, no major changes in *il1b*, *tnfa*, or *cxcl18b* were observed indicating a lack of inflammation in the gills (Figure 5.6A-C).

Ifnphi1 levels were similar between control and PR8-challenged gills at 1 and 4 dpc (Figure 5.6D). *Ifng1* transcripts were more frequently detected in PR8-challenged gills at 4 dpc however, the transcript levels were similar to the control samples at both timepoints (Figure 5.6E). No changes in *rsad2* transcript levels were observed at either timepoint (Figure 5.6F). This suggests that a robust interferon response did not occur.

In the WKM, no significant changes in *il1b*, *tnfa*, or *cxcl18b* were observed at any timepoint. This indicates a lack of inflammation in the WKM following virus challenge. No changes were observed for *ifnphi1*, *ifng1*, or *rsad2* in the WKM.

Overall, these results indicate a negligible host response in the gills and WKM. Only 3 fish were analysed per group therefore, more samples would be needed to determine whether small changes in transcript levels are reproducible and statistically significant. However, it is clear that PR8 did not induce a robust immune response in these fish.

Due to the COVID-19 pandemic, access to raw data for M gene mRNA levels is not currently possible. These data are stored on laptops that were used for COVID-19 testing and are currently under repair. Preliminary analysis during the qRT-PCR run indicated that M gene mRNA was undetected or at least was lower than the PR8 positive control. However, access to the original data files are needed to confirm and quantify this. If the data can be recovered it will be subsequently fully analysed.

Overall, results from these challenges show that gill application of PR8 did not induce detectable disease, or a substantial immune response in adult zebrafish.
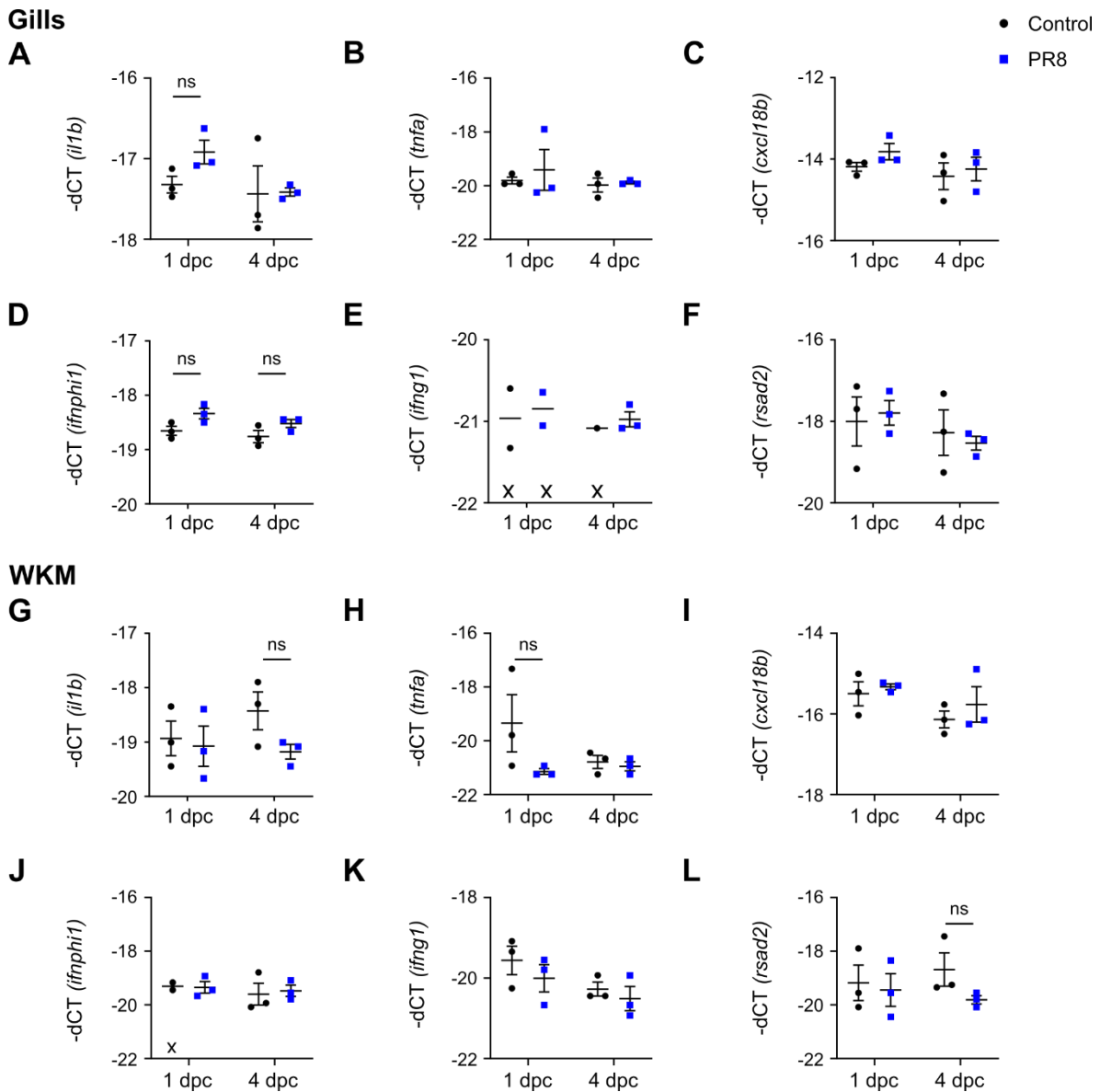
Figure 5.6 Immune gene transcript analysis in fish challenged with PR8 by topical gill application.

Adult *TraNac* zebrafish were acclimatised to 33°C over 5 days and challenged with 5 µl of PR8 (1.4 x 10^5 PFU) or PBS. Gills (A-F) and WKM (G-L) were harvested 1 or 4 dpc. Transcript levels for *il1b* (A, G), *tnfa* (B, H), *cxcl18b* (C, I), *ifnphi1* (D, J), *ifng1* (E, K), and *rsad2* (F, L) were measured by qRT-PCR and are shown relative to 18S transcript levels. Data represents one experiment and each dot represents one fish (n = 3-4). Mean and SEM shown. Two-way ANOVA was performed followed by Tukey's multiple comparisons test. X on the chart indicates ≥ 1 sample in the group had undetected transcripts (SEM not calculated), and therefore statistical testing was not performed for these groups. ns: non-significant ($p > 0.05$).

245

5.3.2.5 Intraperitoneal challenge of adult zebrafish with PR8

Due to the lack of infection in gill topical challenges, i.p. injection was investigated as an alternative route to establish infection. Adult *TraNac* zebrafish were gradually acclimatised to 33°C over 5 days before being i.p. injected with 5 μl of PR8 (1.4×10^5 PFU) and maintained for 1, 4, or 20 dpc at 33°C. 20 dpc was selected as an additional timepoint to assess whether symptoms or viral replication manifested at later timepoints. This was the longest time that challenged fish could be maintained under animal research project licence requirements.

Gills and WKM were harvested at each timepoint and analysed by qRT-PCR for the same panel of immune-related genes as the gill challenge (Figure 5.7 and Figure 5.8). Viral load was assessed by measuring viral M gene mRNA (Figure 5.9).

In PR8-challenged gills, *il1b* was moderately upregulated at 1 dpc but this was not quite statistically significant and not observed at later timepoints (Figure 5.7A and Table 5.2). There was also a trend of increased *cxcl18b* transcripts at 1 dpc but again this was not statistically significant (Figure 5.7C and Table 5.2). *tnfa* was unchanged between control and PR8-challenged fish at all timepoints in the gills (Figure 5.7B). Although *ifnphi1* appeared to be upregulated in PR8-challenged gills at 1 dpc, this was not statistically significant (Figure 5.7D). *Ifng1* and *rsad2* were generally unchanged between control and PR8-challenged groups at all timepoints (Figure 5.7E-F).
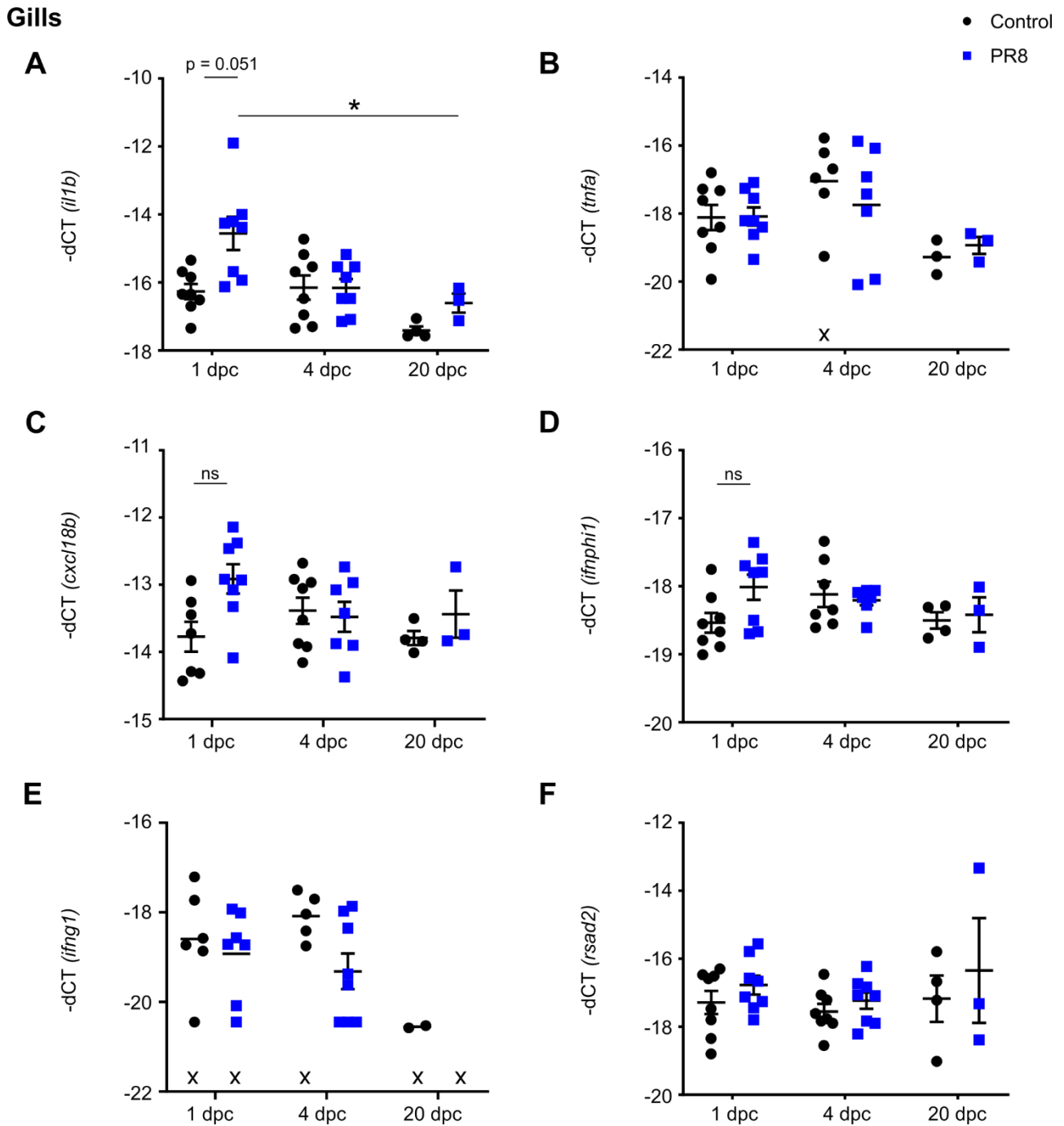
Figure 5.7 Immune gene transcripts in gills of adult fish challenged with PR8 by i.p. injection.

Adult *TraNac* zebrafish were acclimatised to 33°C over 5 days and challenged with 5 µl of PR8 (1.4 x 10^5 PFU) or PBS. Gills were harvested 1-20 dpc. Transcript levels for *il1b* (A), *tnfa* (B), *cxcl18b* (C), *ifnphi1* (D), *ifng1* (E), and *rsad2* (F) were measured by qRT-PCR and are shown relative to 18S transcript levels. Data for 1 and 4 dpc are pooled from two independent experiments (n = 7-8). Data for 20 dpc are from one experiment (n = 3-4). Each dot represents one fish. Mean and SEM shown. Welch's ANOVA followed by Sidak's multiple comparisons test was performed for (A). Two-way ANOVA followed by Tukey's multiple comparisons test was performed for C, D and E. X on the chart indicates ≥ 1 sample in the group had undetected transcripts (SEM not calculated), and therefore statistical testing was not performed for these groups. ns: non-significant (p > 0.05).

Gene	Sample	Relative fold change	SEM
il1b	Control	1.18	0.17
	PR8	5.62	2.32
cxcl18b	Control	1.03	0.13
	PR8	1.89	0.24

Table 5.2 Relative fold change of *il1b* and *cxcl18b* transcript levels in the gills of fish i.p. injected with PBS or PR8, 1 dpc.

Relative fold change calculated with the ΔΔCT method.

No significant changes between control and PR8-challenged fish were detected for any of the genes investigated in the WKM (Figure 5.8).

These results indicate that i.p. injection of PR8 was largely non-inflammatory but may have induced minor, transient, local inflammation in the gills. Furthermore there did not appear to be an IFN response indicating a lack of a broad antiviral immune response.

WKM
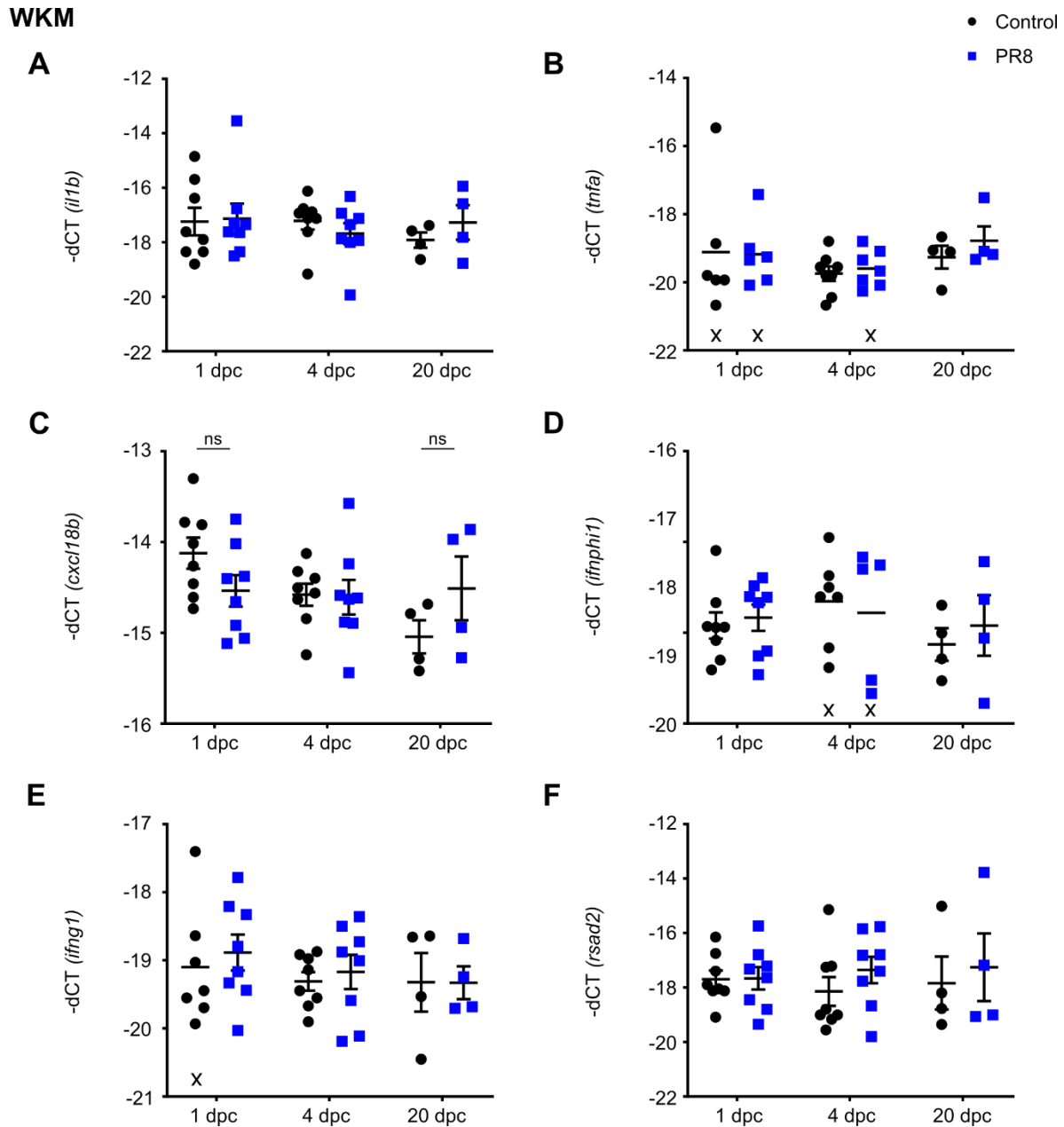
Figure 5.8 Immune gene transcripts in WKM of adult fish challenged with PR8 by i.p. injection.

Adult *TraNac* zebrafish were acclimatised to 33°C over 5 days and challenged with 5 µl of PR8 (1.4 x 10^5 PFU) or PBS. WKM tissue was harvested 1-20 dpc. Transcript levels for *il1b* (A), *tnfa* (B), *cxcl18b* (C), *ifnphi1* (D), *ifng1* (E), and *rsad2* (F) were measured by qRT-PCR and are shown relative to 18S transcript levels. Data for 1 and 4 dpc are pooled from two independent experiments (n = 7-8). Data for 20 dpc are from one experiment (n = 3-4). Each dot represents one fish. Mean and SEM shown. Two-way ANOVA followed by Tukey's multiple comparisons test was performed. X on the chart indicates ≥ 1 sample in the group had undetected transcripts (SEM not calculated), and therefore statistical testing was not performed for these groups. ns: non-significant (p > 0.05).

To measure viral load, mRNA levels of the viral M gene were detected by qRT-PCR (Figure 5.9). Analysis of a positive control sample representing the initial viral dose (gill tissue mixed with 5 µl of virus) revealed that mRNA was present in the viral stock, possibly due to dead cells in the cell culture used to propagate the virus. Viral M gene mRNA was detected at low levels in the WKM in 5/8 challenged fish at 1 dpc and 2/8 fish at 4 dpc. M gene mRNA was not detected in any fish at 20 dpc. The transcript levels at 1 and 4 dpc were all lower than the positive control sample representing the initial dose. These results indicated a decline in viral load over time. Furthermore, M gene mRNA was undetected in the gills at any timepoint.

The lack of viral mRNA in the gills is in contrast to the potential inflammatory response in this tissue. Since earlier timepoints were not investigated, it is possible that viral particles were present in gills following challenge but declined by 1 dpc. It is also possible that virus levels in the gills were too low to detect with the assay used.

In contrast, although the WKM contained viral mRNA, this did not appear to induce any inflammation in the tissue. This suggests that viral presence may not be enough to stimulate an inflammatory response.

Overall, these results show that PR8 was not able to establish a detectable, persistent infection in adult zebrafish through the gill or through i.p. injection. Since there was only a small indication of inflammatory changes in the gills, additional controls would be needed to check potential contributions of the viral stock medium itself. Furthermore, although viral load declined, it is notable that viral mRNA was detectable up to 4 dpc. This suggests that viral mRNA is either stable in zebrafish for extended periods of time, or that a low level of viral replication occurred.
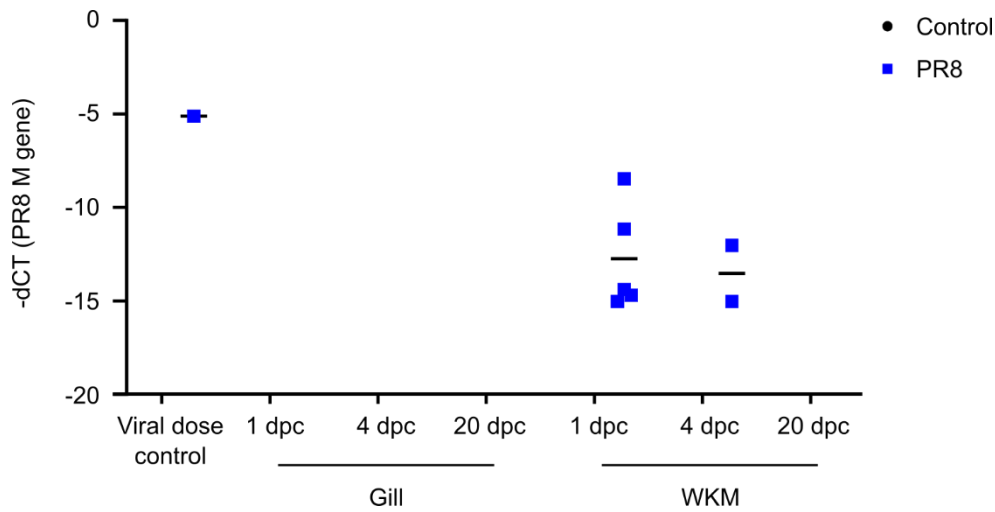
Figure 5.9 Viral load in adult fish challenged with PR8 by i.p. injection.

Adult *TraNac* zebrafish were acclimatised to 33°C over 5 days and challenged with 5 μl of PR8 (1.4 x 10^5 PFU) or PBS (control). Detection controls were made from unchallenged gill tissue mixed with 5 μl of PR8 (1.4 x 10^5 PFU) or PBS (n = 1). Viral load was measured by qRT-PCR of the viral M gene mRNA. M gene levels are shown relative to *actb1* transcript levels. Data for 1 and 4 dpc are pooled from two independent experiments (n = 7-8). Data for 20 dpc are from one experiment (n = 3-4). Each dot represents one fish. Mean shown. Samples with undetected M gene transcripts are not shown on the graph.

5.3.3 IPNV challenges in adult zebrafish

The human respiratory viruses used in this project (RSV and IAV) failed to establish robust infection in zebrafish. The next step was to investigate a virus endemic to fish. As detailed in the introduction of this chapter, several fish viruses have previously been used in zebrafish and some are well established as infection models.

IPNV stocks (strain CD 975/99) were provided by Professor Ross Houston and Dr Jon Pavelin (Roslin Institute, University of Edinburgh). This viral stock was generated by propagation of a clinical isolate in CHSE214 cells.

As with RSV and IAV, IPNV was used to challenge adult zebrafish by topical gill application or i.p. injection and monitored for host immune response and viral load. Challenged fish were maintained at the standard temperature of 28.5°C or a cooler temperature of 15°C. As a virus endemic to fish in cooler environments, IPNV is known to have lower infectivity with increasing temperature (Bang Jensen and Kristoffersen, 2015). However, viral

persistence and vertical transmission has been observed in zebrafish maintained at 24-27°C (Seeley et al., 1977).

5.3.3.1 Immune gene transcripts in fish challenged with IPNV at 28.5°C

Adult *TraNac* fish were injected with 5 µl of undiluted IPNV stock (1.35 x 10^5 PFU) and maintained at 28.5°C for 1 or 6 dpc. Changes in immune gene transcript levels, viral load, or haematopoietic tissue have been observed in previous IPNV infection studies at these timepoints (Lapatra et al., 2000; McBeath et al., 2007). Gills and WKM were harvested and analysed by qRT-PCR for *il1b*, *tnfa*, *cxcl18b*, *ifnphi1*, and *ifng1* zebrafish transcripts. Viral load was assessed by measuring the viral VP2 gene with qRT-PCR.

Il1b and *cxcl18b* appeared slightly lower at 1 dpc in the gills of viral-challenged fish but this was not found to be statistically significant (Figure 5.10A-B). In addition, *tnfa* and *ifng1* was undetectable in several virus-challenged and control gills further indicating a lack of immune response to the virus. No changes were observed at 6 dpc.

No significant changes were observed in *ifnphi1* or *ifng1* transcript levels in the gills (Figure 5.10D-E). Furthermore, no significant changes were observed in the WKM of virus-challenged fish for any of the genes investigated (Figure 5.10G-K). These qRT-PCR results suggest that IPNV did not induce an immune response in the gills or WKM of i.p.-challenged fish.

Gills
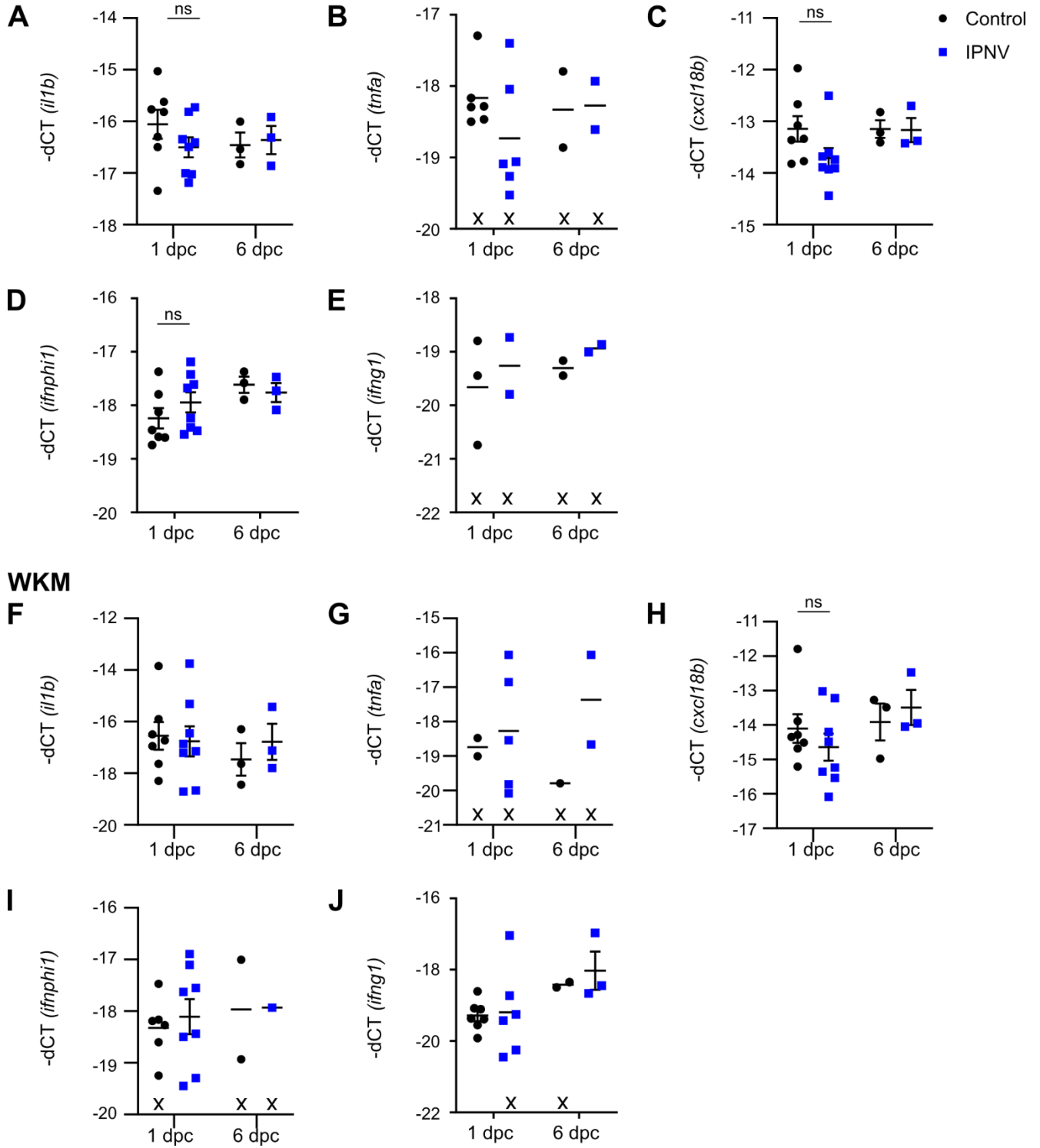
Figure 5.10 Immune gene transcript analysis in fish challenged with IPNV by i.p. injection.

Adult *TraNac* zebrafish were injected with 5 μl of IPNV (1.35×10^5 PFU) or PBS. Gills (A-E) and WKM (F-J) were harvested 1 or 6 dpc. Transcript levels for *il1b* (A, F), *tnfa* (B, G), *cxcl18b* (C, H), *ifnphi1* (D, I), and *ifng1* (E, J) were measured by qRT-PCR and are shown relative to 18S transcript levels. Data for 1 dpc groups are pooled from two independent experiments (n = 7-8). Data for 6 dpc groups are from one experiment. Each dot represents one fish (n = 3-4). Mean and SEM shown. Two-way ANOVA followed by Tukey's multiple comparisons test was performed. X on the chart indicates ≥ 1 sample in the group had undetected transcripts (SEM not calculated), and therefore statistical testing was not performed for these groups. ns: non-significant (p > 0.05).

For the gill challenges, adult *TraNac* fish were topically challenged with 5 μl of IPNV (1.35×10^5 PFU) or PBS and maintained at 28.5°C for 1 dpc. In i.p. challenged fish, the only change in immune genes was observed at 1 dpc, therefore the focus was to first assess early changes in immune-related genes.

No significant changes in *il1b*, *tnfa*, or *cxcl18b* were observed in the gills or WKM (Figure 5.11A-C and F-H). However, there did appear to be a trend of lower *cxcl18b* transcript levels in the WKM (Figure 5.11H). *ifnphi1* and *ifng1* were increased in virus-challenged gills, although this upregulation was fairly small (Figure 5.11D-E and I-J). Overall, despite a possible induction in a low interferon response, no robust immune response was detected in the gills or WKM of fish challenged topically with IPNV.
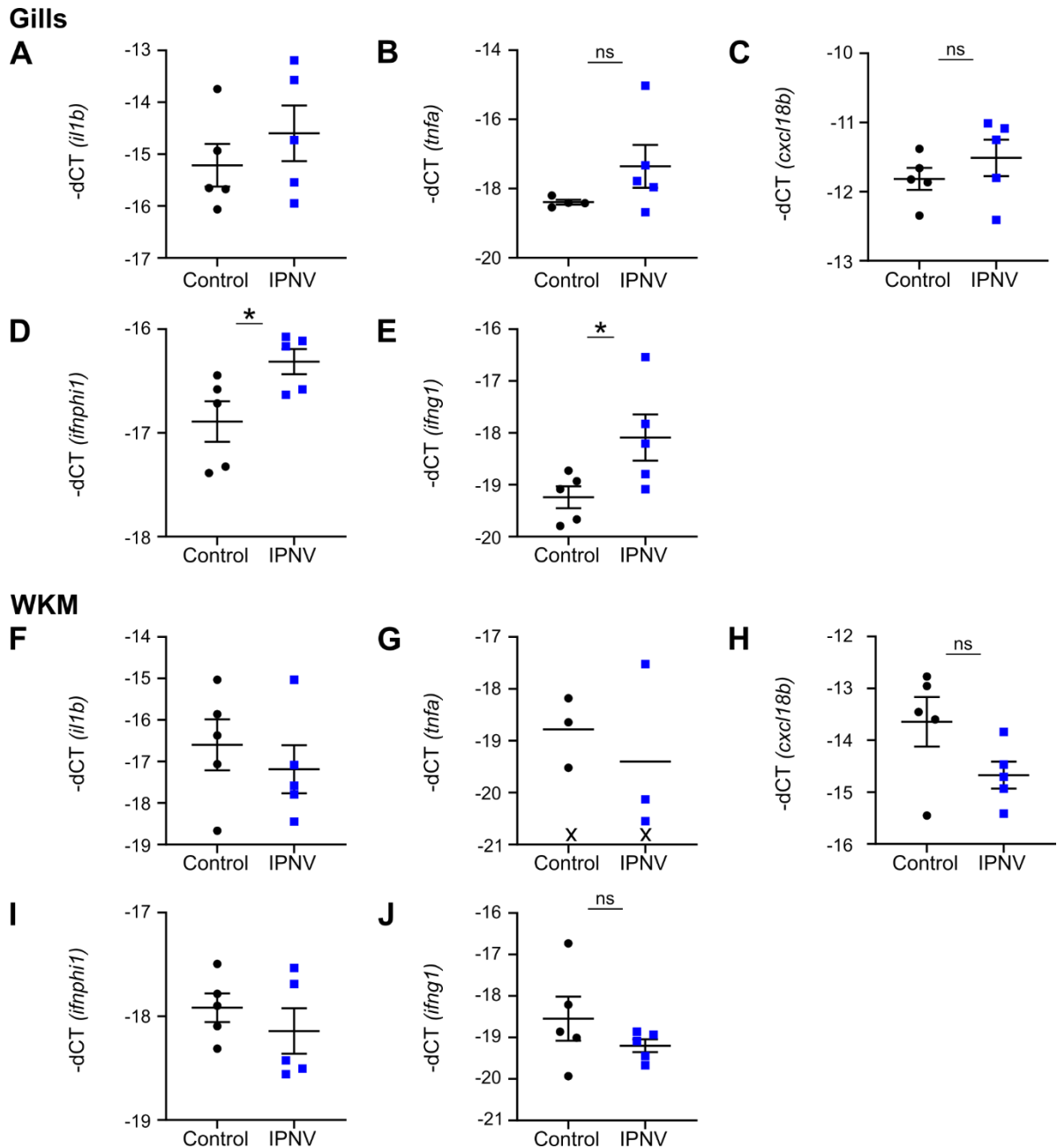
Gills

Figure 5.11 Immune gene transcript analysis in fish challenged with IPNV by topical gill application.

Adult *TraNac* zebrafish were challenged with 5 µl of IPNV (1.35×10^5 PFU) or PBS. Gills (A-E) and WKM (F-J) were harvested 1 dpc. Transcript levels for *il1b* (A, F), *tnfa* (B, G), *cxcl18b* (C, H), *ifnphi1* (D, I), and *ifng1* (E, J) were measured by qRT-PCR and are shown relative to 18S transcript levels. Data represents one experiment and each dot represents one fish (n = 4-5). Mean and SEM shown. Unpaired t-test or Welch's test performed, *: $p \leq 0.05$, ns: non-significant ($p > 0.05$). X on the chart indicates ≥ 1 sample in the group had undetected transcripts (SEM not calculated), and therefore statistical testing was not performed for these groups.

5.3.3.2 Viral load in fish challenged with IPNV at 28.5°C

To measure viral load, gill and WKM samples were analysed by qRT-PCR for the IPNV VP2 gene. To evaluate VP2 detection in zebrafish tissue, gills from unchallenged fish were dissected, mixed with 5 µl of IPNV (1.35×10^5 PFU) and processed for qRT-PCR in the same way as experimental samples. qRT-PCR for VP2 was performed on a 1:5 dilution of this sample (Figure 5.12). This showed that VP2 could be reliably detected when up to 125 times less than in the initial dose used in zebrafish challenges.

For i.p. challenged fish, control gills and WKM (n = 4) at 1 dpc had CT values of ≥33. Furthermore, amplified products of some of the samples had two melting temperatures indicating non-specific amplification. This was also the case for IPNV-challenged gills and WKM (n = 5) indicating a lack of detectable VP2 in these samples.

Due to the COVID-19 pandemic, access to raw data for an additional set samples at 1 dpc (n = 3) and 6 dpc (n = 3) is not currently possible. Preliminary analysis during the qRT-PCR run indicated that VP2 was not detected in any of these samples. Should the data be recoverable, it will be fully analysed.

In topical gill challenges, control and IPNV-challenged gills and WKM at 1 dpc (n = 4 - 5) had CT values of ≥32. Some samples also exhibited multiple melting temperatures for the amplified products, again indicating non-specific amplification. This shows that VP2 was not detected in challenged fish.
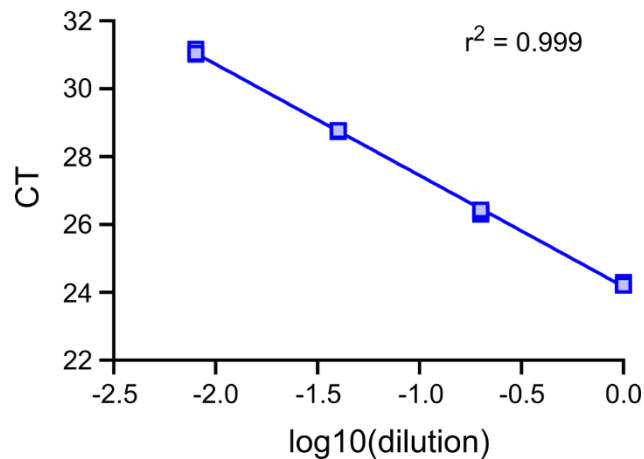
Figure 5.12 Standard curve of IPNV VP2 gene by qRT-PCR analysis.

Gill tissue was mixed with 5 μl of IPNV (1.35 x 10^5 PFU) and used for RNA extraction and cDNA synthesis (n = 2). cDNA was serially diluted 1:5 and used for qRT-PCR for the IPNV VP2 gene. Reactions for each dilution were run in triplicate. CT values for dilutions with standard deviations ≤ 0.4, and a single melting temperature were used to generate the standard curve. Simple linear regression was performed. Data shown is from one sample but representative of both samples.

5.3.3.3 Viral load in fish challenged with IPNV at 15°C

Since challenges at 28.5°C were unsuccessful in establishing IPNV infection, the next aim was to assess infection in zebrafish challenged at 15°C. As previously mentioned, zebrafish can tolerate a large range of temperatures including cooler temperatures (Vergauwen et al., 2010). Adult *TraNac* zebrafish were acclimatised to 15°C by reducing the water temperature gradually over 5 days (reduction by 0.5°C every 4 h). The fish were then challenged with 5 μl of IPNV (1.35 x 10^5 PFU) (n = 5) or PBS (n = 5) by i.p. injection. Another set of fish were also challenged with 5 μl of IPNV (1.35 x 10^5 PFU) by gill application (n =5).

Due to the lack of immune response and viral presence in challenged fish at 28.5°C, the focus for these challenges was to first assess viral load. Gills and WKM were harvested at 1 dpc and analysed for viral VP2 by qRT-PCR. Control and IPNV-challenged samples had similar CT values (31-33) showing that VP2 was not detected in any sample. This shows that IPNV did not establish detectable infection at 15°C.

Due to the lack of viral presence and no gross pathology, these samples were not tested further for changes in immune-related genes.

5.4 Summary

1. **RSV challenges in adults.** RSV did not induce robust inflammation, pathology or increasing viral load in adult zebrafish. This lack of infection was observed at 28.5°C and 33°C and in gill and i.p. challenges.

2. **IAV challenges in zebrafish embryos.** Two IAV strains, PR8 and IAV, did not cause pathology or affect mortality in zebrafish embryos, suggesting a possible lack of infection.

3. **IAV PR8 challenges in zebrafish adults.** I.p. challenge with PR8 may have induced a low level of inflammation in the gills of adult zebrafish and retention of virus in the WKM. However, no pathological disease was observed. Topical gill challenge with PR8 did not induce any pathology, inflammation or retention of virus. Despite the minor response in i.p. challenges, robust infection was not observed in adult zebrafish.

4. **IPNV challenges in zebrafish adults.** Challenge with IPNV did not induce inflammation or pathology regardless of route of exposure or environmental temperature. Furthermore, IPNV virus was not detected in challenged fish at any timepoint.

5.5 Discussion

5.5.1 Assessing viral infection in challenged zebrafish

5.5.1.1 *Virus levels do not increase following challenge in adult zebrafish*

RSV and IPNV RNA were not detected at any timepoint in i.p. injected or gill challenged zebrafish. IAV RNA was also undetectable in gill challenges. This points to three possible explanations: 1) zebrafish are not permissive to the viruses used, 2) virus levels were too low to be detected by the qRT-PCR assays used or 3) the viruses established local infections in other tissues. In one study, IPNV RNA was detected in i.p. injected zebrafish at 2 and 30 dpi using primers for segment A of the IPNV genome (Bello-Perez et al., 2019). This suggests that other qRT-PCR assays may be more sensitive than the ones used in this study. In Atlantic salmon, infectious IPNV was detected by cell culture despite a lack of detectable viral RNA in some samples (Skjesol et al., 2011). This further suggests that viral titre may be a more sensitive measure and thus more appropriate for zebrafish viral models where virus may be present at low levels. This includes asymptomatic IPNV

infections where persistent and low levels of virus have been observed (Bello-Perez et al., 2019; Robledo et al., 2016).

5.5.1.2 *Embryos are not susceptible to pathological infection with IAV in contrast to existing literature*

IAV was previously shown to infect zebrafish embryos (Gabor et al., 2014) therefore this virus was used to test differences in susceptibility between developmental stages. In contrast to previous studies, embryos in this project were not susceptible to pathological infection by PR8 or X31. This does not definitively show a lack of infection since other studies have found that SINV and ZfPV can infect and replicate in larvae without causing major pathology (Balla et al., 2020; Boucontet et al., 2018). However, impaired infection is still one potential explanation for the lack of pathology observed. Both PR8 and X31 replicated efficiently in MDCK cells but it is unknown if viral replication occurred in zebrafish embryos as viral load was not measured. There could be differences between the viral stocks used in this project and those used by Gabor et al. due to the high mutation rate of IAV. Even if the viruses had the same original sequence, propagation of the viruses would likely have resulted in accumulation of different mutations (Van den Hoecke et al., 2015). This could affect the fitness and pathogenicity of the virus in zebrafish. PR8 and X31 were found to increase 10-20 fold over 3 days in the study by Gabor et al., which is much less than the increases observed here in MDCK cells and in other studies in mice (Toapanta and Ross, 2009; Verbist et al., 2012). This indicates that the viruses do not replicate efficiently in zebrafish and therefore any impairments in replication would likely lead to major reductions in viral load.

The discrepancies between this project and the results of Gabor et al. could also be due to differences in the zebrafish host. Animals maintained in different facilities are known to have differences in their microbiota and may be exposed to different facility pathogens, both of which could influence immune responses to viral challenge. Recent studies have detected a zebrafish picornavirus (ZfPV) in fish from several facilities around the world including some in the UK (Altan et al., 2019; Balla et al., 2020). This picornavirus was detected in larvae from at least 5 dpf and induced a robust antiviral response (Balla et al., 2020). Therefore, embryos positive for ZfPV may respond differently to IAV than zebrafish negative for ZfPV. This is supported by co-challenge experiments in adult zebrafish which showed that IPNV can interfere with SVCV infections, enhancing the

immune response and improving survival (Bello-Perez et al., 2019). It is currently unknown if zebrafish in this project or those used by Gabor et al. contained ZfPV however this is clearly an important factor to account for in future immunological studies.

5.5.2 Zebrafish immune response to viral exposure

5.5.2.1 *Possible reasons for the lack of response to RSV and minimal response to IPNV*

Neither RSV nor IPNV had major alterations on cytokine, chemokine or IFN transcript levels in the gills or WKM indicating the lack of a robust immune response. Transient changes could have occurred outside of the 2-3 timepoints measured but it is clear that a sustained response was not present in these tissues. Experiments in human bronchial epithelial cells have shown that inactivated virus and individual RSV proteins can induce chemokine production therefore an immune response does not always require live replicating virus (Oshansky et al., 2010). This response can involve interactions with cell-surface TLR4 although it is unknown whether zebrafish Tlr4a/b would also form these interactions (Kurt-Jones et al., 2000). Experiments in mice have also shown that neutrophil recruitment and production of neutrophil-associated proteins are dependent on live virus (Kirsebom et al. 2019). Therefore, lack of RSV replication in zebrafish could also have led to the lack of immune response. This could have been due to the viruses being unable to enter cells and thus unable to interact with endosomal and cytosolic PRRs. Several receptors for RSV have been proposed but their relative importance in infection is unclear. Even if RSV was internalised in zebrafish cells by receptor-independent pathways, the virus may not be able to undergo uncoating without receptor binding. This would likely limit or alter interactions between PRRs and viral genomic material.

Since undetectable levels of viral replication may have occurred it is also possible that the viral load was too low to stimulate an immune response. Furthermore, live RSV has been found to inhibit IFN response pathways which may have also occurred in zebrafish (Ling et al., 2009; Ramaswamy et al., 2004). This may also be the case for IPNV which has been found to persist in zebrafish without inducing changes in type I IFN, ISG, or cytokine transcript levels (Bello-Perez et al., 2019). This aligns with the results of this thesis where only a minimal response was observed in fish topically challenged with IPNV. This is

further supported by studies showing immunosuppressive activities of the virus *in vitro* (Lauksund et al., 2015; Novoa et al., 1996; Skjesol et al., 2009). It is important to note that only five genes were investigated in RSV and IPNV challenges and other inflammatory or pathological changes may have occurred. In a previous zebrafish study, IPNV induced a transient reduction in the number of erythrocytes in the kidney although inflammatory markers were not assessed (Lapatra et al., 2000).

The lack of detectable viral or robust immune response to RSV supports evidence that this virus replicates poorly in non-human hosts. Many restriction factors have been suggested to influence RSV infection and replication including several host cell surface components, host cytoskeleton elements and heat shock proteins (Griffiths et al., 2017; Kallewaard et al., 2005; Radhakrishnan et al., 2010). Therefore, it may be difficult to identify the factors limiting infection in zebrafish. I propose that IPNV is a more useful zebrafish model since previous evidence indicates that the virus does infect zebrafish and this may provide an opportunity to assess host resistance and viral persistence, including in the gills. However, the minimal immune response indicates that IPNV is not a useful model to investigate inflammation in the gills. This would be better studied using R848 which consistently induces robust immune responses in the gills, including antiviral pathways.

5.5.2.2 Possible transient response to IAV i.p. injection

In contrast to RSV and IPNV, IAV i.p. challenge may have induced a moderate increase in *il1b* and *cxcl18b* transcript levels in the gills suggesting possible low level inflammation. However, viral RNA was undetected in these gills. Another study in rainbow trout also observed altered chemokine transcript levels in response to VHSV infection despite a lack of detectable viral RNA in the gills (Montero et al., 2011). The results in zebrafish and rainbow trout suggest that the gills may respond efficiently to very low levels of local or circulating virus. Alternatively, immune cells may be activated in infected sites like the kidney or fin bases and rapidly home to the gills, perhaps attracted by the increase in chemokines. Although many studies have investigated cellular responses to infection in zebrafish, there do not appear to be any studies focused on the gills. Given that we lack comprehensive understanding on the origins, dynamics and functions of a major immunological structure, the ILT, more investigation on immune cell migration would greatly improve our understanding of the gills.

In rainbow trout VHSV infections, viral RNA was found in the fin bases but the chemokine response occurred later and involved fewer genes than the gills (Montero et al., 2011). The authors suggested that this could be due to the virus inhibiting responses. This could also be the case in zebrafish PR8 infections since cytokine and chemokine transcript levels were unchanged in the WKM whilst viral RNA was present in some samples for at least 1-4 dpc. IAV has previously been shown to interfere with IFN signalling and inflammasome activation (Stasakova et al., 2005; Xia et al., 2016). Conversely the response in the gills could make them more resistant to infection thus leading to lower virus levels. Although cytokine and chemokines were upregulated in zebrafish gills, IFNs/ISGs remained unchanged suggesting that an antiviral response may not have occurred. It is therefore possible that fish responded to other components in the viral stock rather than the virus itself. Controls using uninfected cell supernatant or inactivated virus would be needed to assess the contributions from these components and live virus respectively.

6   Chapter 6 – Final discussion

6.1   Significance and key findings

Our ability to address unanswered questions about the role of the respiratory mucosa depends on the experimental models available. There are currently numerous *in vitro* and *in vivo* models, but the ability to monitor and manipulate an intact mucosa and recapitulate elements of human respiratory infection varies considerably between models. In this thesis I sought to expand and evaluate the zebrafish gill model, particularly with regards to viral infection and immune responses. To achieve this, I developed and assessed several experimental methods and investigated different aspects of immune cells, immune pathways, and viral susceptibility in the gills.

In **Chapter 3**, flow cytometry and microscopy tools were validated for assessment of immune cell morphology, *in situ* localisation and abundance in zebrafish gills. This revealed that the gills contain diverse and abundant innate and adaptive immune cells which are present from early stages of development. These immune cells are capable of antigen-uptake and form dynamic interactions showing that the gills are a useful model to study functional aspects of mucosal immune cells. ILT was identified in the gills displaying both similarities and differences to mammalian MALT and extending further than previously described in other species (Dalum et al. 2015). This provides a unique opportunity to study development, function and responses of mucosal lymphoid aggregates in zebrafish as similar structures have not been described in other mucosal tissues.

In **Chapter 4**, gill immune responses were investigated by challenging zebrafish with compounds mimicking or derived from pathogens. R848, a viral mimic, and LPS, a bacterial component, induced inflammatory responses in the gills but only R848 induced an IFN response. This highlighted that foreign materials stimulate specific immune pathways in the gills. This aligns with our understanding of PAMP recognition through different PRRs although the specific receptors for the ligands used are not fully defined in zebrafish. The response to R848 involved changes in neutrophils and lymphocytes and may have also involved *cd4-1*:mCherry+ myeloid cells which interacted with fluorophore-labelled R848. The response was intact but marginally affected by acute antibiotic treatment. This highlighted R848 gill challenge as a useful model to investigate the

initiation, progression and modulation of antiviral immune pathways in the respiratory mucosa.

In **Chapter 5**, zebrafish were challenged with RSV, IAV or IPNV and were resistant to pathological infection with all three viruses. This revealed discrepancies with previous studies with IAV in zebrafish (Gabor et al., 2014) and highlighted the remaining gap for a zebrafish gill viral infection model. Many of the factors influencing viral tropism are still unknown which can make it difficult to develop new infection models. However, the lack of infection observed in this project provides the opportunity to interrogate some of these factors.

6.2   Future work

6.2.1   Further defining the structure of the ILT

In teleosts, highly organized lymphoid structures have not been identified beyond the gills. This contrasts with the presence of lymph nodes and MALT structures in mammals. This thesis expands on previous work on ILT in the gills, but there are remaining questions on the evolutionary origins and functional properties of this tissue. It is currently unclear what role this tissue plays compared to lymphocytes diffusely distributed in mucosal tissues of teleosts. Furthermore, ILT is absent in some teleost species so it is not clear if this tissue arose independently in some species or was lost during evolution (Rességuier et al., 2020). To address these questions the ILT needs to be more precisely defined both in terms of structure and ontogeny. In this thesis the ILT was identified by accumulations of lymphocytes but other structural elements were not investigated. In the ILT of Atlantic salmon, lymphocytes are embedded in a network of cytokeratin+ epithelial cells and this could be similarly assessed in zebrafish using immunostaining (Haugarvoll et al., 2008; Paquette et al., 2015). In addition, the ILT in salmon is separated from underlying tissue by a thin basal lamina which is often identified by electron microscopy of gill sections (Haugarvoll et al. 2008; Dalum et al. 2016). In zebrafish this could be investigated using immunostaining of laminin in intact gill arches which would preserve the 3D structure of the tissue and could be used alongside transgenic lines for lymphocytes (Nagendran et al., 2015). Confocal microscopes can only image a limited depth so future studies would benefit from additional imaging techniques to identify the complete 3D structure of the ILT. This

would allow more accurate quantification of the tissue than estimations from sections (Dalum et al. 2016) or measurements performed on confocal images. Optical projection tomography (OPT) is a technique which has been used to obtain complete 3D structures in fluorescent transgenic embryos, adult zebrafish, and dissected tissues (Andrews et al., 2016; Kumar et al., 2016; Lindsey et al., 2018). It could be used with *Tg(lck:GFP)* zebrafish to visualise the 3D distribution of lymphocytes in the ILT. Furthermore, OPT can be used to visualise live fish so the ILT could also be imaged longitudinally to track changes in the structure during development.

Some cellular features were not investigated in this thesis but are important features of mammalian MALT and should be investigated in future studies. This includes M cells and dendritic cells which mediate antigen-sampling. There is little investigation of M cells in teleosts but one study has identified cells in rainbow trout gills with similar lectin-binding patterns to murine M cells (Kato et al., 2018). Some of these cells were identified at the edge of the ILT although their ability to sample antigen was not assessed. DCs have also been identified in dissociated zebrafish gill tissue but without corresponding spatial information (Lugo-Villarino et al., 2010). In this thesis endothelial vessels were identified near the ILT but the *Tg(fli:GFP)* line used did not distinguish venous cells from lymphatic cells. This could be further interrogated using *Tg(lyve1:eGFP)* or *Tg(lyve1:DsRed2)* lines which have been reported to label lymphatic endothelial cells (Okuda et al., 2012). Further study of gill antigen-sampling cells will not only allow comparison to other model organisms, but it would also provide insight for development of fish vaccines, particularly those that target mucosal tissues. Understanding which cells are involved and their mechanism of action could guide strategies to target these cells and potentially enhance vaccine efficacy. In mammalian species, specific antigens have been identified targeting antigen-presenting cells, and with more investigation, novel conserved or fish-specific antigens could similarly be identified.

The identity of *lck*:GFP+ lymphocytes in the gills and ILT was only partially addressed in this project with a minority of cells being *cd4-1*:mCherry+ T cells. Future work could use *rag1-/-* zebrafish mutants, which lack T and B cells, to determine the contribution of adaptive cells to these tissues (Petrie-Hanson et al., 2009). *Rag1-/-* fish still contain *lck*+ NK-like and ILC-like cells however loss of adaptive cells could fundamentally impair ILT development (Hernández et al., 2018; Tang et al., 2017). Furthermore, *rag1-/-* mutants

have poor survival and are thus difficult to raise to adulthood (Tang et al., 2014). Alternative mutants include *rag2-/-* fish and *prkdc-/-* fish which both show impairments in T and B cell populations (Jung et al., 2016; Tang et al., 2014).

6.2.2 Determining the ontogeny and dynamics of immune cells in the gills

Another way to compare the ILT to mammalian MALT is to determine its ontogeny. In this project I identified the narrow window in which ILT appears but the factors driving this development are unknown in zebrafish and in other species. In mammals, specialised lymphoid tissue inducer (LTi) cells are involved in the development of several MALTs through lymphotoxin production (Randall and Mebius, 2014). Some MALTs are not completely dependent on lymphotoxin but display an impaired architecture in its absence. This gene has been identified in zebrafish and found to be upregulated in *Mycobacterium marinum* bacterial infection (Ojanen et al., 2015). However, there is little additional literature on this gene and the only zebrafish mutant reported has not been characterised. Lymphotoxin induces expression of chemokines CXCL13, CCL19, and CCL21 which are also important to the development and organisation of MALT (Rangel-Moreno et al., 2005, 2007). Orthologues of these chemokines have been identified in zebrafish but some are better characterised than others. Future studies could assess transcripts of lymphotoxin and the mentioned chemokines in zebrafish gills at different developmental stages using ISH and qRT-PCR. CCL19 transcripts are highly enriched in salmon ILT indicating that there may be some conservation with mammalian MALT (Bjørgen et al., 2019). Morpholinos could be used to knockdown these genes at in embryos (1 to 8 cell stage) and assess effects on lymphocyte presence in developing gills. However, morpholino knockdown is transient with effects lasting only a few days. Given that ILT develops around 1 month post fertilization, morpholinos are unlikely to affect gene expression around this time. The generation of knockout mutants whilst more laborious are more appropriate to investigate development at later stages. Mutants could be developed with a conditional CreER system to allow temporal regulation of gene knockout.

This thesis identified an early presence of immune cells in the gills but did not determine the origins these cells. In zebrafish, definitive haematopoiesis occurs in the caudal haematopoietic tissue in embryos and in the kidney in later stages. Like in mammals,

zebrafish T cell precursors migrate from this primary haematopoeitic tissue and mature in the thymus. There are several lineage tracing techniques which could be used to determine the origins of immune cells in the gills. Genetic modification techniques like ScarTrace introduce mutations in a targeted genomic site which can be identified by single-cell sequencing (Alemany et al., 2018). This has been used to compare cell lineages and identities in adult zebrafish tissues revealing that the fins contained a macrophage-like population with distinct origins to all other haematopoietic cells. However spatial resolution is lost with this technique. Alternatively the *Tg(ubi:Zebrabow)* line uses a CreLox system to induce expression of multiple fluorescent proteins in cells of developing embryos (Pan et al., 2013). This system can produce around 30 different expression patterns allowing different cell lineages to be visualized from embryonic to adult stages. Due to the multiple fluorescent proteins expressed, specific cell types cannot be identified by crossing Zebrabow fish to other transgenic lines. However, endogenous markers of immune cells, such as zap70 could be detected by immunostaining where a wider range of fluorophores are available (Rességuier et al., 2020). Neither ScarTrace nor Zebrabow reveal the tissue origins of the cells of interest, only the clonal relationships between cells. Spatial origins could be assessed with CreLox transgenic systems where heat-shock is used to induced Cre expression in specific regions, leading to fluorescent protein expression. Recent studies using this system have shown that *mpeg1+* cells in mucosal tissues derive from embryonic caudal hematopoietic tissue and non-haematopoietic tissue (Lin et al., 2019, 2020). Investigation of lymphocytes with this system would require development of a new transgenic line using *lck* or *cd4-1* promoters.

Based on live imaging in this thesis, it is clear that immune cells in the ILT and wider gill tissue are motile. Therefore, the ILT should not be solely defined by the presence of structural and cellular features but also by the behaviour of its cells. It is unknown whether these motile cells are tissue-resident cells or whether they recirculate through the vasculature as observed in lymph nodes. This could be investigated by generating heat-inducible CreLox systems as described above or transgenic lines expressing photoswitching fluorescent proteins. Previous literature shows that these proteins can be photoconverted in internal organs of adult zebrafish (Bek et al., 2020). In these systems, Cre expression or photoconversion could be induced in the gills and photoconverted cells analysed in various tissues to monitor cell migration at different timepoints. These systems could be combined with R848 challenge to determine whether

changes in immune cell distribution are a result of gill-resident or recruited cells. These systems would likely require considerable optimization to ensure efficient and specific Cre expression and photoconversion in the tissues of interest.

6.2.3 Adaptive immune responses in zebrafish gills

In mammals, MALTs are important sites for the induction of adaptive immune responses. In this thesis I identified antigen-sampling cells, T cells, and B cells in close proximity in the gills indicating that this tissue may similarly drive adaptive immune responses. This is supported by studies measuring antibody responses to bacteria in zebrafish gills (Ji et al., 2020). This tissue is easily accessible and can be used to monitor immune responses live making it an attractive model for further studies on mucosal adaptive immunity. However adaptive responses are infrequently studied in zebrafish and fundamental concepts like immunological memory are poorly understood. This should be addressed by further work assessing secondary responses to immune challenges. These could be performed using antigens such as keyhole limpet hemocyanin which is known to stimulate responses in zebrafish and is available as a standardised reagent (Lugo-Villarino et al., 2010; Page et al., 2013). Responses could be assessed by measuring antibody levels, including antigen-specific antibodies. This was achieved in the study by Ji et al. using antibodies against zebrafish IgM and IgZ however, commercially produced antibodies are rarely available (Ji et al., 2020). As an alternative, zebrafish B cell numbers, including antigen-binding B cells, and immunoglobulin transcripts could be measured instead. Increased lymphocyte proliferation is another important feature of memory responses and this could be more precisely investigated using the thymidine analogue, 5-bromo-2′-deoxyuridine (BrdU) and transgenic lines. Pulsing live zebrafish with this compound labels the DNA of proliferating cells and any arising daughter cells (Hinsch and Zupanc, 2007). BrdU can be detected with antibodies allowing quantification with flow cytometry or visualisation *in situ*. Given that lymphocytes in mammalian MALT and lymph nodes proliferate considerably following challenge it would be of interest to evaluate proliferation in the ILT. Proliferating cells have been identified in salmon ILT but it is not clear if the rate of lymphocyte proliferation is altered by immune challenge (Dalum et al. 2016). Cellular organisation and behaviour in the ILT should also be

assessed following challenges as these may provide further insights into the function of this tissue.

6.2.4 Effects of antibiotics and microbiota on the immune response

The microbiota and environmental pathogens are important factors in animal research as they can influence many biological processes. The microbiota of animals housed in different facilities can be considerably different and this is currently a major issue for the reproducibility of experimental studies (Rausch et al., 2016). Within the field of zebrafish research many viral infection models have only been recently developed or have only been reported in a few studies. Given the discrepancies observed between the IAV embryos challenges in this thesis and those previously reported by Gabor et al., it would be sensible to evaluate whether microbial differences can affect infection in the gills. As previously discussed, a first step would be to assess zebrafish facilities for the presence of ZfPV. The effect of antibiotics used in raising zebrafish should also be assessed. In this project zebrafish were raised for two weeks in the presence of penicillin-streptomycin but this is not used in all zebrafish facilities. The correlations between antibiotics use and development of atopic conditions in humans suggests that early exposure in zebrafish could have long-term effects on the immune system.

Understanding the impact of antibiotics on immunity is also important for aquaculture where antibiotics are heavily used. If antibiotics impair the immune system, this could have negative effects on overall fish health but also on vaccine efficacy. In this thesis, acute antibiotic treatment with OTC did not significantly impact the inflammatory response to R848 despite having inflammatory or inhibitory effects in other models. This could be an opportunity to investigate the environmental and host-intrinsic factors that influence the action of antibiotics.

6.2.5 Alternative viruses and pathogens to infect zebrafish gills

The work in this thesis builds on existing gill studies providing a more comprehensive understanding of the different components of the gill immune environment. The gills provide an opportunity to investigate mucosal responses and would benefit from further work to establish an infection model. This would expand our ability to study lymphoid

tissue function, immune cell functions, and differences between mucosal and systemic immune responses. In addition, an infection model would allow investigation of immunoregulatory mechanisms of the gills in an infection context. This would complement insights gained on the role of *il4/13a*, *il4/13b* and *il10* in R848 challenges (Bottiglione et al., 2020). Pathogen exposure could also be combined with other insults such as cigarette exposure and cryoinjury to investigate infection in damaged respiratory tissue (Progatzky, 2014; Progatzky et al., 2015). This would complement ongoing work in the Dallman lab on the ability of zebrafish to repair extensive gill tissue damage without pathological scarring. Given the recent expansion of zebrafish viral infection models, including those using human viruses, a gill infection model could provide new insights relevant to many of these models.

Although use of SVCV is restricted in the UK, this virus could be used to assess gill infection and immunity by other researchers in regions where this is permitted. Alternatively, natural infection with ZfPV could provide new insights about the role of the gills in viral persistence and possibly transmission (Balla et al., 2020). Although antiviral responses were the focus in this thesis, other pathogens could be used to expand the tools available for zebrafish gill studies. *Edwardsiella tarda* is a Gram-negative bacterium which has been used to infect embryos and adult zebrafish and has been detected in the gills. It is a pathogen of major importance in aquaculture as it has a wide species tropism and has caused livestock losses for decades (Xu and Zhang, 2014). Virulent strains rapidly lead to high mortality, but this can be partially rescued by prior vaccination highlighting the potential to study memory responses (Gao et al., 2014). In the gills, *E. tarda* induced a clear adaptive response with higher IgZ and IgZ2 expression and greater B cell numbers (Ji et al., 2020). IgZ production was impaired following reduction of T cell numbers showing that T cell-dependent B cell activation seems to occur in this tissue.

In the absence of an existing gill infection model, the work described in this thesis shows that R848 can be used to investigate antiviral pathways. Future work could exploit this model to identify IFN-producing cells using transgenic *ifnphi1* reporter fish or *in situ* hybridsation (Palha et al., 2013). This work was started in this thesis but required further optimization of ISH probes. R848 could also be assessed for its properties as an adjuvant in future gill infection or vaccination models.

6.2.6 Mechanisms of IPNV persistence or host resistance in zebrafish

In this thesis it was not clear if IPNV persisted at low levels or if the virus failed to establish an infection. Understanding both host resistance and viral persistence, including immune evasion strategies, is important for tackling disease in aquaculture and developing mucosal vaccines that induce protective immune responses. Although findings from studies on IPNV would not be directly translatable to human disease they would expand our broader understanding of viral infections. The current SARS-CoV 2 pandemic powerfully highlights the importance of improving our understanding on viruses to tackle emerging pathogens as rapidly and as effectively as possible.

Future work on IPNV in zebrafish would benefit from using cell culture assays to assess viral load as these may be more sensitive than RNA analyses. In this thesis temperature did not affect viral load, pathology or the immune response in contrast to studies in other fish species (Bang Jensen and Kristoffersen, 2015). Future work should focus on the impact of fish developmental stage since IPNV has not yet been tested in zebrafish larvae. IPNV strains with different virulences should also be assessed in zebrafish to determine whether host or virus factors are more important in the development of infection.

6.3 Wider implications

Our current paradigms of mucosal immunology are largely based on our understanding of mammalian systems however, mucosal surfaces arose long before the emergence of vertebrates. The earliest known mucosal surfaces are present in members of the *Cnidaria* phylum which lack a specialised immune system but contain a mucosal epithelium with a commensal microbiome (Schröder and Bosch, 2016). Mucosal surfaces in different species have been shaped by different selection pressures and are therefore likely to exhibit differences in function and development. Continued studies in fish will broaden our understanding of mucosal immunity and how this intersects with other physiological demands in organisms. In this thesis the gills were evaluated as a model for studying respiratory mucosal immunology and they displayed some similarities to the mammalian respiratory tract. However, the gills also have some major functional differences to the lungs and are more directly exposed to ingested food which is likely to impact immunity. Exploring these differences may reveal new insights into the mechanisms regulating immune cells in mucosal tissues. The identification of ILT in salmonid species and now in

zebrafish has stimulated new questions about fish immunity. Fish species were long thought to lack organized lymphoid tissues and ILT challenges this paradigm. Further study of this tissue could address fundamental questions about why lymphocytes aggregate, how this is achieved and what drove the evolution of lymphoid tissues. New insights from this work could direct future studies on mammalian tertiary lymphoid tissue whose function and development are not well understood. Work in fish could also interrogate some of the debated theories on mucosal immunity such as cross-talk between different mucosal tissues.

In addition to providing opportunities to study the wider role of mucosal immune systems, the gills provide an opportunity to better understand factors affecting fish health and immunity. This is highly relevant for aquaculture where infectious diseases jeopardise food safety and result in major economic losses (Assefa and Abunna, 2018). This is also relevant for assessing the impact of environmental changes on fish species, which is a major concern given the level of human-driven pollution in aquatic ecosystems. The insights gained in this thesis on immune cell presence and function should be used to guide new research into methods to prevent and treat insults to fish immunity. For example, the finding that zebrafish gill ILT develops within a short window could be used to further explore factors that can enhance protective immune responses in young fish, as has been done for other tissues (Salinas et al., 2015). This is important in aquaculture as vaccinating fish early can help avoid future disease outbreaks and livestock loss - especially given that younger fish are more susceptible to some infections. Although research in this thesis focused on fish, these insights may translate to other gill-bearing organisms such as molluscs and some salamanders.

In conclusion, this thesis reports that zebrafish gills are immune-rich tissues containing diverse immune cells and a distinct lymphoid structure. Several methods were used to gain new insights into the development, properties and functions of these cells demonstrating the toolkit available to study the gill mucosa. Although the viruses used here did not establish detectable infection, immune responses in the gills can still be studied using pathogen-related compounds such as R848 and LPS. Overall zebrafish gills complement existing respiratory models and continued study will shed further light on the dynamics and complexities of mucosal tissues.

7 References

Aas, I.B., Austbø, L., König, M., Syed, M., Falk, K., Hordvik, I., and Koppang, E.O. (2014). Transcriptional Characterization of the T Cell Population within the Salmonid Interbranchial Lymphoid Tissue. J. Immunol. *193*, 3463–3469.

Aas, I.B., Austbø, L., Falk, K., Hordvik, I., and Koppang, E.O. (2017). The interbranchial lymphoid tissue likely contributes to immune tolerance and defense in the gills of Atlantic salmon. Dev. Comp. Immunol. *76*, 247–254.

Abt, M.C., Osborne, L.C., Monticelli, L.A., Doering, T.A., Alenghat, T., Sonnenberg, G.F., Paley, M.A., Antenus, M., Williams, K.L., Erikson, J., et al. (2012). Commensal Bacteria Calibrate the Activation Threshold of Innate Antiviral Immunity. Immunity *37*, 158–170.

Abt, M.C., Buffie, C.G., Sušac, B., Becattini, S., Carter, R.A., Leiner, I., Keith, J.W., Artis, D., Osborne, L.C., and Pamer, E.G. (2016). TLR-7 activation enhances IL-22-mediated colonization resistance against vancomycin-resistant enterococcus. Sci. Transl. Med. *8*, 327ra25.

Abu-Siniyeh, A., and Al-Zyoud, W. (2020). Highlights on selected microscopy techniques to study zebrafish developmental biology. Lab. Anim. Res. *36*.

Adamek, M., Hazerli, D., Matras, M., Teitge, F., Reichert, M., and Steinhagen, D. (2017). Viral infections in common carp lead to a disturbance of mucin expression in mucosal tissues. Fish Shellfish Immunol. *71*, 353–358.

Agace, W.W. (2006). Tissue-tropic effector T cells: Generation and targeting opportunities. Nat. Rev. Immunol. *6*, 682–692.

Aggad, D., Mazel, M., Boudinot, P., Mogensen, K.E., Hamming, O.J., Hartmann, R., Kotenko, S., Herbomel, P., Lutfalla, G., and Levraud, J.-P. (2009). The two groups of zebrafish virus-induced interferons signal via distinct receptors with specific and shared chains. J. Immunol. *183*, 3924–3931.

Aggad, D., Stein, C., Sieger, D., Mazel, M., Boudinot, P., Herbomel, P., Levraud, J.-P., Lutfalla, G., and Leptin, M. (2010). In vivo analysis of Ifn-γ1 and Ifn-γ2 signaling in zebrafish. J. Immunol. *185*, 6774–6782.

Agius, C., and Roberts, R.J. (2003). Melano-macrophage centres and their role in fish pathology. J. Fish Dis. *26*, 499–509.

Agrawal, A.S., Garron, T., Tao, X., Peng, B.-H., Wakamiya, M., Chan, T.-S., Couch, R.B., and Tseng, C.-T.K. (2015). Generation of a Transgenic Mouse Model of Middle East Respiratory Syndrome Coronavirus Infection and Disease. J. Virol. *89*, 3659–3670.

Ahmed, R., Oldstone, M.B.A., and Palese, P. (2007). Protective immunity and susceptibility to infectious diseases: Lessons from the 1918 influenza pandemic. Nat. Immunol. *8*, 1188–1193.

Al-Garawi, A.A., Fattouh, R., Walker, T.D., Jamula, E.B., Botelho, F., Goncharova, S., Reed, J., Stampfli, M.R.,

O'Byrne, P.M., Coyle, A.J., et al. (2009). Acute, but Not Resolved, Influenza A Infection Enhances Susceptibility to House Dust Mite-Induced Allergic Disease. J. Immunol. *182*, 3095–3104.

Alemany, A., Florescu, M., Baron, C.S., Peterson-Maduro, J., and van Oudenaarden, A. (2018). Whole-organism clone tracing using single-cell sequencing. Nature.

Aleshina, E., Miroshnikova, E., and Sizova, E. (2019). Transformation of microbiota of fish intestines and gills against the background of molybdenum oxide nanoparticles in environment. Int. J. Environ. Sci. Technol.

Allard, B., Panariti, A., and Martin, J.G. (2018). Alveolar Macrophages in the Resolution of Inflammation, Tissue Repair, and Tolerance to Infection. Front. Immunol. *9*, 1777.

Allen, C.D.C., Okada, T., and Cyster, J.G. (2007). Germinal-Center Organization and Cellular Dynamics. Immunity *27*, 190–202.

Allie, S.R., and Randall, T.D. (2017). Pulmonary immunity to viruses. Clin. Sci. *131*, 1737–1762.

Altan, E., Kubiski, S. V., Boros, Á., Reuter, G., Sadeghi, M., Deng, X., Creighton, E.K., Crim, M.J., and Delwart, E. (2019). A Highly Divergent Picornavirus Infecting the Gut Epithelia of Zebrafish (Danio rerio) in Research Institutions Worldwide. Zebrafish *16*, 291–299.

Alturki, S.O., Alturki, S.O., Connors, J., Cusimano, G., Kutzler, M.A., Izmirly, A.M., and Haddad, E.K. (2020). The 2020 Pandemic: Current SARS-CoV-2 Vaccine Development. Front. Immunol. *11*, 1880.

Anderson, A.J., Snelling, T.L., Moore, H.C., and Blyth, C.C. (2017). Advances in Vaccines to Prevent Viral Respiratory Illnesses in Children. Pediatr. Drugs *19*, 523–531.

Andrews, N. (2016). Spatio-temporal Mapping of Protein Activity in Live Zebrafish using FRET FLIM OPT. Imperial College London.

Andrews, N., Ramel, M.-C., Kumar, S., Alexandrov, Y., Kelly, D.J., Warren, S.C., Kerry, L., Lockwood, N., Frolov, A., Frankel, P., et al. (2016). Visualising apoptosis in live zebrafish using fluorescence lifetime imaging with optical projection tomography to map FRET biosensor activity in space and time. J. Biophotonics *9*, 414–424.

Angelidis, I., Simon, L.M., Fernandez, I.E., Strunz, M., Mayr, C.H., Greiffo, F.R., Tsitsiridis, G., Ansari, M., Graf, E., Strom, T.M., et al. (2019). An atlas of the aging lung mapped by single cell transcriptomics and deep tissue proteomics. Nat. Commun. *10*, 1–17.

Angulo, C., Alamillo, E., Hirono, I., Kondo, H., Jirapongpairoj, W., Perez-Urbiola, J.C., and Reyes-Becerril, M. (2018). Class B CpG-ODN2006 is highly associated with IgM and antimicrobial peptide gene expression through TLR9 pathway in yellowtail Seriola lalandi. Fish Shellfish Immunol. *77*, 71–82.

Antinucci, P., and Hindges, R. (2016). A crystal-clear zebrafish for in vivo imaging. Sci. Rep. *6*, 1–10.

Anwar, M.A., Shah, M., Kim, J., and Choi, S. (2019). Recent clinical trends in Toll-like receptor targeting

References

therapeutics. Med. Res. Rev. *39*, 1053–1090.

Aquilino, C., Castro, R., Fischer, U., and Tafalla, C. (2014). Transcriptomic responses in rainbow trout gills upon infection with viral hemorrhagic septicemia virus (VHSV). Dev. Comp. Immunol. *44*, 12–20.

Ardain, A., Porterfield, J.Z., Kløverpris, H.N., and Leslie, A. (2019). Type 3 ILCs in lung disease. Front. Immunol. *10*, 92.

Arimura, H. (1975). Correlation between molecular size and interferon- inducing activity of poly I:C. Acta Virol. *19*, 457–466.

Armstrong, S.M., Wang, C., Tigdi, J., Si, X., Dumpit, C., Charles, S., Gamage, A., Moraes, T.J., and Lee, W.L. (2012). Influenza Infects Lung Microvascular Endothelium Leading to Microvascular Leak: Role of Apoptosis and Claudin-5. PLoS One *7*, e47323.

Ascough, S., Paterson, S., and Chiu, C. (2018). Induction and Subversion of Human Protective Immunity: Contrasting Influenza and Respiratory Syncytial Virus. Front. Immunol. *9*, 323.

Ascough, S., Vlachantoni, I., Kalyan, M., Haijema, B.J., Wallin-Weber, S., Dijkstra-Tiekstra, M., Ahmed, M.S., Van Roosmalen, M., Grimaldi, R., Zhang, Q., et al. (2019). Local and Systemic Immunity against Respiratory Syncytial Virus Induced by a Novel Intranasal Vaccine A Randomized, Double-Blind, Placebo-controlled Clinical Trial. Am. J. Respir. Crit. Care Med. *200*, 481–492.

Assefa, A., and Abunna, F. (2018). Maintenance of Fish Health in Aquaculture: Review of Epidemiological Approaches for Prevention and Control of Infectious Disease of Fish. Vet. Med. Int. *2018*.

ATCC (2012). Converting TCID50 to plaque forming units PFU.

Austbø, L., Aas, I.B., König, M., Weli, S.C., Syed, M., Falk, K., and Koppang, E.O. (2014). Transcriptional response of immune genes in gills and the interbranchial lymphoid tissue of Atlantic salmon challenged with infectious salmon anaemia virus. Dev. Comp. Immunol. *45*, 107–114.

Bailey, E.S., Fieldhouse, J.K., Choi, J.Y., and Gray, G.C. (2018). A Mini Review of the Zoonotic Threat Potential of Influenza Viruses, Coronaviruses, Adenoviruses, and Enteroviruses. Front. Public Heal. *6*, 104.

Bajoghli, B., Aghaallaei, N., Hess, I., Rode, I., Netuschil, N., Tay, B.H., Venkatesh, B., Yu, J.K., Kaltenbach, S.L., Holland, N.D., et al. (2009). Evolution of Genetic Networks Underlying the Emergence of Thymopoiesis in Vertebrates. Cell *138*, 186–197.

Balla, K.M., Lugo-Villarino, G., Spitsbergen, J.M., Stachura, D.L., Hu, Y., Bañuelos, K., Romo-Fewell, O., Aroian, R. V, and Traver, D. (2010). Eosinophils in the zebrafish: prospective isolation, characterization, and eosinophilia induction by helminth determinants. Blood *116*, 3944–3954.

Balla, K.M., Rice, M.C., Gagnon, J.A., and Elde, N.C. (2020). Linking Virus Discovery to Immune Responses Visualized during Zebrafish Infections. Curr. Biol. *30*, 2092-2103.e5.

Bang Jensen, B., and Kristoffersen, A. (2015). Risk factors for outbreaks of infectious pancreatic necrosis

275

(IPN) and associated mortality in Norwegian salmonid farming. Dis. Aquat. Organ. *114*, 177–187.

Bao, L., Deng, W., Huang, B., Gao, H., Liu, J., Ren, L., Wei, Q., Yu, P., Xu, Y., Qi, F., et al. (2020). The pathogenicity of SARS-CoV-2 in hACE2 transgenic mice. Nature *583*, 830–833.

Baptista, A.P., Gola, A., Huang, Y., Milanez-Almeida, P., Torabi-Parizi, P., Urban, J.F., Shapiro, V.S., Gerner, M.Y., and Germain, R.N. (2019). The Chemoattractant Receptor Ebi2 Drives Intranodal Naive CD4+ T Cell Peripheralization to Promote Effective Adaptive Immunity. Immunity *50*, 1188-1201.e6.

Barbalat, R., Lau, L., Locksley, R.M., and Barton, G.M. (2009). Toll-like receptor 2 on inflammatory monocytes induces type i interferon in response to viral but not bacterial ligands. Nat. Immunol. *10*, 1200–1209.

Barros-Becker, F., Romero, J., Pulgar, A., and Feijóo, C.G. (2012). Persistent Oxytetracycline Exposure Induces an Inflammatory Process That Improves Regenerative Capacity in Zebrafish Larvae. PLoS One *7*, e36827.

Bartlett, N.W., Walton, R.P., Edwards, M.R., Aniscenko, J., Caramori, G., Zhu, J., Glanville, N., Choy, K.J., Jourdan, P., Burnet, J., et al. (2008). Mouse models of rhinovirus-induced disease and exacerbation of allergic airway inflammation. Nat. Med. *14*, 199–204.

Basnet, S., Palmenberg, A.C., and Gern, J.E. (2019). Rhinoviruses and Their Receptors. Chest *155*, 1018–1025.

Bawage, S.S., Tiwari, P.M., Pillai, S., Dennis, V.A., and Singh, S.R. (2019). Antibiotic Minocycline Prevents Respiratory Syncytial Virus Infection. Viruses *11*, 739.

Beare, A.S., Schild, G.C., and Craig, J.W. (1975). Trials in man with live recombinants made from A/PR/8/34 (H0 N1) and wild H3 N2 influenza viruses. Lancet *306*, 729–732.

Becker, S., and Soukup, J.M. (1999). Airway epitheliol cell-induced activation of monocytes and eosinophils in respiratory syncytial viral infection. Immunobiology *201*, 88–106.

Behzadi, M.A., and Leyva-Grado, V.H. (2019). Overview of current therapeutics and novel candidates against influenza, respiratory syncytial virus, and Middle East respiratory syndrome coronavirus infections. Front. Microbiol. *10*, 1327.

Bek, J.W., De Clercq, A., De Saffel, H., Soenens, M., Huysseune, A., Witten, P.E., Coucke, P.J., and Willaert, A. (2020). Photoconvertible fluorescent proteins: a versatile tool in zebrafish skeletal imaging. J. Fish Biol. jfb.14335.

Beli, E., Clinthorne, J.F., Duriancik, D.M., Hwang, Ii., Kim, S., and Gardner, E.M. (2011). Natural killer cell function is altered during the primary response of aged mice to influenza infection. Mech. Ageing Dev. *132*, 503–510.

Bello-Perez, M., Medina-Gali, R., Coll, J., and Perez, L. (2019). Viral interference between infectious pancreatic necrosis virus and spring viremia of carp virus in zebrafish. Aquaculture *500*, 370–377.

Bem, R.A., Domachowske, J.B., and Rosenberg, H.F. (2011). Animal models of human respiratory syncytial virus disease. Am. J. Physiol. Lung Cell. Mol. Physiol. *3*, 148–156.

Benam, K.H., Villenave, R., Lucchesi, C., Varone, A., Hubeau, C., Lee, H.H., Alves, S.E., Salmon, M., Ferrante, T.C., Weaver, J.C., et al. (2016). Small airway-on-a-chip enables analysis of human lung inflammation and drug responses in vitro. Nat. Methods *13*, 151–157.

Bermúdez, R., Losada, A.P., de Azevedo, A.M., Guerra-Varela, J., Pérez-Fernández, D., Sánchez, L., Padrós, F., Nowak, B., and Quiroga, M.I. (2018). First description of a natural infection with spleen and kidney necrosis virus in zebrafish. J. Fish Dis. *41*, 1283–1294.

Bernard, J.J., Cowing-Zitron, C., Nakatsuji, T., Muehleisen, B., Muto, J., Borkowski, A.W., Martinez, L., Greidinger, E.L., Yu, B.D., and Gallo, R.L. (2012). Ultraviolet radiation damages self noncoding RNA and is detected by TLR3. Nat. Med. *18*, 1286–1290.

Bernasconi, E., Pattaroni, C., Koutsokera, A., Pison, C., Kessler, R., Benden, C., Soccal, P.M., Magnan, A., Aubert, J.D., Marsland, B.J., et al. (2016). Airway microbiota determines innate cell inflammatory or tissue remodeling profiles in lung transplantation. Am. J. Respir. Crit. Care Med. *194*, 1252–1263.

Bessa, J., Jegerlehner, A., Hinton, H.J., Pumpens, P., Saudan, P., Schneider, P., and Bachmann, M.F. (2009). Alveolar Macrophages and Lung Dendritic Cells Sense RNA and Drive Mucosal IgA Responses. J. Immunol. *183*, 3788–3799.

Bhowmick, R., and Gappa-Fahlenkamp, H. (2016). Cells and Culture Systems Used to Model the Small Airway Epithelium. Lung *194*, 419–428.

Bieback, K., Lien, E., Klagge, I.M., Avota, E., Schneider-Schaulies, J., Duprex, W.P., Wagner, H., Kirschning, C.J., ter Meulen, V., and Schneider-Schaulies, S. (2002). Hemagglutinin Protein of Wild-Type Measles Virus Activates Toll-Like Receptor 2 Signaling. J. Virol. *76*, 8729–8736.

Birmingham, J.M., Patil, S., Li, X.M., and Busse, P.J. (2013). The effect of oral tolerance on the allergic airway response in younger and aged mice. J. Asthma *50*, 122–132.

Bjørgen, H., Løken, O.M., Aas, I.B., Fjelldal, P.G., Hansen, T., Austbø, L., and Koppang, E.O. (2019). Visualization of CCL19-like transcripts in the ILT, thymus and head kidney of Atlantic salmon (Salmo salar L.). Fish Shellfish Immunol. *93*, 763–765.

Björklund, A.K., Forkel, M., Picelli, S., Konya, V., Theorell, J., Friberg, D., Sandberg, R., and Mjösberg, J. (2016). The heterogeneity of human CD127+ innate lymphoid cells revealed by single-cell RNA sequencing. Nat. Immunol. *17*, 451–460.

Blazewicz, S.J., Barnard, R.L., Daly, R.A., and Firestone, M.K. (2013). Evaluating rRNA as an indicator of microbial activity in environmental communities: Limitations and uses. ISME J. *7*, 2061–2068.

Boehm, T., and Swann, J.B. (2014). Origin and Evolution of Adaptive Immunity. Annu. Rev. Anim. Biosci. *2*, 259–283.

Boehm, T., Hess, I., and Swann, J.B. (2012). Evolution of lymphoid tissues. Trends Immunol. *33*, 315–321.

Boltana, S., Rey, S., Roher, N., Vargas, R., Huerta, M., Huntingford, F.A., Goetz, F.W., Moore, J., Garcia-Valtanen, P., Estepa, A., et al. (2013). Behavioural fever is a synergic signal amplifying the innate immune response. Proc. R. Soc. B Biol. Sci. *280*, 20131381–20131381.

Borsutzky, S., Cazac, B.B., Roes, J., and Guzmán, C.A. (2004). TGF-β Receptor Signaling Is Critical for Mucosal IgA Responses. J. Immunol. *173*, 3305–3309.

Borvinskaya, E., Gurkov, A., Shchapova, E., Karnaukhov, D., Sadovoy, A., Meglinski, I., and Timofeyev, M. (2018). Simple and effective administration and visualization of microparticles in the circulatory system of small fishes using kidney injection. J. Vis. Exp. *2018*, e57491.

Botos, I., Segal, D.M., and Davies, D.R. (2011). The structural biology of Toll-like receptors. Structure *19*, 447–459.

Bottiglione, F., Dee, C.T., Lea, R., Zeef, L.A.H., Badrock, A.P., Wane, M., Bugeon, L., Dallman, M.J., Allen, J.E., and Hurlstone, A.F.L. (2020). Zebrafish IL-4–like Cytokines and IL-10 Suppress Inflammation but Only IL-10 Is Essential for Gill Homeostasis. J. Immunol. ji2000372.

Boucontet, L., Passoni, G., Thiry, V., Maggi, L., Herbomel, P., Levraud, J.P., and Colucci-Guyon, E. (2018). A model of superinfection of virus-infected zebrafish larvae: Increased susceptibility to bacteria associated with neutrophil death. Front. Immunol. *9*, 1084.

Bouvier, N.M., and Lowen, A.C. (2010). Animal Models for Influenza Virus Pathogenesis and Transmission. Viruses *2*, 1530–1563.

Boyden, A.W., Legge, K.L., and Waldschmidt, T.J. (2012). Pulmonary infection with influenza A virus induces site-specific germinal center and T follicular helper cell responses. PLoS One *7*, 40733.

Braciale, T.J., Sun, J., and Kim, T.S. (2012). Regulating the adaptive immune response to respiratory virus infection. Nat. Rev. Immunol. *12*, 295–305.

Branchett, W.J., and Lloyd, C.M. (2019). Regulatory cytokine function in the respiratory tract. Mucosal Immunol. 2019 1.

Brandtzaeg, P., Kiyono, H., Pabst, R., and Russell, M.W. (2008). Terminology: nomenclature of mucosa-associated lymphoid tissue. Mucosal Immunol. *1*, 31–37.

Briolat, V., Jouneau, L., Carvalho, R., Palha, N., Langevin, C., Herbomel, P., Schwartz, O., Spaink, H.P., Levraud, J.-P., and Boudinot, P. (2014). Contrasted innate responses to two viruses in zebrafish: insights into the ancestral repertoire of vertebrate IFN-stimulated genes. J. Immunol. *192*, 4328–4341.

de Bruijn, I., Liu, Y., Wiegertjes, G.F., and Raaijmakers, J.M. (2018). Exploring fish microbial communities to mitigate emerging diseases in aquaculture. FEMS Microbiol. Ecol. *94*, 161.

Bry, K., Whitsett, J.A., and Lappalainen, U. (2007). IL-1β disrupts postnatal lung morphogenesis in the

mouse. Am. J. Respir. Cell Mol. Biol. *36*, 32–42.

Bueno, J.M., Martínez-Ojeda, R.M., Mugnier, L.M., and Artal, P. (2019). Deconvolution method for multiphoton microscopy: An application to thick ocular tissues. In International Conference on Transparent Optical Networks, (IEEE Computer Society), p.

Bueno, S.M., González, P.A., Pacheco, R., Leiva, E.D., Cautivo, K.M., Tobar, H.E., Mora, J.E., Prado, C.E., Zúñiga, J.P., Jiménez, J., et al. (2008). Host immunity during RSV pathogenesis. Int. Immunopharmacol. *8*, 1320–1329.

Burgos, J.S., Ripoll-Gomez, J., Alfaro, J.M., Sastre, I., and Valdivieso, F. (2008). Zebrafish as a new model for herpes simplex virus type 1 infection. Zebrafish *5*, 323–333.

Bustamante-Marin, X.M., and Ostrowski, L.E. (2017). Cilia and mucociliary clearance. Cold Spring Harb. Perspect. Biol. *9*.

Button, B., Cai, L.H., Ehre, C., Kesimer, M., Hill, D.B., Sheehan, J.K., Boucher, R.C., and Rubinstein, M. (2012). A periciliary brush promotes the lung health by separating the mucus layer from airway epithelia. Science (80-.). *337*, 937–941.

Caccia, E., Agnello, M., Ceci, M., Strickler Dinglasan, P., Vasta, G., and Romano, N. (2017). Antimicrobial Peptides Are Expressed during Early Development of Zebrafish (Danio rerio) and Are Inducible by Immune Challenge. Fishes *2*, 20.

Cahill, R.N.P., Frost, H., and Trnka, Z. (1976). The effects of antigen on the migration of recirculating lymphocytes through single lymph nodes. J. Exp. Med. *143*, 870–888.

Calderón, L., and Boehm, T. (2011). Three chemokine receptors cooperatively regulate homing of hematopoietic progenitors to the embryonic mouse thymus. Proc. Natl. Acad. Sci. U. S. A. *108*, 7517–7522.

Calvi, C.L., Podowski, M., D'Alessio, F.R., Metzger, S.L., Misono, K., Poonyagariyagorn, H., Lopez-Mercado, A., Ku, T., Lauer, T., Cheadle, C., et al. (2011). Critical Transition in Tissue Homeostasis Accompanies Murine Lung Senescence. PLoS One *6*, e20712.

Cameron, R., Buck, C., Merrill, D., and Luttick, A. (2003). Identification of contaminating adenovirus type 1 in the ATCC reference strain of respiratory syncytial virus A2 (VR-1302). Virus Res. *92*, 151–156.

Camp, J. V., and Jonsson, C.B. (2017). A Role for Neutrophils in Viral Respiratory Disease. Front. Immunol. *8*, 550.

Camp, J. V., Bagci, U., Chu, Y.-K., Squier, B., Fraig, M., Uriarte, S.M., Guo, H., Mollura, D.J., and Jonsson, C.B. (2015). Lower Respiratory Tract Infection of the Ferret by 2009 H1N1 Pandemic Influenza A Virus Triggers Biphasic, Systemic, and Local Recruitment of Neutrophils. J. Virol. *89*, 8733–8748.

Campillo-Navarro, M., Chávez-Blanco, A.D., Wong-Baeza, I., Serafín-López, J., Flores-Mejía, R., Estrada-Parra, S., Estrada-García, I., and Chacón-Salinas, R. (2005). Mast cells in lung homeostasis: Beyond type i hypersensitivity. Corp. Commun. *10*, 115–123.

Carmona, S.J., Teichmann, S.A., Ferreira, L., Macaulay, I.C., Stubbington, M.J.T., Cvejic, A., and Gfeller, D. (2017). Single-cell transcriptome analysis of fish immune cells provides insight into the evolution of vertebrate immune cell types. Genome Res. *27*, 451–461.

Caron, G., Duluc, D., Frémaux, I., Jeannin, P., David, C., Gascan, H., and Delneste, Y. (2005). Direct Stimulation of Human T Cells via TLR5 and TLR7/8: Flagellin and R-848 Up-Regulate Proliferation and IFN-γ Production by Memory CD4 + T Cells . J. Immunol. *175*, 1551–1557.

Carradice, D., and Lieschke, G.J. (2008). Zebrafish in hematology: Sushi or science? Blood *111*, 3331–3342.

Carragher, D.M., Rangel-Moreno, J., and Randall, T.D. (2008). Ectopic lymphoid tissues and local immunity. Semin. Immunol. *20*, 26–42.

Carrasco, Y.R., and Batista, F.D. (2007). B Cells Acquire Particulate Antigen in a Macrophage-Rich Area at the Boundary between the Follicle and the Subcapsular Sinus of the Lymph Node. Immunity *27*, 160–171.

Casadei, E., and Salinas, I. (2019). Comparative models for human nasal infections and immunity. Dev. Comp. Immunol. *92*, 212–222.

Castro, R., Jouneau, L., Pham, H.-P., Bouchez, O., Giudicelli, V., Lefranc, M.-P., Quillet, E., Benmansour, A., Cazals, F., Six, A., et al. (2013). Teleost fish mount complex clonal IgM and IgT responses in spleen upon systemic viral infection. PLoS Pathog. *9*, e1003098.

Castro, R., Bromage, E., Abós, B., Pignatelli, J., González Granja, A., Luque, A., and Tafalla, C. (2014). CCR7 Is Mainly Expressed in Teleost Gills, Where It Defines an IgD + IgM − B Lymphocyte Subset . J. Immunol. *192*, 1257–1266.

Cervantes, J.L., Weinerman, B., Basole, C., and Salazar, J.C. (2012). TLR8: The forgotten relative revindicated. Cell. Mol. Immunol. *9*, 434–438.

Cesta, M.F. (2006). Normal Structure, Function, and Histology of Mucosa-Associated Lymphoid Tissue. Toxicol. Pathol. *34*, 599–608.

Chan, M.C.W., Chan, R.W.Y., Yu, W.C.L., Ho, C.C.C., Yuen, K.M., Fong, J.H.M., Tang, L.L.S., Lai, W.W., Lo, A.C.Y., Chui, W.H., et al. (2010). Tropism and innate host responses of the 2009 pandemic H1N1 influenza virus in ex vivo and in vitro cultures of human conjunctiva and respiratory tract. Am. J. Pathol. *176*, 1828–1840.

Chan, R.W.Y., Chan, M.C.W., Agnihothram, S., Chan, L.L.Y., Kuok, D.I.T., Fong, J.H.M., Guan, Y., Poon, L.L.M., Baric, R.S., Nicholls, J.M., et al. (2013). Tropism of and Innate Immune Responses to the Novel Human Betacoronavirus Lineage C Virus in Human Ex Vivo Respiratory Organ Cultures. J. Virol. *87*, 6604–6614.

Channappanavar, R., Zhao, J., and Perlman, S. (2014). T cell-mediated immune response to respiratory coronaviruses. Immunol. Res. *59*, 118–128.

Charman, M., Herrmann, C., and Weitzman, M.D. (2019). Viral and cellular interactions during adenovirus DNA replication. FEBS Lett. *593*, 3531–3550.

de Chaumont, F., Dallongeville, S., Chenouard, N., Hervé, N., Pop, S., Provoost, T., Meas-Yedid, V., Pankajakshan, P., Lecomte, T., Le Montagner, Y., et al. (2012). Icy: an open bioimage informatics platform for extended reproducible research. Nat. Methods *9*, 690–696.

Chaves-Moreno, D., Plumeier, I., Kahl, S., Krismer, B., Peschel, A., Oxley, A.P.A., Jauregui, R., and Pieper, D.H. (2015). The microbial community structure of the cotton rat nose. Environ. Microbiol. Rep. *7*, 929–935.

Chen, K., and Kolls, J.K. (2013). T cell-mediated host immune defenses in the lung. Annu. Rev. Immunol. *31*, 605–633.

Chen, H., Zhang, L., Ke, L., Chen, X., and Lin, C. (2020). CpG-ODN 2007 protects zebrafish (Danio rerio) against Vibrio vulnificus infection. Aquac. Res. are.14944.

Chen, Y.W., Huang, S.X., De Carvalho, A.L.R.T., Ho, S.H., Islam, M.N., Volpi, S., Notarangelo, L.D., Ciancanelli, M., Casanova, J.L., Bhattacharya, J., et al. (2017). A three-dimensional model of human lung development and disease from pluripotent stem cells. Nat. Cell Biol. *19*, 542–549.

Chiavolini, D., Rangel-Moreno, J., Berg, G., Christian, K., Oliveira-Nascimento, L., Weir, S., Alroy, J., Randall, T.D., and Wetzler, L.M. (2010). Bronchus-Associated Lymphoid Tissue (BALT) and Survival in a Vaccine Mouse Model of Tularemia. PLoS One *5*, e11156.

Chiu, C., and Openshaw, P.J. (2015). Antiviral B cell and T cell immunity in the lungs. Nat Immunol *16*, 18–26.

Chiu, B.C., Stolberg, V.R., Zhang, H., and Chensue, S.W. (2007). Increased Foxp3+ Treg cell activity reduces dendritic cell co-stimulatory molecule expression in aged mice. Mech. Ageing Dev. *128*, 618–627.

Cho, S.-Y., Protzman, R.A., Kim, Y.O., Vaidya, B., Oh, M.-J., Kwon, J., and Kim, D. (2019). Elucidation of mechanism for host response to VHSV infection at varying temperatures in vitro and in vivo through proteomic analysis. Fish Shellfish Immunol. *88*, 244–253.

Cho, W.G., Albuquerque, R.J.C., Kleinman, M.E., Tarallo, V., Greco, A., Nozaki, M., Green, M.G., Baffi, J.Z., Ambati, B.K., De Falco, M., et al. (2009). Small interfering RNA-induced TLR3 activation inhibits blood and lymphatic vessel growth. Proc. Natl. Acad. Sci. U. S. A. *106*, 7137–7142.

Chonmaitree, T., Jennings, K., Golovko, G., Khanipov, K., Pimenova, M., Patel, J.A., McCormick, D.P., Loeffelholz, M.J., and Fofanov, Y. (2017). Nasopharyngeal microbiota in infants and changes during viral upper respiratory tract infection and acute otitis media. PLoS One *12*, e0180630.

Van Cleemput, J., Poelaert, K.C.K., Laval, K., Maes, R., Hussey, G.S., Van Den Broeck, W., and Nauwynck, H.J. (2017). Access to a main alphaherpesvirus receptor, located basolaterally in the respiratory epithelium, is masked by intercellular junctions. Sci. Rep. *7*.

Cohen, M., Zhang, X.Q., Senaati, H.P., Chen, H.W., Varki, N.M., Schooley, R.T., and Gagneux, P. (2013). Influenza A penetrates host mucus by cleaving sialic acids with neuraminidase. Virol. J. *10*, 321.

Collins, P.L., Fearns, R., and Graham, B.S. (2013). Respiratory Syncytial Virus: Virology, Reverse Genetics,

and Pathogenesis of Disease. In Current Topics in Microbiology and Immunology, (NIH Public Access), pp. 3–38.

Cosmi, L., Maggi, L., Santarlasci, V., Liotta, F., and Annunziato, F. (2014). T helper cells plasticity in inflammation. Cytom. Part A *85*, 36–42.

Crosse, K.M., Monson, E.A., Beard, M.R., and Helbig, K.J. (2018). Interferon-Stimulated Genes as Enhancers of Antiviral Innate Immune Signaling. J. Innate Immun. *10*, 85–93.

Crotta, S., Davidson, S., Mahlakoiv, T., Desmet, C.J., Buckwalter, M.R., Albert, M.L., Staeheli, P., and Wack, A. (2013). Type I and Type III Interferons Drive Redundant Amplification Loops to Induce a Transcriptional Signature in Influenza-Infected Airway Epithelia. PLoS Pathog. *9*, 1003773.

Cyr, S.L., Angers, I., Guillot, L., Stoica-Popescu, I., Lussier, M., Qureshi, S., Burt, D.S., and Ward, B.J. (2009). TLR4 and MyD88 control protection and pulmonary granulocytic recruitment in a murine intranasal RSV immunization and challenge model. Vaccine *27*, 421–430.

D'Agati, G., Beltre, R., Sessa, A., Burger, A., Zhou, Y., Mosimann, C., and White, R.M. (2017). A defect in the mitochondrial protein Mpv17 underlies the transparent casper zebrafish. Dev. Biol. *430*, 11–17.

Dakhama, A., Park, J.-W., Taube, C., El Gazzar, M., Kodama, T., Miyahara, N., Takeda, K., Kanehiro, A., Balhorn, A., Joetham, A., et al. (2005). Alteration of airway neuropeptide expression and development of airway hyperresponsiveness following respiratory syncytial virus infection. Am. J. Physiol. Cell. Mol. Physiol. *288*, L761–L770.

Dalum, A.S., Austbø, L., Bjørgen, H., Skjødt, K., Hordvik, I., Hansen, T., Fjelldal, P.G., Press, C.M., Griffiths, D.J., and Koppang, E.O. (2015). The interbranchial lymphoid tissue of Atlantic Salmon (Salmo salar L) extends as a diffuse mucosal lymphoid tissue throughout the trailing edge of the gill filament. J. Morphol. *276*, 1075–1088.

Dalum, A.S., Griffiths, D.J., Valen, E.C., Amthor, K.S., Austbø, L., Koppang, E.O., Press, C.M., and Kvellestad, A. (2016). Morphological and functional development of the interbranchial lymphoid tissue (ILT) in Atlantic salmon (Salmo salar L). Fish Shellfish Immunol. *58*, 153–164.

Danilova, N., Bussmann, J., Jekosch, K., and Steiner, L.A. (2005). The immunoglobulin heavy-chain locus in zebrafish: identification and expression of a previously unknown isotype, immunoglobulin Z. Nat. Immunol. *6*, 295–302.

Davidson, S., Crotta, S., McCabe, T.M., Wack, A., and Furth, A.M. van (2014). Pathogenic potential of interferon αβ in acute influenza infection. Nat. Commun. *5*, L1315–L1321.

Davis, A.S., Chertow, D.S., Moyer, J.E., Suzich, J., Sandouk, A., Dorward, D.W., Logun, C., Shelhamer, J.H., and Taubenberger, J.K. (2015). Validation of Normal Human Bronchial Epithelial Cells as a Model for Influenza A Infections in Human Distal Trachea. J. Histochem. Cytochem. *63*, 312–328.

Dee, C.T., Nagaraju, R.T., Athanasiadis, E.I., Gray, C., Fernandez Del Ama, L., Johnston, S.A., Secombes, C.J.,

Cvejic, A., and Hurlstone, A.F.L. (2016). CD4-Transgenic Zebrafish Reveal Tissue-Resident Th2- and Regulatory T Cell-like Populations and Diverse Mononuclear Phagocytes. J. Immunol.

Delgado, M.F., Coviello, S., Monsalvo, A.C., Melendi, G.A., Hernandez, J.Z., Batalle, J.P., Diaz, L., Trento, A., Chang, H.Y., Mitzner, W., et al. (2009). Lack of antibody affinity maturation due to poor Toll-like receptor stimulation leads to enhanced respiratory syncytial virus disease. Nat. Med. *15*, 34–41.

Demedts, I.K., Bracke, K.R., Maes, T., Joos, G.F., and Brusselle, G.G. (2006). Different roles for human lung dendritic cell subsets in pulmonary immune defense mechanisms. Am. J. Respir. Cell Mol. Biol. *35*, 387–393.

Deng, Y., Herbert, J.A., Smith, C.M., and Smyth, R.L. (2018). An in vitro transepithelial migration assay to evaluate the role of neutrophils in Respiratory Syncytial Virus (RSV) induced epithelial damage. Sci. Rep. *8*, 1–12.

Deng, Y., Herbert, J.A., Robinson, E., Ren, L., Smyth, R.L., and Smith, C.M. (2020). Neutrophil-Airway Epithelial Interactions Result in Increased Epithelial Damage and Viral Clearance during Respiratory Syncytial Virus Infection. J. Virol. *94*.

Denney, L., and Ho, L.P. (2018). The role of respiratory epithelium in host defence against influenza virus infection. Biomed. J. *41*, 218–233.

Deprez, M., Zaragosi, L.-E., Truchi, M., Becavin, C., Ruiz García, S., Arguel, M.-J., Plaisant, M., Magnone, V., Lebrigand, K., Abelanet, S., et al. (2020). A Single-cell Atlas of the Human Healthy Airways. Am. J. Respir. Crit. Care Med.

Derksen, J.A., Ostland, V.E., and Ferguson, H.W. (1998). Particle clearance from the gills of rainbow trout (Oncorhynchus mykiss). J. Comp. Pathol. *118*, 245–256.

Dijkman, R., Jebbink, M.F., Koekkoek, S.M., Deijs, M., Jonsdottir, H.R., Molenkamp, R., Ieven, M., Goossens, H., Thiel, V., and van der Hoek, L. (2013). Isolation and Characterization of Current Human Coronavirus Strains in Primary Human Epithelial Cell Cultures Reveal Differences in Target Cell Tropism. J. Virol. *87*, 6081–6090.

Ding, C.B., Zhang, J.P., Zhao, Y., Peng, Z.G., Song, D.Q., and Jiang, J.D. (2011). Zebrafish as a potential model organism for drug test against hepatitis C virus. PLoS One *6*.

Dobbs, L.G., Johnson, M.D., Vanderbilt, J., Allen, L., and Gonzalez, R. (2010). The Great Big Alveolar TI Cell: Evolving Concepts and Paradigms.

Dobson, J.T., Seibert, J., Teh, E.M., Da'as, S., Fraser, R.B., Paw, B.H., Lin, T.-J., and Berman, J.N. (2008). Carboxypeptidase A5 identifies a novel mast cell lineage in the zebrafish providing new insight into mast cell fate determination. Blood *112*.

Domingo-Gonzalez, R., Zanini, F., Che, X., Liu, M., Jones, R.C., Swift, M.A., Quake, S.R., Cornfield, D.N., and Alvira, C.M. (2020). Diverse homeostatic and immunomodulatory roles of immune cells in the developing

mouse lung at single cell resolution. Elife *9*, 1–39.

Dopazo, C.P. (2020). The infectious pancreatic necrosis virus (IPNV) and its virulence determinants: What is known and what should be known. Pathogens *9*, 94.

Dou, D., Revol, R., Östbye, H., Wang, H., and Daniels, R. (2018). Influenza A Virus Cell Entry, Replication, Virion Assembly and Movement. Front. Immunol. *9*, 1581.

Douville, N.J., Zamankhan, P., Tung, Y.C., Li, R., Vaughan, B.L., Tai, C.F., White, J., Christensen, P.J., Grotberg, J.B., and Takayama, S. (2011). Combination of fluid and solid mechanical stresses contribute to cell death and detachment in a microfluidic alveolar model. Lab Chip *11*, 609–619.

Du, Y., Tang, X., Sheng, X., Xing, J., and Zhan, W. (2017). The influence of concentration of inactivated Edwardsiella tarda bacterin and immersion time on antigen uptake and expression of immune-related genes in Japanese flounder (Paralichthys olivaceus). Microb. Pathog. *103*, 19–28.

Dufour, A., Meas-Yedid, V., Grassart, A., and Olivo-Marin, J.C. (2008). Automated quantification of cell endocytosis using active contours and wavelets. In Proceedings - International Conference on Pattern Recognition, (Institute of Electrical and Electronics Engineers Inc.), p.

Dufour, A., Thibeaux, R., Labruyère, E., Guillén, N., and Olivo-Marin, J.C. (2011). 3-D active meshes: Fast discrete deformable models for cell tracking in 3-D time-lapse microscopy. IEEE Trans. Image Process. *20*, 1925–1937.

Van Dycke, J., Ny, A., Conceição-Neto, N., Maes, J., Hosmillo, M., Cuvry, A., Goodfellow, I., Nogueira, T.C., Verbeken, E., Matthijnssens, J., et al. (2019). A robust human norovirus replication model in zebrafish larvae. PLOS Pathog. *15*, e1008009.

Ege, M.J., Bieli, C., Frei, R., van Strien, R.T., Riedler, J., Üblagger, E., Schram-Bijkerk, D., Brunekreef, B., van Hage, M., Scheynius, A., et al. (2006). Prenatal farm exposure is related to the expression of receptors of the innate immunity and to atopic sensitization in school-age children. J. Allergy Clin. Immunol. *117*, 817–823.

Ellett, F., Pase, L., Hayman, J.W., Andrianopoulos, A., and Lieschke, G.J. (2011). mpeg1 promoter transgenes direct macrophage-lineage expression in zebrafish. Blood *117*.

Ellis, A.E., Cavaco, A., Petrie, A., Lockhart, K., Snow, M., and Collet, B. (2010). Histology, immunocytochemistry and qRT-PCR analysis of Atlantic salmon, Salmo salar L., post-smolts following infection with infectious pancreatic necrosis virus (IPNV). J. Fish Dis. *33*, 803–818.

Encinas, P., Garcia-Valtanen, P., Chinchilla, B., Gomez-Casado, E., Estepa, A., and Coll, J. (2013). Identification of Multipath Genes Differentially Expressed in Pathway-Targeted Microarrays in Zebrafish Infected and Surviving Spring Viremia Carp Virus (SVCV) Suggest Preventive Drug Candidates. PLoS One *8*, e73553.

Endres, R., Alimzhanov, M.B., Plitz, T., Fütterer, A., Kosco-Vilbois, M.H., Nedospasov, S.A., Rajewsky, K., and

Pfeffer, K. (1999). Mature follicular dendritic cell networks depend on expression of lymphotoxin β receptor by radioresistant stromal cells and of lymphotoxin β and tumor necrosis factor by B cells. J. Exp. Med. *189*, 159–167.

Epaulard, O., Adam, L., Poux, C., Zurawski, G., Salabert, N., Rosenbaum, P., Dereuddre-Bosquet, N., Zurawski, S., Flamar, A.-L., Oh, S., et al. (2014). Macrophage- and Neutrophil-Derived TNF-α Instructs Skin Langerhans Cells To Prime Antiviral Immune Responses. J. Immunol. *193*, 2416–2426.

Van Erp, E.A., Luytjes, W., Ferwerda, G., and Van Kasteren, P.B. (2019). Fc-mediated antibody effector functions during respiratory syncytial virus infection and disease. Front. Immunol. *10*, 548.

Evans, D.H., Piermarini, P.M., and Choe, K.P. (2005). The Multifunctional Fish Gill: Dominant Site of Gas Exchange, Osmoregulation, Acid-Base Regulation, and Excretion of Nitrogenous Waste. Physiol. Rev. *85*.

Fahy, J. V., and Dickey, B.F. (2010). Medical progress: Airway mucus function and dysfunction. N. Engl. J. Med. *363*, 2233–2247.

Farrell, A.P., Sobin, S.S., Randall, D.J., and Crosby, S. (1980). Intralamellar blood flow patterns in fish gills. Am. J. Physiol. - Regul. Integr. Comp. Physiol. *8*.

Ferrer, M., Méndez-García, C., Rojo, D., Barbas, C., and Moya, A. (2017). Antibiotic use and microbiome function. Biochem. Pharmacol. *134*, 114–126.

Ferrero, G., Gomez, E., Lyer, S., Rovira, M., Miserocchi, M., Langenau, D.M., Bertrand, J.Y., and Wittamer, V. (2020). The macrophage-expressed gene (mpeg) 1 identifies a subpopulation of B cells in the adult zebrafish. J. Leukoc. Biol. *107*, 431–443.

Fiole, D., and Tournier, J.-N. (2016). Intravital microscopy of the lung: minimizing invasiveness. J. Biophotonics *9*, 868–878.

Fischer, A.J., Pino-Argumedo, M.I., Hilkin, B.M., Shanrock, C.R., Gansemer, N.D., Chaly, A.L., Zarei, K., Allen, P.D., Ostedgaard, L.S., Hoffman, E.A., et al. (2019). Mucus strands from submucosal glands initiate mucociliary transport of large particles. JCI Insight *4*, 124863.

Fischer, T., Klinger, A., von Smolinski, D., Orzekowsky-Schroeder, R., Nitzsche, F., Bölke, T., Vogel, A., Hüttmann, G., and Gebert, A. (2020). High-resolution imaging of living gut mucosa: lymphocyte clusters beneath intestinal M cells are highly dynamic structures. Cell Tissue Res. *380*, 539–546.

Fischer, U., Utke, K., Somamoto, T., Köllner, B., Ototake, M., and Nakanishi, T. (2006). Cytotoxic activities of fish leucocytes. In Fish and Shellfish Immunology, (Academic Press), pp. 209–226.

Fischer, U., Koppang, E.O., and Nakanishi, T. (2013). Teleost T and NK cell immunity. Fish Shellfish Immunol. *35*, 197–206.

Flores-Torres, A.S., Salinas-Carmona, M.C., Salinas, E., and Rosas-Taraco, A.G. (2019). Eosinophils - Respiratory Viruses. Viral Immunol. *32*, 198–207.

Foo, S.Y., Zhang, V., Lalwani, A., Lynch, J.P., Zhuang, A., Lam, C.E., Foster, P.S., King, C., Steptoe, R.J., Mazzone, S.B., et al. (2015). Regulatory T Cells Prevent Inducible BALT Formation by Dampening Neutrophilic Inflammation. J. Immunol. *194*, 4567–4576.

Forn-Cuní, G., Varela, M., Pereiro, P., Novoa, B., and Figueras, A. (2017). Conserved gene regulation during acute inflammation between zebrafish and mammals. Sci. Rep. *7*, 41905.

Forum of International Respiratory Societies (2017). The Global Impact of Respiratory Disease (Sheffield: European Respiratory Society).

Frasca, D., Diaz, A., Romero, M., Landin, A.M., Phillips, M., Lechner, S.C., Ryan, J.G., and Blomberg, B.B. (2010). Intrinsic defects in B cell response to seasonal influenza vaccination in elderly humans. Vaccine *28*, 8077–8084.

Fraser, E. (2020). Long term respiratory complications of covid-19. BMJ *370*, m3001.

Fuchs, R., and Blaas, D. (2012). Productive entry pathways of human rhinoviruses. Adv. Virol. *2012*.

Gabor, K.A., Goody, M.F., Mowel, W.K., Breitbach, M.E., Gratacap, R.L., Witten, P.E., and Kim, C.H. (2014). Influenza A virus infection in zebrafish recapitulates mammalian infection and sensitivity to anti-influenza drug treatment. Dis. Model. Mech. *7*, 1227–1237.

Gadan, K., Sandtrø, A., Marjara, I.S., Santi, N., Munang'andu, H.M., and Evensen, Ø. (2013). Stress-Induced Reversion to Virulence of Infectious Pancreatic Necrosis Virus in Naïve Fry of Atlantic Salmon (Salmo salar L.). PLoS One *8*, 54656.

Ganesan, S., Comstock, A.T., and Sajjan, U.S. (2013). Barrier function of airway tract epithelium. Tissue Barriers *1*, e24997.

Gao, H., Wu, L., Sun, J.-S., Geng, X.-Y., and Pan, B.-P. (2013). Molecular characterization and expression analysis of Toll-like receptor 21 cDNA from Paralichthys olivaceus. Fish Shellfish Immunol. *35*, 1138–1145.

Gao, Y., Wu, H., Wang, Q., Qu, J., Liu, Q., Xiao, J., and Zhang, Y. (2014). A live attenuated combination vaccine evokes effective immune-mediated protection against Edwardsiella tarda and Vibrio anguillarum. Vaccine *32*, 5937–5944.

Gao, Y., Tang, X., Sheng, X., Xing, J., and Zhan, W. (2016). Antigen uptake and expression of antigen presentation-related immune genes in flounder (Paralichthys olivaceus) after vaccination with an inactivated Edwardsiella tarda immersion vaccine, following hyperosmotic treatment. Fish Shellfish Immunol. *55*, 274–280.

Garcia-Verdugo, I., Descamps, D., Chignard, M., Touqui, L., and Sallenave, J.M. (2010). Lung protease/anti-protease network and modulation of mucus production and surfactant activity. Biochimie *92*, 1608–1617.

Ge, R., Zhou, Y., Peng, R., Wang, R., Li, M., Zhang, Y., Zheng, C., and Wang, C. (2015). Conservation of the STING-mediated cytosolic DNA sensing pathway in zebrafish. J. Virol. *89*, JVI.01049-15-.

Geerdink, R.J., Pillay, J., Meyaard, L., and Bont, L. (2015). Neutrophils in respiratory syncytial virus infection: A target for asthma prevention. J. Allergy Clin. Immunol. *136*, 838–847.

Geijtenbeek, T.B.H., and Gringhuis, S.I. (2009). Signalling through C-type lectin receptors: Shaping immune responses. Nat. Rev. Immunol. *9*, 465–479.

Geller, A., and Yan, J. (2019). The role of membrane bound complement regulatory proteins in tumor development and cancer immunotherapy. Front. Immunol. *10*, 1074.

Gentek, R., and Bajénoff, M. (2017). Lymph Node Stroma Dynamics and Approaches for Their Visualization. Trends Immunol. *38*, 236–247.

Georas, S.N., and Rezaee, F. (2014). Epithelial barrier function: at the front line of asthma immunology and allergic airway inflammation. J. Allergy Clin. Immunol. *134*, 509–520.

von Gersdorff Jørgensen, L. (2016). Infection and immunity against Ichthyophthirius multifiliis in zebrafish (Danio rerio). Fish Shellfish Immunol. *57*, 335–339.

von Gersdorff Jørgensen, L., Heinecke, R.D., Skjødt, K., Rasmussen, K.J., and Buchmann, K. (2011). Experimental evidence for direct in situ binding of IgM and IgT to early trophonts of Ichthyophthirius multifiliis (Fouquet) in the gills of rainbow trout, Oncorhynchus mykiss (Walbaum). J. Fish Dis. *34*, 749–755.

GeurtsvanKessel, C.H., Willart, M.A.M., Van Rijt, L.S., Muskens, F., Kool, M., Baas, C., Thielemans, K., Bennett, C., Clausen, B.E., Hoogsteden, H.C., et al. (2008). Clearance of influenza virus from the lung depends on migratory langerin+CD11b- but not plasmacytoid dendritic cells. J. Exp. Med. *205*, 1621–1634.

Giarmarco, M.M., Cleghorn, W.M., Hurley, J.B., and Brockerhoff, S.E. (2018). Preparing fresh retinal slices from adult zebrafish for ex vivo imaging experiments. J. Vis. Exp. *2018*, e56977.

Glaser, L., Coulter, P.J., Shields, M., Touzelet, O., Power, U.F., and Broadbent, L. (2019). Airway epithelial derived cytokines and chemokines and their role in the immune response to respiratory syncytial virus infection. Pathogens *8*.

Gohy, S.T., Hupin, C., Pilette, C., and Ladjemi, M.Z. (2016). Chronic inflammatory airway diseases: the central role of the epithelium revisited. Clin. Exp. Allergy *46*, 529–542.

Gomez, D., Sunyer, J.O., and Salinas, I. (2013). The mucosal immune system of fish: The evolution of tolerating commensals while fighting pathogens. Fish Shellfish Immunol. *35*, 1729–1739.

Gonzalez, S.F., Lukacs-Kornek, V., Kuligowski, M.P., Pitcher, L.A., Degn, S.E., Kim, Y.A., Cloninger, M.J., Martinez-Pomares, L., Gordon, S., Turley, S.J., et al. (2010). Capture of influenza by medullary dendritic cells via SIGN-R1 is essential for humoral immunity in draining lymph nodes. Nat. Immunol. *11*, 427–434.

Good, D.W., George, T., and Watts, B.A. (2012). Toll-like receptor 2 is required for LPS-induced toll-like receptor 4 signaling and inhibition of ion transport in renal thick ascending limb. J. Biol. Chem. *287*, 20208–20220.

Goody, M., Jurczyszak, D., Kim, C., and Henry, C. (2017). Influenza A Virus Infection Damages Zebrafish Skeletal Muscle and Exacerbates Disease in Zebrafish Modeling Duchenne Muscular Dystrophy. PLoS Curr. *9*.

Goody, M.F., Sullivan, C., and Kim, C.H. (2014). Studying the immune response to human viral infections using zebrafish. Dev. Comp. Immunol. *46*, 84–95.

Gopinath, S., Kim, M. V., Rakib, T., Wong, P.W., Zandt, M., Barry, N.A., Kaisho, T., Goodman, A.L., and Iwasaki, A. (2018). Topical application of aminoglycoside antibiotics enhances host resistance to viral infections in a microbiota-independent manner. Nat. Microbiol. 2018 1.

Gorden, K.K.B., Qiu, X.X., Binsfeld, C.C.A., Vasilakos, J.P., and Alkan, S.S. (2006). Cutting Edge: Activation of Murine TLR8 by a Combination of Imidazoquinoline Immune Response Modifiers and PolyT Oligodeoxynucleotides. J. Immunol. *177*, 6584–6587.

Goris, K., Uhlenbruck, S., Schwegmann-Wessels, C., Köhl, W., Niedorf, F., Stern, M., Hewicker-Trautwein, M., Bals, R., Taylor, G., Braun, A., et al. (2009). Differential Sensitivity of Differentiated Epithelial Cells to Respiratory Viruses Reveals Different Viral Strategies of Host Infection. J. Virol. *83*, 1962–1968.

Goritzka, M., Makris, S., Kausar, F., Durant, L.R., Pereira, C., Kumagai, Y., Culley, F.J., Mack, M., Akira, S., and Johansson, C. (2015). Alveolar macrophage-derived type I interferons orchestrate innate immunity to RSV through recruitment of antiviral monocytes. J. Exp. Med. *212*, jem.20140825-.

Goritzka, M., Pereira, C., Makris, S., Durant, L.R., and Johansson, C. (2016). T cell responses are elicited against Respiratory Syncytial Virus in the absence of signalling through TLRs, RLRs and IL-1R/IL-18R. Sci. Rep. *5*, 18533.

Grasa, L., Abecia, L., Forcén, R., Castro, M., de Jalón, J.A.G., Latorre, E., Alcalde, A.I., and Murillo, M.D. (2015). Antibiotic-Induced Depletion of Murine Microbiota Induces Mild Inflammation and Changes in Toll-Like Receptor Patterns and Intestinal Motility. Microb. Ecol. *70*, 835–848.

Gray, J., Oehrle, K., Worthen, G., Alenghat, T., Whitsett, J., and Deshmukh, H. (2017). Intestinal commensal bacteria mediate lung mucosal immunity and promote resistance of newborn mice to infection. Sci. Transl. Med. *9*.

Greiff, L., Ahlström-Emanuelsson, C., Alenäs, M., Almqvist, G., Andersson, M., Cervin, A., Dolata, J., Lindgren, S., Mårtensson, A., Young, B., et al. (2015). Biological effects and clinical efficacy of a topical Toll-like receptor 7 agonist in seasonal allergic rhinitis: a parallel group controlled phase IIa study. Inflamm. Res. *64*, 903–915.

Griffith, M.B. (2017). Toxicological perspective on the osmoregulation and ionoregulation physiology of major ions by freshwater animals: Teleost fish, crustacea, aquatic insects, and Mollusca. Environ. Toxicol. Chem. *36*, 576–600.

Griffiths, C., Drews, S.J., and Marchant, D.J. (2017). Respiratory syncytial virus: Infection, detection, and new options for prevention and treatment. Clin. Microbiol. Rev. *30*, 277–319.

Griffiths, C.D., Bilawchuk, L.M., McDonough, J.E., Jamieson, K.C., Elawar, F., Cen, Y., Duan, W., Lin, C., Song, H., Casanova, J.L., et al. (2020). IGF1R is an entry receptor for respiratory syncytial virus. Nature *583*, 615–619.

Guerra-Varela, J., Baz-Martínez, M., Da Silva-Álvarez, S., Losada, A.P., Quiroga, M.I., Collado, M., Rivas, C., and Sánchez, L. (2018). Susceptibility of Zebrafish to Vesicular Stomatitis Virus Infection. Zebrafish *15*, 124–132.

Le Guyader, D., Redd, M.J., Colucci-Guyon, E., Murayama, E., Kissa, K., Briolat, V., Mordelet, E., Zapata, A., Shinomiya, H., and Herbomel, P. (2008). Origins and unconventional behavior of neutrophils in developing zebrafish. Blood *111*, 132–141.

Habibi, M.S., Jozwik, A., Makris, S., Dunning, J., Paras, A., DeVincenzo, J.P., De Haan, C.A.M., Wrammert, J., Openshaw, P.J.M., and Chiu, C. (2015). Impaired antibody-mediated protection and defective IgA B-cell memory in experimental infection of adults with respiratory syncytial virus. Am. J. Respir. Crit. Care Med. *191*, 1040–1049.

Haig, D.M., Hopkins, J., and Miller, H.R. (1999). Local immune responses in afferent and efferent lymph. Immunology *96*, 155–163.

Hall, C., Flores, M., Storm, T., Crosier, K., and Crosier, P. (2007). The zebrafish lysozyme C promoter drives myeloid-specific expression in transgenic fish. BMC Dev. Biol. *7*, 42.

Hamada, H., Bassity, E., Flies, A., Strutt, T.M., Garcia-Hernandez, M. de L., McKinstry, K.K., Zou, T., Swain, S.L., and Dutton, R.W. (2013). Multiple Redundant Effector Mechanisms of CD8 + T Cells Protect against Influenza Infection . J. Immunol. *190*, 296–306.

Hamley, I.W., Kirkham, S., Dehsorkhi, A., Castelletto, V., Reza, M., and Ruokolainen, J. (2014). Toll-like receptor agonist lipopeptides self-assemble into distinct nanostructures. Chem. Commun. *50*, 15948–15951.

Hancock, G.E., Heers, K.M., Pryharski, K.S., Smith, J.D., and Tiberio, L. (2003). Adjuvants recognized by toll-like receptors inhibit the induction of polarized type 2 T cell responses by natural attachment (G) protein of respiratory syncytial virus. Vaccine *21*, 4348–4358.

Haneberg, B., Glette, J., Talstad, I., Sørnes, S., and Solberg, C.O. (1984). In vitro release of lysozyme from monocytes and granulocytes. J. Leukoc. Biol. *35*, 573–582.

Hansel, T.T., Johnston, S.L., and Openshaw, P.J. (2013). Microbes and mucosal immune responses in asthma. Lancet *381*, 861–873.

Hansen, A., Reutter, K., and Zeiske, E. (2002). Taste bud development in the zebrafish,Danio rerio. Dev. Dyn. *223*, 483–496.

Haq, K., and McElhaney, J.E. (2014). Ageing and respiratory infections: The airway of ageing. Immunol. Lett. *162*, 323–328.

Harkema, J.R., Carey, S.A., and Wagner, J.G. (2006). The Nose Revisited: A Brief Review of the Comparative Structure, Function, and Toxicologic Pathology of the Nasal Epithelium. Toxicol. Pathol. *34*, 252–269.

Harrison, M.R., Feng, X., Mo, G., Aguayo, A., Villafuerte, J., Yoshida, T., Pearson, C.A., Schulte-Merker, S., and Ching-Ling, L. (2019). Late developing cardiac lymphatic vasculature supports adult zebrafish heart function and regeneration. Elife *8*.

Harrison, M.R.M., Bussmann, J., Huang, Y., Zhao, L., Osorio, A., Burns, C.G., Burns, C.E., Sucov, H.M., Siekmann, A.F., and Lien, C.L. (2015). Chemokine-Guided Angiogenesis Directs Coronary Vasculature Formation in Zebrafish. Dev. Cell *33*, 442–454.

Hart, O.M., Athie-Morales, V., O'Connor, G.M., and Gardiner, C.M. (2005). TLR7/8-Mediated Activation of Human NK Cells Results in Accessory Cell-Dependent IFN-γ Production. J. Immunol. *175*, 1636–1642.

Harton, J.A., Linhoff, M.W., Zhang, J., and Ting, J.P.-Y. (2002). Cutting Edge: CATERPILLER: A Large Family of Mammalian Genes Containing CARD, Pyrin, Nucleotide-Binding, and Leucine-Rich Repeat Domains. J. Immunol. *169*, 4088–4093.

Hasan, U., Chaffois, C., Gaillard, C., Saulnier, V., Merck, E., Tancredi, S., Guiet, C., Brière, F., Vlach, J., Lebecque, S., et al. (2005). Human TLR10 Is a Functional Receptor, Expressed by B Cells and Plasmacytoid Dendritic Cells, Which Activates Gene Transcription through MyD88. J. Immunol. *174*, 2942–2950.

Hasegawa, Y., Mark Welch, J.L., Rossetti, B.J., and Borisy, G.G. (2017). Preservation of three-dimensional spatial structure in the gut microbiome. PLoS One *12*, e0188257.

Hashimoto, Y., Moki, T., Takizawa, T., Shiratsuchi, A., and Nakanishi, Y. (2007). Evidence for Phagocytosis of Influenza Virus-Infected, Apoptotic Cells by Neutrophils and Macrophages in Mice. J. Immunol. *178*, 2448–2457.

Haugarvoll, E., Bjerkås, I., Nowak, B.F., Hordvik, I., and Koppang, E.O. (2008). Identification and characterization of a novel intraepithelial lymphoid tissue in the gills of Atlantic salmon. J. Anat. *213*, 202–209.

Hauptmann, M., and Schaible, U.E. (2016). Linking microbiota and respiratory disease. FEBS Lett. *590*, 3721–3738.

Hayashi, F., Smith, K.D., Ozinsky, A., Hawn, T.R., Yi, E.C., Goodlett, D.R., Eng, J.K., Akira, S., Underhill, D.M., and Aderem, A. (2001). The innate immune response to bacterial flagellin is mediated by Toll-like receptor 5. Nature *410*, 1099–1103.

Heesters, B.A., Chatterjee, P., Kim, Y.A., Gonzalez, S.F., Kuligowski, M.P., Kirchhausen, T., and Carroll, M.C. (2013). Endocytosis and Recycling of Immune Complexes by Follicular Dendritic Cells Enhances B Cell Antigen Binding and Activation. Immunity *38*, 1164–1175.

Heier, I., Malmström, K., Sajantila, A., Lohi, J., Mäkelä, M., and Jahnsen, F.L. (2011). Characterisation of bronchus-associated lymphoid tissue and antigen-presenting cells in central airway mucosa of children.

Thorax *66*, 151–156.

Van Der Heijden, M.H.T., Helders, G.M., Booms, G.H.R., Huisman, E.A., Rombout, J.H.W.M., and Boon, J.H. (1996). Influence of flumequine and oxytetracycline on the resistance of the European eel against the parasitic swimbladder nematode Anguillicola crassus. Vet. Immunol. Immunopathol. *52*, 127–134.

Heil, F., Hemmi, H., Hochrein, H., Ampenberger, F., Kirschning, C., Akira, S., Lipford, G., Wagner, H., and Bauer, S. (2004). Species-Specific Recognition of Single-Stranded RNA via Till-like Receptor 7 and 8. Science (80-.). *303*, 1526–1529.

Herbomel, P., Thisse, B., and Thisse, C. (1999). Ontogeny and behaviour of early macrophages in the zebrafish embryo. Development *126*, 3735–3745.

Hernández, P.P., Strzelecka, P.M., Athanasiadis, E.I., Hall, D., Robalo, A.F., Collins, C.M., Boudinot, P., Levraud, J.-P., and Cvejic, A. (2018). Single-cell transcriptional analysis reveals ILC-like cells in zebrafish. Sci. Immunol. *3*.

Hetland, D.L., Jørgensen, S.M., Skjødt, K., Dale, O.B., Falk, K., Xu, C., Mikalsen, A.B., Grimholt, U., Gjøen, T., and Press, C.M. (2010). In situ localisation of major histocompatibility complex class I and class II and CD8 positive cells in infectious salmon anaemia virus (ISAV)-infected Atlantic salmon. Fish Shellfish Immunol. *28*, 30–39.

Heycock, M. (2017). Immune Characterisation of the Zebrafish Gill. Imperial College London.

Hiller, Tschernig, Kleemann, and Pabst (1998). Bronchus-Associated Lymphoid Tissue (BALT) and Larynx-Associated Lymphoid Tissue (LALT) are Found at Different Frequencies in Children, Adolescents and Adults. Scand. J. Immunol. *47*, 159–162.

Hinsch, K., and Zupanc, G.K.H. (2007). Generation and long-term persistence of new neurons in the adult zebrafish brain: A quantitative analysis. Neuroscience *146*, 679–696.

Ho, J., Yang, X., Nikou, S.A., Kichik, N., Donkin, A., Ponde, N.O., Richardson, J.P., Gratacap, R.L., Archambault, L.S., Zwirner, C.P., et al. (2019). Candidalysin activates innate epithelial immune responses via epidermal growth factor receptor. Nat. Commun. *10*, 1–12.

Hoeben, R.C., and Uil, T.G. (2013). Adenovirus DNA replication. Cold Spring Harb. Perspect. Biol. *5*.

Van den Hoecke, S., Verhelst, J., Vuylsteke, M., and Saelens, X. (2015). Analysis of the genetic diversity of influenza A viruses using next-generation DNA sequencing. BMC Genomics *16*, 79.

Hoegger, M.J., Fischer, A.J., McMenimen, J.D., Ostedgaard, L.S., Tucker, A.J., Awadalla, M.A., Moninger, T.O., Michalski, A.S., Hoffman, E.A., Zabner, J., et al. (2014). Impaired mucus detachment disrupts mucociliary transport in a piglet model of cystic fibrosis. Science (80-.). *345*, 818–822.

Van Hoeven, N., Belser, J.A., Szretter, K.J., Zeng, H., Staeheli, P., Swayne, D.E., Katz, J.M., and Tumpey, T.M. (2009). Pathogenesis of 1918 Pandemic and H5N1 Influenza Virus Infections in a Guinea Pig Model: Antiviral Potential of Exogenous Alpha Interferon To Reduce Virus Shedding. J. Virol. *83*, 2851–2861.

Hogan, B.M., Hunter, M.P., Oates, A.C., Crowhurst, M.O., Hall, N.E., Heath, J.K., Prince, V.E., and Lieschke, G.J. (2004). Zebrafish gcm2 is required for gill filament budding from pharyngeal ectoderm. Dev. Biol. *276*, 508–522.

Hohn, C., and Petrie-Hanson, L. (2012). Rag1–/– Mutant Zebrafish Demonstrate Specific Protection following Bacterial Re-Exposure. PLoS One *7*, e44451.

Hol, J., Wilhelmsen, L., and Haraldsen, G. (2010). The murine IL-8 homologues KC, MIP-2, and LIX are found in endothelial cytoplasmic granules but not in Weibel-Palade bodies. J. Leukoc. Biol. *87*, 501–508.

Holbrook, B.C., Kim, J.R., Blevins, L.K., Jorgensen, M.J., Kock, N.D., D'Agostino, R.B., Aycock, S.T., Hadimani, M.B., King, S.B., Parks, G.D., et al. (2016). A Novel R848-Conjugated Inactivated Influenza Virus Vaccine Is Efficacious and Safe in a Neonate Nonhuman Primate Model. J. Immunol. *197*, 555–564.

Holden, J.A., Layfield, L.L., and Matthews, J.L. (2013). The Zebrafish: Atlas of Macroscopic and Microscopic Anatomy (Cambridge University Press).

Hoong, S. (2018). Characterization of immune cells and the inflammatory response in zebrafish gills. Imperial College London.

Hornick, E.E., Zacharias, Z.R., and Legge, K.L. (2019). Kinetics and Phenotype of the CD4 T Cell Response to Influenza Virus Infections. Front. Immunol. *10*, 2351.

Hou, Y.J., Okuda, K., Edwards, C.E., Martinez, D.R., Asakura, T., Dinnon, K.H., Kato, T., Lee, R.E., Yount, B.L., Mascenik, T.M., et al. (2020). SARS-CoV-2 Reverse Genetics Reveals a Variable Infection Gradient in the Respiratory Tract. Cell *182*, 429-446.e14.

Houston, R.D., Haley, C.S., Hamilton, A., Guy, D.R., Mota-Velasco, J.C., Gheyas, A.A., Tinch, A.E., Taggart, J.B., Bron, J.E., Starkey, W.G., et al. (2010). The susceptibility of Atlantic salmon fry to freshwater infectious pancreatic necrosis is largely explained by a major QTL. Heredity (Edinb). *105*, 318–327.

Howe, K., Clark, M.D., Torroja, C.F., Torrance, J., Berthelot, C., Muffato, M., Collins, J.E., Humphray, S., Mclaren, K., Matthews, L., et al. (2013). The zebrafish reference genome sequence and its relationship to the human genome. Nature.

Howe, K., Schiffer, P.H., Zielinski, J., Wiehe, T., Laird, G.K., Marioni, J.C., Soylemez, O., Kondrashov, F., and Leptin, M. (2016). Structure and evolutionary history of a large family of NLR proteins in the zebrafish. Open Biol. *6*.

Hsia, C.C.W., Schmitz, A., Lambertz, M., Perry, S.F., and Maina, J.N. (2013). Evolution of air breathing: Oxygen homeostasis and the transitions from water to land and sky. Compr. Physiol. *3*, 849–915.

Hsu, A.C.-Y., Parsons, K., Barr, I., Lowther, S., Middleton, D., Hansbro, P.M., and Wark, P.A.B. (2012). Critical Role of Constitutive Type I Interferon Response in Bronchial Epithelial Cell to Influenza Infection. PLoS One *7*, e32947.

Hu, Y.-L., Xiang, L.-X., and Shao, J.-Z. (2010). Identification and characterization of a novel immunoglobulin

Z isotype in zebrafish: Implications for a distinct B cell receptor in lower vertebrates. Mol. Immunol. *47*, 738–746.

Hu, Y., Carpio, Y., Scott, C., Alnabulsi, A., Alnabulsi, A., Wang, T.T., Liu, F., Monte, M., Wang, T.T., and Secombes, C.J. (2019). Induction of IL-22 protein and IL-22-producing cells in rainbow trout Oncorhynchus mykiss. Dev. Comp. Immunol. *101*.

Huang, Y., Cyr, S.L., Burt, D.S., and Anderson, R. (2009). Murine host responses to respiratory syncytial virus (RSV) following intranasal administration of a Protollin-adjuvanted, epitope-enhanced recombinant G protein vaccine. J. Clin. Virol. *44*, 287–291.

Hui, S.P., Sheng, D.Z., Sugimoto, K., Gonzalez-Rajal, A., Nakagawa, S., Hesselson, D., and Kikuchi, K. (2017). Zebrafish Regulatory T Cells Mediate Organ-Specific Regenerative Programs. Dev. Cell *43*, 659-672.e5.

Huising, M.O., Kruiswijk, C.P., and Flik, G. (2006). Phylogeny and evolution of class-I helical cytokines. J. Endocrinol. *189*, 1–25.

Huttenhuis, H.B.T., Romano, N., Oosterhoud, C.N., Taverne-Thiele, A.J., Mastrolia, L., Muiswinkel, W.B., and Rombout, J.H.W.M. (2005). The ontogeny of mucosal immune cells in common carp (Cyprinus carpio L.). Anat. Embryol. (Berl). *211*, 19–29.

Hwang, P.P., and Lee, T.H. (2007). New insights into fish ion regulation and mitochondrion-rich cells. Comp. Biochem. Physiol. - A Mol. Integr. Physiol. *148*, 479–497.

Hwang, J.Y., Randall, T.D., and Silva-Sanchez, A. (2016). Inducible bronchus-associated lymphoid tissue: Taming inflammation in the lung. Front. Immunol. *7*, 1.

Hwang, S.D., Kondo, H., Hirono, I., and Aoki, T. (2011). Molecular cloning and characterization of Toll-like receptor 14 in Japanese flounder, Paralichthys olivaceus. Fish Shellfish Immunol. *30*, 425–429.

Hynicka, L.M., and Ensor, C.R. (2012). Prophylaxis and Treatment of Respiratory Syncytial Virus in Adult Immunocompromised Patients. Ann. Pharmacother. *46*, 558–566.

Ibricevic, A., Pekosz, A., Walter, M.J., Newby, C., Battaile, J.T., Brown, E.G., Holtzman, M.J., and Brody, S.L. (2006). Influenza Virus Receptor Specificity and Cell Tropism in Mouse and Human Airway Epithelial Cells. J. Virol. *80*, 7469–7480.

Ichinohe, T., Lee, H.K., Ogura, Y., Flavell, R., and Iwasaki, A. (2009). Inflammasome recognition of influenza virus is essential for adaptive immune responses. J. Exp. Med. *206*, 79–87.

Ichinohe, T., Pang, I.K., Kumamoto, Y., Peaper, D.R., Ho, J.H., Murray, T.S., and Iwasaki, A. (2011). Microbiota regulates immune defense against respiratory tract influenza A virus infection. Proc. Natl. Acad. Sci. U. S. A. *108*, 5354–5359.

Igarashi, K., Matsunaga, R., Hirakawa, S., Hosoya, S., Suetake, H., Kikuchi, K., Suzuki, Y., Nakamura, O., Miyadai, T., Tasumi, S., et al. (2017). Mucosal IgM Antibody with d-Mannose Affinity in Fugu Takifugu rubripes Is Utilized by a Monogenean Parasite Heterobothrium okamotoi for Host Recognition . J.

Immunol. *198*, 4107–4114.

Inamura, S., Fujimoto, Y., Kawasaki, A., Shiokawa, Z., Woelk, E., Heine, H., Lindner, B., Inohara, N., Kusumoto, S., and Fukase, K. (2006). Synthesis of peptidoglycan fragments and evaluation of their biological activity. Org. Biomol. Chem. *4*, 232–242.

Invernizzi, R., Lloyd, C.M., and Molyneaux, P.L. (2020). Respiratory microbiome and epithelial interactions shape immunity in the lungs. Immunology *160*, 171–182.

Ioannidis, I., McNally, B., Willette, M., Peeples, M.E., Chaussabel, D., Durbin, J.E., Ramilo, O., Mejias, A., and Flano, E. (2012). Plasticity and Virus Specificity of the Airway Epithelial Cell Immune Response during Respiratory Virus Infection. J. Virol. *86*, 5422–5436.

Ishak, A., and Everard, M.L. (2017). Persistent and recurrent bacterial Bronchitis-A paradigm shift in our understanding of chronic respiratory disease. Front. Pediatr. *5*, 1.

İşisağ, S., and Karakişi, H. (1998). Fine Structure of the Chloride Cell in the Gill Epithelium of Brachydanio rerio (Cyprinidae, Teleostei).

Isobe, Y., Kasai, M., Nakamura, T., Tojo, S., and Kurebayashi, H. (2011). Imidazoquinolines which act via Toll-like receptors (TLR)) (World Intellectual Property Organization).

Itano, A.A., McSorley, S.J., Reinhardt, R.L., Ehst, B.D., Ingulli, E., Rudensky, A.Y., and Jenkins, M.K. (2003). Distinct dendritic cell populations sequentially present antigen to CD4 T cells and stimulate different aspects of cell-mediated immunity. Immunity *19*, 47–57.

Ivashkiv, L.B., and Donlin, L.T. (2014). Regulation of type i interferon responses. Nat. Rev. Immunol. *14*, 36–49.

Ivinson, K., Deliyannis, G., McNabb, L., Grollo, L., Gilbertson, B., Jackson, D., and Brown, L.E. (2017). Salivary Blockade Protects the Lower Respiratory Tract of Mice from Lethal Influenza Virus Infection. J. Virol. *91*.

Iwane, M.K., Edwards, K.M., Szilagyi, P.G., Walker, F.J., Griffin, M.R., Weinberg, G.A., Coulen, C., Poehling, K.A., Shone, L.P., Balter, S., et al. (2004). Population-Based Surveillance for Hospitalizations Associated With Respiratory Syncytial Virus, Influenza Virus, and Parainfluenza Viruses Among Young Children. Pediatrics *113*.

Iwasaki, A., Foxman, E.F., and Molony, R.D. (2016). Early local immune defences in the respiratory tract. Nat. Publ. Gr.

Jacobs, S.E., Lamson, D.M., Kirsten, S., and Walsh, T.J. (2013). Human rhinoviruses. Clin. Microbiol. Rev. *26*, 135–162.

Jagadeeswaran, P., Sheehan, J.P., Craig, F.E., and Troyer, D. (1999). Identification and characterization of zebrafish thrombocytes. Br. J. Haematol. *107*, 731–738.

Jansen, A.G.S.C., Sanders, E.A.M., Hoes, A.W., Van Loon, A.M., and Hak, E. (2007). Influenza- and respiratory syncytial virus- associated mortality and hospitalisations. Eur. Respir. J. *30*, 1158–1166.

Jardine, L., Barge, D., Ames-Draycott, A., Pagan, S., Cookson, S., Spickett, G., Haniffa, M., Collin, M., and Bigley, V. (2013). Rapid detection of dendritic cell and monocyte disorders using CD4 as a lineage marker of the human peripheral blood antigen-presenting cell compartment. Front. Immunol. *4*.

Jault, C., Pichon, L., and Chluba, J. (2004). Toll-like receptor gene family and TIR-domain adapters in Danio rerio. Mol. Immunol. *40*, 759–771.

Jemielita, M., Taormina, M.J., Burns, A.R., Hampton, J.S., Rolig, A.S., Guillemin, K., and Parthasarathy, R. (2014). Spatial and temporal features of the growth of a bacterial species colonizing the zebrafish gut. MBio *5*, 1751–1765.

Jewell, N.A., Cline, T., Mertz, S.E., Smirnov, S. V, Flaño, E., Schindler, C., Grieves, J.L., Durbin, R.K., Kotenko, S. V, and Durbin, J.E. (2010). Lambda interferon is the predominant interferon induced by influenza A virus infection in vivo. J. Virol. *84*, 11515–11522.

Ji, J., Rao, Y., Wan, Q., Liao, Z., and Su, J. (2018). Teleost-Specific TLR19 Localizes to Endosome, Recognizes dsRNA, Recruits TRIF, Triggers both IFN and NF-κB Pathways, and Protects Cells from Grass Carp Reovirus Infection. J. Immunol. *200*, 573–585.

Ji, J., Hu, C., Shao, T., Fan, D., Zhang, N., Lin, A., Xiang, L., and Shao, J. (2020). Differential immune responses of immunoglobulin Z subclass members in antibacterial immunity in a zebrafish model. Immunology imm.13269.

Johansson, M.E.V., and Hansson, G.C. (2016). Immunological aspects of intestinal mucus and mucins. Nat. Rev. Immunol. *16*, 639–649.

Johnson, N.P.A.S., and Mueller, J. (2002). Updating the accounts: global mortality of the 1918-1920 "Spanish" influenza pandemic. Bull. Hist. Med. *76*, 105–115.

Johnson, J.E., Gonzales, R.A., Olson, S.J., Wright, P.F., and Graham, B.S. (2007a). The histopathology of fatal untreated human respiratory syncytial virus infection. Mod. Pathol. *20*, 108–119.

Johnson, J.E., Gonzales, R.A., Olson, S.J., Wright, P.F., and Graham, B.S. (2007b). The histopathology of fatal untreated human respiratory syncytial virus infection. Mod. Pathol. *20*, 108–119.

Joint Formulary Committee (2020). Oxytetracycline. Br. Natl. Formul.

Jones, G.W., and Jones, S.A. (2016). Ectopic lymphoid follicles: Inducible centres for generating antigen-specific immune responses within tissues. Immunology *147*, 141–151.

Jones, C. V., Williams, T.M., Walker, K.A., Dickinson, H., Sakkal, S., Rumballe, B.A., Little, M.H., Jenkin, G., and Ricardo, S.D. (2013). M2 macrophage polarisation is associated with alveolar formation during postnatal lung development. Respir. Res. *14*, 41.

Jonsdottir, H.R., and Dijkman, R. (2016). Coronaviruses and the human airway: A universal system for virus-host interaction studies Coronaviruses: Emerging and re-emerging pathogens in humans and animals Susanna Lau Emerging viruses. Virol. J. *13*, 1–9.

Jonz, M.G., and Nurse, C.A. (2005). Development of oxygen sensing in the gills of zebrafish. J. Exp. Biol. *208*.

Jorquera, P.A., and Tripp, R.A. (2017). Respiratory syncytial virus: prospects for new and emerging therapeutics. Expert Rev. Respir. Med. 1–7.

Jung, I.H., Chung, Y.-Y., Jung, D.E., Kim, Y.J., Kim, D.H., Kim, K.-S., and Park, S.W. (2016). Impaired Lymphocytes Development and Xenotransplantation of Gastrointestinal Tumor Cells in Prkdc-Null SCID Zebrafish Model. Neoplasia *18*, 468–479.

Junt, T., Moseman, E.A., Iannacone, M., Massberg, S., Lang, P.A., Boes, M., Fink, K., Henrickson, S.E., Shayakhmetov, D.M., Di Paolo, N.C., et al. (2007). Subcapsular sinus macrophages in lymph nodes clear lymph-borne viruses and present them to antiviral B cells. Nature *450*, 110–114.

Jurk, M., Heil, F., Vollmer, J., Schetter, C., Krieg, A.M., Wagner, H., Lipford, G., and Bauer, S. (2002). Human TLR7 or TLR8 independently confer responsiveness to the antiviral compound R-848. Nat. Immunol. *3*, 499.

Kaiser, L., Fritz, R.S., Straus, S.E., Gubareva, L., and Hayden, F.G. (2001). Symptom pathogenesis during acute influenza: Interleukin-6 and other cytokine responses. J. Med. Virol. *64*, 262–268.

Kallewaard, N.L., Bowen, A.L., and Crowe, J.E. (2005). Cooperativity of actin and microtubule elements during replication of respiratory syncytial virus. Virology *331*, 73–81.

Kalymbetova, T. V, Selvakumar, B., Rodríguez-Castillo, J.A., Gunjak, M., Malainou, C., Heindl, M.R., Moiseenko, A., Chao, C.-M., Vadász, I., Mayer, K., et al. (2018). Resident alveolar macrophages are master regulators of arrested alveolarization in experimental bronchopulmonary dysplasia. J. Pathol. *245*, 153–159.

Kao, Y.J., Piedra, P.A., Larsen, G.L., and Colasurdo, G.N. (2001). Induction and regulation of nitric oxide synthase in airway epithelial cells by respiratory syncytial virus. Am. J. Respir. Crit. Care Med. *163*, 532–539.

Kasheta, M., Painter, C.A., Moore, F.E., Lobbardi, R., Bryll, A., Freiman, E., Stachura, D., Rogers, A.B., Houvras, Y., Langenau, D.M., et al. (2017). Identification and characterization of T reg-like cells in zebrafish. J. Exp. Med. *214*, 3519–3530.

Kato, G., Miyazawa, H., Nakayama, Y., Ikari, Y., Kondo, H., Yamaguchi, T., Sano, M., and Fischer, U. (2018). A Novel Antigen-Sampling Cell in the Teleost Gill Epithelium With the Potential for Direct Antigen Presentation in Mucosal Tissue. Front. Immunol. *9*, 2116.

Kaur, G., and Dufour, J.M. (2012). Cell lines. Spermatogenesis *2*, 1–5.

Kavaliauskis, A., Arnemo, M., Speth, M., Lagos, L., Rishovd, A.-L., Estepa, A., Griffiths, G., and Gjøen, T.

(2016). Protective effect of a recombinant VHSV-G vaccine using poly(I:C) loaded nanoparticles as an adjuvant in zebrafish (Danio rerio) infection model. Dev. Comp. Immunol. *61*, 248–257.

Kavanagh, D.P.J., and Kalia, N. (2019). Live Intravital Imaging of Cellular Trafficking in the Cardiac Microvasculature—Beating the Odds. Front. Immunol. *10*, 2782.

Kawai, T., and Akira, S. (2010). The role of pattern-recognition receptors in innate immunity: Update on toll-like receptors. Nat. Immunol. *11*, 373–384.

Kawasaki, T., and Kawai, T. (2014). Toll-like receptor signaling pathways. Front. Immunol. *5*, 1–8.

Keck, T., Leiacker, R., Riechelmann, H., and Rettinger, G. (2000). Temperature Profile in the Nasal Cavity. Laryngoscope *110*, 651–654.

van Kessel, M.A.H.J., Mesman, R.J., Arshad, A., Metz, J.R., Spanings, F.A.T., van Dalen, S.C.M., van Niftrik, L., Flik, G., Wendelaar Bonga, S.E., Jetten, M.S.M., et al. (2016). Branchial nitrogen cycle symbionts can remove ammonia in fish gills. Environ. Microbiol. Rep. *8*, 590–594.

Khurana, S., Loving, C.L., Manischewitz, J., King, L.R., Gauger, P.C., Henningson, J., Vincent, A.L., and Golding, H. (2013). Vaccine-induced anti-HA2 antibodies promote virus fusion and enhance influenza virus respiratory disease. Sci. Transl. Med. *5*, 200ra114-200ra114.

Kim, T.H., and Lee, H.K. (2014). Differential Roles of Lung Dendritic Cell Subsets Against Respiratory Virus Infection. Immune Netw. *14*, 128.

Kim, C.H., Hashimoto-Hill, S., and Kim, M. (2016). Migration and Tissue Tropism of Innate Lymphoid Cells. Trends Immunol. *37*, 68–79.

Kim, T.S., Hufford, M.M., Sun, J., Fu, Y.-X., and Braciale, T.J. (2010). Antigen persistence and the control of local T cell memory by migrant respiratory dendritic cells after acute virus infection. J. Exp. Med. *207*, 1161–1172.

Kirsebom, F., Michalaki, C., Agueda-Oyarzabal, M., and Johansson, C. (2020). Neutrophils do not impact viral load or the peak of disease severity during RSV infection. Sci. Rep. *10*, 1–12.

Kirsebom, F.C.M., Kausar, F., Nuriev, R., Makris, S., and Johansson, C. (2019). Neutrophil recruitment and activation are differentially dependent on MyD88/TRIF and MAVS signaling during RSV infection. Mucosal Immunol. *12*, 1244–1255.

Kishi, S., Uchiyama, J., Baughman, A.M., Goto, T., Lin, M.C., and Tsai, S.B. (2003). The zebrafish as a vertebrate model of functional aging and very gradual senescence. Exp. Gerontol. *38*, 777–786.

Kissenpfennig, A., Henri, S., Dubois, B., Laplace-Builhé, C., Perrin, P., Romani, N., Tripp, C.H., Douillard, P., Leserman, L., Kaiserlian, D., et al. (2005). Dynamics and function of langerhans cells in vivo: Dermal dendritic cells colonize lymph node areasdistinct from slower migrating langerhans cells. Immunity *22*, 643–654.

Kitiyodom, S., Kaewmalun, S., Nittayasut, N., Suktham, K., Surassmo, S., Namdee, K., Rodkhum, C., Pirarat, N., and Yata, T. (2019). The potential of mucoadhesive polymer in enhancing efficacy of direct immersion vaccination against Flavobacterium columnare infection in tilapia. Fish Shellfish Immunol. *86*, 635–640.

Kleiman, E., Salyakina, D., De Heusch, M., Hoek, K.L., Llanes, J.M., Castro, I., Wright, J.A., Clark, E.S., Dykxhoorn, D.M., Capobianco, E., et al. (2015). Distinct transcriptomic features are associated with transitional and mature B-cell populations in the mouse spleen. Front. Immunol. *6*, 30.

Koppang, E.O., Fischer, U., Moore, L., Tranulis, M.A., Dijkstra, J.M., Köllner, B., Aune, L., Jirillo, E., and Hordvik, I. (2010). Salmonid T cells assemble in the thymus, spleen and in novel interbranchial lymphoid tissue. J. Anat. *217*, 728–739.

Krasteva, G., Canning, B.J., Hartmann, P., Veres, T.Z., Papadakis, T., Muhlfeld, C., Schliecker, K., Tallini, Y.N., Braun, A., Hackstein, H., et al. (2011). Cholinergic chemosensory cells in the trachea regulate breathing. Proc. Natl. Acad. Sci. *108*, 9478–9483.

Krasteva, G., Canning, B.J., Papadakis, T., and Kummer, W. (2012). Cholinergic brush cells in the trachea mediate respiratory responses to quorum sensing molecules. In Life Sciences, (Pergamon), pp. 992–996.

Krauss, J., Astrinidis, P., Astrinides, P., Frohnhöfer, H.G., Walderich, B., and Nüsslein-Volhard, C. (2013). transparent, a gene affecting stripe formation in Zebrafish, encodes the mitochondrial protein Mpv17 that is required for iridophore survival. Biol. Open *2*, 703–710.

Kreda, S.M., Davis, C.W., and Rose, M.C. (2012). CFTR, mucins, and mucus obstruction in cystic fibrosis. Cold Spring Harb. Perspect. Med. *2*.

Krege, J., Seth, S., Hardtke, S., Davalos-Misslitz, A.C.M., and Förster, R. (2009). Antigen-dependent rescue of nose-associated lymphoid tissue (NALT) development independent of LTβR and CXCR5 signaling. Eur. J. Immunol. *39*, 2765–2778.

Kreijtz, J.H.C.M., Fouchier, R.A.M., and Rimmelzwaan, G.F. (2011). Immune responses to influenza virus infection. Virus Res. *162*, 19–30.

Kuil, L.E., Oosterhof, N., Ferrero, G., Mikulášová, T., Hason, M., Dekker, J., Rovira, M., van der Linde, H.C., van Strien, P.M.H., de Pater, E., et al. (2020). Zebrafish macrophage developmental arrest underlies depletion of microglia and reveals Csf1r-independent metaphocytes. Elife *9*.

Kulkarni, U., Zemans, R.L., Smith, C.A., Wood, S.C., Deng, J.C., and Goldstein, D.R. (2019). Excessive neutrophil levels in the lung underlie the age-associated increase in influenza mortality. Mucosal Immunol. *12*, 545–554.

Kumar, S., Lockwood, N., Ramel, M.-C., Correia, T., Ellis, M., Alexandrov, Y., Andrews, N., Patel, R., Bugeon, L., Dallman, M.J., et al. (2016). Quantitative in vivo optical tomography of cancer progression & vasculature development in adult zebrafish. Oncotarget *7*, 2–11.

Kumari, J., Bogwald, J., and Dalmo, R.A. (2009a). Transcription factor GATA-3 in Atlantic salmon (Salmo

salar): molecular characterization, promoter activity and expression analysis. Mol. Immunol. *46*, 3099–3107.

Kumari, U., Yashpal, M., Mittal, S., and Mittal, A.K. (2009b). Histochemical analysis of glycoproteins in the secretory cells in the gill epithelium of a catfish, Rita rita (Siluriformes, Bagridae). Tissue Cell *41*, 271–280.

Kuper, C.F. (2006). Histopathology of Mucosa-Associated Lymphoid Tissue. Toxicol. Pathol. *34*, 609–615.

Kurt-Jones, E.A., Popova, L., Kwinn, L., Haynes, L.M., Jones, L.P., Tripp, R.A., Walsh, E.E., Freeman, M.W., Golenbock, D.T., Anderson, L.J., et al. (2000). Pattern recognition receptors TLR4 and CD14 mediate response to respiratory syncytial virus. Nat. Immunol. *1*, 398–401.

Lam, S.. H., Chua, H.. L., Gong, Z., Lam, T.. J., and Sin, Y.. M. (2004). Development and maturation of the immune system in zebrafish, Danio rerio: a gene expression profiling, in situ hybridization and immunological study. Dev. Comp. Immunol. *28*, 9–28.

Lam, S.H., Chua, H.L., Gong, Z., Wen, Z., Lam, T.J., and Sin, Y.M. (2002). Morphologic transformation of the thymus in developing zebrafish. Dev. Dyn. *225*, 87–94.

Lambert, L., and Culley, F.J. (2017). Innate immunity to respiratory infection in early life. Front. Immunol. *8*, 1570.

Lambrecht, B.N., and Hammad, H. (2009). Biology of Lung Dendritic Cells at the Origin of Asthma. Immunity *31*, 412–424.

Lamers, C.H.J., and De Haas, M.J.H. (1985). Antigen localization in the lymphoid organs of carp (Cyprinus carpio). Cell Tissue Res. *242*, 491–498.

Langenau, D.M., and Zon, L.I. (2005). The zebrafish: a new model of T-cell and thymic development. Nat. Rev. Immunol. *5*, 307–317.

Langenau, D.M., Ferrando, A.A., Traver, D., Kutok, J.L., Hezel, J.-P.D., Kanki, J.P., Zon, L.I., Look, A.T., and Trede, N.S. (2004). In vivo tracking of T cell development, ablation, and engraftment in transgenic zebrafish. Proc. Natl. Acad. Sci. U. S. A. *101*, 7369–7374.

Langevin, C., Aleksejeva, E., Passoni, G., Palha, N., Levraud, J.-P.P., and Boudinot, P. (2013a). The antiviral innate immune response in fish: Evolution and conservation of the IFN system. J. Mol. Biol. *425*, 4904–4920.

Langevin, C., Van Der Aa, L.M., Houel, A., Torhy, C., Briolat, V., Lunazzi, A., Harmache, A., Bremont, M., Levraud, J.-P., and Boudinot, P. (2013b). Zebrafish ISG15 Exerts a Strong Antiviral Activity against RNA and DNA Viruses and Regulates the Interferon Response.

Lapatra, S.E., Barone, L., Jones, G.R., and Zon, L.I. (2000). Effects of Infectious Hematopoietic Necrosis Virus and Infectious Pancreatic Necrosis Virus Infection on Hematopoietic Precursors of the Zebrafish. Blood Cells, Mol. Dis. *26*, 445–452.

Lauksund, S., Greiner-Tollersrud, L., Chang, C.J., and Robertsen, B. (2015). Infectious pancreatic necrosis virus proteins VP2, VP3, VP4 and VP5 antagonize IFNa1 promoter activation while VP1 induces IFNa1. Virus Res. *196*, 113–121.

Lawson, N.D., and Weinstein, B.M. (2002). In vivo imaging of embryonic vascular development using transgenic zebrafish. Dev. Biol. *248*, 307–318.

Lay, M.K., Bueno, S.M., Gálvez, N., Riedel, C.A., and Kalergis, A.M. (2015). New insights on the viral and host factors contributing to the airway pathogenesis caused by the respiratory syncytial virus. Crit. Rev. Microbiol. 1–13.

Leal, J., Smyth, H.D.C., and Ghosh, D. (2017). Physicochemical properties of mucus and their impact on transmucosal drug delivery. Int. J. Pharm. *532*, 555–572.

Lebold, K.M., Jacoby, D.B., and Drake, M.G. (2016). Toll-Like Receptor 7-Targeted Therapy in Respiratory Disease. Transfus. Med. Hemotherapy *43*, 114–119.

Lee, P., and Kim, D.-J. (2020). Newly Emerging Human Coronaviruses: Animal Models and Vaccine Research for SARS, MERS, and COVID-19. Immune Netw. *20*, 1–25.

Lee, D.C.P., Harker, J.A.E., Tregoning, J.S., Atabani, S.F., Johansson, C., Schwarze, J., and Openshaw, P.J.M. (2010). CD25+ Natural Regulatory T Cells Are Critical in Limiting Innate and Adaptive Immunity and Resolving Disease following Respiratory Syncytial Virus Infection. J. Virol. *84*, 8790–8798.

Lee, J.J., McGarry, M.P., Farmer, S.C., Denzler, K.L., Larson, K.A., Carrigan, P.E., Brenneise, I.E., Horton, M.A., Haczku, A., Gelfand, E.W., et al. (1997). Interleukin-5 expression in the lung epithelium of transgenic mice leads to pulmonary changes pathognomonic of asthma. J. Exp. Med. *185*, 2143–2156.

Lee, N., Wong, C.K., Chan, M.C.W., Yeung, E.S.L., Tam, W.W.S., Tsang, O.T.Y., Choi, K.W., Chan, P.K.S., Kwok, A., Lui, G.C.Y., et al. (2017). Anti-inflammatory effects of adjunctive macrolide treatment in adults hospitalized with influenza: A randomized controlled trial. Antiviral Res. *144*, 48–56.

Lee, S.M.Y., Kok, K.H., Jaume, M., Cheung, T.K.W., Yip, T.F., Lai, J.C.C., Guan, Y., Webster, R.G., Jin, D.Y., and Malik Peiris, J.S. (2014). Toll-like receptor 10 is involved in induction of innate immune responses to influenza virus infection. Proc. Natl. Acad. Sci. U. S. A. *111*, 3793–3798.

Legg, J.P., Hussain, I.R., Warner, J.A., Johnston, S.L., and Warner, J.O. (2003). Type 1 and type 2 cytokine imbalance in acute respiratory syncytial virus bronchiolitis. Am. J. Respir. Crit. Care Med. *168*, 633–639.

Legrand, T.P.R.A., Catalano, S.R., Wos-Oxley, M.L., Stephens, F., Landos, M., Bansemer, M.S., Stone, D.A.J., Qin, J.G., and Oxley, A.P.A. (2018). The Inner Workings of the Outer Surface: Skin and Gill Microbiota as Indicators of Changing Gut Health in Yellowtail Kingfish. Front. Microbiol. *8*.

Leguen, I. (2018). Gills of the medaka (Oryzias latipes): A scanning electron microscopy study. J. Morphol. *279*, 97–108.

Lepiller, S., Franche, N., Solary, E., Chluba, J., and Laurens, V. (2009). Comparative analysis of zebrafish

nos2a and nos2b genes. Gene *445*, 58–65.

Levican, J., Miranda-Cárdenas, C., Soto-Rifo, R., Aguayo, F., Gaggero, A., and León, O. (2017). Infectious pancreatic necrosis virus enters CHSE-214 cells via macropinocytosis. Sci. Rep. *7*, 1–12.

Lewis, K.L., Del Cid, N., and Traver, D. (2014). Perspectives on antigen presenting cells in zebrafish. Dev. Comp. Immunol. *46*, 63–73.

Li, J.Y., Wang, Y.Y., Shao, T., Fan, D.D., Lin, A.F., Xiang, L.X., and Shao, J.Z. (2020). The zebrafish NLRP3 inflammasome has functional roles in ASC-dependent interleukin-1β maturation and gasdermin E-mediated pyroptosis. J. Biol. Chem. *295*, 1120–1141.

Li, P., Ye, J., Zeng, S., and Yang, C. (2019). Florfenicol alleviated lipopolysaccharide (LPS)-induced inflammatory responses in Ctenopharyngodon idella through inhibiting toll / NF-κB signaling pathways. Fish Shellfish Immunol. *94*, 479–484.

Li, Y.Y., Li, Y.Y., Cao, X., Jin, X., and Jin, T. (2016). Pattern recognition receptors in zebrafish provide functional and evolutionary insight into innate immune signaling pathways. Cell. Mol. Immunol. *14*, 1–10.

Liang, B., Hyland, L., and Hou, S. (2001). Nasal-Associated Lymphoid Tissue Is a Site of Long-Term Virus-Specific Antibody Production following Respiratory Virus Infection of Mice. J. Virol. *75*, 5416–5420.

Limbu, S.M., Zhou, L., Sun, S.-X., Zhang, M.-L., and Du, Z.-Y. (2018). Chronic exposure to low environmental concentrations and legal aquaculture doses of antibiotics cause systemic adverse effects in Nile tilapia and provoke differential human health risk. Environ. Int. *115*, 205–219.

Lin, X., Zhou, Q., Zhao, C., Lin, G., Xu, J., and Wen, Z. (2019). An Ectoderm-Derived Myeloid-like Cell Population Functions as Antigen Transporters for Langerhans Cells in Zebrafish Epidermis. Dev. Cell *49*, 605-617.e5.

Lin, X., Zhou, Q., Lin, G., Zhao, C., and Wen, Z. (2020). Endoderm-Derived Myeloid-like Metaphocytes in Zebrafish Gill Mediate Soluble Antigen-Induced Immunity. Cell Rep. *33*.

Lindsey, B.W., Douek, A.M., Loosli, F., and Kaslin, J. (2018). A Whole Brain Staining, Embedding, and Clearing Pipeline for Adult Zebrafish to Visualize Cell Proliferation and Morphology in 3-Dimensions. Front. Neurosci. *11*, 750.

Ling, Z., Tran, K.C., and Teng, M.N. (2009). Human Respiratory Syncytial Virus Nonstructural Protein NS2 Antagonizes the Activation of Beta Interferon Transcription by Interacting with RIG-I. J. Virol. *83*, 3734–3742.

Liu, F., and Wen, Z. (2002). Cloning and expression pattern of the lysozyme C gene in zebrafish. Mech. Dev. *113*, 69–72.

Liu, G., Betts, C., Cunoosamy, D.M., Åberg, P.M., Hornberg, J.J., Sivars, K.B., and Cohen, T.S. (2019a). Use of precision cut lung slices as a translational model for the study of lung biology. Respir. Res. *20*.

Liu, J., Xu, C., Hsu, L.C., Luo, Y., Xiang, R., and Chuang, T.H. (2010). A five-amino-acid motif in the undefined region of the TLR8 ectodomain is required for species-specific ligand recognition. Mol. Immunol. *47*, 1083–1090.

Liu, W., Fontanet, A., Zhang, P., Zhan, L., Xin, Z., Baril, L., Tang, F., Lv, H., and Cao, W. (2006). Two-Year Prospective Study of the Humoral Immune Response of Patients with Severe Acute Respiratory Syndrome. J. Infect. Dis. *193*, 792–795.

Liu, W., Kuang, M., Zhang, Z., Lu, Y., and Liu, X. (2019b). Molecular Characterization and Expression Analysis of ftr01, ftr42, and ftr58 in Zebrafish (Danio rerio). Virol. Sin. *34*, 434–443.

Liu, X., Wu, H., Chang, X., Tang, Y., Liu, Q., and Zhang, Y. (2014). Notable mucosal immune responses induced in the intestine of zebrafish (Danio rerio) bath-vaccinated with a live attenuated Vibrio anguillarum vaccine. Fish Shellfish Immunol. *40*, 99–108.

Livak, K.J., and Schmittgen, T.D. (2001). Analysis of Relative Gene Expression Data Using Real- Time Quantitative PCR and the 2-^ddCT Method. Methods *25*, 402–408.

Lizundia, R., Sauter, K.S., Taylor, G., and Werling, D. (2008). Host species-specific usage of the TLR4-LPS receptor complex. Innate Immun. *14*, 223–231.

Lo, M.S., Brazas, R.M., and Holtzman, M.J. (2005). Respiratory Syncytial Virus Nonstructural Proteins NS1 and NS2 Mediate Inhibition of Stat2 Expression and Alpha/Beta Interferon Responsiveness. J. Virol. *79*, 9315–9319.

Loebbermann, J., Schnoeller, C., Thornton, H., Durant, L., Sweeney, N.P., Schuijs, M., O'Garra, A., Johansson, C., and Openshaw, P.J. (2012). IL-10 Regulates Viral Lung Immunopathology during Acute Respiratory Syncytial Virus Infection in Mice. PLoS One *7*, e32371.

Loffredo, L.F., Coden, M.E., Jeong, B.M., Walker, M.T., Anekalla, K.R., Doan, T.C., Rodriguez, R., Browning, M., Nam, K., Lee, J.J., et al. (2020). Eosinophil accumulation in postnatal lung is specific to the primary septation phase of development. Sci. Rep. *10*, 1–14.

Long, J.S., Giotis, E.S., Moncorgé, O., Frise, R., Mistry, B., James, J., Morisson, M., Iqbal, M., Vignal, A., Skinner, M.A., et al. (2016). Species difference in ANP32A underlies influenza A virus polymerase host restriction. Nature *529*, 101–104.

Long, Y., Li, L., Li, Q., He, X., and Cui, Z. (2012). Transcriptomic Characterization of Temperature Stress Responses in Larval Zebrafish. PLoS One *7*, e37209.

López-Muñoz, A., Roca, F.J., Meseguer, J., and Mulero, V. (2009). New insights into the evolution of IFNs: zebrafish group II IFNs induce a rapid and transient expression of IFN-dependent genes and display powerful antiviral activities. J. Immunol. *182*, 3440–3449.

López-Muñoz, A., Roca, F.J., Sepulcre, M.P., Meseguer, J., and Mulero, V. (2010). Zebrafish larvae are unable to mount a protective antiviral response against waterborne infection by spring viremia of carp virus.

Dev. Comp. Immunol. *34*, 546–552.

López-Muñoz, A., Sepulcre, M.P., Roca, F.J., Figueras, A., Meseguer, J., and Mulero, V. (2011). Evolutionary conserved pro-inflammatory and antigen presentation functions of zebrafish IFNγ revealed by transcriptomic and functional analysis. Mol. Immunol. *48*, 1073–1083.

López-Olmeda, J.F., and Sánchez-Vázquez, F.J. (2011). Thermal biology of zebrafish (Danio rerio). J. Therm. Biol. *36*, 91–104.

López Nadal, A., Peggs, D., Wiegertjes, G.F., and Brugman, S. (2018). Exposure to Antibiotics Affects Saponin Immersion-Induced Immune Stimulation and Shift in Microbial Composition in Zebrafish Larvae. Front. Microbiol. *9*, 2588.

Lowery, E.M., Brubaker, A.L., Kuhlmann, E., and Kovacs, E.J. (2013). The aging lung. Clin. Interv. Aging *8*, 1489–1496.

Lu, M.W., Chao, Y.M., Guo, T.C., Santi, N., Evensen, Ø., Kasani, S.K., Hong, J.R., and Wu, J.L. (2008). The interferon response is involved in nervous necrosis virus acute and persistent infection in zebrafish infection model. Mol. Immunol. *45*, 1146–1152.

Lü, A., Hu, X., Wang, Y., Shen, X., Li, X., Zhu, A., Tian, J., Ming, Q., and Feng, Z. (2014). ITRAQ analysis of gill proteins from the zebrafish (Danio rerio) infected with Aeromonas hydrophila. Fish Shellfish Immunol. *36*, 229–239.

Lugo-Villarino, G., Balla, K.M., Stachura, D.L., Bañuelos, K., Werneck, M.B.F., and Traver, D. (2010). Identification of dendritic antigen-presenting cells in the zebrafish. Proc. Natl. Acad. Sci. U. S. A. *107*, 15850–15855.

Lukens, M. V., Kruijsen, D., Coenjaerts, F.E.J., Kimpen, J.L.L., and van Bleek, G.M. (2009a). Respiratory Syncytial Virus-Induced Activation and Migration of Respiratory Dendritic Cells and Subsequent Antigen Presentation in the Lung-Draining Lymph Node. J. Virol. *83*, 7235–7243.

Lukens, M. V., van de Pol, A.C., Coenjaerts, F.E.J., Jansen, N.J.G., Kamp, V.M., Kimpen, J.L.L., Rossen, J.W.A., Ulfman, L.H., Tacke, C.E.A., Viveen, M.C., et al. (2010). A Systemic Neutrophil Response Precedes Robust CD8+ T-Cell Activation during Natural Respiratory Syncytial Virus Infection in Infants. J. Virol. *84*, 2374–2383.

Lukens, M. V, Kruijsen, D., Coenjaerts, F.E.J., Kimpen, J.L.L., and van Bleek, G.M. (2009b). Respiratory syncytial virus-induced activation and migration of respiratory dendritic cells and subsequent antigen presentation in the lung-draining lymph node. J. Virol. *83*, 7235–7243.

Lumsden, J.S., and Ferguson, H.W. (1994). Isolation and partial characterization of rainbow trout (Oncorhynchus mykiss) gill mucin. Fish Physiol. Biochem. *12*, 387–398.

Lumsden, J.S., Ostland, V.E., MacPhee, D.D., and Ferguson, H.W. (1995). Production of gill-associated and serum antibody byrainbow trout (Oncorhynchus mykiss) following immersion immunization with

acetone-killed Flavobacterium branchiophilum and the relationship to protection from experimental challenge. Fish Shellfish Immunol. *5*, 151–165.

Lundén, T., Miettinen, S., Lönnström, L.G., Lllius, E.M., and Bylund, G. (1998). Influence of oxytetracycline and oxolinic acid on the immune response of rainbow trout (Oncorhynchus mykiss). Fish Shellfish Immunol. *8*, 217–230.

Ma, J., Rubin, B.K., and Voynow, J.A. (2018). Mucins, Mucus, and Goblet Cells. Chest *154*, 169–176.

Maarouf, O.H., Uehara, M., Kasinath, V., Solhjou, Z., Banouni, N., Bahmani, B., Jiang, L., Yilmam, O.A., Guleria, I., Lovitch, S.B., et al. (2018). Repetitive ischemic injuries to the kidneys result in lymph node fibrosis and impaired healing. JCI Insight *3*.

Macirella, R., and Brunelli, E. (2017). Morphofunctional alterations in zebrafish (Danio rerio) gills after exposure to mercury chloride. Int. J. Mol. Sci. *18*.

Mackay, C.R., Marston, W., and Dudler, L. (1992). Altered patterns of T cell migration through lymph nodes and skin following antigen challenge. Eur. J. Immunol. *22*, 2205–2210.

MacKenzie, S.A., Roher, N., Boltaña, S., and Goetz, F.W. (2010). Peptidoglycan, not endotoxin, is the key mediator of cytokine gene expression induced in rainbow trout macrophages by crude LPS☆. Mol. Immunol. *47*, 1450–1457.

Maikawa, C.L., Zimmerman, N., Rais, K., Shah, M., Hawley, B., Pant, P., Jeong, C.H., Delgado-Saborit, J.M., Volckens, J., Evans, G., et al. (2016). Murine precision-cut lung slices exhibit acute responses following exposure to gasoline direct injection engine emissions. Sci. Total Environ. *568*, 1102–1109.

Majumdar, S., and Nandi, D. (2018). Thymic Atrophy: Experimental Studies and Therapeutic Interventions. Scand. J. Immunol. *87*, 4–14.

Makris, S., and Johansson, C. (2020). R848 or influenza virus can induce potent innate immune responses in the lungs of neonatal mice. Mucosal Immunol. 1–10.

Malinina, A., Dikeman, D., Westbrook, R., Moats, M., Gidner, S., Poonyagariyagorn, H., Walston, J., and Neptune, E.R. (2020). IL10 deficiency promotes alveolar enlargement and lymphoid dysmorphogenesis in the aged murine lung. Aging Cell *19*.

Man, S.M., and Kanneganti, T.-D. (2015). Regulation of inflammasome activation. Immunol. Rev. *265*, 6–21.

Man, W.H., De Steenhuijsen Piters, W.A.A., and Bogaert, D. (2017). The microbiota of the respiratory tract: Gatekeeper to respiratory health. Nat. Rev. Microbiol. *15*, 259–270.

Mancuso, G., Gambuzza, M., Midiri, A., Biondo, C., Papasergi, S., Akira, S., Teti, G., and Beninati, C. (2009). Bacterial recognition by TLR7 in the lysosomes of conventional dendritic cells. Nat. Immunol. *10*, 587–594.

Van Der Marel, M., Adamek, M., Gonzalez, S.F., Frost, P., Rombout, J.H.W.M., Wiegertjes, G.F., Savelkoul,

H.F.J., and Steinhagen, D. (2012). Molecular cloning and expression of two beta-defensin and two mucin genes in common carp (Cyprinus carpio L.) and their up-regulation after beta-glucan feeding. Fish Shellfish Immunol. *32*, 494–501.

Marin, N.D., Dunlap, M.D., Kaushal, D., and Khader, S.A. (2019). Friend or Foe: The Protective and Pathological Roles of Inducible Bronchus-Associated Lymphoid Tissue in Pulmonary Diseases. J. Immunol. *202*, 2519–2526.

Marr, N., and Turvey, S.E. (2012). Role of human TLR4 in respiratory syncytial virus-induced NF-κB activation, viral entry and replication. Innate Immun. *18*, 856–865.

Martín, V., Mavian, C., López Bueno, A., de Molina, A., Díaz, E., Andrés, G., Alcami, A., and Alejo, A. (2015). Establishment of a Zebrafish Infection Model for the Study of Wild-Type and Recombinant European Sheatfish Virus. J. Virol. *89*, 10702–10706.

Martins, R.R., Ellis, P.S., MacDonald, R.B., Richardson, R.J., and Henriques, C.M. (2019a). Resident Immunity in Tissue Repair and Maintenance: The Zebrafish Model Coming of Age. Front. Cell Dev. Biol. *7*, 12.

Martins, R.R., Ellis, R.S., Macdonald, P.B., Richardson, R.J., and Martins Henriques, B. (2019b). Resident Immunity in Tissue Repair and Maintenance: The Zebrafish Model Coming of Age. Front. Cell Dev. Biol. *7*.

Matikainen, S., Pirhonen, J., Miettinen, M., Lehtonen, A., Govenius-Vintola, C., Sareneva, T., and Julkunen, I. (2000). Influenza A and Sendai viruses induce differential chemokine gene expression and transcription factor activation in human macrophages. Virology *276*, 138–147.

Matsuo, A., Oshiumi, H., Tsujita, T., Mitani, H., Kasai, H., Yoshimizu, M., Matsumoto, M., and Seya, T. (2008). Teleost TLR22 recognizes RNA duplex to induce IFN and protect cells from birnaviruses. J. Immunol. *181*, 3474–3485.

May, A. (2017). Characterisation of Immune Cells in Adult Zebrafish Gills. Imperial College London.

McBeath, A.J.A., Snow, M., Secombes, C.J., Ellis, A.E., and Collet, B. (2007). Expression kinetics of interferon and interferon-induced genes in Atlantic salmon (Salmo salar) following infection with infectious pancreatic necrosis virus and infectious salmon anaemia virus. Fish Shellfish Immunol. *22*, 230–241.

McGhee, J.R.R., Fujihashi, K., Getachew, H., Bromberg, J., and Lira, S. (2012). Inside the Mucosal Immune System. PLoS Biol. *10*, e1001397.

McGinniss, J.E., and Collman, R.G. (2018). Of mice and men and microbes: Conclusions and cautions from a murine study of the lung microbiome and microbiome-immune interactions. Am. J. Respir. Crit. Care Med. *198*, 419–422.

McLaren, C., and Butchko, G.M. (1978). Regional T- and B- cell responses in influenza-infected ferrets. Infect. Immun. *22*, 189–194.

Meeker, N.D., and Trede, N.S. (2008). Immunology and zebrafish: Spawning new models of human disease. Dev. Comp. Immunol. *32*, 745–757.

Mehta, R., Gerardin, P., de Brito, C.A.A., Soares, C.N., Ferreira, M.L.B., and Solomon, T. (2018). The neurological complications of chikungunya virus: A systematic review. Rev. Med. Virol. *28*, 28.

Meijer, A.H., Gabby Krens, S., Medina Rodriguez, I.A., He, S., Bitter, W., Ewa Snaar-Jagalska, B., and Spaink, H.P. (2004). Expression analysis of the Toll-like receptor and TIR domain adaptor families of zebrafish. Mol. Immunol. *40*, 773–783.

Meijer, A.H., van der Sar, A.M., Cunha, C., Lamers, G.E.M., Laplante, M.A., Kikuta, H., Bitter, W., Becker, T.S., and Spaink, H.P. (2008). Identification and real-time imaging of a myc-expressing neutrophil population involved in inflammation and mycobacterial granuloma formation in zebrafish. Dev. Comp. Immunol. *32*, 36–49.

Meischel, T., Villalon-Letelier, F., Saunders, P.M., Reading, P.C., and Londrigan, S.L. (2020). Influenza A virus interactions with macrophages: Lessons from epithelial cells. Cell. Microbiol. *22*.

Mierzwa, A.S., Nguyen, F., Xue, M., and Jonz, M.G. (2020). Regeneration of the gill filaments and replacement of serotonergic neuroepithelial cells in adult zebrafish (Danio rerio). Respir. Physiol. Neurobiol. *274*.

Miller, A.J., and Spence, J.R. (2017). In vitro models to study human lung development, disease and homeostasis. Physiology *32*, 246–260.

Mitchell, S.O., and Rodger, H.D. (2011). A review of infectious gill disease in marine salmonid fish. J. Fish Dis. *34*, 411–432.

Miyauchi, K. (2017). Helper T Cell Responses to Respiratory Viruses in the Lung: Development, Virus Suppression, and Pathogenesis. Viral Immunol. *30*, 421–430.

Miyazawa, R., Matsuura, Y., Shibasaki, Y., Imamura, S., and Nakanishi, T. (2016). Cross-reactivity of monoclonal antibodies against CD4-1 and CD8α of ginbuna crucian carp with lymphocytes of zebrafish and other cyprinid species. Dev. Comp. Immunol.

Mizuno, D., Kimoto, T., Sakai, S., Takahashi, E., Kim, H., and Kido, H. (2016). Induction of systemic and mucosal immunity and maintenance of its memory against influenza A virus by nasal vaccination using a new mucosal adjuvant SF-10 derived from pulmonary surfactant in young cynomolgus monkeys. Vaccine *34*, 1881–1888.

Mjösberg, J.M., Trifari, S., Crellin, N.K., Peters, C.P., Van Drunen, C.M., Piet, B., Fokkens, W.J., Cupedo, T., and Spits, H. (2011). Human IL-25-and IL-33-responsive type 2 innate lymphoid cells are defined by expression of CRTH2 and CD161. Nat. Immunol. *12*, 1055–1062.

Montero, J., Garcia, J., Ordas, M.C., Casanova, I., Gonzalez, A., Villena, A., Coll, J., and Tafalla, C. (2011). Specific regulation of the chemokine response to viral hemorrhagic septicemia virus at the entry site. J. Virol. *85*, 4046–4056.

Montoro, D.T., Haber, A.L., Biton, M., Vinarsky, V., Lin, B., Birket, S.E., Yuan, F., Chen, S., Leung, H.M.,

Villoria, J., et al. (2018). A revised airway epithelial hierarchy includes CFTR-expressing ionocytes. Nat. 2018 1.

Moore, F.E., Garcia, E.G., Lobbardi, R., Jain, E., Tang, Q., Moore, J.C., Cortes, M., Molodtsov, A., Kasheta, M., Luo, C.C., et al. (2016a). Single-cell transcriptional analysis of normal, aberrant, and malignant hematopoiesis in zebrafish. J. Exp. Med. *213*, 979–992.

Moore, J.C., Tang, Q., Yordán, N.T., Moore, F.E., Garcia, E.G., Lobbardi, R., Ramakrishnan, A., Marvin, D.L., Anselmo, A., Sadreyev, R.I., et al. (2016b). Single-cell imaging of normal and malignant cell engraftment into optically clear prkdc-null SCID zebrafish. J. Exp. Med. *213*, 2575–2589.

Mordstein, M., Kochs, G., Dumoutier, L., Renauld, J.-C., Paludan, S.R., Klucher, K., and Staeheli, P. (2008). Interferon-λ Contributes to Innate Immunity of Mice against Influenza A Virus but Not against Hepatotropic Viruses. PLoS Pathog. *4*, e1000151.

Morick, D., Faigenbaum, O., Smirnov, M., Fellig, Y., Inbal, A., Kotler, M., Development, N., and David, I. (2015). Mortality Caused by Bath Exposure of Zebrafish (Danio rerio) Larvae to Nervous Necrosis Virus is Limited to the fourth Day Post-Fertilization.

Mowat, A.M., and Viney, J.L. (1997). The anatomical basis of intestinal immunity. Immunol. Rev. *156*, 145–166.

Moyse, B.R., and Richardson, R.J. (2020). A Population of Injury-Responsive Lymphoid Cells Expresses mpeg1.1 in the Adult Zebrafish Heart . ImmunoHorizons *4*, 464–474.

Muire, P.J., Hanson, L.A., Wills, R., and Petrie-Hanson, L. (2017). Differential gene expression following TLR stimulation in rag1-/- mutant zebrafish tissues and morphological descriptions of lymphocyte-like cell populations. PLoS One *12*, e0184077.

Mukherjee, S., Karmakar, S., and Babu, S.P.S. (2016). TLR2 and TLR4 mediated host immune responses in major infectious diseases: A review. Brazilian J. Infect. Dis. *20*, 193–204.

Mulero, I., Chaves-Pozo, E., García-Alcázar, A., Meseguer, J., Mulero, V., and García Ayala, A. (2007). Distribution of the professional phagocytic granulocytes of the bony fish gilthead seabream (Sparus aurata L.) during the ontogeny of lymphomyeloid organs and pathogen entry sites. Dev. Comp. Immunol. *31*, 1024–1033.

Müller-Anstett, M.A., Müller, P., Albrecht, T., Nega, M., Wagener, J., Gao, Q., Kaesler, S., Schaller, M., Biedermann, T., and Götz, F. (2010). Staphylococcal peptidoglycan co-localizes with Nod2 and TLR2 and activates innate immune response via both receptors in primary murine keratinocytes. PLoS One *5*, 13153.

Murray, P.J., Allen, J.E., Biswas, S.K., Fisher, E.A., Gilroy, D.W., Goerdt, S., Gordon, S., Hamilton, J.A., Ivashkiv, L.B., Lawrence, T., et al. (2014). Macrophage activation and polarization: nomenclature and experimental guidelines. Immunity *41*, 14–20.

Nagendran, M., Arora, P., Gori, P., Mulay, A., Ray, S., Jacob, T., and Sonawane, M. (2015). Canonical Wnt signalling regulates epithelial patterning by modulating levels of laminins in zebrafish appendages. Development *142*, 320–330.

Nakanishi, T., Toda, H., Shibasaki, Y., and Somamoto, T. (2011). Cytotoxic T cells in teleost fish. Dev. Comp. Immunol. *35*, 1317–1323.

Neish, A.S. (2014). Mucosal immunity and the microbiome. In Annals of the American Thoracic Society, (American Thoracic Society), p. S28.

Neyt, K., and Lambrecht, B.N. (2013). The role of lung dendritic cell subsets in immunity to respiratory viruses. Immunol. Rev. *255*, 57–67.

Neyt, K., Perros, F., GeurtsvanKessel, C.H., Hammad, H., and Lambrecht, B.N. (2012). Tertiary lymphoid organs in infection and autoimmunity. Trends Immunol. *33*, 297–305.

Ngai, J.C., Ko, F.W., Ng, S.S., To, K.W., Tong, M., and Hui, D.S. (2010). The long-term impact of severe acute respiratory syndrome on pulmonary function, exercise capacity and health status. Respirology *15*, 543–550.

Nguyen-Chi, M., Laplace-Builhe, B., Travnickova, J., Luz-Crawford, P., Tejedor, G., Phan, Q.T., Duroux-Richard, I., Levraud, J.-P., Kissa, K., Lutfalla, G., et al. (2015). Identification of polarized macrophage subsets in zebrafish. Elife *4*, e07288.

Ni, K., Li, S., Xia, Q., Zang, N., Deng, Y., Xie, X., Luo, Z., Luo, Y., Wang, L., Fu, Z., et al. (2012). Pharyngeal Microflora Disruption by Antibiotics Promotes Airway Hyperresponsiveness after Respiratory Syncytial Virus Infection. PLoS One *7*, e41104.

Ni, L.Y., Chen, H.P., Han, R., Luo, X.C., Li, A.X., Li, J.Z., Dan, X.M., and Li, Y.W. (2020). Distribution of Mpeg1+ cells in healthy grouper (Epinephelus coioides) and after Cryptocaryon irritans infection. Fish Shellfish Immunol. *104*, 222–227.

Nochi, T., Jansen, C.A., Toyomizu, M., and Eden, W. van (2018). The Well-Developed Mucosal Immune Systems of Birds and Mammals Allow for Similar Approaches of Mucosal Vaccination in Both Types of Animals. Front. Nutr. *5*.

Noton, S.L., Tremaglio, C.Z., and Fearns, R. (2019). Killing two birds with one stone: How the respiratory syncytial virus polymerase initiates transcription and replication. PLOS Pathog. *15*, e1007548.

Novoa, B., and Figueras, A. (2012). Zebrafish: Model for the Study of Inflammation and the Innate Immune Response to Infectious Diseases (New York, NY: Springer New York).

Novoa, B., Barja, J.L., and Figueras, A. (1995). Entry and sequential distribution of an aquatic birnavirus in turbot (Scophthalmus maximus). Aquaculture *131*, 1–9.

Novoa, B., Figueras, A., and Secombes, C.J. (1996). Effects of in vitro addition of infectious pancreatic necrosis virus (IPNV) on rainbow trout Oncorhynchus mykiss leucocyte responses. Vet. Immunol.

Immunopathol. *51*, 365–376.

Novoa, B., Romero, A., Mulero, V., Rodríguez, I., Fernández, I., and Figueras, A. (2006). Zebrafish (Danio rerio) as a model for the study of vaccination against viral haemorrhagic septicemia virus (VHSV). Vaccine *24*, 5806–5816.

Novoa, B., Bowman, T.V., Zon, L., and Figueras, A. (2009). LPS response and tolerance in the zebrafish (Danio rerio). Fish Shellfish Immunol. *26*, 326–331.

O'Dowd, A.M., Bricknell, I.R., Secombes, C.J., and Ellis, A.E. (1999). The primary and secondary antibody responses to IROMP antigens in Atlantic salmon (Salmo salar L) immunised with A+ and A- Aeromonas salmonicida bacterins. Fish Shellfish Immunol. *9*, 125–138.

Office International des Épizooties (2003). Manual of Diagnostic Tests for Aquatic Animals.

Oh, C.K., Murray, L.A., and Molfino, N.A. (2012). Smoking and idiopathic pulmonary fibrosis. Pulm. Med.

Ohtani, M., Villumsen, K.R., Strøm, H.K., Raida, M.K., and Hinnebusch, B. (2014). 3D Visualization of the Initial Yersinia ruckeri Infection Route in Rainbow Trout (Oncorhynchus mykiss) by Optical Projection Tomography. PLoS One *9*, e89672.

Ojanen, M.J.T., Turpeinen, H., Cordova, Z.M., Hammarén, M.M., Harjula, S.K.E., Parikka, M., Rämet, M., and Pesu, M. (2015). The proprotein convertase subtilisin/kexin FurinA regulates zebrafish host response against Mycobacterium marinum. Infect. Immun. *83*, 1431–1442.

Okabayashi, T., Kojima, T., Masaki, T., Yokota, S. ichi, Imaizumi, T., Tsutsumi, H., Himi, T., Fujii, N., and Sawada, N. (2011). Type-III interferon, not type-I, is the predominant interferon induced by respiratory viruses in nasal epithelial cells. Virus Res. *160*, 360–366.

Okuda, K.S., Astin, J.W., Misa, J.P., Flores, M. V., Crosier, K.E., and Crosier, P.S. (2012). Lyve1 expression reveals novel lymphatic vessels and new mechanisms for lymphatic vessel development in zebrafish. Dev. *139*, 2381–2391.

Oliveira-Nascimento, L., Massari, P., and Wetzler, L.M. (2012). The role of TLR2 ininfection and immunity. Front. Immunol. *3*.

de Oliveira, S., Reyes-Aldasoro, C.C., Candel, S., Renshaw, S.A., Mulero, V., and Calado, A. (2013). Cxcl8 (IL-8) mediates neutrophil recruitment and behavior in the zebrafish inflammatory response. J. Immunol. *190*, 4349–4359.

Olivo-Marin, J.C. (2002). Extraction of spots in biological images using multiscale products. Pattern Recognit. *35*, 1989–1996.

Olson, K.R. (2002). Vascular anatomy of the fish gill. J. Exp. Zool. *293*, 214–231.

Openshaw, P.J.M., Chiu, C., Culley, F.J., and Johansson, C. (2017). Protective and Harmful Immunity to RSV Infection. Annu. Rev. Immunol. *35*, 501–532.

Ordás, M.C., Castro, R., Dixon, B., Sunyer, J.O., Bjork, S., Bartholomew, J., Korytar, T., Köllner, B., Cuesta, A., and Tafalla, C. (2012). Identification of a novel CCR7 gene in rainbow trout with differential expression in the context of mucosal or systemic infection. Dev. Comp. Immunol. *38*, 302–311.

Oshansky, C.M., Barber, J.P., Crabtree, J., and Tripp, R.A. (2010). Respiratory syncytial virus F and G proteins induce interleukin lα, CC, and CXC chemokine responses by normal human bronchoepithelial cells. J. Infect. Dis. *201*, 1201–1207.

Osman, R., Malmuthuge, N., Gonzalez-Cano, P., and Griebel, P. (2018). Development and Function of the Mucosal Immune System in the Upper Respiratory Tract of Neonatal Calves. Annu. Rev. Anim. Biosci. *6*, 141–155.

Øvergård, A.-C., Nepstad, I., Nerland, A.H., and Patel, S. (2012). Characterisation and expression analysis of the Atlantic halibut (Hippoglossus hippoglossus L.) cytokines: IL-1β, IL-6, IL-11, IL-12β and IFNγ. Mol. Biol. Rep. *39*, 2201–2213.

Padra, J.T., Murugan, A.V.M., Sundell, K., Sundh, H., Benktander, J., and Lindén, S.K. (2019). Fish pathogen binding to mucins from Atlantic salmon and Arctic char differs in avidity and specificity and is modulated by fluid velocity. PLoS One *14*, e0215583.

Page, D.M., Wittamer, V., Bertrand, J.Y., Lewis, K.L., Pratt, D.N., Delgado, N., Schale, S.E., Mcgue, C., Jacobsen, B.H., Doty, A., et al. (2013). An evolutionarily conserved program of B-cell development and activation in zebrafish. Blood *122*, e1-11.

Paget, C., Ivanov, S., Fontaine, J., Renneson, J., Blanc, F., Pichavant, M., Dumoutier, L., Ryffel, B., Renauld, J.C., Gosset, P., et al. (2012). Interleukin-22 is produced by invariant natural killer T lymphocytes during influenza A virus infection: Potential role in protection against lung epithelial damages. J. Biol. Chem. *287*, 8816–8829.

Palha, N., Guivel-Benhassine, F., Briolat, V., Lutfalla, G., Sourisseau, M., Ellett, F., Wang, C.H., Lieschke, G.J., Herbomel, P., Schwartz, O., et al. (2013). Real-Time Whole-Body Visualization of Chikungunya Virus Infection and Host Interferon Response in Zebrafish. PLoS Pathog. *9*.

Palti, Y., Gahr, S.A., Purcell, M.K., Hadidi, S., Rexroad, C.E., and Wiens, G.D. (2010). Identification, characterization and genetic mapping of TLR7, TLR8a1 and TLR8a2 genes in rainbow trout (Oncorhynchus mykiss). Dev. Comp. Immunol. *34*, 219–233.

Pan, W., Godoy, R., Cook, D., Scott, A.L., Nurse, C.A., and Jonz, M.G. (2020). Unfolding the Mysteries of Oxygen Sensing - A Comprehensive Analysis of the Hypoxic Response in Zebrafish Gills One Cell at a Time via Single Cell RNA Sequencing. FASEB J. *34*, 1–1.

Pan, Y.A., Freundlich, T., Weissman, T.A., Schoppik, D., Wang, X.C., Zimmerman, S., Ciruna, B., Sanes, J.R., Lichtman, J.W., and Schier, A.F. (2013). Zebrabow: multispectral cell labeling for cell tracing and lineage analysis in zebrafish. Development *140*.

Pang, S.S., Bayly-Jones, C., Radjainia, M., Spicer, B.A., Law, R.H.P., Hodel, A.W., Parsons, E.S., Ekkel, S.M.,

Conroy, P.J., Ramm, G., et al. (2019). The cryo-EM structure of the acid activatable pore-forming immune effector Macrophage-expressed gene 1. Nat. Commun. *10*.

Paquette, C.E., Kent, M.L., Peterson, T.S., Wang, R., Dashwood, R.H., and Löhr, C. V. (2015). Immunohistochemical characterization of intestinal neoplasia in zebrafish Danio rerio indicates epithelial origin. Dis. Aquat. Organ. *116*, 191–197.

Parichy, D.M., Elizondo, M.R., Mills, M.G., Gordon, T.N., and Engeszer, R.E. (2009). Normal table of postembryonic zebrafish development: Staging by externally visible anatomy of the living fish. Dev. Dyn. *238*, 2975–3015.

Passoni, G., Langevin, C., Palha, N., Mounce, B.C., Briolat, V., Affaticati, P., De Job, E., Joly, J.-S., Vignuzzi, M., Saleh, M.-C., et al. (2017). Imaging of viral neuroinvasion in the zebrafish reveals that Sindbis and chikungunya viruses favour different entry routes. Dis. Model. Mech.

Patel, V.I., and Metcalf, J.P. (2018). Airway macrophage and dendritic cell subsets in the resting human lung. Crit. Rev. Immunol. *38*, 303–331.

Pattaroni, C., Watzenboeck, M.L., Schneidegger, S., Kieser, S., Wong, N.C., Bernasconi, E., Pernot, J., Mercier, L., Knapp, S., Nicod, L.P., et al. (2018). Early-Life Formation of the Microbial and Immunological Environment of the Human Airways. Cell Host Microbe *24*, 857-865.e4.

Perdiguero, P., Martín-Martín, A., Benedicenti, O., Díaz-Rosales, P., Morel, E., Muñoz-Atienza, E., García-Flores, M., Simón, R., Soleto, I., Cerutti, A., et al. (2019). Teleost IgD+IgM– B Cells Mount Clonally Expanded and Mildly Mutated Intestinal IgD Responses in the Absence of Lymphoid Follicles. Cell Rep. *29*, 4223-4235.e5.

Pereiro, P., Varela, M., Diaz-Rosales, P., Romero, A., Dios, S., Figueras, A., and Novoa, B. (2015). Zebrafish Nk-lysins: First insights about their cellular and functional diversification. Dev. Comp. Immunol. *51*, 148–159.

Pereiro, P., Forn-Cuní, G., Dios, S., Coll, J., Figueras, A., and Novoa, B. (2017). Interferon-independent antiviral activity of 25-hydroxycholesterol in a teleost fish. Antiviral Res. *145*, 146–159.

Perrin, S., Rich, C.B., Morris, S.M., Stone, P.J., and Foster, J.A. (1999). The zebrafish swimbladder: A simple model for lung elastin injury and repair. Connect. Tissue Res. *40*, 105–112.

Perrone, L.A., Plowden, J.K., García-Sastre, A., Katz, J.M., and Tumpey, T.M. (2008). H5N1 and 1918 Pandemic Influenza Virus Infection Results in Early and Excessive Infiltration of Macrophages and Neutrophils in the Lungs of Mice. PLoS Pathog. *4*, e1000115.

Petrie-Hanson, L., Hohn, C., and Hanson, L. (2009). Characterization of rag1 mutant zebrafish leukocytes. BMC Immunol. *10*, 8.

Pezzulo, A.A., Starner, T.D., Scheetz, T.E., Traver, G.L., Tilley, A.E., Harvey, B.G., Crystal, R.G., McCray, P.B., and Zabner, J. (2011). The air-liquid interface and use of primary cell cultures are important to

recapitulate the transcriptional profile of in vivo airway epithelia. Am. J. Physiol. - Lung Cell. Mol. Physiol. *300*, 25–31.

Phan, Q.T., Sipka, T., Gonzalez, C., Levraud, J.-P., Lutfalla, G., and Nguyen-Chi, M. (2018). Neutrophils use superoxide to control bacterial infection at a distance. PLOS Pathog. *14*, e1007157.

Phan, T.G., Grigorova, I., Okada, T., and Cyster, J.G. (2007). Subcapsular encounter and complement-dependent transport of immune complexes by lymph node B cells. Nat. Immunol. *8*, 992–1000.

Phan, T.G., Gray, E.E., and Cyster, J.G. (2009). The microanatomy of B cell activation. Curr. Opin. Immunol. *21*, 258–265.

Phelan, P.E., Pressley, M.E., Witten, P.E., Mellon, M.T., Blake, S., and Kim, C.H. (2005). Characterization of snakehead rhabdovirus infection in zebrafish (Danio rerio). J. Virol. *79*, 1842–1852.

Pieretti, A.C., Ahmed, A.M., Roberts, J.D., and Kelleher, C.M. (2014). A novel in vitro model to study alveologenesis. Am. J. Respir. Cell Mol. Biol. *50*, 459–469.

Pietretti, D., Scheer, M., Fink, I.R., Taverne, N., Savelkoul, H.F.J., Spaink, H.P., Forlenza, M., and Wiegertjes, G.F. (2014). Identification and functional characterization of nonmammalian Toll-like receptor 20. Immunogenetics *66*, 123–141.

Pikarsky, E., Ronen, A., Abramowitz, J., Levavi-Sivan, B., Hutoran, M., Shapira, Y., Steinitz, M., Perelberg, A., Soffer, D., and Kotler, M. (2004). Pathogenesis of Acute Viral Disease Induced in Fish by Carp Interstitial Nephritis and Gill Necrosis Virus. J. Virol. *78*, 9544–9551.

Pizzolla, A., and Wakim, L.M. (2019). Memory T Cell Dynamics in the Lung during Influenza Virus Infection. J. Immunol. *202*, 374–381.

Plasschaert, L.W., Žilionis, R., Choo-Wing, R., Savova, V., Knehr, J., Roma, G., Klein, A.M., and Jaffe, A.B. (2018). A single-cell atlas of the airway epithelium reveals the CFTR-rich pulmonary ionocyte. Nature *560*, 377–381.

van Pomeren, M., Peijnenburg, W.J.G.M., Vlieg, R.C., van Noort, S.J.T., and Vijver, M.G. (2019). The biodistribution and immuno-responses of differently shaped non-modified gold particles in zebrafish embryos. Nanotoxicology *13*, 558–571.

Porotto, M., Ferren, M., Chen, Y.W., Siu, Y., Makhsous, N., Rima, B., Briese, T., Greninger, A.L., Snoeck, H.W., and Moscona, A. (2019). Authentic modeling of human respiratory virus infection in human pluripotent stem cell-derived lung organoids. MBio *10*.

Powell, M.D., Wright, G.M., and Burka, J.F. (1990). Eosinophilic granule cells in the gills of rainbow trout, Oncorhynchusmykiss: evidence of migration? J. Fish Biol. *37*, 495–497.

Progatzky, F. (2014). Using zebrafish as a model to study acute and chronic mucosal inflammation. Imperial College London.

Progatzky, F., Cook, H.T., Lamb, J.R., Bugeon, L., and Dallman, M.J. (2015). Mucosal inflammation at the respiratory interface: a zebrafish model. Am. J. Physiol. Lung Cell. Mol. Physiol. *310*, L551-61.

Progatzky, F., Jha, A., Wane, M., Thwaites, R.S., Makris, S., Shattock, R.J., Johansson, C., Openshaw, P.J., Bugeon, L., Hansel, T.T., et al. (2019). Induction of innate cytokine responses by respiratory mucosal challenge with R848 in zebrafish, mice, and humans. J. Allergy Clin. Immunol.

Proud, D., Sanders, S.P., and Wiehler, S. (2004). Human Rhinovirus Infection Induces Airway Epithelial Cell Production of Human β-Defensin 2 Both In Vitro and In Vivo. J. Immunol. *172*, 4637–4645.

Qiao, J., Li, A., and Jin, X. (2011). TSLP from RSV-stimulated rat airway epithelial cells activates myeloid dendritic cells. Immunol. Cell Biol. *89*, 231–238.

Qin, Z., Lewis, J.E., and Perry, S.F. (2010). Zebrafish (*Danio rerio*) gill neuroepithelial cells are sensitive chemoreceptors for environmental CO_2. J. Physiol. *588*, 861–872.

Quatromoni, J.G., Singhal, S., Bhojnagarwala, P., Hancock, W.W., Albelda, S.M., and Eruslanov, E. (2015). An optimized disaggregation method for human lung tumors that preserves the phenotype and function of the immune cells. J. Leukoc. Biol. *97*, 201–209.

Radhakrishnan, A., Yeo, D., Brown, G., Myaing, M.Z., Iyer, L.R., Fleck, R., Tan, B.H., Aitken, J., Sanmun, D., Tang, K., et al. (2010). Protein analysis of purified respiratory syncytial virus particles reveals an important role for heat shock protein 90 in virus particle assembly. Mol. Cell. Proteomics *9*, 1829–1848.

Rajão, D.S., and Pérez, D.R. (2018). Universal Vaccines and Vaccine Platforms to Protect against Influenza Viruses in Humans and Agriculture. Front. Microbiol. *9*, 123.

Rajão, D.S., Chen, H., Perez, D.R., Sandbulte, M.R., Gauger, P.C., Loving, C.L., Dennis Shanks, G., and Vincent, A. (2016). Vaccine-associated enhanced respiratory disease is influenced by haemagglutinin and neuraminidase in whole inactivated influenza virus vaccines. J. Gen. Virol. *97*, 1489–1499.

Rajasekaran, K., Riese, M.J., Rao, S., Wang, L., Thakar, M.S., Sentman, C.L., and Malarkannan, S. (2016). Signaling in effector lymphocytes: Insights toward safer immunotherapy. Front. Immunol. *7*, 176.

Rakhilin, N., Garrett, A., Eom, C.Y., Chavez, K.R., Small, D.M., Daniel, A.R., Kaelberer, M.M., Mejooli, M.A., Huang, Q., Ding, S., et al. (2019). An intravital window to image the colon in real time. Nat. Commun. *10*.

Rakus, K., Adamek, M., Mojżesz, M., Podlasz, P., Chmielewska-Krzesińska, M., Naumowicz, K., Kasica-Jarosz, N., Kłak, K., Rakers, S., Way, K., et al. (2019). Evaluation of zebrafish (Danio rerio) as an animal model for the viral infections of fish. J. Fish Dis. jfd.12994.

Rakus, K., Mojzesz, M., Widziolek, M., Pooranachandran, N., Teitge, F., Surachetpong, W., Chadzinska, M., Steinhagen, D., and Adamek, M. (2020). Antiviral response of adult zebrafish (Danio rerio) during tilapia lake virus (TiLV) infection. Fish Shellfish Immunol. *101*, 1–8.

Ramaswamy, M., Shi, L., Monick, M.M., Hunninghake, G.W., and Look, D.C. (2004). Specific inhibition of type I interferon signal transduction by respiratory syncytial virus. Am. J. Respir. Cell Mol. Biol. *30*, 893–

900.

Randall, T.D. (2015). Structure, Organization, and Development of the Mucosal Immune System of the Respiratory Tract. In Mucosal Immunology: Fourth Edition, (Elsevier Inc.), pp. 43–61.

Randall, T.D., and Mebius, R.E. (2014). The development and function of mucosal lymphoid tissues: a balancing act with micro-organisms. Mucosal Immunol. *7*, 455–466.

Rangel-Moreno, J., Moyron-Quiroz, J., Kusser, K., Hartson, L., Nakano, H., and Randall, T.D. (2005). Role of CXC Chemokine Ligand 13, CC Chemokine Ligand (CCL) 19, and CCL21 in the Organization and Function of Nasal-Associated Lymphoid Tissue. J. Immunol. *175*, 4904–4913.

Rangel-Moreno, J., Moyron-Quiroz, J.E., Hartson, L., Kusser, K., and Randall, T.D. (2007). Pulmonary expression of CXC chemokine ligand 13, CC chemokine ligand 19, and CC chemokine ligand 21 is essential for local immunity to influenza. Proc. Natl. Acad. Sci. U. S. A. *104*, 10577–10582.

Rangel-Moreno, J., Carragher, D.M., de la Luz Garcia-Hernandez, M., Hwang, J.Y., Kusser, K., Hartson, L., Kolls, J.K., Khader, S.A., and Randall, T.D. (2011). The development of inducible bronchus-associated lymphoid tissue depends on IL-17. Nat. Immunol. *12*, 639–646.

Rausch, K., Hackett, B.A., Weinbren, N.L., Reeder, S.M., Sadovsky, Y., Hunter, C.A., Schultz, D.C., Coyne, C.B., and Cherry, S. (2017). Screening Bioactives Reveals Nanchangmycin as a Broad Spectrum Antiviral Active against Zika Virus. Cell Rep. *18*, 804–815.

Rausch, P., Basic, M., Batra, A., Bischoff, S.C., Blaut, M., Clavel, T., Gläsner, J., Gopalakrishnan, S., Grassl, G.A., Günther, C., et al. (2016). Analysis of factors contributing to variation in the C57BL/6J fecal microbiota across German animal facilities. Int. J. Med. Microbiol. *306*, 343–355.

Ravi, V., and Venkatesh, B. (2018). The Divergent Genomes of Teleosts. Annu. Rev. Anim. Biosci. *6*, 47–68.

Regan, T., Nally, K., Carmody, R., Houston, A., Shanahan, F., MacSharry, J., and Brint, E. (2013). Identification of TLR10 as a Key Mediator of the Inflammatory Response to Listeria monocytogenes in Intestinal Epithelial Cells and Macrophages . J. Immunol. *191*, 6084–6092.

Reite, O.B., and Evensen, Ø. (2006). Inflammatory cells of teleostean fish: A review focusing on mast cells/eosinophilic granule cells and rodlet cells. In Fish and Shellfish Immunology, (Academic Press), pp. 192–208.

Renshaw, S.A., Loynes, C.A., Trushell, D.M.I., Elworthy, S., Ingham, P.W., and Whyte, M.K.B. (2006). A transgenic zebrafish model of neutrophilic inflammation. Blood *108*.

Rességuier, J., Delaune, E., Coolen, A.-L., Levraud, J.-P., Boudinot, P., Le Guellec, D., and Verrier, B. (2017). Specific and Efficient Uptake of Surfactant-Free Poly(Lactic Acid) Nanovaccine Vehicles by Mucosal Dendritic Cells in Adult Zebrafish after Bath Immersion. Front. Immunol. *8*, 190.

Rességuier, J., Dalum, A.S., Du Pasquier, L., Zhang, Y., Koppang, E.O., Boudinot, P., and Wiegertjes, G.F. (2020). Lymphoid Tissue in Teleost Gills: Variations on a Theme. Biology (Basel). *9*, 127.

Retallack, H., Di Lullo, E., Arias, C., Knopp, K.A., Laurie, M.T., Sandoval-Espinosa, C., Leon, W.R.M., Krencik, R., Ullian, E.M., Spatazza, J., et al. (2016). Zika virus cell tropism in the developing human brain and inhibition by azithromycin. Proc. Natl. Acad. Sci. U. S. A. *113*, 14408–14413.

Reyes-Cerpa, S., Reyes-López, F.E., Toro-Ascuy, D., Ibañez, J., Maisey, K., Sandino, A.M., and Imarai, M. (2012). IPNV modulation of pro and anti-inflammatory cytokine expression in Atlantic salmon might help the establishment of infection and persistence. Fish Shellfish Immunol. *32*, 291–300.

Reyes-Cerpa, S.S., Reyes-López, F.E., Toro-Ascuy, D., An Reyes-Cerpa, S., Reyes-L Opez, F., Montero, R., Maisey, K., Acu, C., Na-Castillo, ∼, Sunyer, J.O., et al. (2014). Induction of anti-inflammatory cytokine expression by IPNV in persistent infection. Fish Shellfish Immunol. *41*, 172–182.

Reyes-López, F.E., Romeo, J.S., Vallejos-Vidal, E., Reyes-Cerpa, S., Sandino, A.M., Tort, L., Mackenzie, S., and Imarai, M. (2015). Differential immune gene expression profiles in susceptible and resistant full-sibling families of Atlantic salmon (Salmo salar) challenged with infectious pancreatic necrosis virus (IPNV). Dev. Comp. Immunol. *53*, 210–221.

Reyfman, P.A., Walter, J.M., Joshi, N., Anekalla, K.R., McQuattie-Pimentel, A.C., Chiu, S., Fernandez, R., Akbarpour, M., Chen, C.I., Ren, Z., et al. (2019). Single-cell transcriptomic analysis of human lung provides insights into the pathobiology of pulmonary fibrosis. Am. J. Respir. Crit. Care Med. *199*, 1517–1536.

Ribeiro, C.M.S., Hermsen, T., Taverne-Thiele, A.J., Savelkoul, H.F.J., and Wiegertjes, G.F. (2010). Evolution of Recognition of Ligands from Gram-Positive Bacteria: Similarities and Differences in the TLR2-Mediated Response between Mammalian Vertebrates and Teleost Fish. J. Immunol. *184*, 2355–2368.

Ricciardolo, F.L.M. (2003). Multiple roles of nitric oxide in the airways. Thorax *58*, 175–182.

Richert, L.E., Harmsen, A.L., Rynda-Apple, A., Wiley, J.A., Servid, A.E., Douglas, T., and Harmsen, A.G. (2013). Inducible bronchus-associated lymphoid tissue (ibalt) synergizes with local lymph nodes during antiviral CD4+ T Cell Responses. Lymphat. Res. Biol. *11*, 196–202.

van Riel, D., Munster, V.J., de Wit, E., Rimmelzwaan, G.F., Fouchier, R.A.M., Osterhaus, A.D.M.E., and Kuiken, T. (2007). Human and Avian Influenza Viruses Target Different Cells in the Lower Respiratory Tract of Humans and Other Mammals. Am. J. Pathol. *171*, 1215–1223.

van Riet, E., Ainai, A., Suzuki, T., and Hasegawa, H. (2012). Mucosal IgA responses in influenza virus infections; thoughts for vaccine design. Vaccine *30*, 5893–5900.

Rigos, G., and Troisi, G.M. (2005). Antibacterial agents in Mediterranean finfish farming: A synopsis of drug pharmacokinetics in important euryhaline fish species and possible environmental implications. Rev. Fish Biol. Fish. *15*, 53–73.

Risnes, K.R., Belanger, K., Murk, W., and Bracken, M.B. (2011). Antibiotic exposure by 6 months and asthma and allergy at 6 years: Findings in a cohort of 1,401 US children. Am. J. Epidemiol. *173*, 310–318.

Roberts, S.D., and Powell, M.D. (2005). The viscosity and glycoprotein biochemistry of salmonid mucus

varies with species, salinity and the presence of amoebic gill disease. J. Comp. Physiol. B Biochem. Syst. Environ. Physiol. *175*, 1–11.

Robledo, D., Taggart, J.B., Ireland, J.H., McAndrew, B.J., Starkey, W.G., Haley, C.S., Hamilton, A., Guy, D.R., Mota-Velasco, J.C., Gheyas, A.A., et al. (2016). Gene expression comparison of resistant and susceptible Atlantic salmon fry challenged with Infectious Pancreatic Necrosis virus reveals a marked contrast in immune response. BMC Genomics *17*, 279.

Rodrigues, S., Antunes, S.C., Nunes, B., and Correia, A.T. (2017). Histological alterations in gills and liver of rainbow trout (Oncorhynchus mykiss) after exposure to the antibiotic oxytetracycline. Environ. Toxicol. Pharmacol. *53*, 164–176.

Rodrigues, S., Antunes, S.C., Nunes, B., and Correia, A.T. (2019). Histopathological effects in gills and liver of Sparus aurata following acute and chronic exposures to erythromycin and oxytetracycline. Environ. Sci. Pollut. Res. *26*, 15481–15495.

Rogan, M.P., Geraghty, P., Greene, C.M., O'Neill, S.J., Taggart, C.C., and McElvaney, N.G. (2006). Antimicrobial proteins and polypeptides in pulmonary innate defence. Respir. Res. *7*, 29.

Rombough, P. (2002). Gills are needed for ionoregulation before they are needed for O2 uptake in developing zebrafish, Danio rerio. J. Exp. Biol. *205*.

Rombough, P. (2007). The functional ontogeny of the teleost gill: Which comes first, gas or ion exchange? Comp. Biochem. Physiol. - A Mol. Integr. Physiol. *148*, 732–742.

Rosado, D., Xavier, R., Severino, R., Tavares, F., Cable, J., and Pérez-Losada, M. (2019). Effects of disease, antibiotic treatment and recovery trajectory on the microbiome of farmed seabass (Dicentrarchus labrax). Sci. Rep. *9*, 1–11.

Rose, M.C., and Voynow, J.A. (2006). Respiratory tract mucin genes and mucin glycoproteins in health and disease. Physiol. Rev. *86*, 245–278.

Rosewich, M. (2010). Ultra-short course immunotherapy in children and adolescents during a 3-yrs post-marketing surveillance study. Pediatr. Allergy Immunol. *21*, e185–e189.

Ruch, T.R., and Machamer, C.E. (2012). The coronavirus E protein: Assembly and beyond. Viruses *4*, 363–382.

Ruddle, N.H., and Akirav, E.M. (2009). Secondary Lymphoid Organs: Responding to Genetic and Environmental Cues in Ontogeny and the Immune Response. J. Immunol. *183*, 2205–2212.

Rueden, C.T., Schindelin, J., Hiner, M.C., DeZonia, B.E., Walter, A.E., Arena, E.T., and Eliceiri, K.W. (2017). ImageJ2: ImageJ for the next generation of scientific image data. BMC Bioinformatics *18*, 529.

Russell, C.D., Unger, S.A., Walton, M., and Schwarze, J. (2017). The Human Immune Response to Respiratory Syncytial Virus Infection. Clin. Microbiol. Rev. *30*, 481–502.

Ryo, S., Wijdeven, R.H.M., Tyagi, A., Hermsen, T., Kono, T., Karunasagar, I., Rombout, J.H.W.M., Sakai, M., Kemenade, B.M.L.V., and Savan, R. (2010). Common carp have two subclasses of bonyfish specific antibody IgZ showing differential expression in response to infection. Dev. Comp. Immunol. *34*, 1183–1190.

Rzepka, J.P., Haick, A.K., and Miura, T.A. (2012). Virus-infected alveolar epithelial cells direct neutrophil chemotaxis and inhibit their apoptosis. Am. J. Respir. Cell Mol. Biol. *46*, 833–841.

Sackstein, R., Schatton, T., and Barthel, S.R. (2017). T-lymphocyte homing: An underappreciated yet critical hurdle for successful cancer immunotherapy. Lab. Investig. *97*, 669–697.

Salinas, I. (2015). The Mucosal Immune System of Teleost Fish. Biology (Basel). *4*, 525–539.

Salinas, I., Zhang, Y.A., and Sunyer, J.O. (2011). Mucosal immunoglobulins and B cells of teleost fish. Dev. Comp. Immunol. *35*, 1346–1365.

Salinas, I., LaPatra, S.E., and Erhardt, E.B. (2015). Nasal vaccination of young rainbow trout (Oncorhynchus mykiss) against infectious hematopoietic necrosis and enteric red mouth disease. Dev. Comp. Immunol. *53*, 105–111.

Samji, T. (2009). Influenza A: Understanding the viral life cycle. Yale J. Biol. Med. *82*, 153–159.

Sanders, G.E., Batts, W.N., and Winton, J.R. (2003). Susceptibility of zebrafish (Danio rerio) to a model pathogen, spring viremia of carp virus. Comp. Med. *53*, 514–521.

Santos, L., and Ramos, F. (2018). Antimicrobial resistance in aquaculture: Current knowledge and alternatives to tackle the problem. Int. J. Antimicrob. Agents *52*, 135–143.

Sarder, P., and Nehorai, A. (2006). Deconvolution methods for 3-D fluorescence microscopy images. IEEE Signal Process. Mag. *23*, 32–45.

Sarris, M., Masson, J.-B., Maurin, D., Van der Aa, L.M., Boudinot, P., Lortat-Jacob, H., and Herbomel, P. (2012). Inflammatory Chemokines Direct and Restrict Leukocyte Migration within Live Tissues as Glycan-Bound Gradients.

Sato, S., and Kiyono, H. (2012). The mucosal immune system of the respiratory tract. Curr. Opin. Virol. *2*, 225–232.

Scapigliati, G., Buonocore, F., Randelli, E., Casani, D., Meloni, S., Zarletti, G., Tiberi, M., Pietretti, D., Boschi, I., Manchado, M., et al. (2010). Cellular and molecular immune responses of the sea bass (Dicentrarchus labrax) experimentally infected with betanodavirus. Fish Shellfish Immunol. *28*, 303–311.

Schmidt, M.E., and Varga, S.M. (2018). The CD8 T cell response to respiratory virus infections. Front. Immunol. *9*, 678.

Schmitz, N., Kurrer, M., Bachmann, M.F., and Kopf, M. (2005). Interleukin-1 Is Responsible for Acute Lung Immunopathology but Increases Survival of Respiratory Influenza Virus Infection. J. Virol. *79*, 6441–6448.

Schoggins, J.W. (2019). Interferon-Stimulated Genes: What Do They All Do? Annu. Rev. Virol. *6*, 567–584.

Schröder, K., and Bosch, T.C.G. (2016). The Origin of Mucosal Immunity: Lessons from the Holobiont Hydra. MBio *7*, e01184-16.

Seeley, R.J., Perlmutter, A., and Seeley, V.A. (1977). Inheritance and longevity of infectious pancreatic necrosis virus in the zebra fish, Brachydanio rerio (Hamilton-Buchanan). Appl. Environ. Microbiol. *34*, 50–55.

Sepahi, A., and Salinas, I. (2016). The evolution of nasal immune systems in vertebrates. Mol. Immunol. *69*, 131–138.

Sepahi, A., Cordero, H., Goldfine, H., Esteban, M.Á., and Salinas, I. (2016a). Symbiont-derived sphingolipids modulate mucosal homeostasis and B cells in teleost fish. Sci. Rep. *6*, 1–13.

Sepahi, A., Casadei, E., Tacchi, L., Muñoz, P., LaPatra, S.E., and Salinas, I. (2016b). Tissue Microenvironments in the Nasal Epithelium of Rainbow Trout (Oncorhynchus mykiss) Define Two Distinct CD8α + Cell Populations and Establish Regional Immunity . J. Immunol. *197*, 4453–4463.

Sepulcre, M.P., López-Castejón, G., Meseguer, J., and Mulero, V. (2007). The activation of gilthead seabream professional phagocytes by different PAMPs underlines the behavioural diversity of the main innate immune cells of bony fish. Mol. Immunol. *44*, 2009–2016.

Sepulcre, M.P., Alcaraz-Pérez, F., López-Muñoz, A., Roca, F.J., Meseguer, J., Cayuela, M.L., and Mulero, V. (2009). Evolution of Lipopolysaccharide (LPS) Recognition and Signaling: Fish TLR4 Does Not Recognize LPS and Negatively Regulates NF-κB Activation. J. Immunol. *182*, 1836–1845.

Serezlí, R. (2005). The Effect of Oxytetracycline on Non-Specific Immune Response in Sea Bream (Sparus aurata L. 1758).

Shaikh, F.Y., and Crowe, J.E. (2013). Molecular mechanisms driving respiratory syncytial virus assembly. Future Microbiol. *8*, 123–131.

Shaykhiev, R. (2019). Emerging biology of persistent mucous cell hyperplasia in COPD. Thorax *74*, 4–6.

Shike, H., Shimizu, C., Lauth, X., and Burns, J.C. (2004). Organization and expression analysis of the zebrafish hepcidin gene, an antimicrobial peptide gene conserved among vertebrates. Dev. Comp. Immunol. *28*, 747–754.

Shimoda, M., Nakamura, T., Takahashi, Y., Asanuma, H., Tamura, S.I., Kurata, T., Mizuochi, T., Azuma, N., Kanno, C., and Takemori, T. (2001). Isotype-specific selection of high affinity memory B cells in nasal-associated lymphoid tissue. J. Exp. Med. *194*, 1597–1607.

Shin, D.-L., Hatesuer, B., Bergmann, S., Nedelko, T., and Schughart, K. (2015). Protection from Severe Influenza Virus Infections in Mice Carrying the Mx1 Influenza Virus Resistance Gene Strongly Depends on Genetic Background . J. Virol. *89*, 9998–10009.

Shivappa, R.B., Song, H., Yao, K., Aas-Eng, A., Evensen, and Vakharia, V.N. (2004). Molecular characterization of Sp serotype strains of infectious pancreatic necrosis virus exhibiting differences in virulence. Dis. Aquat. Organ. *61*, 23–32.

Short, K.R., Kroeze, E.J.B.V., Fouchier, R.A.M., and Kuiken, T. (2014). Pathogenesis of influenza-induced acute respiratory distress syndrome. Lancet Infect. Dis. *14*, 57–69.

Shulman, Z., Gitlin, A.D., Weinstein, J.S., Lainez, B., Esplugues, E., Flavell, R.A., Craft, J.E., and Nussenzweig, M.C. (2014). Germinal centers: Dynamic signaling by T follicular helper cells during germinal center B cell selection. Science (80-.). *345*, 1058–1062.

Silva-Sanchez, A., and Randall, T.D. (2020). Role of iBALT in Respiratory Immunity. In Current Topics in Microbiology and Immunology, (Springer), pp. 21–43.

Simmons, G., Zmora, P., Gierer, S., Heurich, A., and Pöhlmann, S. (2013). Proteolytic activation of the SARS-coronavirus spike protein: Cutting enzymes at the cutting edge of antiviral research. Antiviral Res. *100*, 605–614.

Simoni, Y., Fehlings, M., Kløverpris, H.N., McGovern, N., Koo, S.L., Loh, C.Y., Lim, S., Kurioka, A., Fergusson, J.R., Tang, C.L., et al. (2017). Human Innate Lymphoid Cell Subsets Possess Tissue-Type Based Heterogeneity in Phenotype and Frequency. Immunity *46*, 148–161.

Skinner, A.M.J., and Watt, P.J. (2007). Strategic egg allocation in the zebra fish, Danio rerio. Behav. Ecol. *18*, 905–909.

Skjesol, A., Aamo, T., Hegseth, M.N., Robertsen, B., and Jørgensen, J.B. (2009). The interplay between infectious pancreatic necrosis virus (IPNV) and the IFN system: IFN signaling is inhibited by IPNV infection. Virus Res. *143*, 53–60.

Skjesol, A., Skjæveland, I., Elnæs, M., Timmerhaus, G., Fredriksen, B.N., Jørgensen, S., Krasnov, A., and Jørgensen, J.B. (2011). IPNV with high and low virulence: Host immune responses and viral mutations during infection. Virol. J. *8*, 396.

Slight, S.R., Rangel-Moreno, J., Gopal, R., Lin, Y., Junecko, B.A.F., Mehra, S., Selman, M., Becerril-Villanueva, E., Baquera-Heredia, J., Pavon, L., et al. (2013). CXCR5+ T helper cells mediate protective immunity against tuberculosis. J. Clin. Invest. *123*, 712–726.

Smith, J.C., and Sanderson, S.L. (2013). Particle retention in suspension-feeding fish after removal of filtration structures. Zoology *116*, 348–355.

Smith, T.D., and Bhatnagar, K.P. (2004). Microsmatic primates: Reconsidering how and when size matters. Anat. Rec. *279B*, 24–31.

Smith, J.G., Wiethoff, C.M., Stewart, P.L., and Nemerow, G.R. (2010). Adenovirus. In Current Topics in Microbiology and Immunology, (NIH Public Access), pp. 195–224.

Smith, N., Rodero, M.P., Bekaddour, N., Bondet, V., Ruiz-Blanco, Y.B., Harms, M., Mayer, B., Badder-Meunier,

B., Quartier, P., Bodemer, C., et al. (2019). Control of TLR7-mediated type i IFN signaling in pDCs through CXCR4 engagement-A new target for lupus treatment. Sci. Adv. *5*, 9019.

Sollid, J., Weber, R.E., and Nilsson, G.E. (2005). Temperature alters the respiratory surface area of crucian carp Carassius carassius and goldfish Carassius auratus. J. Exp. Biol. *208*, 1109–1116.

Somamoto, T., Miura, Y., Nakanishi, T., and Nakao, M. (2015). Local and systemic adaptive immune responses toward viral infection via gills in ginbuna crucian carp. Dev. Comp. Immunol. *52*, 81–87.

Sorvina, A., Bader, C.A., Lock, M.C., Brooks, D.A., Morrison, J.L., and Plush, S.E. (2018). Label-free imaging of healthy and infarcted fetal sheep hearts by two-photon microscopy. J. Biophotonics *11*, e201600296.

Spann, K.M., Tran, K.-C., Chi, B., Rabin, R.L., and Collins, P.L. (2004). Suppression of the Induction of Alpha, Beta, and Gamma Interferons by the NS1 and NS2 Proteins of Human Respiratory Syncytial Virus in Human Epithelial Cells and Macrophages. J. Virol. *78*, 4363–4369.

Speer, E.M., Dowling, D.J., Xu, J., Ozog, L.S., Mathew, J.A., Chander, A., Yin, D., and Levy, O. (2018). Pentoxifylline, dexamethasone and azithromycin demonstrate distinct age-dependent and synergistic inhibition of TLR- and inflammasome-mediated cytokine production in human newborn and adult blood in vitro. PLoS One *13*, e0196352.

Spence, R., Gerlach, G., Lawrence, C., and Smith, C. (2007). The behaviour and ecology of the zebrafish, Danio rerio. Biol. Rev. *83*, 13–34.

Sridhar, S., Begom, S., Bermingham, A., Hoschler, K., Adamson, W., Carman, W., Bean, T., Barclay, W., Deeks, J.J., and Lalvani, A. (2013). Cellular immune correlates of protection against symptomatic pandemic influenza. Nat. Med. *19*, 1305–1312.

Sridhar, S., Begom, S., Hoschler, K., Bermingham, A., Adamson, W., Carman, W., Riley, S., and Lalvani, A. (2015). Longevity and determinants of protective humoral immunity after pandemic influenza infection. Am. J. Respir. Crit. Care Med. *191*, 325–332.

Stachura, D.L., and Traver, D. (2011). Cellular Dissection of Zebrafish Hematopoiesis.

Stasakova, J., Ferko, B., Kittel, C., Sereinig, S., Romanova, J., Katinger, H., and Egorov, A. (2005). Influenza A mutant viruses with altered NS1 protein function provoke caspase-1 activation in primary human macrophages, resulting in fast apoptosis and release of high levels of interleukins 1β and 18. J. Gen. Virol. *86*, 185–195.

De Steenhuijsen Piters, W.A.A., Heinonen, S., Hasrat, R., Bunsow, E., Smith, B., Suarez-Arrabal, M.C., Chaussabel, D., Cohen, D.M., Sanders, E.A.M., Ramilo, O., et al. (2016). Nasopharyngeal microbiota, host transcriptome, and disease severity in children with respiratory syncytial virus infection. Am. J. Respir. Crit. Care Med. *194*, 1104–1115.

Stehle, C., Hernández, D.C., and Romagnani, C. (2018). Innate lymphoid cells in lung infection and immunity. Immunol. Rev. *286*, 102–119.

Stein, J. V., and F. Gonzalez, S. (2017). Dynamic intravital imaging of cell-cell interactions in the lymph node. J. Allergy Clin. Immunol. *139*, 12–20.

Stein, C., Caccamo, M., Laird, G., and Leptin, M. (2007). Conservation and divergence of gene families encoding components of innate immune response systems in zebrafish. Genome Biol. *8*, R251.

Stein, M.M., Hrusch, C.L., Gozdz, J., Igartua, C., Pivniouk, V., Murray, S.E., Ledford, J.G., Marques dos Santos, M., Anderson, R.L., Metwali, N., et al. (2016). Innate Immunity and Asthma Risk in Amish and Hutterite Farm Children. N. Engl. J. Med. *375*, 411–421.

Steinel, N.C., and Bolnick, D.I. (2017). Melanomacrophage Centers As a Histological Indicator of Immune Function in Fish and Other Poikilotherms. Front. Immunol. *8*, 827.

Stier, M.T., and Peebles, R.S. (2018). Host and viral determinants of respiratory syncytial virus-induced airway mucus. In Annals of the American Thoracic Society, (American Thoracic Society), pp. S205–S209.

Stockhammer, O.W., Zakrzewska, A., Hegedûs, Z., Spaink, H.P., and Meijer, A.H. (2009). Transcriptome profiling and functional analyses of the zebrafish embryonic innate immune response to Salmonella infection. J. Immunol. *182*, 5641–5653.

Stolper, J., Ambrosio, E.M., Danciu, D.P., Buono, L., Elliott, D.A., Naruse, K., Martínez-Morales, J.R., Marciniak-Czochra, A., and Centanin, L. (2019). Stem cell topography splits growth and homeostatic functions in the fish gill. Elife *8*.

Strauss, J., Burnham, N.A., and Camesano, T.A. (2009). Atomic force microscopy study of the role of LPS O-antigen on adhesion of E. coli. In Journal of Molecular Recognition, (J Mol Recognit), pp. 347–355.

Strzepa, A., Pritchard, K.A., and Dittel, B.N. (2017). Myeloperoxidase: A new player in autoimmunity. Cell. Immunol. *317*, 1–8.

Su, J.-G., Zhu, Z.-Y., and Wang, Y.-P. (2009). Up-regulating expressions of toll-like receptor 3 and Mx genes in gills by grass CARP reovirus in rare minnow. Acta Hydrobiol. Sin. *32*, 728–734.

Sullivan, C., Charette, J., Catchen, J., Lage, C.R., Giasson, G., Postlethwait, J.H., Millard, P.J., and Kim, C.H. (2009). The gene history of zebrafish tlr4a and tlr4b is predictive of their divergent functions. J. Immunol. *183*, 5896–5908.

Sullivan, C., Jurcyzszak, D., Goody, M.F., Gabor, K.A., Longfellow, J.R., Millard, P.J., and Kim, C.H. (2017). Using Zebrafish Models of Human Influenza A Virus Infections to Screen Antiviral Drugs and Characterize Host Immune Cell Responses. J. Vis. Exp. e55235–e55235.

Sungnak, W., Huang, N., Bécavin, C., Berg, M., Queen, R., Litvinukova, M., Talavera-López, C., Maatz, H., Reichart, D., Sampaziotis, F., et al. (2020). SARS-CoV-2 entry factors are highly expressed in nasal epithelial cells together with innate immune genes. Nat. Med. *26*, 681–687.

Suresh, N. (2009). Effect of cadmium chloride on liver, spleen and kidney melano macrophage centres in Tilapia mossambica. J. Environ. Biol. *30*, 505–508.

Svingerud, T., Solstad, T., Sun, B., Nyrud, M.L.J., Kileng, Ø., Greiner-Tollersrud, L., and Robertsen, B. (2012). Atlantic salmon type I IFN subtypes show differences in antiviral activity and cell-dependent expression: evidence for high IFNb/IFNc-producing cells in fish lymphoid tissues. J. Immunol. *189*, 5912–5923.

Sweet, C., and Smith, A.H. (1980). Pathogenicity of Influenza Virus. Microbiol. Rev. *44*, 303–330.

Taherali, F., Varum, F., and Basit, A.W. (2018). A slippery slope: On the origin, role and physiology of mucus. Adv. Drug Deliv. Rev. *124*, 16–33.

Takano, T., Kondo, H., Hirono, I., Endo, M., Saito-Taki, T., and Aoki, T. (2007). Molecular cloning and characterization of Toll-like receptor 9 in Japanese flounder, Paralichthys olivaceus. Mol. Immunol. *44*, 1845–1853.

Takizawa, F., Koppang, E.O., Ohtani, M., Nakanishi, T., Hashimoto, K., Fischer, U., and Dijkstra, J.M. (2011). Constitutive high expression of interleukin-4/13A and GATA-3 in gill and skin of salmonid fishes suggests that these tissues form Th2-skewed immune environments. Mol. Immunol. *48*, 1360–1368.

Tanaka, K., Sawamura, S., Satoh, T., Kobayashi, K., and Noda, S. (2007). Role of the Indigenous Microbiota in Maintaining the Virus-Specific CD8 Memory T Cells in the Lung of Mice Infected with Murine Cytomegalovirus. J. Immunol. *178*, 5209–5216.

Tang, Q., Abdelfattah, N.S., Blackburn, J.S., Moore, J.C., Martinez, S.A., Moore, F.E., Lobbardi, R., Tenente, I.M., Ignatius, M.S., Berman, J.N., et al. (2014). Optimized cell transplantation using adult rag2 mutant zebrafish. Nat. Methods *11*, 821–824.

Tang, Q., Iyer, S., Lobbardi, R., Moore, J.C., Chen, H., Lareau, C., Hebert, C., Shaw, M.L., Neftel, C., Suva, M.L., et al. (2017). Dissecting hematopoietic and renal cell heterogeneity in adult zebrafish at single-cell resolution using RNA sequencing. J. Exp. Med. *214*, 2875–2887.

Tate, M.D., Brooks, A.G., and Reading, P.C. (2008). The role of neutrophils in the upper and lower respiratory tract during influenza virus infection of mice. Respir. Res. *9*, 57.

Tate, M.D., Pickett, D.L., van Rooijen, N., Brooks, A.G., and Reading, P.C. (2010). Critical Role of Airway Macrophages in Modulating Disease Severity during Influenza Virus Infection of Mice. J. Virol. *84*, 7569–7580.

Tate, M.D., Brooks, A.G., Reading, P.C., and Mintern, J.D. (2012). Neutrophils sustain effective CD8+ T-cell responses in the respiratory tract following influenza infection. Immunol. Cell Biol. *90*, 197–205.

Tavares, L.P., Teixeira, M.M., and Garcia, C.C. (2017). The inflammatory response triggered by Influenza virus: a two edged sword. Inflamm. Res. *66*, 283–302.

Taylor, G. (2017). Animal models of respiratory syncytial virus infection. Vaccine *35*, 469–480.

Tayyari, F., Marchant, D., Moraes, T.J., Duan, W., Mastrangelo, P., and Hegele, R.G. (2011). Identification of nucleolin as a cellular receptor for human respiratory syncytial virus. Nat. Med. *17*, 1132–1135.

Thangavel, R.R., and Bouvier, N.M. (2014). Animal models for influenza virus pathogenesis, transmission, and immunology. J. Immunol. Methods *410*, 60–79.

Thoen, E., Tartor, H., Amundsen, M., Dale, O.B., Sveinsson, K., Rønning, H.P., Grønneberg, E., Dahle, M.K., and Gjessing, M.C. (2020). First record of experimentally induced salmon gill poxvirus disease (SGPVD) in Atlantic salmon (Salmo salar L.). Vet. Res. *51*, 63.

Thorlund, K., Awad, T., Boivin, G., and Thabane, L. (2011). Systematic review of influenza resistance to the neuraminidase inhibitors. BMC Infect. Dis. *11*, 134.

Thornton, D.J., Rousseau, K., and McGuckin, M.A. (2008). Structure and Function of the Polymeric Mucins in Airways Mucus. Annu. Rev. Physiol. *70*, 459–486.

Toapanta, F.R., and Ross, T.M. (2009). Impaired immune responses in the lungs of aged mice following influenza infection. Respir. Res. *10*, 1–19.

Tognarelli, E.I., Bueno, S.M., and González, P.A. (2019). Immune-modulation by the human respiratory syncytial virus: Focus on dendritic cells. Front. Immunol. *10*, 810.

Torgersen, Y., and Håstein, T. (1995). Disinfection in aquaculture.

Travassos, L.H., Girardin, S.E., Philpott, D.J., Blanot, D., Nahori, M., Werts, C., and Boneca, I.G. (2004). Toll-like receptor 2-dependent bacterial sensing does not occur via peptidoglycan recognition. EMBO Rep. *5*, 1000–1006.

Traver, D., Paw, B.H., Poss, K.D., Penberthy, W.T., Lin, S., and Zon, L.I. (2003). Transplantation and in vivo imaging of multilineage engraftment in zebrafish bloodless mutants. Nat. Immunol. *4*, 1238–1246.

Trede, N.S., Langenau, D.M., Traver, D., Look, A.T., and Zon, L.I. (2004). The use of zebrafish to understand immunity. Immunity *20*, 367–379.

Tsai, S.B., Tucci, V., Uchiyama, J., Fabian, N.J., Lin, M.C., Bayliss, P.E., Neuberg, D.S., Zhdanova, I. V., and Kishi, S. (2007). Differential effects of genotoxic stress on both concurrent body growth and gradual senescence in the adult zebrafish. Aging Cell *6*, 209–224.

Tschemig, T., Kleemann, W.J., and Pabst, R. (1995). Bronchus-associated lymphoid tissue (BALT) in the lungs of children who had died from sudden infant death syndrome and other causes. Thorax *50*, 658–660.

Tschernig, T., and Pabst, R. (2000). Bronchus-Associated Lymphoid Tissue (BALT) Is Not Present in the Normal Adult Lung but in Different Diseases Mucosa-Associated Lymphoid Tissue.

Tseng, C.-T.K., Tseng, J., Perrone, L., Worthy, M., Popov, V., and Peters, C.J. (2005). Apical Entry and Release of Severe Acute Respiratory Syndrome-Associated Coronavirus in Polarized Calu-3 Lung Epithelial Cells. J. Virol. *79*, 9470–9479.

Tsoi, C.C. (2019). Characterisation of immune cell populations in zebrafish gills and effects of

oxytetracycline on R848-triggered immune response. Imperial College London.

Turan, K., Mibayashi, M., Sugiyama, K., Saito, S., Numajiri, A., and Nagata, K. (2004). Nuclear MxA proteins form a complex with influenza virus NP and inhibit the transcription of the engineered influenza virus genome. Nucleic Acids Res. *32*, 643–652.

Turner, D.L., Bickham, K.L., Thome, J.J., Kim, C.Y., D'Ovidio, F., Wherry, E.J., and Farber, D.L. (2014). Lung niches for the generation and maintenance of tissue-resident memory T cells. Mucosal Immunol. *7*, 501–510.

Ugonna, K., Bingle, C.D., Plant, K., Wilson, K., and Everard, M.L. (2014). Macrophages Are Required for Dendritic Cell Uptake of Respiratory Syncytial Virus from an Infected Epithelium. PLoS One *9*, e91855.

Van Der Vaart, M., Spaink, H.P., and Meijer, A.H. (2012). Pathogen recognition and activation of the innate immune response in zebrafish. Adv. Hematol. *2012*.

Valdenegro-Vega, V.A., Crosbie, P., Bridle, A., Leef, M., Wilson, R., and Nowak, B.F. (2014). Differentially expressed proteins in gill and skin mucus of Atlantic salmon (Salmo salar) affected by amoebic gill disease. Fish Shellfish Immunol. *40*, 69–77.

Vanderheiden, A., Ralfs, P., Chirkova, T., Upadhyay, A.A., Zimmerman, M.G., Bedoya, S., Aoued, H., Tharp, G.M., Pellegrini, K.L., Manfredi, C., et al. (2020). Type I and Type III IFN Restrict SARS-CoV-2 Infection of Human Airway Epithelial Cultures. J. Virol.

Vanderven, H.A., Ana-Sosa-Batiz, F., Jegaskanda, S., Rockman, S., Laurie, K., Barr, I., Chen, W., Wines, B., Hogarth, P.M., Lambe, T., et al. (2016). What Lies Beneath: Antibody Dependent Natural Killer Cell Activation by Antibodies to Internal Influenza Virus Proteins. EBioMedicine *8*, 277–290.

Vareille, M., Kieninger, E., Edwards, M.R., and Regamey, N. (2011). The airway epithelium: Soldier in the fight against respiratory viruses. Clin. Microbiol. Rev. *24*, 210–229.

Varela, M., Dios, S., Novoa, B., and Figueras, A. (2012). Characterisation, expression and ontogeny of interleukin-6 and its receptors in zebrafish (Danio rerio). Dev. Comp. Immunol. *37*, 97–106.

Varela, M., Romero, A., Dios, S., van der Vaart, M., Figueras, A., Meijer, A.H., and Novoa, B. (2014). Cellular visualization of macrophage pyroptosis and interleukin-1β release in a viral hemorrhagic infection in zebrafish larvae. J. Virol. *88*, 12026–12040.

Varela, M., Forn-Cuní, G., Dios, S., Figueras, A., and Novoa, B. (2016). Proinflammatory Caspase A Activation and an Antiviral State Are Induced by a Zebrafish Perforin after Possible Cellular and Functional Diversification from a Myeloid Ancestor. J. Innate Immun. *8*, 43–56.

Varela, M., Figueras, A., and Novoa, B. (2017). Modelling viral infections using zebrafish: Innate immune response and antiviral research. Antiviral Res. *139*, 59–68.

Vargas-Chacoff, L., Regish, A.M., Weinstock, A., and McCormick, S.D. (2018). Effects of elevated temperature on osmoregulation and stress responses in Atlantic salmon *Salmo salar* smolts in fresh water

and seawater. J. Fish Biol. *93*, 550–559.

Verbist, K.C., Rose, D.L., Cole, C.J., Field, M.B., and Klonowski, K.D. (2012). IL-15 Participates in the Respiratory Innate Immune Response to Influenza Virus Infection. PLoS One *7*, e37539.

Veres, T.Z. (2018). Visualizing immune responses of the airway mucosa. Cell. Immunol.

Vergauwen, L., Benoot, D., Blust, R., and Knapen, D. (2010). Long-term warm or cold acclimation elicits a specific transcriptional response and affects energy metabolism in zebrafish. Comp. Biochem. Physiol. Part A Mol. Integr. Physiol. *157*, 149–157.

Vieira Braga, F.A., Kar, G., Berg, M., Carpaij, O.A., Polanski, K., Simon, L.M., Brouwer, S., Gomes, T., Hesse, L., Jiang, J., et al. (2019). A cellular census of human lungs identifies novel cell states in health and in asthma. Nat. Med. *25*, 1153–1163.

Vigliano, F.A., Bermúdez, R., Quiroga, M.I., and Nieto, J.M. (2006). Evidence for melano-macrophage centres of teleost as evolutionary precursors of germinal centres of higher vertebrates: An immunohistochemical study. Fish Shellfish Immunol. *21*, 467–471.

Voils, S.A., Evans, M.E., Lane, M.T., Schosser, R.H., and Rapp, R.P. (2005). Use of macrolides and tetracyclines for chronic inflammatory diseases. Ann. Pharmacother. *39*, 86–94.

Waffarn, E.E., and Baumgarth, N. (2011). Protective B Cell Responses to Flu—No Fluke! J. Immunol. *186*, 3823–3829.

Wali, S., Flores, J.R., Jaramillo, A.M., Goldblatt, D.L., Pantaleón García, J., Tuvim, M.J., Dickey, B.F., and Evans, S.E. (2020). Immune Modulation to Improve Survival of Viral Pneumonia in Mice. Am. J. Respir. Cell Mol. Biol.

Walton, E.M., Cronan, M.R., Beerman, R.W., and Tobin, D.M. (2015). The Macrophage-Specific Promoter mfap4 Allows Live, Long-Term Analysis of Macrophage Behavior during Mycobacterial Infection in Zebrafish. PLoS One *10*, e0138949.

Wan, F., Hu, C., Ma, J., Gao, K., Xiang, L., and Shao, J. (2017). Characterization of γδ T Cells from Zebrafish Provides Insights into Their Important Role in Adaptive Humoral Immunity. Front. Immunol. *7*, 675.

Wang, B.-Z., Xu, R., Quan, F.-S., Kang, S.-M., Wang, L., and Compans, R.W. (2010a). Intranasal Immunization with Influenza VLPs Incorporating Membrane-Anchored Flagellin Induces Strong Heterosubtypic Protection. PLoS One *5*, e13972.

Wang, G., Deering, C., Macke, M., Shao, J., Burns, R., Blau, D.M., Holmes, K. V., Davidson, B.L., Perlman, S., and McCray, P.B. (2000). Human Coronavirus 229E Infects Polarized Airway Epithelia from the Apical Surface. J. Virol. *74*, 9234–9239.

Wang, J., Nikrad, M.P., Phang, T., Gao, B., Alford, T., Ito, Y., Edeen, K., Travanty, E.A., Kosmider, B., Hartshorn, K., et al. (2011). Innate immune response to influenza A virus in differentiated human alveolar type II cells. Am. J. Respir. Cell Mol. Biol. *45*, 582–591.

Wang, Q., Nagarkar, D.R., Bowman, E.R., Schneider, D., Gosangi, B., Lei, J., Zhao, Y., McHenry, C.L., Burgens, R. V., Miller, D.J., et al. (2009). Role of Double-Stranded RNA Pattern Recognition Receptors in Rhinovirus-Induced Airway Epithelial Cell Responses. J. Immunol. *183*, 6989–6997.

Wang, T., Holland, J.W., Bols, N., and Secombes, C.J. (2005). Cloning and expression of the first nonmammalian interleukin-11 gene in rainbow trout Oncorhynchus mykiss. FEBS J. *272*, 1136–1147.

Wang, T., Holland, J.W., Martin, S.A.M., and Secombes, C.J. (2010b). Sequence and expression analysis of two T helper master transcription factors, T-bet and GATA3, in rainbow trout Oncorhynchus mykiss and analysis of their expression during bacterial and parasitic infection. Fish Shellfish Immunol. *29*, 705–715.

Wang, W., Zhou, Z., He, S., Liu, Y., Cao, Y., Shi, P., Yao, B., and Ringø, E. (2010c). Identification of the adherent microbiota on the gills and skin of poly-cultured gibel carp (Carassius auratus gibelio) and bluntnose black bream (Megalobrama amblycephala Yih). Aquac. Res. *41*, e72–e83.

Wang, Z., Zhang, S., Wang, G., and An, Y. (2008a). Complement Activity in the Egg Cytosol of Zebrafish Danio rerio: Evidence for the Defense Role of Maternal Complement Components. PLoS One *3*, e1463.

Wang, Z., Zhang, S., and Wang, G. (2008b). Response of complement expression to challenge with lipopolysaccharide in embryos/larvae of zebrafish Danio rerio: Acquisition of immunocompetent complement. Fish Shellfish Immunol. *25*, 264–270.

Wansleeben, C., Bowie, E., Hotten, D.F., Yu, Y.-R.A., and Hogan, B.L.M. (2014). Age-Related Changes in the Cellular Composition and Epithelial Organization of the Mouse Trachea. PLoS One *9*, e93496.

Warburton, D. (2017). Overview of Lung Development in the Newborn Human. Neonatology *111*, 398–401.

Wareing, M.D., Lyon, A.B., Lu, B., Gerard, C., and Sarawar, S.R. (2004). Chemokine expression during the development and resolution of a pulmonary leukocyte response to influenza A virus infection in mice. J. Leukoc. Biol. *76*, 886–895.

Weitnauer, M., Mijošek, V., and Dalpke, A.H. (2016). Control of local immunity by airway epithelial cells. Mucosal Immunol. *9*, 287–298.

Weli, S.C., Aamelfot, M., Dale, O.B., Koppang, E.O., and Falk, K. (2013). Infectious salmon anaemia virus infection of Atlantic salmon gill epithelial cells. Virol. J. *10*.

Wenz, R., Conibear, E., Bugeon, L., and Dallman, M. (2020). Fast, easy and early (larval) identification of transparent mutant zebrafish using standard fluorescence microscopy. F1000Research *9*.

Westerfield, M. (2000). The Zebrafish Book (University of Oregon Press, Eugene).

White, R.M., Sessa, A., Burke, C., Bowman, T., LeBlanc, J., Ceol, C., Bourque, C., Dovey, M., Goessling, W., Burns, C.E., et al. (2008). Transparent adult zebrafish as a tool for in vivo transplantation analysis. Cell Stem Cell *2*, 183–189.

Whitsett, J.A., Kalin, T. V., Xu, Y., and Kalinichenko, V. V. (2019). Building and regenerating the lung cell by cell. Physiol. Rev. *99*, 513–554.

Widdicombe, J.H., and Wine, J.J. (2015). Airway gland structure and function. Physiol. Rev. *95*, 1241–1319.

Widdicombe, J.H., Chen, L.L.-K., Sporer, H., Choi, H.K., Pecson, I.S., and Bastacky, S.J. (2001). Distribution of tracheal and laryngeal mucous glands in some rodents and the rabbit. J. Anat. *198*, 207–221.

Wiles, T.J., Jemielita, M., Baker, R.P., Schlomann, B.H., Logan, S.L., Ganz, J., Melancon, E., Eisen, J.S., Guillemin, K., and Parthasarathy, R. (2016). Host Gut Motility Promotes Competitive Exclusion within a Model Intestinal Microbiota. PLOS Biol. *14*, e1002517.

Willis, A.R., Torraca, V., Gomes, M.C., Shelley, J., Mazon-Moya, M., Filloux, A., Lo Celso, C., and Mostowy, S. (2018). Shigella-induced emergency granulopoiesis protects Zebrafish Larvae from secondary infection. MBio *9*.

Wilson, J.M., and Laurent, P. (2002). Fish gill morphology: inside out. J. Exp. Zool. *293*, 192–213.

Wilson, S.S., Wiens, M.E., and Smith, J.G. (2013). Antiviral mechanisms of human defensins. J. Mol. Biol. *425*, 4965–4980.

Winarski, K.L., Tang, J., Klenow, L., Lee, J., Coyle, E.M., Manischewitz, J., Turner, H.L., Takeda, K., Ward, A.B., Golding, H., et al. (2019). Antibody-dependent enhancement of influenza disease promoted by increase in hemagglutinin stem flexibility and virus fusion kinetics. Proc. Natl. Acad. Sci. U. S. A. *116*, 15194–15199.

Wittamer, V., Bertrand, J.Y., Gutschow, P.W., and Traver, D. (2011). Characterization of the mononuclear phagocyte system in zebrafish. Blood *117*, 7126–7135.

Witten, J., Samad, T., and Ribbeck, K. (2018). Selective permeability of mucus barriers. Curr. Opin. Biotechnol. *52*, 124–133.

Wong, L.-Y.R., Lui, P.-Y., and Jin, D.-Y. (2016). A molecular arms race between host innate antiviral response and emerging human coronaviruses. Virol. Sin. 12–23.

Wu, L.P., Wang, N.C., Chang, Y.H., Tian, X.Y., Na, D.Y., Zhang, L.Y., Zheng, L., Lan, T., Wang, L.F., and Liang, G.D. (2007). Duration of antibody responses after severe acute respiratory syndrome. Emerg. Infect. Dis. *13*, 1562–1564.

Wu, W., Patel, K.B., Booth, J.L., Zhang, W., and Metcalf, J.P. (2011). Cigarette smoke extract suppresses the RIG-I-initiated innate immune response to influenza virus in the human lung. Am. J. Physiol. Cell. Mol. Physiol. *300*, L821–L830.

Xia, C., Vijayan, M., Pritzl, C.J., Fuchs, S.Y., McDermott, A.B., and Hahm, B. (2016). Hemagglutinin of Influenza A Virus Antagonizes Type I Interferon (IFN) Responses by Inducing Degradation of Type I IFN Receptor 1. J. Virol. *90*, 2403–2417.

Xiang, Z., Dong, C., Qi, L., Chen, W., Huang, L., Li, Z., Xia, Q., Liu, D., Huang, M., Weng, S., et al. (2010).

Characteristics of the interferon regulatory factor pairs zfIRF5/7 and their stimulation expression by ISKNV Infection in zebrafish (Danio rerio). Dev. Comp. Immunol. *34*, 1263–1273.

Xu, T., and Zhang, X.H. (2014). Edwardsiella tarda: An intriguing problem in aquaculture. Aquaculture *431*, 129–135.

Xu, C., Volkery, S., and Siekmann, A.F. (2015). Intubation-based anesthesia for long-term time-lapse imaging of adult zebrafish. Nat. Protoc. *10*, 2064–2073.

Xu, J., Jia, W., Wang, P., Zhang, S., Shi, X., Wang, X., and Zhang, L. (2019). Antibodies and vaccines against Middle East respiratory syndrome coronavirus. Emerg. Microbes Infect. *8*, 841–856.

Xu, X., Zhang, L., Weng, S., Huang, Z., Lu, J., Lan, D., Zhong, X., Yu, X., Xu, A., and He, J. (2008). A zebrafish (Danio rerio) model of infectious spleen and kidney necrosis virus (ISKNV) infection. Virology *376*, 1–12.

Xu, Z., Takizawa, F., Parra, D., Gómez, D., von Gersdorff Jørgensen, L., LaPatra, S.E., Sunyer, J.O., Maina, J.N., Glover, C.N., Bucking, C., et al. (2016). Mucosal immunoglobulins at respiratory surfaces mark an ancient association that predates the emergence of tetrapods. Nat. Commun. *7*, 10728.

Xu, Z., Takizawa, F., Casadei, E., Shibasaki, Y., Ding, Y., Sauters, T.J.C., Yu, Y., Salinas, I., and Sunyer, J.O. (2020). Specialization of mucosal immunoglobulins in pathogen control and microbiota homeostasis occurred early in vertebrate evolution. Sci. Immunol. *5*, 3254.

Yadava, K., Bollyky, P., and Lawson, M.A. (2016). The formation and function of tertiary lymphoid follicles in chronic pulmonary inflammation. Immunology *149*, 262–269.

Yamamoto, K., Yamamoto, S., Ogasawara, N., Takano, K., Shiraishi, T., Sato, T., Miyata, R., Kakuki, T., Kamekura, R., Kojima, T., et al. (2016). Clarithromycin prevents human respiratory syncytial virus-induced airway epithelial responses by modulating activation of interferon regulatory factor-3. Pharmacol. Res. *111*, 804–814.

Yang, D., Zheng, X., Chen, S., Wang, Z., Xu, W., Tan, J., Hu, T., Hou, M., Wang, W., Gu, Z., et al. (2018). Sensing of cytosolic LPS through caspy2 pyrin domain mediates noncanonical inflammasome activation in zebrafish. Nat. Commun. *9*, 3052.

Yang, H.T., Zou, S.S., Zhai, L.J., Wang, Y., Zhang, F.M., An, L.G., and Yang, G.W. (2017). Pathogen invasion changes the intestinal microbiota composition and induces innate immune responses in the zebrafish intestine. Fish Shellfish Immunol. *71*, 35–42.

Yang, S., Marín-Juez, R., Meijer, A.H., and Spaink, H.P. (2015). Common and specific downstream signaling targets controlled by Tlr2 and Tlr5 innate immune signaling in zebrafish. BMC Genomics *16*, 547.

Yang, X.-H., Deng, W., Tong, Z., Liu, Y.-X., Zhang, L.-F., Zhu, H., Gao, H., Huang, L., Liu, Y.-L., Ma, C.-M., et al. (2007). Comparative Medicine Mice Transgenic for Human Angiotensin-converting Enzyme 2 Provide a Model for SARS Coronavirus Infection.

Yang, X., Steukers, L., Forier, K., Xiong, R., Braeckmans, K., Van Reeth, K., and Nauwynck, H. (2014). A

Beneficiary Role for Neuraminidase in Influenza Virus Penetration through the Respiratory Mucus. PLoS One *9*, e110026.

Yang, Y., Peng, F., Wang, R., Guan, K., Jiang, T., Xu, G., Sun, J., and Chang, C. (2020). The deadly coronaviruses: The 2003 SARS pandemic and the 2020 novel coronavirus epidemic in China. J. Autoimmun. *109*, 102434.

Yeh, D.-W., Liu, Y.-L., Lo, Y.-C., Yuh, C.-H., Yu, G.-Y., Lo, J.-F., Luo, Y., Xiang, R., and Chuang, T.-H. (2013). Toll-like receptor 9 and 21 have different ligand recognition profiles and cooperatively mediate activity of CpG-oligodeoxynucleotides in zebrafish. Proc. Natl. Acad. Sci. U. S. A. *110*, 20711–20716.

Yonar, M.E. (2012). The effect of lycopene on oxytetracycline-induced oxidative stress and immunosuppression in rainbow trout (Oncorhynchus mykiss, W.). Fish Shellfish Immunol. *32*, 994–1001.

Yoo, S.K., and Huttenlocher, A. (2011). Spatiotemporal photolabeling of neutrophil trafficking during inflammation in live zebrafish. J. Leukoc. Biol. *89*, 661–667.

Yoon, S., Mitra, S., Wyse, C., Alnabulsi, A., Zou, J., Weerdenburg, E.M., van der Sar, A.M., Wang, D., Secombes, C.J., and Bird, S. (2015). First Demonstration of Antigen Induced Cytokine Expression by CD4-1+ Lymphocytes in a Poikilotherm: Studies in Zebrafish (Danio rerio). PLoS One *10*, e0126378.

York, A., and Fodor, E. (2013). Biogenesis, assembly and export of viral messenger ribonucleoproteins in the influenza A virus infected cell. RNA Biol. *10*, 1274–1282.

Zahradník, J., Kolářová, L., Pařízková, H., Kolenko, P., and Schneider, B. (2018). Interferons type II and their receptors R1 and R2 in fish species: Evolution, structure, and function. Fish Shellfish Immunol. *79*, 140–152.

Zakrzewska, A., Cui, C., Stockhammer, O.W., Benard, E.L., Spaink, H.P., and Meijer, A.H. (2010). Macrophage-specific gene functions in Spi1-directed innate immunity. Blood *116*, e1–e11.

Zanin, M., Marathe, B., Wong, S.-S., Yoon, S.-W., Collin, E., Oshansky, C., Jones, J., Hause, B., and Webby, R. (2015). Pandemic Swine H1N1 Influenza Viruses with Almost Undetectable Neuraminidase Activity Are Not Transmitted via Aerosols in Ferrets and Are Inhibited by Human Mucus but Not Swine Mucus. J. Virol. *89*, 5935–5948.

Zanin, M., Baviskar, P., Webster, R., and Webby, R. (2016). The Interaction between Respiratory Pathogens and Mucus. Cell Host Microbe *19*, 159–168.

Zhang, D.C., Shao, Y.Q., Huang, Y.Q., and Jiang, S.G. (2005). Cloning, characterization and expression analysis of interleukin-10 from the zebrafish (Danio reriori). J. Biochem. Mol. Biol. *38*, 571–576.

Zhang, H., Shen, B., Wu, H., Gao, L., Liu, Q., Wang, Q., Xiao, J., and Zhang, Y. (2014). Th17-like immune response in fish mucosal tissues after administration of live attenuated Vibrio anguillarum via different vaccination routes. Fish Shellfish Immunol. *37*, 229–238.

Zhang, K., Xu, W.W., Zhang, Z., Liu, J., Li, J., Sun, L., Sun, W., Jiao, P., Sang, X., Ren, Z., et al. (2017). The innate

immunity of guinea pigs against highly pathogenic avian influenza virus infection. Oncotarget *8*, 30422–30437.

Zhang, Q.-M., Zhao, X., Li, Z., Wu, M., Gui, J.-F., and Zhang, Y.-B. (2018). Alternative Splicing Transcripts of Zebrafish LGP2 Gene Differentially Contribute to IFN Antiviral Response. J. Immunol. *200*, 688–703.

Zhang, Q., Cheng, J., and Xin, Q. (2015a). Effects of tetracycline on developmental toxicity and molecular responses in zebrafish (Danio rerio) embryos. Ecotoxicology *24*, 707–719.

Zhang, Z., Huang, T., Yu, F., Liu, X., Zhao, C., Chen, X., Kelvin, D.J., and Gu, J. (2015b). Infectious Progeny of 2009 A (H1N1) influenza virus replicated in and released from human neutrophils. Sci. Rep. *5*, 17809.

Zhao, K., Rong, G., Hao, Y., Yu, L., Kang, H., Wang, X., Wang, X., Jin, Z., Ren, Z., and Li, Z. (2016). IgA response and protection following nasal vaccination of chickens with Newcastle disease virus DNA vaccine nanoencapsulated with Ag@SiO2 hollow nanoparticles. Sci. Rep. *6*.

Zhao, X., Dai, J., Xiao, X., Wu, L., Zeng, J., Sheng, J., Su, J., Chen, X., Wang, G., and Li, K. (2014). PI3K/Akt Signaling Pathway Modulates Influenza Virus Induced Mouse Alveolar Macrophage Polarization to M1/M2b. PLoS One *9*, e104506.

Zheng, J.-L., Guo, S.-N., Yuan, S.-S., Xia, H., Zhu, Q.-L., and Lv, Z.-M. (2017). Preheating mitigates cadmium toxicity in zebrafish livers: Evidence from promoter demethylation, gene transcription to biochemical levels. Aquat. Toxicol. *190*, 104–111.

Zheng, W., Wang, Z., Collins, J.E., Andrews, R.M., Stemple, D., and Gong, Z. (2011). Comparative Transcriptome Analyses Indicate Molecular Homology of Zebrafish Swimbladder and Mammalian Lung. PLoS One *6*, e24019.

Zheng, Z., Diaz-Arévalo, D., Guan, H., and Zeng, M. (2018). Noninvasive vaccination against infectious diseases. Hum. Vaccines Immunother. *14*, 1717–1733.

Zhou, Z., and Sun, L. (2015). Immune effects of R848: Evidences that suggest an essential role of TLR7/8-induced, Myd88- and NF-κB-dependent signaling in the antiviral immunity of Japanese flounder (Paralichthys olivaceus). Dev. Comp. Immunol. *49*, 113–120.

Zhou, G., Juang, S.W.W., and Kane, K.P. (2013). NK cells exacerbate the pathology of influenza virus infection in mice. Eur. J. Immunol. *43*, 929–938.

Zhou, L., Limbu, S.M.H., Qiao, F., Du, Z.-Y.Y., and Zhang, M. (2018). Influence of Long-Term Feeding Antibiotics on the Gut Health of Zebrafish. Zebrafish *15*, 340–348.

Zhu, J., Liu, X., Cai, X., Ouyang, G., Fan, S., Wang, J., and Xiao, W. (2020). Zebrafish prmt7 negatively regulates antiviral responses by suppressing the retinoic acid-inducible gene-I-like receptor signaling. FASEB J. *34*, 988–1000.

Zhu, L., Wang, X., Wang, K., Yang, Q., He, J., Qin, Z., Geng, Y., Ouyang, P., and Huang, X. (2017). Outbreak of infectious pancreatic necrosis virus (IPNV) in farmed rainbow trout in China. Acta Trop. *170*, 63–69.

Zuercher, A.W., and Cebra, J.J. (2002). Structural and functional differences between putative mucosal inductive sites of the rat. Eur. J. Immunol. *32*, 3191–3196.

Zuercher, A.W., Coffin, S.E., Thurnheer, M.C., Fundova, P., and Cebra, J.J. (2002). Nasal-Associated Lymphoid Tissue Is a Mucosal Inductive Site for Virus-Specific Humoral and Cellular Immune Responses. J. Immunol. *168*, 1796–1803.

8 Appendices

Gills
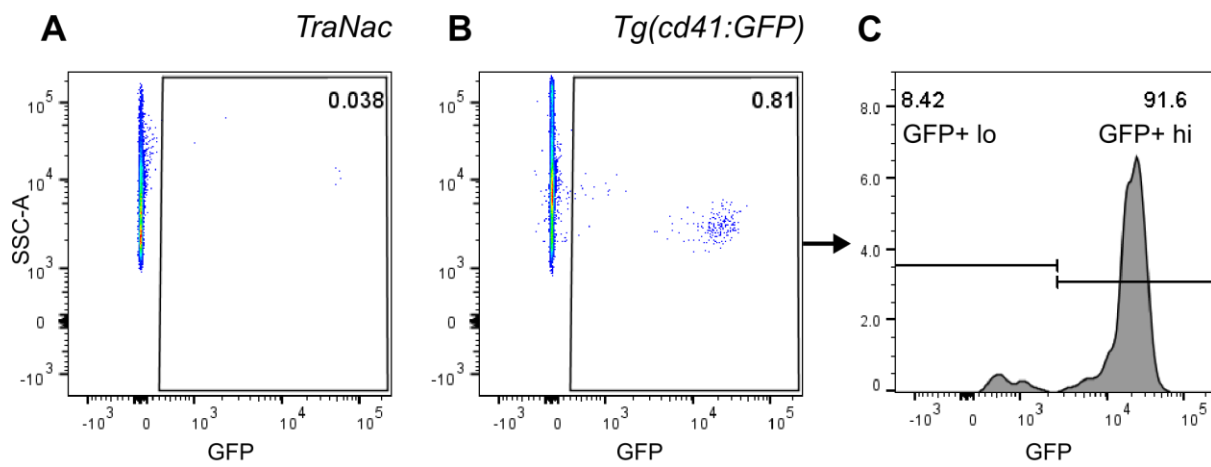
WKM
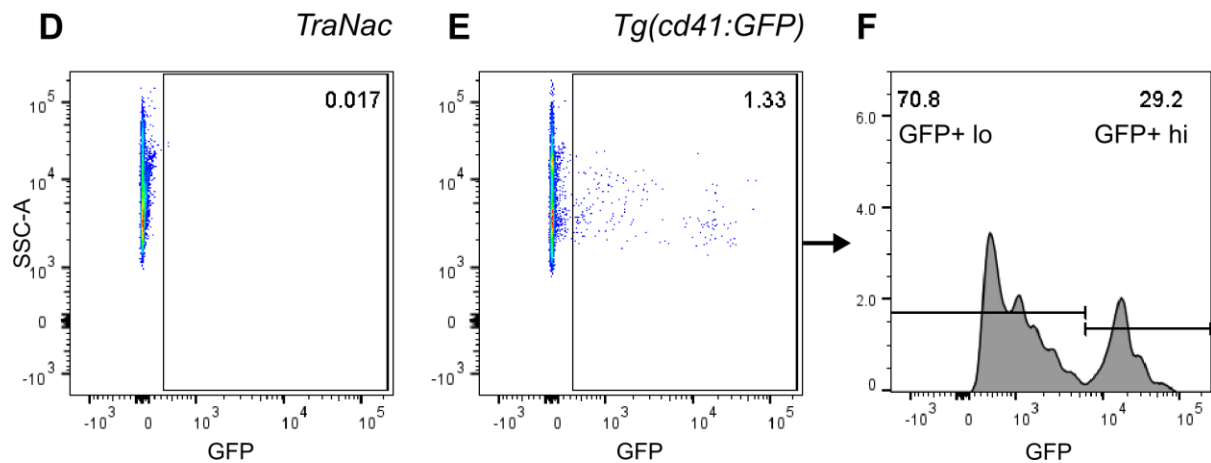
Appendix 1 Flow cytometry of cells from *Tg(cd41:GFP)* adult zebrafish.

Tg(cd41:GFP) and *TraNac* gills and WKM were digested with collagenase and manually triturated into single cell suspensions. (A, D) Background fluorescence was identified from *TraNac* control gills (A) and WKM (D) and excluded in subsequent gating. (B, E) This gating was used to identify GFP+ cells in *Tg(cd41:GFP)* samples. (C, F) Histogram of GFP+ cells. Values in (A-F) reflect percentages of events in each gate compared to total events in plot. N = 1 for *TraNac* fish, N = 4 for *Tg(cd41:GFP)* fish.

Page No.	Type of work:	Name of work	Source of work	Copyright holder and contact	Permission requested on	I have permission yes /no	Permission note
344	Figure	Fig. 2 R848 induces lymphocyte migration in zebrafish gills	Induction of innate cytokine responses by respiratory mucosal challenge with R848 in zebrafish, mice, and humans. J. Allergy Clin. Immunol. (2019)	© 2019 The Authors. m.dallman@imperial.ac.uk	29.10.20	Yes	This is an open access article under the CC BY license (http://creativecommons.org/licenses/by/3.0/).

Appendix 2 Table of copyright permissions obtained to reproduce work.